

**NIST Technical Note 2121**

**Structural Performance of Nuclear Power  
Plant Concrete Structures Affected by  
Alkali-Silica Reaction (ASR)**

**Task 1: Assessing In-Situ Mechanical  
Properties of ASR-Affected Concrete**

Fahim Sadek  
Travis Thonstad  
Sorin Marcu  
Jonathan M. Weigand  
Timothy J. Barrett  
Hai S. Lew  
Long T. Phan  
Adam L. Pintar

This publication is available free of charge from:  
<https://doi.org/10.6028/NIST.TN.2121>

**NIST Technical Note 2121**

**Structural Performance of Nuclear Power  
Plant Concrete Structures Affected by  
Alkali-Silica Reaction (ASR)**

**Task 1: Assessing In-Situ Mechanical  
Properties of ASR-Affected Concrete**

Fahim Sadek  
Travis Thonstad  
Sorin Marcu  
Jonathan M. Weigand  
Timothy J. Barrett  
Hai S. Lew  
Long T. Phan  
*Engineering Laboratory  
National Institute of Standards and Technology*

Adam L. Pintar  
*Information Technology Laboratory  
National Institute of Standards and Technology*

This publication is available free of charge from:  
<https://doi.org/10.6028/NIST.TN.2121>

February 2021



U.S. Department of Commerce  
*Wynn Coggins, Acting Secretary*

National Institute of Standards and Technology  
*James K. Olthoff, Performing the Non-Exclusive Functions and Duties of the Under Secretary of Commerce  
for Standards and Technology & Director, National Institute of Standards and Technology*

#### Disclaimer No. 1

Certain commercial entities, equipment, or materials may be identified in this document in order to describe an experimental procedure or concept adequately. Such identification is not intended to imply recommendation or endorsement by the National Institute of Standards and Technology, nor is it intended to imply that the entities, materials, or equipment are necessarily the best available for the purpose.

#### Disclaimer No. 2

The policy of NIST is to use the International System of Units in all publications. In this document, however, units are presented in the system prevalent in the relevant discipline, although in some cases more than one system of units may be presented.

#### Use in Legal Proceedings

No part of any report resulting from a NIST investigation into a structural failure or from an investigation under the National Construction Safety Team Act may be used in any suit or action for damages arising out of any matter mentioned in such report (15 U.S.C. 281a, as amended).

#### Copyright

This NIST publication is a work of the United States Government not subject to copyright protection within the United States under Title 17 United States Code § 105. This publication may include copyrighted content (such as photographs) used with permission of the credited copyright holder. Reproduction, redistribution or reuse of such copyrighted content apart from this publication may require permission, which should be sought from the credited copyright holder. Where no copyright holder or source is credited for a figure or table in this publication, the source is NIST, which would appreciate attribution.

**National Institute of Standards and Technology Technical Note 2121**  
**Natl. Inst. Stand. Technol. Tech. Note 2121, 217 pages (February 2021)**  
**<https://doi.org/10.6028/NIST.TN.2121>**  
**CODEN: NTN0EF**

## ACKNOWLEDGEMENTS

---

The authors wish to express gratitude and appreciation to the following current and former NIST colleagues who have provided advice and guidance, ideas and expertise, collaborations, technical contributions, and assistance throughout the duration of this research effort:

- Meses. Bridget Kowalchek, Ami Reisinger, Jennifer Horning, Gwynaeth Broome, and Melissa Logan for budgetary advice and administrative and logistical supports, including procurements, acquisitions, meetings, and shipping and receiving.
- Drs. Ken Snyder, Steve Feldman, Michael Bishop, and Mr. Richard Eason: For sharing information and advice on aggregates reactivity, procurement, and concrete expansion, and for providing assistance with specimen preparation, instrumentation, construction, and testing.
- Ms. Gerry Cheok: For lending her expertise, time, and equipment for laser scanning measurement, and for providing assistance with data collection and analysis for our surface expansion measurement.
- Dr. Vance Payne: For providing expertise and advice in heating, air conditioning, and ventilation for control of the NIST environmental chamber and curing of the test specimens.
- Messrs. Shawn Harris, Jason Garver, James Ratino: For their contributions and technical assistance in the construction of the test specimens, and
- Messrs. Rudy Villegas and Louis Potts: For their contributions in all the experimental phases of this research, including samples preparation and testing, through a related NIST laboratory project.

Last but not least, the authors would like to sincerely thank Mr. Jacob Philip, from the U.S. Nuclear Regulatory Commission (NRC), for his support and technical guidance throughout the entire duration of this NRC's sponsored research to study structural performance of Nuclear Power Plant's concrete structures affected by Alkali-Silica Reaction.

## ABSTRACT

---

This report describes the results of Task 1 of a five-task comprehensive research program conducted at the National Institute of Standards and Technology (NIST) under the sponsorship of the U.S. Nuclear Regulatory Commission (NRC). The overall study aims to develop a technical basis for evaluating effects of Alkali-Silica Reaction (ASR), which occurs when the high pH concrete pore solution reacts with certain aggregate mineral phases to form expansive ASR gel and create internal expansive forces that cause cracking in concrete, and may result in degradation of engineering properties of materials and structural capacities of reinforced concrete structures. The report provides detailed information on experimental planning, measurements, and testing performed to achieve the objective of Task 1, assessing in-situ mechanical properties of ASR-affected concrete, and presents experimental results that quantified the effects of: (1) the influence of different degrees of steel confinement and (2) different levels of ASR-induced expansions (0.1 %; 0.3 %; and 0.5 % designed linear target ultimate expansion) on concrete's mechanical properties, surface expansion, and crack development.

**Keywords:**

Alkali-silica Reaction; ASR; Compressive Strength; Concrete; Crack; Expansion; Experimental; Mechanical Property; Modulus of Elasticity; Steel Reinforcement; Triaxial Compression Test

## PREFACE

---

The technical work reported herein is part of a comprehensive research program carried out by the Engineering Laboratory of the National Institute of Standards and Technology (NIST) on the structural performance of nuclear power plant concrete structures affected by alkali-silica reaction (ASR). The work is funded by the U.S. Nuclear Regulatory Commission (NRC) under Inter-agency agreement NRC-HQ-60-14-I-0004.

# TABLE OF CONTENTS

---

---

<b>Acknowledgements</b> .....	<b>iii</b>
<b>Abstract</b> .....	<b>iv</b>
<b>Preface</b> .....	<b>v</b>
<b>Table of Contents</b> .....	<b>vi</b>
<b>List of Figures</b> .....	<b>ix</b>
<b>List of Tables</b> .....	<b>xiv</b>
<b>List of Acronyms, Abbreviations, and Notations</b> .....	<b>xv</b>
<b>Metric Conversion Table</b> .....	<b>xviii</b>
<b>Executive Summary</b> .....	<b>xxi</b>
E.1 Introduction .....	xxi
E.2 NIST Task 1 Experimental Program .....	xxii
E.3 Findings And Conclusions .....	xxiii
E.3.1 Findings .....	xxiii
Strain Developments in Reinforcing Bars .....	xxiii
Concrete Strains.....	xxiv
Surface Expansion and Crack Mapping.....	xxiv
Mechanical Properties of ASR-Affected Concrete .....	xxv
Effect of Confinement Pressure on Compressive Strength of ASR-Affected Concrete .....	xxvi
E.3.2 Conclusions .....	xxvi
<b>Chapter 1 Introduction</b> .....	<b>1</b>
1.1 Background .....	1
1.2 Scope of Study .....	2
1.3 Report Outline .....	3

---

<b>Chapter 2 Experimental Plan For Assessing Mechanical Properties Of ASR-Affected Concrete .....</b>	<b>5</b>
2.1 Materials Selection and Mixture Proportioning .....	6
2.2 Design of Block Specimens .....	9
2.3 Instrumentation and Data Acquisition.....	13
2.3.1 Strain Gages.....	16
2.3.2 Tri-directional Concrete Strain Transducers.....	16
2.3.3 Thermocouples and Relative Humidity Sensors.....	17
2.3.4 Targets for Laser Tracking System .....	17
2.3.5 Data Acquisition System (DAQ) .....	21
2.4 Specimens Construction .....	22
2.4.1 Erection of Reinforcing Bar Cages and Steel Formwork .....	22
2.4.2 Concrete Placement .....	24
2.5 Properties of Fresh Concrete .....	27
2.6 Curing.....	30
2.6.1 Initial Curing after Concrete Placement.....	30
2.6.2 Long-Term Curing .....	30
2.7 NIST Triaxial Pressure Vessel .....	32
<b>Chapter 3 MEASUREMENT AND DATA ANALYSIS .....</b>	<b>35</b>
3.1 Environmental Conditions .....	35
3.2 Strain-Time Histories .....	37
3.2.1 Strains on Reinforcing Bars .....	37
3.2.2 Strains in Concrete .....	64
3.3 Surface Expansion and Crack Mapping .....	70
3.3.1 Surface Expansion Measurements Using A Laser Tracker .....	71
3.3.2 Surface Crack Mapping and Expansion Using Cracking Index Method.....	80
3.3.3 Summary .....	86
3.4 Mechanical Properties of Concrete .....	86
3.4.1 Overview of Mechanical Property Testing Program .....	86
3.4.2 Results of mechanical property tests .....	93
3.4.3 Analysis of Core Test Results.....	99
3.4.4 Normalized Mechanical Properties .....	108
3.5 Triaxial Testing of Core Specimens .....	113
3.5.1 Estimate of confinement pressure.....	113

---

3.5.2 Design of TPV experiment.....	114
3.5.3 TPV test procedure and data correction.....	116
3.5.4 TPV Test Results and Data Analysis .....	121
<b>CHAPTER 4 FINDINGS AND CONCLUSIONS.....</b>	<b>129</b>
4.1 Summary .....	129
4.2 Findings.....	129
4.2.1 Strain Developments in Reinforcing Bars.....	129
4.2.2 Concrete Core Strains .....	130
4.2.3 Surface Expansion and Crack Mapping.....	131
4.2.4 Mechanical Properties of ASR-Affected Concrete.....	131
4.2.5 Effect of Confinement Pressure on Compressive Strength of ASR-Affected Concrete .....	132
4.3 Conclusions .....	133
<b>References .....</b>	<b>135</b>
<b>APPENDIX A STRAIN GAGES ON REINFORCING BARS .....</b>	<b>137</b>
A.1 strain gages on stirrups .....	138
A.2 strain gages on longitudinal reinforcing bars.....	140
A.3 strain gages on corner reinforcing bars.....	142
A.4 strain gages on cross ties.....	144
<b>APPENDIX B AVERAGE SURFACE STRAINS USING LASER MEASUREMENTS .....</b>	<b>145</b>
<b>APPENDIX C AVERAGE SURFACE STRAINS USING LASER AND CALIPER MEASUREMENTS ALONG WITH CRACKING INDEX AND REINFORCING BAR STRAINS.....</b>	<b>177</b>
<b>APPENDIX D MEASUREMENT UNCERTAINTIES .....</b>	<b>187</b>

## LIST OF FIGURES

---

---

Figure 2-1: Elevation view of typical block specimen showing different confinement regions ....	10
Figure 2-2: Reinforcement details for the blocks: (a) elevation and (b) cross sections.....	12
Figure 2-3: Threaded mechanical headed anchors at ends of longitudinal reinforcing bars.....	13
Figure 2-4: Layout of strain gages on reinforcing bars, triaxial concrete strain transducers, and thermocouples for blocks ASR 1, ASR 2, and ASR 3.....	14
Figure 2-5: Layout of strain gages on reinforcing bars, triaxial concrete strain transducers, and thermocouples for control block .....	15
Figure 2-6: Tri-directional concrete strain transducers.....	16
Figure 2-7: Targets for surface expansion measurements: (a) plywood sheet with targets, (b) target construction, and (c) target design .....	18
Figure 2-8: Layout of targets for surface expansion measurements: (a) elevation and (b) side view. ....	20
Figure 2-9: Reference target for laser measurement tracking mounted on stainless steel framing installed around the environmental chamber.....	20
Figure 2-10: (a) Routing of instrumentation cables though PVC conduits and into (b) the DAQ in an adjacent room .....	21
Figure 2-11: Assembled reinforcing bar cage for block ASR 1 .....	22
Figure 2-12: Steel formwork details: (a) plan view and (b) sectional view.....	23
Figure 2-13: Photographs showing erection of steel formwork .....	24
Figure 2-14: Mobile batch plant and three cubic yard concrete mixer.....	25
Figure 2-15: Consolidation of concrete using vibrators.....	25
Figure 2-16: Concrete mixer discharging control concrete into telebelt. ....	26
Figure 2-17: Concrete placement into formwork of control specimen using an elephant trunk hose.....	26
Figure 2-18: Phase 1 of curing of reactive block specimens.....	30
Figure 2-19: Phase 2 of curing of reactive block specimens.....	31
Figure 2-20: Phase 3 of curing of reactive block specimens.....	31
Figure 2-21: (a) Triaxial pressure vessel and (b) cross section of triaxial pressure vessel with a prepared cored concrete specimen.....	33
Figure 2-22: Triaxial pressure vessel and hydraulic power unit and controls situated in 220 kip servohydraulic load frame .....	33
Figure 3-1: Temperature histories inside the environmental chamber .....	36
Figure 3-2: Measured temperatures inside the control block .....	37

---

Figure 3-3: Measured strains on reinforcing bars of Region 1 of block ASR 1: (a) longitudinal bars, (b) top corner bars, (c) bottom corner bars, (d) vertical legs of stirrups, (e) top horizontal leg of stirrups, and (f) bottom horizontal leg of stirrupsAnchorage channel assembly (a) excluding high-strength anchor rod, and .....	41
Figure 3-4: Measured strains on corner reinforcing bars of Region 2 of block ASR 1 .....	42
Figure 3-5: Measured strains on reinforcing bars of Region 3 of block ASR 1: (a) longitudinal bars, (b) top corner bars, (c) bottom corner bars, (d) vertical legs of stirrups, (e) top horizontal leg of stirrups, (f) bottom horizontal leg of stirrups, and (g) cross ties .....	46
Figure 3-6: Measured strains on reinforcing bars of Region 1 of block ASR 2: (a) longitudinal bars, (b) top corner bars, (c) bottom corner bars, (d) vertical legs of stirrups, (e) top horizontal leg of stirrups, and (f) bottom horizontal leg of stirrups.....	49
Figure 3-7: Measured strains on corner reinforcing bars of Region 2 of block ASR 2.....	50
Figure 3-8: Measured strains on reinforcing bars of Region 3 of block ASR 2: (a) longitudinal bars, (b) top corner bars, (c) bottom corner bars, (d) vertical legs of stirrups, (e) top horizontal leg of stirrups, (f) bottom horizontal leg of stirrups, and (g) cross ties .....	54
Figure 3-9: Measured strains on reinforcing bars of Region 1 of block ASR 3: (a) longitudinal bars, (b) top corner bars, (c) bottom corner bars, (d) vertical legs of stirrups, (e) top horizontal leg of stirrups, and (f) bottom horizontal leg of stirrups.....	57
Figure 3-10: Measured strains on corner reinforcing bars of Region 2 of block ASR 3.....	58
Figure 3-11: Measured strains on reinforcing bars of Region 3 of block ASR 3: (a) longitudinal bars, (b) top corner bars, (c) bottom corner bars, (d) vertical legs of stirrups, (e) top horizontal leg of stirrups, (f) bottom horizontal leg of stirrups, and (g) cross ties .....	62
Figure 3-12: Measured strains on reinforcing bars for the control block .....	64
Figure 3-13: Measured strains at the core of block ASR 1: (a) Region 1, and (b) Region 2.....	66
Figure 3-14: Measured strains at the core of block ASR 2: (a) Region 1, and (b) Region 2.....	67
Figure 3-15: Measured strains at the core of block ASR 3: (a) Region 1, and (b) Region 2.....	68
Figure 3-16: Automated Precision Inc. (API) Tracker 3 used in surface expansion measurements .....	71
Figure 3-17: (a) 1.5 in laser tracker SMR, (b) 1.5 in SMR holder used in surface expansion measurements (both from <a href="https://www.metrologyworks.com/">https://www.metrologyworks.com/</a> ) .....	72
Figure 3-18: Plan view of environmental chamber showing locations of laser tracker for scanning of surfaces of reactive blocks.....	74
Figure 3-19: Average surface strains using laser measurements between neighboring targets versus measured strains on corresponding reinforcing bars .....	77
Figure 3-20: Average surface strains using laser measurements along target lines versus average measured strains on corresponding reinforcing bars .....	78
Figure 3-21: Mean value and upper and lower bounds for average surface strains using laser measurements along target lines versus measured strains on corresponding reinforcing bars.....	79
Figure 3-22: Grid used for measurement of surface cracking using an optical microscope and surface expansion using a high-precision caliper .....	81

---

Figure 3-23: Average surface strains using caliper measurements versus average surface strains using laser measurements for blocks (a) ASR 1, (b) ASR 2, and (c) ASR 3.....	83
Figure 3-24: Cracking Index versus average surface strains using laser measurements for blocks (a) ASR 1, (b) ASR 2, and (c) ASR 3 .....	85
Figure 3-25: Extraction of cores from the blocks .....	87
Figure 3-26: Compressive strength and elastic modulus testing of concrete cylinders .....	88
Figure 3-27: Splitting Tensile Strength testing of concrete cylinders.....	88
Figure 3-28: Potential core locations. Center line of potential core locations indicated by red line, black lines indicate approximate centerline of reinforcement, circles represent surface cast targets, and orange boxes indicate regions with embedded concrete strain transducers .....	89
Figure 3-29: Elevation cross section of idealized confinement zones in (a) Region 1 and (b) Region 3 of the blocks.....	90
Figure 3-30: Core specimen numbering system.....	91
Figure 3-31: Example of linear regression lines (dashed lines) calculated from each of three cycles of a cylinder's stress-strain data for a core extracted from block ASR 3 at 634 days. The modulus of elasticity was taken as the average slope of the three linear regression lines .....	92
Figure 3-32: Comparison of the modulus of elasticity values calculated using ASTM C469/469M-14's secant stiffness method to values calculated using linear regression .....	92
Figure 3-33: Average compressive strength test results for cylinders and cores from (a) block ASR 1, (b) block ASR 2, (c) block ASR 3, and (d) control block .....	95
Figure 3-34: Average modulus of elasticity test results for cylinders and cores from (a) block ASR 1, (b) block ASR 2, (c) block ASR 3, and (d) Control block .....	97
Figure 3-35: Average splitting tensile strength test results for cylinders and cores from (a) block ASR 1, (b) block ASR 2, (c) block ASR 3, and (d) Control block .....	99
Figure 3-36: Comparison of measured modulus of elasticity and calculated modulus of elasticity based on ACI 318-14 equation for cores extracted from reactive blocks (a) ASR 1, (b) ASR 2, and (c) ASR 3 .....	101
Figure 3-37: Comparison of measured splitting tensile strength and calculated tensile strength based on ACI 318-14 equation for cores extracted from reactive blocks (a) ASR 1, (b) ASR 2, and (c) ASR 3 .....	103
Figure 3-38: Effect of confinement region on compressive strength of cores extracted from blocks (a) ASR 1, (b) ASR 2, and (c) ASR 3 .....	105
Figure 3-39: Effect of core height on compressive strength of cores extracted from blocks (a) ASR 1, (b) ASR 2, and (c) ASR 3.....	107
Figure 3-40: Average compressive strength normalized to 28-day compressive strength versus unconfined expansion for cores from (a) ASR 1, (b) ASR 2, and (c) ASR 3 blocks .....	110
Figure 3-41: Average modulus of elasticity normalized to 28-day modulus of elasticity versus unconfined expansion for cores from (a) ASR 1, (b) ASR 2, and (c) ASR 3 blocks .....	111
Figure 3-42: Average splitting tensile strength normalized to 28-day tensile strength versus unconfined expansion for cores from (a) ASR 1, (b) ASR 2, and (c) ASR 3 blocks .....	113

---

Figure 3-43: Concrete stresses in the (a) vertical, (b) transverse, and (c) longitudinal direction .....	114
Figure 3-44: Variables considered in the design of experiment .....	115
Figure 3-45: Triaxial compression test procedure: (a) specimen was with a shrink tub and O-rings, (b) specimen inside TPV with metallic screen, (c) assembled TPV with bolts tightened, (d) TPV test setup in servohydraulic load frame, and (e) failed specimen .....	118
Figure 3-46: Schematic of TPV assembly showing load transfer mechanism .....	119
Figure 3-47: Measured force during pressurized tests without core specimen at pressure of (a) 350 psi and (b) 700 psi .....	120
Figure 3-48: Corrected and normalized triaxial test data using average unconfined strength at time of testing .....	125
Figure 3-49: Estimates and associated uncertainties for the $\beta_i$ 's in Equation (3.5). The red points are the estimates, and the violin plots depict the bootstrap distributions, which quantify uncertainty. The numbers are the proportions of the bootstrap datasets for which the coefficients are estimated to be non-zero .....	126
Figure 3-50: Comparison of developed expression with equations from Richart et al. (1928) and Mander et al. (1988). The thick black line is the developed expression in Equation (3.6), and the grey lines are 1000 bootstrap replicates conveying uncertainty due to sampling variability. The black points are the observed measurements from Table 3-10. ....	128
Figure A-1: Strain gages on stirrups in Region 1 of the blocks. ....	138
Figure A-2: Strain gages on stirrups in Region 3 of the blocks. ....	139
Figure A-3: Strain gages on longitudinal reinforcing bars in Region 1 of the blocks.....	140
Figure A-4: Strain gages on longitudinal reinforcing bars in Region 3 of the blocks.....	141
Figure A-5: Strain gages on upper corner reinforcing bars. ....	142
Figure A-6: Strain gages on lower corner reinforcing bars.....	143
Figure A-7: Strain gages on cross ties in Region 3 of the blocks.....	144
Figure B-1: Average surface strains using laser measurements between neighboring targets for block ASR 1: (a) horizontal strains on east face, (b) vertical strains on east face, (c) horizontal strains on west face, (d) vertical strains on west face, (e) horizontal strains on north and south ends, and (f) vertical strains on north and south ends.....	151
Figure B-2: Average surface strains using laser measurements between neighboring targets for block ASR 2: (a) horizontal strains on north face, (b) vertical strains on north face, (c) horizontal strains on south face, (d) vertical strains on south face, (e) horizontal strains on east and west ends, and (f) vertical strains on east and west ends. ....	157
Figure B-3: Average surface strains using laser measurements between neighboring targets for block ASR 3: (a) horizontal strains on east face, (b) vertical strains on east face, (c) horizontal strains on west face, (d) vertical strains on west face, (e) horizontal strains on north and south ends, and (f) vertical strains on north and south ends.....	163
Figure B-4: Average surface strains using laser measurements along target lines for block ASR 1: (a) horizontal strains on east face, (b) vertical strains on east face, (c) horizontal strains on west face, and (d) vertical strains on west face. ....	167

---

Figure B-5: Average surface strains using laser measurements along target lines for block ASR 2: (a) horizontal strains on north face, (b) vertical strains on north face, (c) horizontal strains on south face, and (d) vertical strains on south face. ....	171
Figure B-6: Average surface strains using laser measurements along target lines for block ASR 3: (a) horizontal strains on east face, (b) vertical strains on east face, (c) horizontal strains on west face, and (d) vertical strains on west face. ....	175
Figure C-1: Average surface strains using laser and caliper measurements along with cracking index and reinforcing bar strains for block ASR 1 on (a) east face, (b) west face, and (c) north and south ends (all values are percentages). ....	180
Figure C-2: Average surface strains using laser and caliper measurements along with cracking index and reinforcing bar strains for block ASR 2 on (a) north face, (b) south face, and (c) east and west ends (all values are percentages). ....	183
Figure C-3: Average surface strains using laser and caliper measurements along with cracking index and reinforcing bar strains for block ASR 3 on (a) east face, (b) west face, and (c) north and south ends (all values are percentages). ....	186

---

## LIST OF TABLES

---

Table E-1: Test matrix showing primary variables for Task 1 experimental program .....	xxiii
Table 2-1: Test matrix showing primary variables for Task 1 experimental program. ....	5
Table 2-2: Mixture proportioning for concretes in the NIST experimental program .....	8
Table 2-3: Steel reinforcement ratio for Confinement Regions 1, 2, and 3 of the block specimens .....	11
Table 2-4: Types and numbers of instruments used in the block specimens .....	13
Table 2-5: Fresh concrete properties for each batch used in the production of block ASR 3 .....	28
Table 2-6: Fresh concrete properties for each batch used in the production of block ASR 2 .....	28
Table 2-7: Fresh concrete properties for each batch used in the production of block ASR 1. ....	29
Table 2-8: Fresh concrete properties for each batch used in the production of control block.....	29
Table 3-1: History of surface expansion and crack mapping measurements .....	71
Table 3-2: Statistics of the ratio of the average measured strains using laser measurements between neighboring targets to the corresponding measured strains or reinforcing bars ...	77
Table 3-3: Statistics of the ratio of the average measured strains along target lines and the corresponding average measured strains on reinforcing bars .....	79
Table 3-4: Average vertical surface strains in Region 2 of the three reactive blocks (% in/in)....	80
Table 3-5: Statistics of the ratio of the average measured strains between targets using Caliper measurement and the corresponding average strains using laser tracker .....	82
Table 3-6: Statistics of the ratio of the cracking index to the average measured strains between targets using laser tracker .....	84
Table 3-7: Test matrix for triaxial testing of cores. ....	116
Table 3-8: Raw data from triaxial testing of core specimens.....	122
Table 3-9: Average unconfined compressive strength of core specimens .....	123
Table 3-10: Corrected and normalized data using average unconfined strength at time of triaxial testing .....	124
Table D-1: Measurement uncertainty .....	187

---

## LIST OF ACRONYMS, ABBREVIATIONS, AND NOTATIONS

---

### Acronyms

ACI	American Concrete Institute
API	Automated Precision Inc.
ASR	Alkali-silica reaction
ASTM	American Society for Testing and Materials
CI	Cracking index
DAQ	Data acquisition
DEMEC	Demountable mechanical
FHWA	Federal Highway Administration
HRWRA	High-range water-reducing admixture
LASSO	Least absolute shrinkage and selection operator
MTS	Materials Testing Systems
NIST	National Institute of Standards and Technology
NPP	Nuclear power plant
NRC	Nuclear Regulatory Commission
PCle	Peripheral component interconnect express
RH	Relative humidity
RT	Reference targets
RMS	Root mean square
SCXI	Signal conditioning extension for instrumentation
SMR	Spherically mounted retroreflector
TPV	Triaxial pressure vessel
TRE	target registration error

### Abbreviations

d	day
ft	foot
in	inch
kip	a force equal to 1,000 pounds
ksi	kip per square inch
lbf	pound force

---

min	minute
psi	pounds per square inch
s	second

## Notations

$A_c$	Area of concrete cylinder or core
$A_p$	Area of the TPV's piston
$A_s$	Area of reinforcing bars
$b_c, d_c$	Dimensions of concrete cross section bounded by reinforcing bars
$B$	Identifier for block (ASR 1 or ASR 3)
$E_c$	Modulus of elasticity of concrete, psi
$F_0$	Offset reading of load cell at zero applied load in load frame
$F_\mu$	Friction force in the TPV's rod seal due to piston motion
$F_p$	Upward force on concrete core due to pressure in the TPV
$f'_c$	Specified compressive strength of concrete
$f_{cc}$	Confined compressive strength of concrete
$f_{cm}$	Measured average compressive strength of concrete
$f_{ct}$	Measured average splitting tensile strength of concrete
$f_{cu}$	Average unconfined strength of concrete
$f_l$	Confinement pressure
$f_y$	Specified yield strength of reinforcement
$k$	Coverage factor (in Sections 3.3.1 and 3.4.2), rate of compressive strength increase with increasing lateral pressure (elsewhere)
$n$	Number of independent measurements
$N$	Number of degrees of freedom
$P$	Total force on concrete cylinder
$R$	Identifier for confinement region (Region 1 or 3)
$u_c$	Standard uncertainty
$U$	Uncertainty measure
$\beta_i$	Regression coefficient
$\epsilon$	Term representing random error
$\epsilon_{ASR}$	ASR-induced linear expansion
$\epsilon_{avg}$	Average surface strain

---

$\mu_c$	Mean value of a variable
$\rho_v$	Volumetric reinforcement ratio
$\rho_x, \rho_y, \rho_z$	Ratio of area of steel reinforcement to area of concrete in x, y, and z directions
$\sigma_{avg}$	Average stress in confined concrete

---

## METRIC CONVERSION TABLE

---

To convert from	to	Multiply by
<b>AREA AND SECOND MOMENT OF AREA</b>		
square foot (ft <sup>2</sup> )	square meter (m <sup>2</sup> )	9.290 304 E-02
square inch (in. <sup>2</sup> )	square meter (m <sup>2</sup> )	6.4516 E-04
<b>FORCE</b>		
kilogram-force (kgf)	newton (N)	9.806 65 E+00
kilopond (kilogram-force) (kp)	newton (N)	9.806 65 E+00
kip (1 kip=1,000 lbf)	newton (N)	4.448 222 E+03
kip (1 kip=1,000 lbf)	kilonewton (kN)	4.448 222 E+00
pound-force (lbf)	newton (N)	4.448 222 E+00
<b>FORCE DIVIDED BY LENGTH</b>		
pound-force per foot (lbf/ft)	newton per meter (N/m)	1.459 390 E+01
pound-force per inch (lbf/in.)	newton per meter (N/m)	1.751 268 E+02
<b>LENGTH</b>		
foot (ft)	meter (m)	3.048 E-01
inch (in)	meter (m)	2.54 E-02
<b>MASS and MOMENT OF INERTIA</b>		
kilogram-force second squared per meter (kgf · s <sup>2</sup> /m)	kilogram (kg)	9.806 65 E+00
pound foot squared (lb · ft <sup>2</sup> )	kilogram meter squared (kg · m <sup>2</sup> )	4.214 011 E-02
pound inch squared (lb · in. <sup>2</sup> )	kilogram meter squared (kg · m <sup>2</sup> )	2.926 397 E-04

---

<b>To convert from</b>	<b>to</b>	<b>Multiply by</b>
<b>PRESSURE or STRESS (FORCE DIVIDED BY AREA)</b>		
kilogram–force per square centimeter (kgf/cm <sup>2</sup> )	pascal (Pa)	9.806 65 E+04
kilogram–force per square meter (kgf/m <sup>2</sup> )	pascal (Pa)	9.806 65 E+00
kilogram–force per square millimeter (kgf/mm <sup>2</sup> )	pascal (Pa)	9.806 65 E+06
kip per square inch (ksi) (kip/in. <sup>2</sup> )	pascal (Pa)	6.894 757 E+06
kip per square inch (ksi) (kip/in. <sup>2</sup> )	kilopascal (kPa)	6.894 757 E+03
pound–force per square foot (lbf/ft <sup>2</sup> )	pascal (Pa)	4.788 026 E+01
pound–force per square inch (psi) (lbf/in. <sup>2</sup> )	pascal (Pa)	6.894 757 E+03
pound–force per square inch (psi) (lbf/in. <sup>2</sup> )	kilopascal (kPa)	6.894 757 E+00
psi (pound–force per square inch) (lbf/in. <sup>2</sup> )	pascal (Pa)	6.894 757 E+03
psi (pound–force per square inch) (lbf/in. <sup>2</sup> )	kilopascal (kPa)	6.894 757 E+00



This page intentionally left blank.

---

# EXECUTIVE SUMMARY

---

## E.1 INTRODUCTION

Alkali-silica reaction (ASR) has long been recognized as a major cause of concrete internal microcracking and deterioration (Stanton 1940; Swenson 1957). This concrete deterioration mechanism begins with a chemical reaction between the alkali hydroxides in the cement paste and certain amorphous or micro-crystalline siliceous phases in the aggregates, which produces an alkali-silica gel that forms initially in the partially-saturated pore space of the hardened cement paste. The alkali-silica gel is hygroscopic, and will absorb, through osmotic action, moisture in the concrete matrix and expand. This expansion will persist if moisture and other necessary conditions are present. The expansion of alkali-silica gel creates an increasing internal pressure that ultimately leads to internal cracking and degradation of the mechanical properties of concrete (Hansen 1944, Taylor 1990).

Generally, the rate of ASR expansion is relatively slow and is a function of the reactivity of the aggregate mineral phases, the alkalinity of the pore solution, and the availability of moisture. Thus, the onset of ASR-induced cracking can take years or decades after construction to occur. However, once occurred, this deterioration at the material level may affect the bonding characteristics between the concrete and reinforcement and may further influence the overall capacity and service life of reinforced concrete structural member or system.

At present, the industry solution is to identify the reactive aggregates and avoid using them through sourcing of materials for construction and/or use fly ash pozzolan to control reactivity. Although this approach helps to avoid or mitigate ASR in new construction, it does not address the problem in existing structures. Given the current knowledge gaps on ASR effects on structural behavior and lack of associated consensus standard and code provisions to account for these effects on structural capacities, questions remain on how to (1) predict the progression of ASR-induced deterioration once initiated and (2) assess the residual material properties and in-situ structural capacity of the affected structures. These considerations are relevant for certain safety-critical components of the nation's infrastructure (e.g., dams, bridges, and nuclear power plants). Reasonable predictions of the progression of ASR and future, residual structural capacities can provide critical support for decision on whether the affected structures can continue to perform their intended safety functions without significant increase in risk to public safety.

This report describes work that is part of a comprehensive research program being conducted by the Engineering Laboratory of the National Institute of Standards and Technology (NIST) to study the effects of ASR on the structural performance of nuclear power plant concrete structures. The work is funded by the U.S. Nuclear Regulatory Commission (NRC) under Inter-Agency Agreement NRC-HQ-60-14-I-0004. The objective of this research program is to develop a technical basis for generic regulatory guidance for evaluation of ASR-affected nuclear power plant (NPP) reinforced concrete structures through its service life. Specifically, the program is intended to develop measurements for evaluation of (1) effects of ASR on structural performance and capability to perform intended function under design basis static and dynamic loads, and (2) characteristics of an aging management program to adequately monitor and manage aging effects of ASR degradation such that intended functions are maintained through periods of extended operation of renewed licenses. The intended outcome is a methodology for determining for an existing ASR-

---

affected reinforced concrete structure (1) the in-situ structural capacity to resist design-basis static and dynamic loads and (2) future structural capacity.

The overall research program conducted by NIST on behalf of the NRC consisted of five tasks, intended to:

- Task 1: Assess effects of ASR on in-situ mechanical properties of concrete
- Task 2: Assess development and lap-splice lengths of reinforcing bars in ASR-affected concrete
- Task 3: Evaluate seismic response characteristics of ASR-affected reinforced concrete structural members
- Task 4: Estimate the degree of reaction in ASR-affected concrete and the corresponding expansion
- Task 5: Predict future and ultimate ASR expansion in ASR-affected concrete

Specifically, this report describes the experimental planning, measurements and testing, data collection and data analysis, test results, and findings and conclusions that pertain to Task 1 of the overall research program being conducted at NIST under the sponsorship of the NRC.

## **E.2 NIST TASK 1 EXPERIMENTAL PROGRAM**

The NIST Task 1 experimental program utilized three large concrete blocks of different ASR reactivity made with reactive aggregates, along with one control (non-reactive) specimen for comparison. The three reactive blocks were cast with concretes having three different designed target ultimate expansions based on measurements taken on standard prisms: relatively low target linear ASR expansion of 0.15 %; intermediate target linear expansion of 0.3 %; and high target linear expansion of 0.5 %. Each block consisted of three separate regions, each containing different amounts of longitudinal and transverse reinforcements to facilitate examination of the influence of the different levels of confinement provided by the reinforcing bars on the ASR-induced expansion behavior of the blocks. Thus, the combination of three target ASR expansions, from low to high, and three levels of reinforcement confinement, from unconfined to heavily-confined, would encompass a full range of examination of these two variables on the mechanical properties of concrete. Table E.1 shows the overall test matrix with parameters for the two primary variables examined in Task 1 experimental program.

All concrete blocks were cast and kept in a large environmental chamber where they were subjected to a predetermined curing regime with specified temperature and humidity to accelerate their ASR expansion.

All four block specimens were heavily instrumented. The instrumentations allowed measurements of strain development in concrete at the center of the blocks and in the reinforcing bars at various locations, along with internal concrete temperature and relative humidity.

External measuring devices, including a laser tracker, a high-precision caliper, and an optical microscope, were used in measuring ASR-induced expansion and crack development on the surface of the reactive block specimens.

Core samples extracted from the reactive block specimens after different numbers of days, and companion concrete cylinders prepared during concrete placement, were used in mechanical

property testing to quantify the effects of ASR on concrete's properties, including uniaxial compressive strength, modulus of elasticity, and splitting tensile strength. The measured mechanical properties of ASR-affected concrete were compared with the American Concrete Institute (ACI) code equations to evaluate their applicability to concrete affected by ASR.

The influence of confinement pressure on the compressive strength of ASR-affected concrete was also quantified using the NIST-designed Triaxial Pressure Vessel (TPV) test apparatus that allowed simultaneous application of radial confinement pressure of up to 700 psi and uniaxial compressive stress.

**Table E-1 Test matrix showing primary variables for Task 1 experimental program**

Primary Experimental Variables		Block Specimen			
		ASR 1	ASR 2	ASR 3	Control
Concrete with Target Ultimate Expansion $\epsilon_{ASR}$ (%)		0.15	0.3	0.5	0
Levels of Confinement by Volumetric Reinforcement Ratio $\rho_v$ (%)	Region 1	0.72	0.72	0.72	0.72
	Region 2	0.15	0.15	0.15	0.15
	Region 3	1.14	1.14	1.14	1.14

### E.3 FINDINGS AND CONCLUSIONS

This section summarizes the findings and conclusions from this Task 1 experimental program:

#### E.3.1 Findings

##### Strain Developments in Reinforcing Bars

- In the three reactive blocks, the tensile strains measured in the reinforcements were not symmetric with respect to the vertical axis even though the cross section of the blocks was symmetrical both in geometry and in amount of reinforcement. This lack of symmetry may be attributed to (1) a non-uniform ASR expansion within each specimen and (2) to a lesser extent the uneven extraction of core samples from the blocks (cores were not extracted in a symmetric fashion).
- For each block, the strains in Region 1 (mid-confinement) were slightly but consistently larger than those in Region 3 (high-confinement). This trend was expected to occur due to the higher confinement in Region 3 compared with Region 1.
- In general, for a given block and a given region, the strains on the bottom reinforcing bars were smaller than those on the higher bars. This may be due to the friction provided by the ground and/or the larger compaction and overburden pressure, which may have induced higher constraint and resulted in less expansion on the lower portion of the block.

- 
- Block ASR 3, which was designed to be the most reactive, had the largest expansion of the three reactive blocks at the end of Task 1 duration. Blocks ASR 1 and ASR 2 had lower and similar levels of expansion.
  - Most reinforcing bars in block ASR 3 yielded due to the ASR expansion, having strains in excess of their yield strain of typically 0.20 % to 0.23 %. A few reinforcing bars in block ASR 1 also yielded. No reinforcing bars in block ASR 2 yielded.

### **Concrete Strains**

- For each reactive block, the expansions measured in the center of concrete using tri-directional concrete strain transducers in Region 2 were larger than those measured in Region 1 (no data was available from Region 3). This result was expected since Region 2 had virtually no confinement compared with Region 1.
- Consistent with the finding from the strain development using strain gages in the reinforcement above, block ASR 3 (the most reactive block) had the largest measured concrete expansion at its center among the three reactive blocks. Concrete strains at the centers of blocks ASR 1 and ASR 2 had lower and similar expansion values.
- Discrepancies observed between the measured strains in concrete at the center of the blocks and the measured strains on the reinforcing bars, which were located close to the exterior of the blocks (just inside the concrete cover), showed that strains at the exterior of the blocks were larger than those at the center. A similar observation was made using surface expansion measurements taken for Region 2. These measurements showed that the surfaces of the blocks without reinforcing bars had larger in-plane strains/displacements than what was measured by the concrete strain gages at the centers of the three reactive blocks.
  - This highlights one of the challenges associated with evaluation of large ASR-affected concrete structures, where the unconfined expansion is not a single-value, but in reality, an expansion field that can be largely affected by, among other variables, size, exposure to moisture, and potential for alkali leaching.
  - While previous studies provided the mechanical properties of ASR-affected concrete as a function of expansion based on measurements taken from standard prisms, this study provided the mechanical properties of an in-situ structure or element as a function of the measured expansion field (see Section 3.4).

### **Surface Expansion and Crack Mapping**

- A reasonable correlation was observed between the average surface strains/displacements (along target lines in a given region) and the corresponding reinforcing bar strains for blocks ASR 1 and ASR 2, which had maximum measured reinforcing bar strains of about 0.15 %. The correlation was much poorer for block ASR 3, which had maximum measured strains between 0.15 % and 0.35 %, where the average surface strains were smaller than the measured strains on reinforcing bars. These contrasting results suggest that surface

---

expansion measurements may only provide a reasonable estimate of strains at low expansion levels.

- Surface expansion measurements taken using a high-precision caliper were consistent with those taken using the laser tracker. The minor inconsistencies that do exist in the data were likely due to different measurement methodologies, human error, and to a lesser extent small differences in dates of measurements and slight differences in gage length.
- The cracking index (CI) method developed by the Federal Highway Administration (Fournier *et al.*, 2010) yielded results that were not consistent with the surface expansion measurements using the laser tracker and high-precision caliper. In general, the CI results were smaller than the surface strains obtained from the other two techniques, and there was a large scatter in the ratio of the CI to the average surface strains resulting in a coefficient of variation of about 50 %.
- The inability of the surface expansion measurements and the CI method to estimate the level of concrete expansion (or strains on reinforcing bars) was likely because the behavior and thus strains developed in the concrete cover are different from those within the concrete confined by the reinforcing bars. The surface expansion measurements and the CI method remain as useful tools to monitor the progression of ASR, but they do not provide an accurate estimate of the level of expansion.

### **Mechanical Properties of ASR-Affected Concrete**

- Plots of uniaxial compressive strength, modulus of elasticity, and splitting tensile strength (from cylinders and core specimens) versus time and versus unconfined expansion based on (1) Region 2 concrete strain gages and (2) Region 2 surface expansion measurements were developed. Results showed that:
  - *Unconfined uniaxial compressive strength*: Cores extracted from blocks ASR 1 and ASR 2 showed no reduction in the unconfined uniaxial compressive strength compared with the 28-day strength. Cores from block ASR 3 exhibited a reduction in compressive strength of  $13 \% \pm 15 \%$  compared with the 28-day compressive strength. Samples from the control block continued to gain strength over time.
  - *Modulus of elasticity*: Cores extracted from the three reactive blocks showed a reduction of the elastic modulus of  $28 \% \pm 9 \%$  to  $41 \% \pm 6 \%$  compared with the 28-day elastic modulus. On the other hand, samples from the control block exhibited an increase in the modulus of elasticity over time.
  - *Splitting tensile strength*: Extracted cores from blocks ASR 2 and ASR 3 showed no reduction in the tensile strength compared with the 28-day tensile strength. Cores from block ASR 1 showed a reduction of  $15 \% \pm 13 \%$  in tensile strength. For the control block, the splitting tensile strength remained nearly constant over time.
- Modulus of elasticity-compressive strength relationship versus current code:

At the early age of the three reactive blocks, the modulus of elasticity of extracted cores remained, for the most part, within the  $\pm 20 \%$  range of the ACI 318-14 equation ( $E_c = 57000 \sqrt{f'_c}$  [psi]). At increased age (corresponding to increased levels of ASR expansion) of the

---

blocks, the measured modulus of elasticity became significantly lower than that predicted by the ACI equation. This indicates that the modulus of elasticity degraded faster than the compressive strength of concrete with increased ASR expansion.

- Splitting tensile strength-compressive strength relationship versus current code:  
At the early age of the reactive blocks, the splitting tensile strength of extracted cores remained, for the most part, within the  $\pm 20\%$  range of the ACI 318-14 equation ( $f_{ct} = 6.7 \sqrt{f_{cm}}$  [psi]). At increased age (corresponding to increased levels of ASR expansion), the measured splitting tensile strength became higher, on average, than the ACI equation. However, the large scatter in the data prevented definitive conclusions to be drawn regarding the validity of the ACI tensile strength equation for ASR-affected concrete.
- No discernable trend was found regarding the influence of region (i.e., level of confinement) on the uniaxial compressive strength of extracted cores.
- Cores were extracted from both the lower and upper portions of each region in each ASR-affected block. No discernable trend was found regarding the influence of core-height on uniaxial compressive strength of extracted cores.

### **Effect of Confinement Pressure on Compressive Strength of ASR-Affected Concrete**

Based on TPV triaxial compression test results and rigorous statistical analysis, an expression was developed to relate the confined compressive strength of cores,  $f_{cc}$ , that were extracted from ASR-affected specimens; the applied lateral pressure,  $f_l$ ; and the uniaxial compressive strength of cores,  $f_{cu}$ , obtained under standard (unconfined) conditions at the time of the triaxial testing. The expression was found to have the familiar form:

$$f_{cc}/f_{cu} = 1 + k f_l/f_{cu},$$

where the value of  $k$ , the rate of strength increase with increasing lateral pressure, was estimated to be 6, with the associated 95 % confidence interval [4.7, 6.7].

The above expression was not found to depend on the concrete mixture, and therefore the level of ASR induced expansion at the time of testing, or the region where the cores were extracted, which had two different levels of confinement. The expression was consistent with the relationship proposed by Mander *et al.* (1988), commonly used for conventional concrete, within the uncertainty due to sampling variability estimated by a parametric bootstrap algorithm, while the equation proposed by Richart *et al.* (1928) may be used as a conservative lower bound.

### **E.3.2 Conclusions**

For the ranges of experimental parameters examined in this study, i.e. concrete mixtures considered in this experiment with an ultimate ASR-induced target expansion  $\varepsilon_{ASR}$  of 0.5% (based on measurements taken on standard prisms) and a maximum volumetric reinforcement ratio  $\rho_v$  of 1.14%, the following conclusions can be drawn:

- 
- For large structures, ASR-induced expansion is a complex field that varies both by location on the concrete surface and through depth of concrete member. The variation depends on several factors, including degree of confinement and restraint by surrounding conditions. In the block specimens in this test program, the ASR expansion field varies with the largest expansion observed on or near the specimen surface and the smallest expansion at the center of the specimen.
  - Both surface expansion measurements and the CI method are useful tools for monitoring the progression of ASR-induced surface expansion, but may not be used to determine the actual expansion field in the structure.
  - ASR expansion causes degradation of concrete's mechanical properties typically used for structural design (compressive strength and elastic modulus). For the concrete mixtures considered in this study, the degradation varies differently for each property:
    - *Unconfined compressive strength*: a reduction of 13 % ± 15 % of compressive strength obtained using standard uniaxial compression test method compared with 28-day compressive strength can be observed for the most reactive concrete (ASR 3), while no discernable reduction was observed for concretes with lower reactivity (ASR 1 and ASR 2).
    - *Modulus of elasticity*: modulus of elasticity was found to degrade faster with increased ASR expansion than compressive strength. Within the range of ASR reactivity studied in this test program, the reduction in modulus of elasticity ranged from 28 % ± 9 % to 41 % ± 6 % relative to the 28-day elastic modulus.

Note that, in normal concrete (without ASR), both compressive strength and elastic modulus continue to increase as function of time.

- The current ACI code equation for the modulus of elasticity versus compressive strength relationship ( $E_c = 57000 \sqrt{f'_c}$  [psi]) is unconservative and not applicable for the ASR-affected concrete in this study. In general, the ACI empirical equation became unconservative for larger expansions. Note that this conclusion is based on isolated core/material uniaxial testing with no regard to structural surroundings or context, which might enhance the stiffness of the structure.
- Degree of reinforcement confinement (represented by volumetric reinforcement ratio,  $\rho_v$ , in this study) and location of concrete core samples were found not to have an influence on the uniaxial compressive strength of ASR-affected concrete. This suggests that, the uncertainty in compressive strength obtained from field-procured core specimens due to sampling location on the structure may be small. Accordingly, for field core extraction for determining in-situ compressive strength of concrete of real structure, cores can be taken at any locations on the structure as long as they are in the region affected by ASR with careful consideration of site conditions, structural loads that might restrain expansion, and moisture condition.
- In-situ compressive strength of ASR-affected concrete, i.e., compressive strength measured under triaxial stress state (with radial confinement pressure) that simulates the confinement condition of the specimen, is higher than the compressive strength measured under the current, conventional ASTM uniaxial compression test condition. This increase in in-situ

---

compressive strength varies linearly with increasing confinement pressure. The in-situ compressive strength of ASR-affected concrete  $f_{cc}$  can be estimated based on the confinement pressure  $f_l$  and compressive strength  $f_{cu}$  determined based on standardized uniaxial compression test at the time of triaxial testing following this empirical expression:

$f_{cc}/f_{cu} = 1 + k f_l/f_{cu}$ , where the value of  $k$ , the rate of strength increase with increasing lateral pressure, was estimated to be 6, with the associated 95 % confidence interval [4.7, 6.7]. This expression is valid for the range of confinement pressure of up to 700 psi and the range of ASR expansion studied in this test program. This expression is consistent with the relationship proposed by Mander *et al.* (1988), commonly used for conventional concrete, within the uncertainty due to sampling variability estimated by a parametric bootstrap algorithm. The relationship proposed by Richart *et al.* (1928) may also be used as a conservative lower bound for estimating the effects of confinement on the ASR-affected concrete. In an existing structure, determination of confinement pressure is based on the structural context, i.e., amount of external loading, reinforcing bar cage, intersecting/abutting elements, etc.

# Chapter 1

## INTRODUCTION

---

---

### 1.1 BACKGROUND

Alkali-silica reaction (ASR) has long been recognized as a major cause of concrete internal microcracking and deterioration (Stanton 1940; Swenson 1957). This concrete deterioration mechanism begins with a chemical reaction between the alkali hydroxides in the cement paste and certain amorphous or micro-crystalline siliceous phases in the aggregates, which produces an alkali-silica gel that forms initially in the partially saturated pore space of the hardened cement paste. The alkali-silica gel is hygroscopic and will absorb, through osmotic action, moisture in the concrete matrix and expand. This expansion will persist if moisture and other necessary conditions are present. The expansion of alkali-silica gel creates an increasing internal pressure that ultimately leads to internal cracking and degradation of the mechanical properties of concrete (Hansen 1944, Taylor 1990).

Generally, the rate of ASR expansion is relatively slow and is a function of the reactivity of the aggregate mineral phases, the alkalinity of the pore solution, and the availability of moisture. Thus, the onset of ASR-induced cracking can take years or decades after construction to occur. However, once initiated, deterioration occurring at the material level may affect the bonding characteristics between the concrete and the reinforcement and the overall capacity and service life of reinforced concrete structural member or system. From a structural safety perspective, the important consideration is the remaining capacity of a structure after exhibiting distress due to ASR. Particularly, for ASR-affected safety-related concrete structures that are required to perform safety functions over extended periods of operation, a monitoring strategy is needed that can monitor and evaluate the evolution of ASR to ensure that they can continue to perform their intended safety functions without risk to public safety.

The technical work presented in this report is part of a comprehensive research program carried out by the Engineering Laboratory of the National Institute of Standards and Technology (NIST) on the structural performance of nuclear power plant concrete structures affected by ASR. The work is funded by the U.S. Nuclear Regulatory Commission (NRC) under Inter-Agency Agreement NRC-HQ-60-14-I-0004. The research plan was based on a scoping study of ASR effects on concrete by the NIST (Snyder and Lew, 2013). The scoping study identified knowledge gaps in evaluation of the present capacity of concrete structures affected by ASR, and prediction of the future loss of structural capacity. These gaps were identified through a comprehensive search of technical literature, including journal articles, standards, and codes related to ASR. Based on the identified gaps, a technical plan was proposed for closing each knowledge gap.

The objective of this research program is to develop a technical basis for generic regulatory guidance for evaluation of ASR-affected nuclear power plant (NPP) reinforced concrete structures throughout its service life. Specifically, the program will develop measurements for evaluation of (1) effects of ASR on structural performance and capability to perform intended function under design basis static and dynamic loads, and (2) characteristics of an aging management program to adequately monitor and manage aging effects of ASR degradation such that intended functions are maintained through the period of extended operation of renewed licenses. The intended outcome is a methodology for determining, for an existing ASR-affected reinforced concrete structure, (1) the in-situ structural capacity to resist design-basis static and dynamic loads, and (2) future structural capacity.

It should be noted that methodologies developed within the framework of this research program would generally be applicable for evaluating existing reinforced concrete structures affected by ASR. However, the collected data is not intended for direct comparison to any specific real structure under in-service operating conditions due to differences between controlled experiments and in-field conditions including (1) the accelerated rate of ASR in the test environment, (2) use of concrete mixtures having both reactive fine and coarse aggregate to achieve target concrete expansion, (3) levels of concrete confinement provided by steel reinforcing bars, and (4) other age-related degradations of concrete material properties.

## 1.2 SCOPE OF STUDY

The overall NRC-sponsored research program consists of five tasks. The first three tasks (Tasks 1, 2, and 3) deal with the effects of ASR on the structural properties of reinforced concrete structures as they relate to the static and dynamic performance of structure (Phan *et al.*, 2019). The other two tasks (Tasks 4 and 5) are concerned with identifying and evaluating methods for determining the current state and rate of the ASR reaction. These tasks are intended to:

Task 1: Assess effects of ASR on in-situ mechanical properties of concrete

Task 2: Assess development and lap-splice lengths of reinforcing bars in ASR-affected concrete

Task 3: Evaluate seismic response characteristics of ASR-affected reinforced concrete structural members

Task 4: Estimate the degree of reaction in ASR-affected concrete and the corresponding expansion

Task 5: Predict future and ultimate ASR expansion in ASR-affected concrete

This report details Task 1 of the research program: *Assessing In-Situ Mechanical Properties of ASR-Affected Concrete*. This task seeks to establish:

- the relationship between ASR-induced expansion and (1) concrete mechanical properties and (2) surface cracking of concrete
- the effectiveness of steel reinforcing bars in confining ASR-induced expansion.

This task utilized three large concrete blocks of different ASR reactivity made with known, natural reactive aggregates (Feldman *et al.*, 2020), along with one control (non-reactive) block. The blocks were all cast with longitudinal reinforcing bars, but each region of a given block had differently-sized hoop stirrups so that the influence of degree of confinement on the expansion behavior of the blocks could be studied. Each block was densely instrumented to measure internal strains in concrete and strains on reinforcing bars, along with temperature and humidity measurement devices. The concrete blocks were cast and kept in a large environmental chamber to maintain predetermined levels of temperature and humidity. The blocks were designed to allow for:

- correlating level of expansion with changes in mechanical properties of concrete, including compressive strength, tensile strength, and modulus of elasticity;
- studying and mapping surface expansion and cracking due to ASR and correlating surface expansion measurements with internal concrete strains; and
- monitoring development of axial strains in the reinforcing bars, including their potential for yielding or loss of bond.

Periodically, as the ASR reaction progressed, cores were extracted from the concrete blocks, and standard ASTM compressive and tensile testing was performed to determine their mechanical properties. This testing was conducted to determine whether the tensile or compressive strength of concrete degraded with ASR expansion. Cores extracted from the blocks were also subjected to triaxial confinement pressure representing the multi-axial state of stress generated internally in the blocks by the expansion of the ASR gel. In addition, surface strains were measured using both a laser tracker and high-precision caliper. Surface crack formation due to ASR was measured by means of an optical measurement system.

### **1.3 REPORT OUTLINE**

Chapter 2 describes the experimental plan for assessing the effects of ASR-induced expansion on the mechanical properties and crack development in concrete. This description includes proportioning the concrete mixtures, specimen design, reinforcement detailing, instrumentation and data acquisition, specimen construction, specimen curing regime, and special purpose test apparatus designed by NIST for tri-axial compression testing of concrete core samples.

Chapter 3 presents measurement data collected from the sensors embedded at different locations inside the block specimens. These data include strains measured by strain gages on reinforcing bars and concrete strain transducers, and measurements of temperature and relative humidity inside the specimens. Chapter 3 also presents results of data analysis on mechanical properties of concrete obtained from uniaxial and triaxial testing of concrete cylinders and cores, surface expansion measured using a laser tracker and high-precision caliper, and crack mapping using an optical microscope. The correlation between surface measurements and internal strains is also described.

Chapter 4 provides a summary of the findings and conclusions drawn from these findings for Task 1 of this study.

This page intentionally left blank.

## Chapter 2

# EXPERIMENTAL PLAN FOR ASSESSING MECHANICAL PROPERTIES OF ASR-AFFECTED CONCRETE

This chapter describes the NIST experimental plan for achieving the objective of Task 1 of the five-task NRC-sponsored study, which was to assess the effects of ASR on in-situ mechanical properties of concrete. The experimental plan called for use of four large-scale concrete block specimens. Three blocks had reactive aggregate concretes having three different designed target ultimate linear expansions (relatively low ASR linear expansion of 0.15 %; intermediate linear expansion of 0.3 %; and high linear expansion of 0.5 %) to facilitate examination of how the different degrees of ASR expansion would affect concrete’s mechanical properties. These target linear expansions were based on expansion measurements from 3 in × 3 in × 11.25 in prisms (ASTM C1293 - 08b, 2015) along with 4 in × 4 in × 11.25 in prisms, see Feldman *et al.* (2020) for details. Throughout this report, the term “expansion” refers to linear rather than volumetric expansion, unless otherwise indicated. The fourth block was made with non-reactive aggregates (concrete having no ASR-induced expansion) to serve as control specimen. In addition, since it is expected that ASR-induced concrete expansion is influenced by the level of confinement provided by the steel reinforcement, three levels of reinforcement confinement were used in each block specimen, ranging from none to heavy confinement. Thus, the combination of three target ASR expansions, from low to high, and three levels of reinforcement confinement, from none to heavily confined, resulted in a full range of examination of these two variables on the mechanical properties of concrete. Table 2-1 shows the overall test matrix of Task 1 of this study.

**Table 2-1. Test matrix showing primary variables for Task 1 experimental program**

Primary Experimental Variables		Block Specimen			
		ASR 1	ASR 2	ASR 3	Control
Concrete with Target Ultimate Expansion $\epsilon_{ASR}$ (%)		0.15	0.3	0.5	0
Levels of Confinement by Volumetric Reinforcement Ratio $\rho_v$ (%)	Region 1	0.72	0.72	0.72	0.72
	Region 2	0.15	0.15	0.15	0.15
	Region 3	1.14	1.14	1.14	1.14

Details on concrete’s constitutive materials and mixture proportioning, designed to achieve the target ultimate expansions mentioned above, are provided in Section 2.1 below. The design of the four block specimens, including their geometry, dimensions, and reinforcement layout to produce the indicated three levels of reinforcement confinement are described in Section 2.2.

The block specimens were heavily instrumented to facilitate measurements of ASR-induced strain and crack developments inside and on the surface of concrete, strain developments in reinforcing bars, as well as temperature and relative humidity inside the concrete. Section 2.3 describes, in

detail, the instrumentation scheme, types and locations of sensors placed within the specimens, and the data acquisition system used for data collection.

Section 2.4 provides information on the construction of the specimens, including assembly of the reinforcing bar cages, erection of steel formwork, and the concrete placement procedure. Section 2.5 provides a summary of the measured properties of fresh concrete. Section 2.6 describes the curing conditions used to accelerate and attain the designed concrete expansion in the block specimens.

Besides providing platforms for measuring surface cracking of concrete and strains developed within the concrete and steel reinforcing bars, as described above, the blocks were also used to provide concrete core samples for standard materials testing to quantify effects of concrete age, degree of expansion, levels of confinement, and test conditions (uniaxial or triaxial compression test) on concrete in-situ mechanical properties. Uniaxial compression and splitting tensile testing for concrete mechanical properties were performed using a 220 kip Materials Testing Systems (MTS) closed-loop servohydraulic load frame in accordance with standard methods prescribed by:

- ASTM C39 (ASTM C39/C39M-17a, 2017) for compressive strength of concrete,
- ASTM C469 (ASTM C469/C469M-14, 2014) for modulus of elasticity of concrete, and
- ASTM C496 (ASTM C496/C496M-17, 2017) for splitting tensile strength of concrete.

In addition, to facilitate measurements of in-situ concrete compressive strength as a function of degrees of confinement provided by different amounts of steel reinforcement, a specialized test device, designed and fabricated by NIST, called the Triaxial Pressure Vessel (TPV), was used in conjunction with the load frame to simultaneously subject the core samples to both radial and axial pressures to more accurately simulate the in-situ stress condition experienced by the core samples. The NIST TPV can produce a maximum radial pressure of up to 2,300 psi. Descriptions of the TPV are provided in Section 2.7.

Details on strategy for selecting locations of core samples, cores extraction and preparation procedure, and testing under uniaxial compression and triaxial compression conditions for concrete mechanical properties are provided in Chapter 3.

## 2.1 MATERIALS SELECTION AND MIXTURE PROPORTIONING

To facilitate examination of the effects of different degrees of ASR expansion, hereafter referred to as  $\epsilon_{ASR}$ , on in-situ concrete mechanical properties and structural capacities of reinforced concrete beams and walls (see Task 2 and Task 3 reports, respectively), three reactive concrete mixture designs, namely ASR 1 to ASR 3, along with a control mixture were developed. The first three mixtures, ASR 1, ASR 2, and ASR 3, were designed to be reactive for use in the three reactive block specimens mentioned above, with known natural reactive aggregates that were sourced in the United States (U.S.) and expected to produce target ultimate linear expansions,  $\epsilon_{ASR}$ , of 0.15 %; 0.3 %; and 0.5 %, respectively, within 18 months from casting and curing in laboratory conditions based on concrete prism measurements as shown in Feldman *et al.* (2020). Information on the types of reactive aggregates, all other concrete constitutive materials, including mixture proportioning used to achieve the above target expansions in the specimens of this test program are described below:

- **Cementitious Material:** ASTM C150/C150M-16 (2016) Type I/II Portland cement with minimum alkali equivalent ( $\text{Na}_2\text{O}$ ) content of  $\geq 0.87$  %.
- **Coarse Aggregate:** Highly alkali-reactive Placitas coarse aggregate that was sourced from Albuquerque, New Mexico, and

- **Fine Aggregates:** Combinations of highly reactive washed concrete sand (Jobe, sourced from El Paso, TX) and non-reactive (Chaney, sourced from Hagerstown, MD) fine aggregates that meet the grading specification of ASTM C33 (ASTM C33/C33M-16, 2016).
- **Alkalis:** Additional alkali, in the form of water soluble NaOH pellets, was used to increase the alkali level in the cement to 1.40 % (for a total of 4.9 lbf/yd<sup>3</sup> alkali content, including cement alkali + NaOH addition) to further accelerate reactivity in order to achieve the high target expansions within the duration of this test program.

More detailed information and analysis on fine and coarse aggregates' alkali reactivity, mineralogy, and texture are available in Feldman *et al.* (2020). The concrete mixture for the control block was designed to be non-reactive, utilizing ASTM C150/C150M-16 (2016) Type I/II cement with low alkali equivalent (Na<sub>2</sub>O) content (<0.87 %) and non-alkali reactive aggregates, with no alkali additions.

All coarse aggregates had a maximum size of 3/4 in. All four concrete mixtures utilized commercially available high range water reducing admixtures which comply with ASTM C494 (ASTM C494/C494M-16, 2016) to aid with workability. Table 2.2 shows the mixture proportioning for the concretes used in this study.

Table 2-2. Mixture Proportioning for Concretes in the NIST Experimental Program

Mixture	Cement Content			Coarse Aggregate			Fine Aggregate			Alkalis*	Water Gal (lbfyd <sup>3</sup> )
	Type	lbfyd <sup>3</sup>	vol. fraction	Type	lbfyd <sup>3</sup>	vol. fraction	Type	lbfyd <sup>3</sup>	vol. fraction		
<b>ASR 1</b>	I/II, high alkali (≥0.87% Na <sub>2</sub> O)	588	0.111	Placitas	1767	0.420	Chaney	1199	0.274	4.90	35 (294)
<b>ASR 2</b>	"	588	0.111	"	1767	0.420	Jobe	711	0.274	4.90	35 (294)
							Chaney	480			
<b>ASR 3</b>	"	588	0.111	"	1767	0.420	Jobe	1185	0.274	4.90	35 (294)
<b>Control</b>	I/II, low alkali (≤0.87% Na <sub>2</sub> O)	578	0.115	#57	1805	0.399	Washed #33 Sand	1385	0.295	<2.0	35 (294)

\* Total alkali content, including cement alkali + NaOH addition

## **2.2 DESIGN OF BLOCK SPECIMENS**

Four large reinforced concrete block specimens were designed and constructed to facilitate experimental measurements for quantification of how ASR-induced expansion may affect in-situ concrete mechanical properties as well as concrete surface cracking and expansion, and how these relationships may be influenced by the presence and amount of hoop reinforcement (i.e., stirrups). Of the four blocks, three were made with the reactive ASR 1, ASR 2, and ASR 3 concretes (see Table 2-2), and the fourth was made with non-reactive concrete. The block specimens are hereafter referred to as block ASR 1, ASR 2, and ASR 3, and the control specimen is referred to as the control block.

All four blocks have identical geometry, dimensions, and reinforcement arrangements. The dimensions of each block were 3 ft-9 in × 6 ft-1 in × 16 ft-5 in. This large scale was selected both to allow studying the performance of large concrete structures affected by ASR without significant scale effect and at the same time permit sufficient locations on the blocks for extraction of a large number of core samples throughout the duration of Task 1.

Each block was comprised of three confinement regions (Region 1, Region 2, and Region 3). Each region had hoop stirrups of different sizes to simulate different degrees of reinforcement confinement of concrete. Regions 1 and 3 contained reinforcement amounts representing moderate and heavy confinement, respectively, while Region 2 had minimal longitudinal reinforcement and no transverse reinforcement, representing no confinement condition. Figure 2-1 shows the elevation of a typical block specimen in this test program. The lengths of Regions 1, 2, and 3 were 73 in, 45 in, and 75 in, respectively. Between adjacent regions in each block specimen, a two-inch thick polystyrene plastic divider was inserted to separate the regions having different levels of confinement to alleviate the potential for differential expansions that can induce cracking that was not a direct result of the ASR reaction within each respective confinement region.

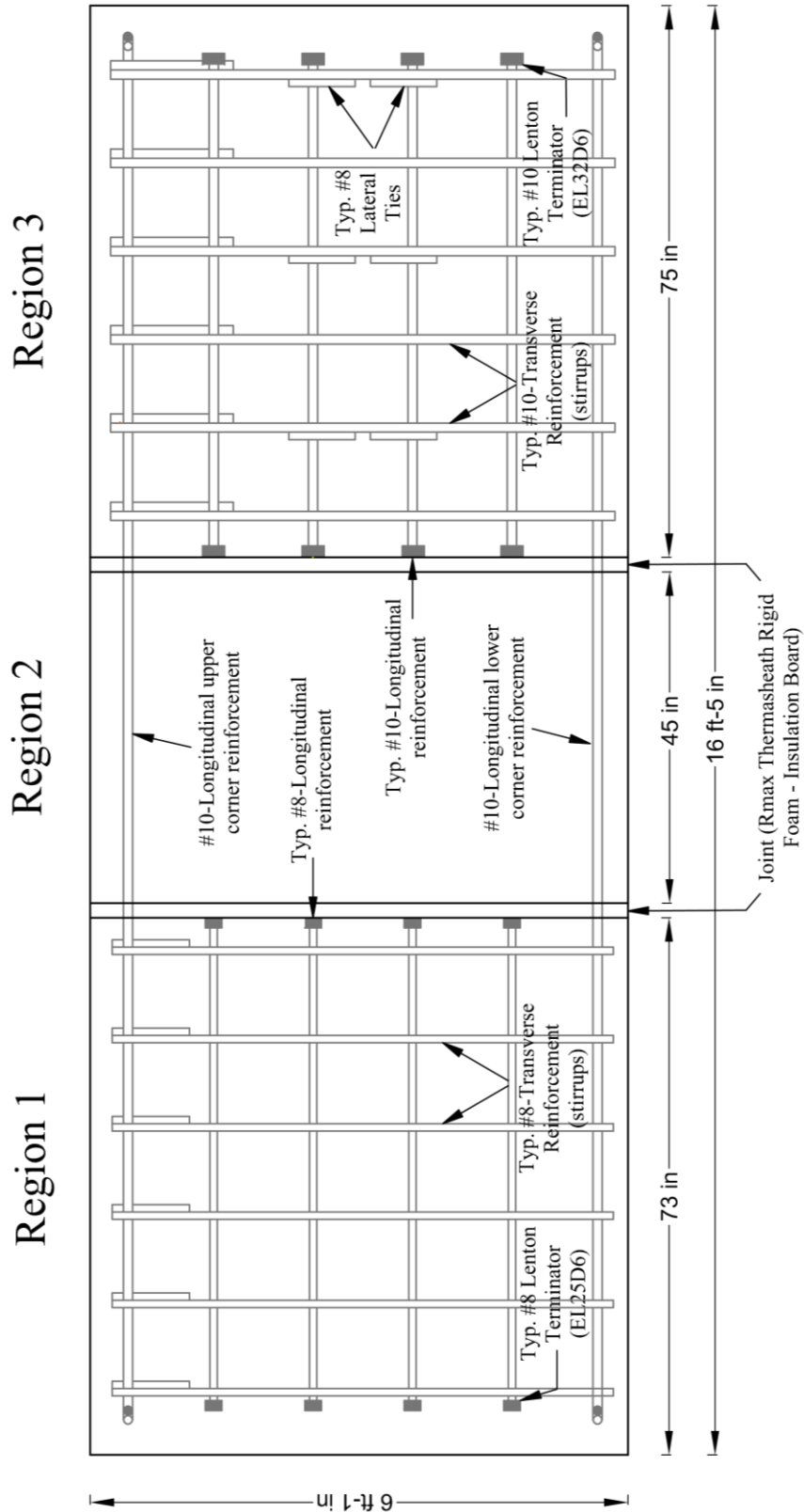


Figure 2-1. Elevation view of typical block specimen showing different confinement regions

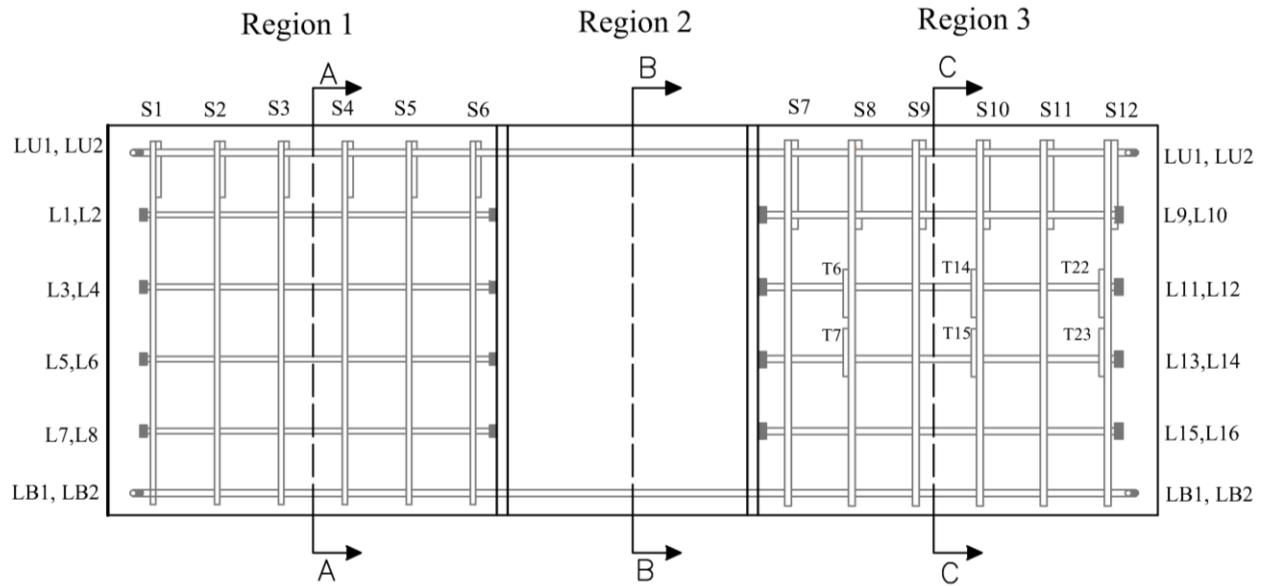
All block specimens were reinforced with ASTM A706-Grade 60 reinforcing bars with a minimum specified yield strength of  $f_y = 60$  ksi. The reinforcement details of each block and the naming convention for the types of reinforcement are shown in Figure 2-2. For each block specimen, there were four #10 longitudinal reinforcing bars placed at the block's top and bottom corners (two top – named LU1 and LU2, and two bottom – named LB1 and LB2). These four longitudinal reinforcing bars extended through all three confinement regions of the block. Additionally, Region 1 was further reinforced longitudinally with eight #8 reinforcing bars (four on each side, named L1 to L8) with a vertical spacing of 13.5 in, and transversely with six #8 stirrups at 12 in spacing (named S1 to S6). In Region 3, similar additional longitudinal reinforcement was provided (eight #10 longitudinal rebars with a vertical spacing of 13.5 in, four on each side, named L9 to L16), but with six #10 stirrups at 12 in-spacing and two #8 cross ties at every other stirrup for a total of six cross ties (named T6, T7, T14, T15, T22, and T23). As shown on Figure 2-2, Region 2 had only the four continuous #10 longitudinal reinforcing bars at the top and bottom corners and no additional longitudinal reinforcement or stirrups. This was done to facilitate the quantification of effects of ASR expansion in concrete without reinforcement confinement.

To avoid reinforcing bar congestion at the ends of each region and to prevent slippage between concrete and the eight longitudinal bars in Regions 1 and 3 at their ends, threaded mechanical anchorage devices designed according to ACI 318-14 (2014) were used (see Figure 2-3).

Table 2-3 shows the reinforcement ratios for the three regions in the three orthogonal directions x, y, and z, along with the volumetric steel reinforcing ratio,  $\rho_v$ , defined as the ratio of the volume of the reinforcing bars to that of the concrete in a given region of the block. Note that the cross section of each block was defined in the x-y plane, where y represented the gravity direction. The Z-axis was defined along the length of the block.

**Table 2–3. Steel reinforcement ratio for Confinement Regions 1, 2, and 3 of the block specimens**

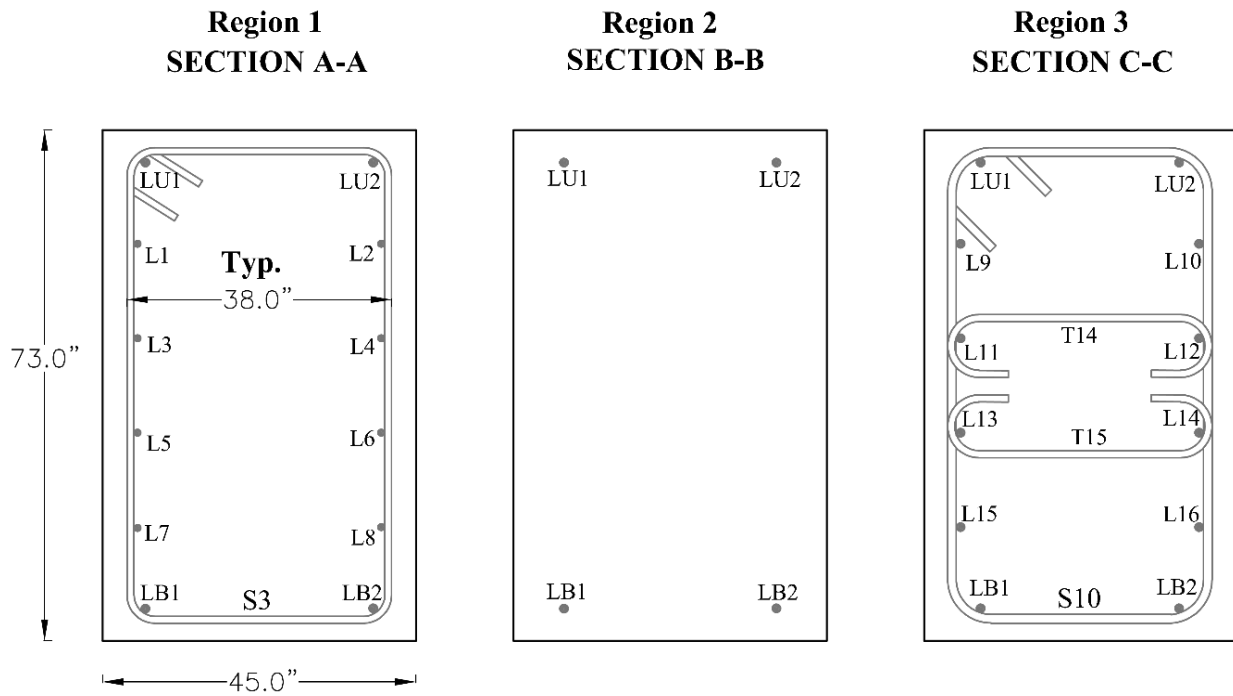
Steel Ratio	Region 1	Region 2	Region 3
$\rho_x$	0.20 %	0.00 %	0.60 %
$\rho_y$	0.40 %	0.00 %	0.60 %
$\rho_z$	0.30 %	0.15 %	0.50 %
$\rho_v$	0.72 %	0.15 %	1.14 %



**Notes:**

- LB1, LB2, LU1, LU2 - #10 continuous longitudinal
- S1..S6 - #8 stirrups @ 12";
- S7..S12 - #10 stirrups @ 12";
- L1..L8 - #8 - headed longitudinal (67" length) @13.5" ;
- L9..L16 - #10 - headed longitudinal (68.5" length) @13.5"
- T6..T23 - #8 ties @24" length

(a)



(b)

**Figure 2-2. Reinforcement details for the blocks: (a) elevation and (b) cross sections**



Figure 2–3. Threaded mechanical headed anchors at ends of longitudinal reinforcing bars

### 2.3 INSTRUMENTATION AND DATA ACQUISITION

The block specimens were heavily instrumented to facilitate measurements of strains developed in the concrete and reinforcing bars, as well as of temperature and relative humidity inside the concrete. The three reactive blocks (ASR 1, ASR 2, and ASR 3) had identical instrumentation layouts, and the control block was less heavily instrumented as it was not expected to have any reaction or expansion. Table 2-4 provides a summary of the types and number of instruments used in the three reactive blocks and control block. Figure 2-4 shows the locations of (1) strain gages on reinforcing bars, (2) tri-directional concrete strain transducers, and (3) thermocouples in reactive blocks ASR 1, ASR 2, and ASR 3. Figure 2-5 shows the locations of the same types of instrumentation, but with lesser number of instruments, for the control block. Descriptions of the sensors used to monitor strain development, temperature, and moisture inside the block specimens are provided in the sub-sections below. In Figures 2-4 and 2-5, the number between brackets indicate the number of strain gages on a given reinforcing bar.

Table 2–4. Types and numbers of instruments used in the block specimens

Instrumentation Type	Instrumentation Number	
	Each of reactive blocks ASR 1, ASR 2, and ASR 3	Non-reactive control block
Strain gages on reinforcing bars	164	94
Triaxial strain transducers in concrete	18	9
Thermocouples	16	8
Wireless temperature and humidity sensors	9	0
Targets for laser tracking system (see Section 2.3.4)	280	280

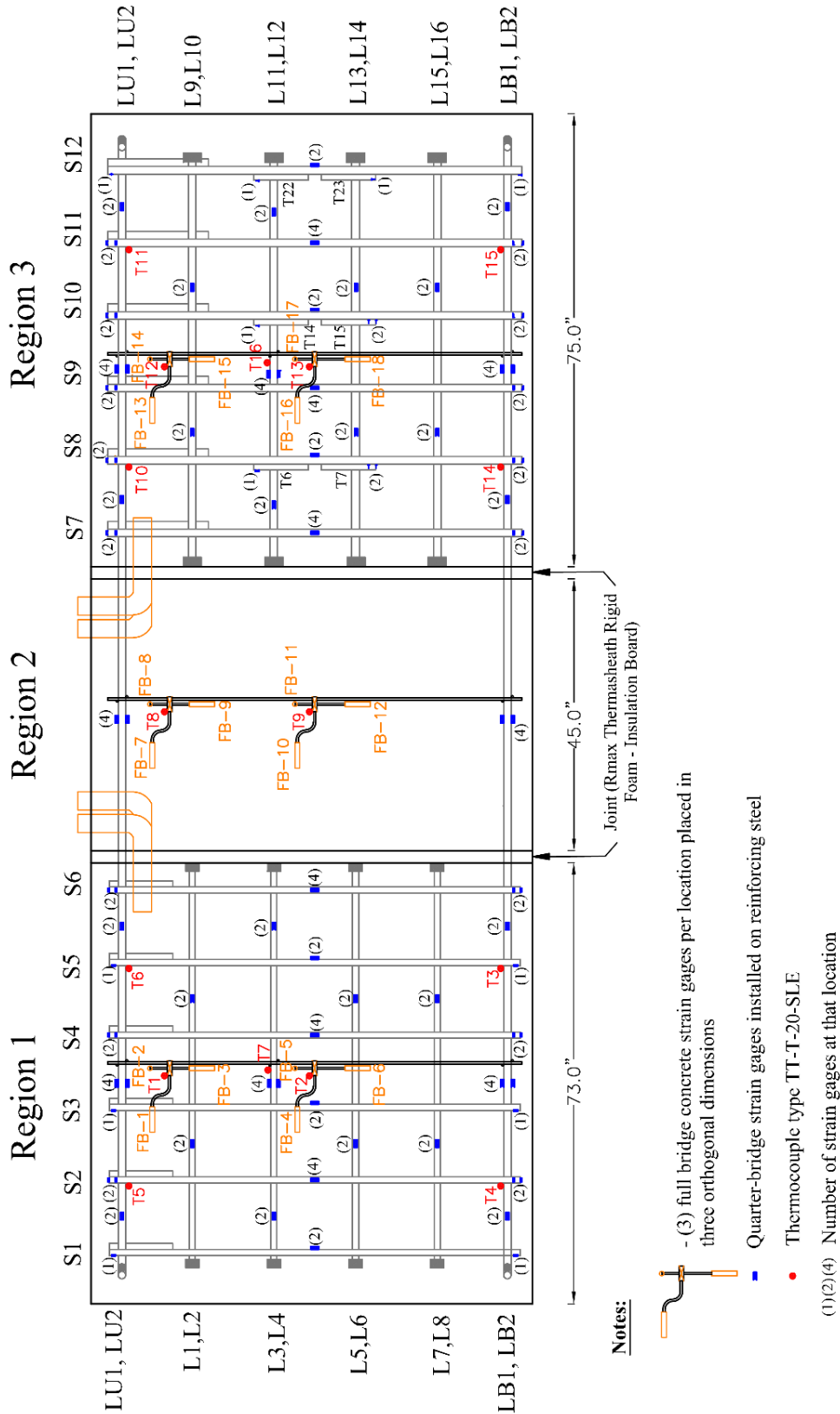


Figure 2-4. Layout of strain gages on reinforcing bars, triaxial concrete strain transducers, and thermocouples for blocks ASR 1, ASR 2, and ASR 3

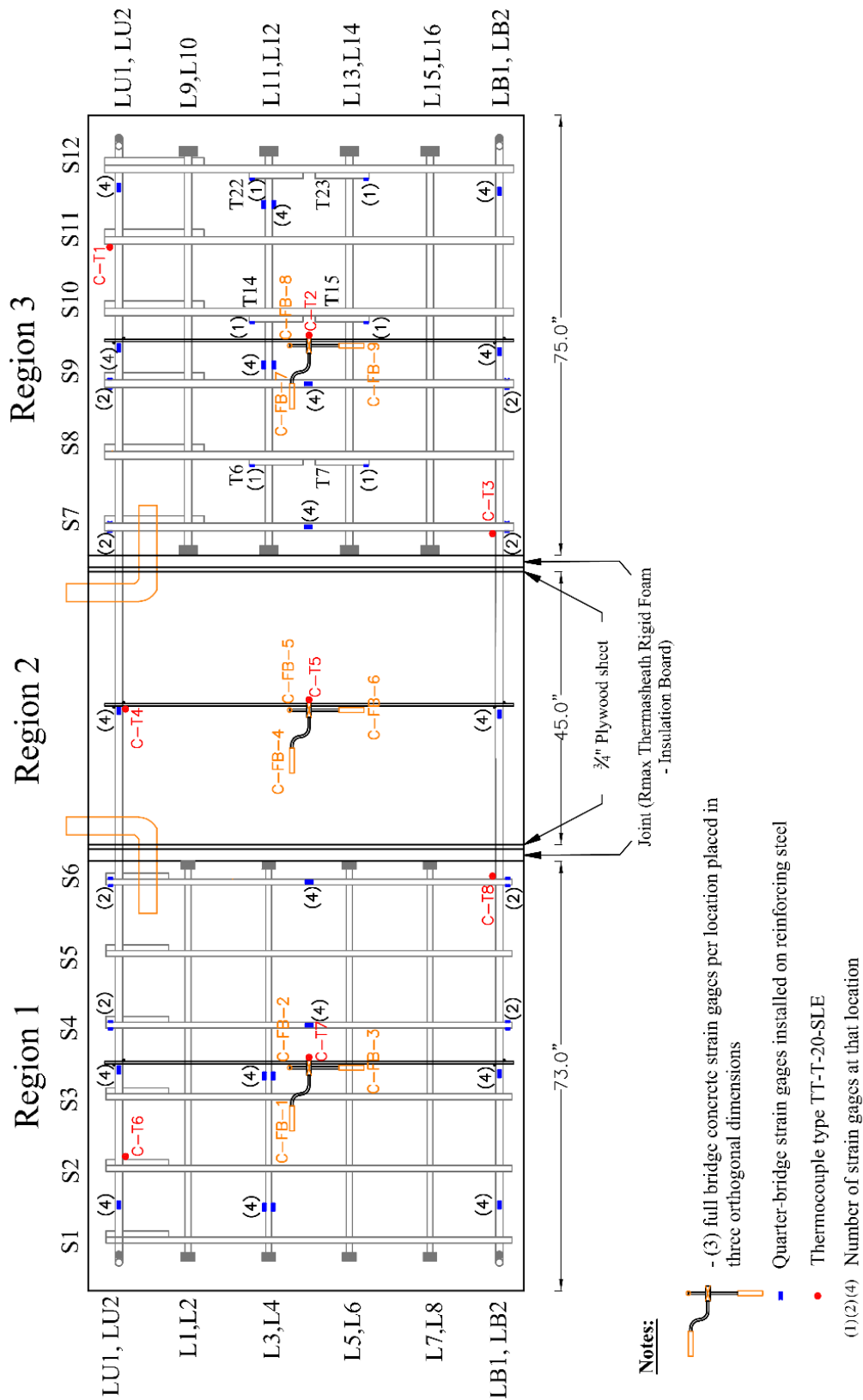


Figure 2-5. Layout of strain gauges on reinforcing bars, triaxial concrete strain transducers, and thermocouples for control block

### 2.3.1 Strain Gages

Electric resistance strain gages were used to measure surface strains on the reinforcing bars. In total, 164 quarter-bridge strain gages were used for each reactive block and 94 strain gages were used for the control block (see Figures 2-4 and 2-5, respectively, and Table 2-4). The number designations for the strain gages are described in Appendix A. Installation of the strain gages on the reinforcing bars was carried out using a two-part epoxy adhesive (M-Bond-AE-10), which is commercially available from Micro-Measurements. This adhesive provided elongation capabilities of 6 % to 10 % at 75 °F, and suitable operating temperature range (-320 °F to 200 °F). A protective coating, M-Coat JA from Micro-Measurements, was applied to provide protection from water penetration. This protective coating is a two-part, polysulfide, liquid polymer compound that, once fully cured, forms a rubber-like protective covering for the strain gages.

### 2.3.2 Tri-directional Concrete Strain Transducers

Tri-directional concrete strain transducers were embedded in the block specimens at selected locations to measure internal strain development, or expansion, of concrete due to the effects of ASR. For that purpose, 18 full-bridge concrete strain transducers, type KM-100B manufactured by Tokyo Sokki Kenkyujo Co. Ltd. (TML), were embedded in the core of the reactive block specimens at six different locations (two in each confinement region), as was shown in Figure 2-4. For the control block, only nine concrete strain transducers were used at three locations (one in each region, see Figure 2-5). At each location, tri-directional concrete gages were grouped to provide strain measurement in three orthogonal directions using a special arrangement of brass rods that was fabricated to support the transducers as shown in Figure 2-6. The brass rod assembly with the KM-100B strain transducers was assembled outside the reinforcement cage, and then mounted in each region at the designated locations within the blocks per the instrumentation plan.



Figure 2-6. Tri-directional concrete strain transducers

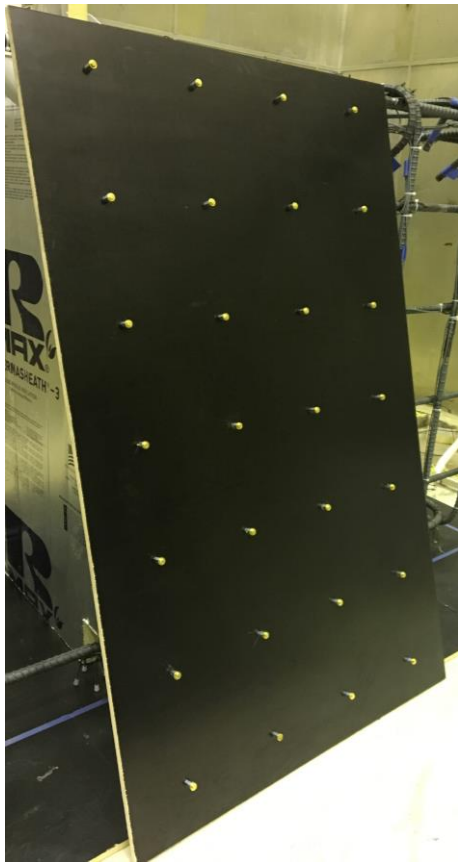
### **2.3.3 Thermocouples and Relative Humidity Sensors**

Thermocouples made of Type T thermocouple wire were embedded in the block specimens to measure internal temperature development over the course of the experiment. The thermocouple layouts for the reactive and control blocks are shown in Figures 2-4 and 2-5, respectively. For the reactive blocks, thermocouples T1 and T2 (Region 1), T8 and T9 (Region 2), and T12 and T16 (Region 3) were installed at the center of the blocks at two different elevations, while the rest of the thermocouples were installed near the surface on one of the exterior sides. For the control block, all thermocouples were installed at the center of the block, but also at different elevations.

In addition, wireless iButton Hygrochron Temperature/Humidity Loggers (DS1923) were inserted in four holes created by the tie rods as part of the formwork, see Section 2.4. For each block, three of these temperature/humidity devices were inserted in each hole, resulting in 3 devices per region. Data were recorded in a protected memory section inside the device at a user-defined rate and could be downloaded to a computer using a serial port interface.

### **2.3.4 Targets for Laser Tracking System**

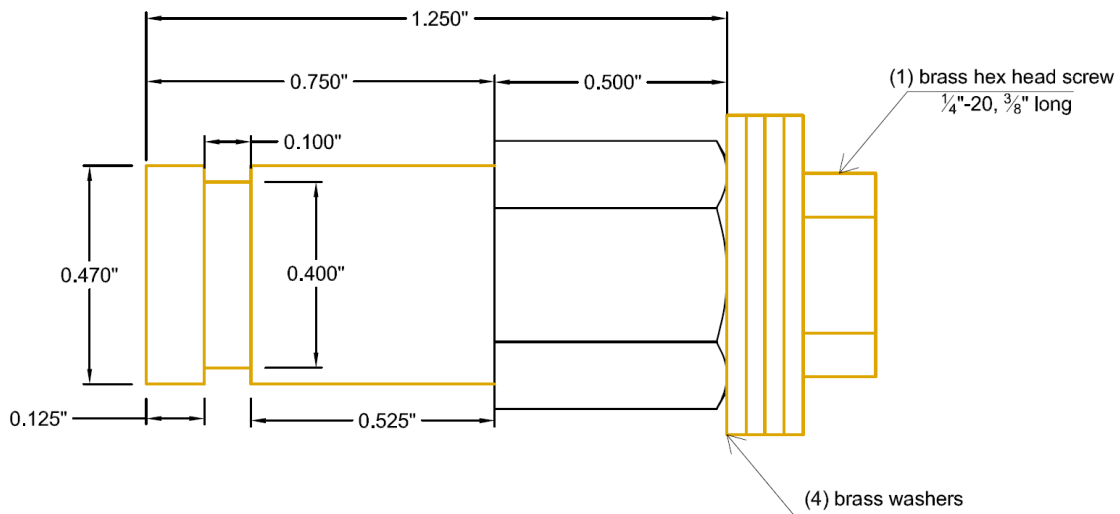
Anchoring devices (targets) to facilitate laser tracking and high-precision caliper measurements for evaluation of ASR-induced concrete surface expansion were installed on the exterior of each block specimen. The targets consisted of brass zinc coated standoffs (1/2 in hex, 1.25 in long, 1/4 in-20 thread), that enabled caliper measurements by using the flat jaws in the 1/10 in machined groove (Figure 2-7(b) and (c)). For laser measurements using the API3 Tracker (see Section 3.3.1 of Chapter 3), the ball probe seat was tightened into the threaded portion of the target. For better embedment into the concrete, four brass washers were installed at the embedded end of the target, using a 3/8 in long brass head hex screw. The exposed 3/4 in length of the target was protected during the curing phases by a removable rubber cap that was removed during caliper/laser measurements. The targets were installed on plywood sheets (Figure 2-7(a)). The plywood sheets, in turn, were attached to the inside face of steel formwork used for concrete placement and were removed after concrete had hardened, leaving the targets in place on the surface of the elevation sides of the block specimens. The total number of targets for each of the four blocks was 280 and the targets layout for all blocks is shown in Figure 2-8.



(a)

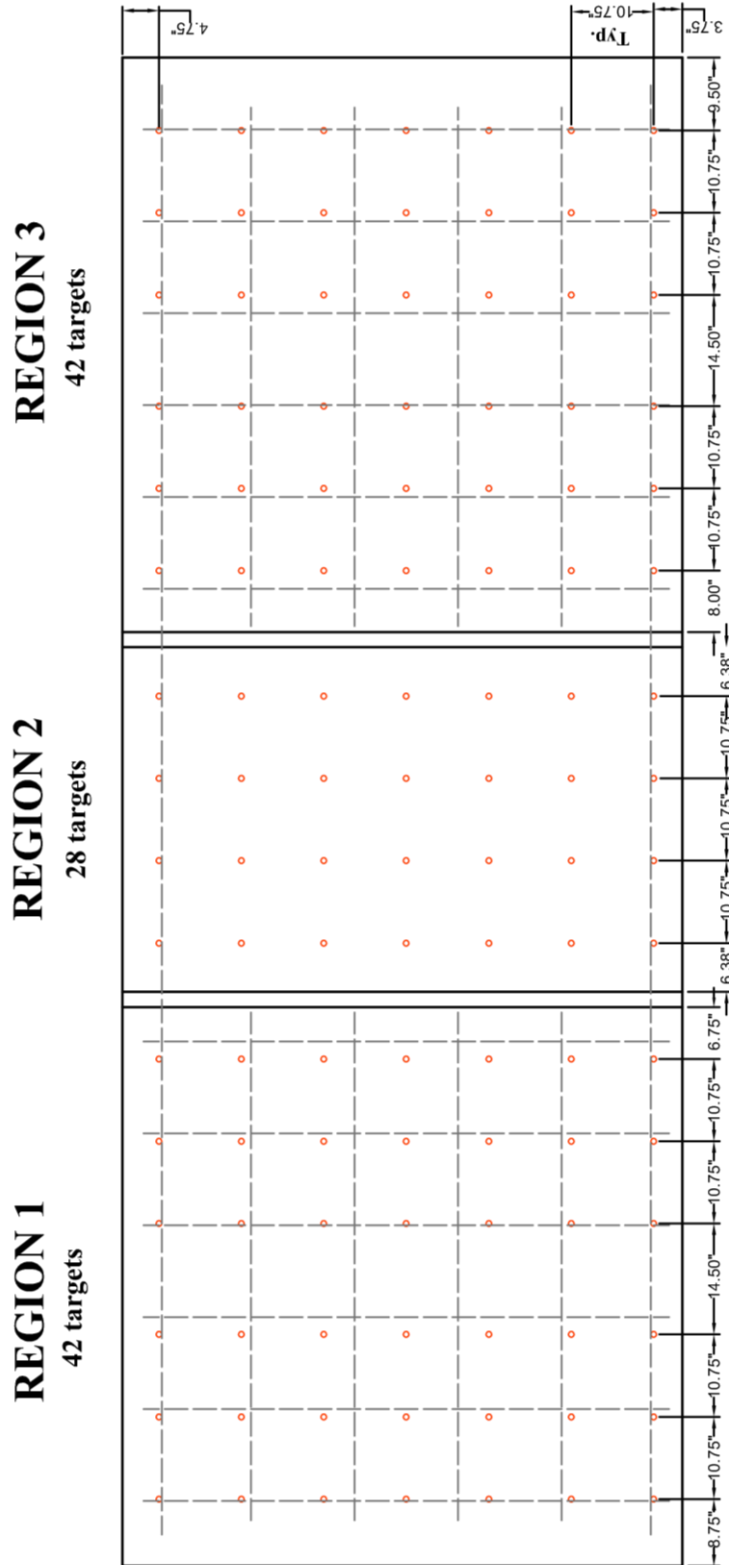


(b)

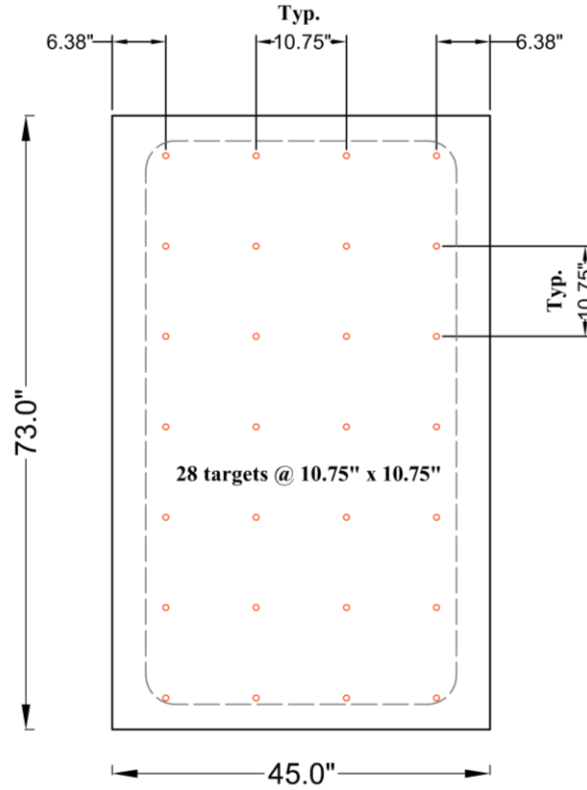


(c)

Figure 2-7. Targets for surface expansion measurements: (a) plywood sheet with targets, (b) target construction, and (c) target design



(a)



(b)

Figure 2–8. Layout of targets for surface expansion measurements: (a) elevation and (b) side view

In addition, a stainless-steel frame was erected along the perimeter of the environmental chamber to (1) support and route instrumentation cables to the data acquisition system and (2) support multiple reference targets for allowing laser measurement using the API3 Tracker (see Figure 2-9).

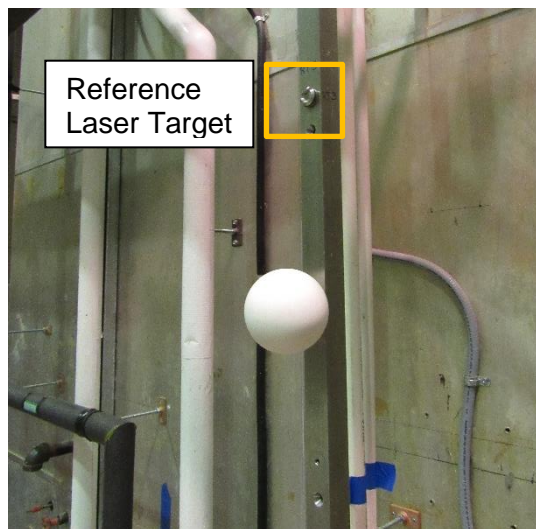


Figure 2–9. Reference target for laser measurement tracking mounted on stainless steel framing installed around the environmental chamber

### 2.3.5 Data Acquisition System (DAQ)

The DAQ was comprised of three National Instruments SCXI-1001 chassis arranged in a multiplex configuration and connected to a peripheral component interconnect express (PCIe-6363) device installed on a desktop computer. Chassis #2 and #3 had the same configuration, each holding twelve SCXI 1521 modules. Each module had a capacity of 24 350- $\Omega$  quarter bridge strain channels – Chassis #1 contained two SCXI 1521 modules, followed by eight SCXI 1520 modules and two SCXI 1102 modules. The SCXI 1520 module has a capacity of eight (8) strain channels that can measure quarter-, half- and full-bridge configurations. The modules were set-up for the full-bridge configuration, to record data from the KM-100B concrete strain transducers. The SCXI 1102 module had 32 channels and was used for conditioning signals from thermocouples. For these modules, the corresponding terminal blocks were installed and for the strain channels (quarter- or full-bridge), the corresponding terminal blocks were pre-wired with 5 ft cables and connected to the instrumentation cables routed from the block specimens using twist-on butt splice connectors.

From the block specimens, instrumentation cables from all specimens were bundled and passed out of the blocks through PVC conduits and connected to the DAQ described above and located in a room adjacent to the environmental chamber where the block specimens were constructed and cured. Figure 2-10 shows the bundles of instrumentation cables and PVC conduits from one block specimen and cables from all four block specimens coming through the wall of the environmental chamber and connected to the DAQ in the adjacent room.



(a)



(b)

Figure 2–10. (a) Routing of instrumentation cables though PVC conduits and into (b) the DAQ in an adjacent room

## 2.4 SPECIMENS CONSTRUCTION

### 2.4.1 Erection of Reinforcing Bar Cages and Steel Formwork

Prior to assembly of the reinforcing bar cages for each block, strain gages were attached to the individual reinforcing bars which were then assembled to form the reinforcing bar cages. Temporary shoring was used to support the cage for stability until after the steel formwork has been erected. The 2 in thick polystyrene plastic dividers between adjacent confinement regions in each block were inserted to separate the three regions with different levels of confinement. Figure 2-11 shows a photograph of an assembled reinforcing bar cage for block ASR 1.



Figure 2-11. Assembled reinforcing bar cage for block ASR 1

The steel formwork was designed to have plan dimensions that are 1.5 in larger than the overall block plan dimensions in both directions to allow for adding two plywood sheets, 3/4 in thick each, holding the targets for laser tracking (see Section 2.3.4). The formwork was designed to resist the hydrostatic lateral pressure exerted by wet concrete prior to setting and maintain the shape of the blocks without lateral deformation during the initial curing period. The formwork consisted of only the vertical steel panels with steel stiffeners to form the walls of the specimen. These wall panels were connected to the base of the formwork for the specimen, which were made of plywood sheets and rested on a rigid concrete floor.

Plan and section views of the formwork are shown in Figure 2-12. As shown in the figure, the formwork consisted of modular steel sections that were bolted together to provide the frame in which concrete was placed. The formwork relied on steel channels at the top and tapered steel tie rods with diameter of 1.25 in/1.50 in at the lower part of the block to provide resistance to the hydrostatic pressure exerted by the fresh concrete. The vertical plywood sheets were attached to the formwork using screws. Figure 2-13 shows photographs of the assembly of the formwork for one of the block specimens.





Figure 2–13. Photographs showing erection of steel formwork

#### 2.4.2 Concrete Placement

Placement of concrete for the three reactive block specimens was carried out in one concrete placement operation that lasted three days, as follows:

- Block ASR 3: Concrete mixture ASR 3, on March 21, 2017
- Block ASR 2: Concrete mixture ASR 2, on March 22, 2017
- Block ASR 1: Concrete mixture ASR 1, on March 23, 2017

The control block specimen was placed in a separate concrete placement operation on June 9, 2017.

For the three reactive specimens, a three-cubic-yard mixer, Figure 2-14, was used in conjunction with a mobile batch plant to mix the concrete. After mixing, concrete was discharged into a concrete bucket which was moved into position over the block formwork by a telescoping forklift. An elephant trunk hose was then attached to the bottom of the bucket to reduce the concrete discharge height to avoid aggregates segregation during discharge. The concrete was consolidated using vibrators (Figure 2-15). Due to its large size, six batches of concrete were required to fill each block specimen.



**Figure 2-14. Mobile batch plant and three cubic yard concrete mixer**



**Figure 2-15. Consolidation of concrete using vibrators**

For the control block that was cast in the second concrete placement operation, concrete was procured from a concrete mixing plant which batched the concrete in accordance with the NIST specifications. The concrete was discharged from the concrete mixer into a telescoping conveyer belt (telebelt), as shown in Figure 2-16, that was used to place concrete into the formwork using an elephant trunk hose, Figure 2-17.

In addition to casting the blocks, companion concrete specimens were prepared for all concrete mixtures. These included prisms for monitoring of ASR expansion and cylinders of sizes 4 in x 8 in and 6 in x 12 in for mechanical properties testing. The companion specimens were kept in the NIST environmental chambers where the four large block specimens were cured to ensure the same curing conditions for both the block and the companion specimens.



**Figure 2–16. Concrete mixer discharging control concrete into telebelt**



**Figure 2–17. Concrete placement into formwork of control specimen using an elephant trunk hose**

## **2.5 PROPERTIES OF FRESH CONCRETE**

To determine compliance with the quality requirements of the specifications under which the concrete was batched or produced, freshly mixed concrete samples were obtained and tested in accordance with ASTM C172 (ASTM C172/C172M-14a, 2014). The following fresh concrete properties were evaluated:

- Consistency (Slump Test): in accordance with ASTM C143 (ASTM C143/C143M-15a, 2015)
- Density (Wet Unit Weight): in accordance with ASTM C138 (ASTM C138/C138M-17a, 2017)
- Air Content: in accordance with ASTM C231 (Pressure Method), ASTM C231/C231M-17a (2017)

The fresh properties of concrete from each individual batch produced during the construction of the three reactive block specimens are reported in Tables 2-5, 2-6, and 2-7. The fresh properties of concrete from the two trucks used for the control block specimen are shown in Table 2-8.

For block ASR 3 (Table 2-5), the measured volumetric air content for each batch varied between 1.4 % to 2.2 % and consisted of primarily entrapped voids, as no air-entraining admixture was utilized. These measured entrapped air contents varied due to the adjustment of dosed high-range water-reducing admixture (HRWRA) which affected the consolidation behavior of each mixture. This measured air content is consistent with the variation in measured slump of 4.0 in to 8.0 in throughout production. The corrected relative density, defined here as the measured density from ASTM C138 (ASTM C138/C138M-17a, 2017) testing divided by the theoretical (i.e., calculated) density of the as-batched mixture proportions corrected for the volume of measured air content. This metric gives an indication of the cumulative error of both the batched proportions and measured air content, which can be contrasted with the typically reported relative yield, which does not account for the air content; the uncertainty in the combined measurements of the air content and unit weight for a typical mixture reported herein resulted in a standard deviation in relative density of approximately  $\pm 1.0$  % while typical limits for concern are  $\pm 2.0$  %. For each batch, it was found that the relative density varied from -0.7 % to +2.5 %. Overall, the mixtures were batched with relatively high-precision and the measurements indicate that the primary difference between any two batches was the consistency which may be primarily attributable to variable dosages of HRWRA during concrete mixing. It should be noted here that companion specimens were taken from Batch 1.

For block ASR 2 (Table 2-6), the entrapped air content was measured as 2.0 % in all but Batch 3, where additional water present on the coarse aggregate resulted in an excessively flowable mixture with a measured slump of 8.3 in. Overall, the corrected relative density varied from +0.3 % to +2.0 %, indicating that the reported batch weights were in general agreement with the measured unit weight and air contents. The measured slump varied from 4.3 in to 8.3 in and was a result of variable moisture contents of the aggregate pile and HRWRA dosage rates. The concrete used to cast the companion specimens for this mixture were taken from Batch 2.

For block ASR 1 (Table 2-7), the measured entrapped air content was between 1.3 % and 2.0 % and the range of measured slump was between 5.0 in and 6.8 in. The corrected relative density computed for each mixture was in the range of +0.8 % to +1.7 % indicating high consistency between reported batch weights and the measured unit weight and air content. The companion specimens for this mixture were taken from Batch 2.

**Table 2–5. Fresh concrete properties for each batch used in the production of block ASR 3**

		Design	Batch						
			Trial	1	2	3	4	5	6
Gross Air Content	[%]	2.0	1.6	1.6	1.5	2.2	2.1	1.8	1.4
Unit Weight	[lb/ft <sup>3</sup> ]	144.3	148.3	146.9	147.9	143.3	144.2	145.6	146.4
Corrected Rel. Density	[-]	-	1.027	1.018	1.025	0.993	0.999	1.008	1.015
Slump	[in]	4-6	4.0	5.25	7.0	6.5	6.5	6.5	8.0

**Table 2–6. Fresh concrete properties for each batch used in the production of block ASR 2**

		Design	Batch						
			Trial	1	2	3	4	5	6
Gross Air Content	[%]	2.0	2.0	2.0	2.0	1.5	2.0	2.0	2.0
Unit Weight	[lb/ft <sup>3</sup> ]	144.6	146.7	146.2	145.1	147.1	146.7	147.2	147.0
Corrected Rel. Density	[-]	-	1.014	1.010	1.003	1.017	1.013	1.019	1.020
Slump	[in]	4-6	5.25	5.75	7.0	8.25	5.0	7.0	4.5

**Table 2–7. Fresh concrete properties for each batch used in the production of block ASR 1**

	Design	Batch							
		Trial	1	2	3	4	5	6	
Gross Air Content	[%]	2.0	1.3	1.3	1.5	1.9	1.9	2.0	2.0
Unit Weight	[lb/ft <sup>3</sup> ]	145.0	147.5	147.5	146.5	146.0	147.0	146.2	146.5
Corrected Rel. Density	[-]	-	1.017	1.017	1.010	1.007	1.013	1.008	1.011
Slump	[in]	4-6	6.0	6.0	6.0	6.75	5.0	5.0	6.0

**Table 2–8. Fresh concrete properties for each batch used in the production of control block**

	Design	Accepted	Ticket	Truck	
		Design	Design	1	2
Gross Air Content	[%]	1.5	2.0	1.5	2.5
Unit Weight	[lb/ft <sup>3</sup> ]	149.5	148.7	147.4	147.2
Corrected Rel. Density	[-]	-	-	0.994	0.977
Slump	[in]	4-8	4-8	7.5	5.5

## 2.6 CURING

### 2.6.1 Initial Curing after Concrete Placement

The intended curing practice for concrete specimens was to provide a stable temperature of approximately 75 °F and a high relative humidity (RH) of greater than approximately 95 % for a minimum of three months to allow for the proper development of mechanical properties prior to increasing the temperatures to accelerate the ASR reaction. Due to delays in the availability of environmental controlling equipment, the exposed surface (top) of each reactive block specimen was initially covered with wet burlap and plastic sheets immediately following completion of concrete placement and top surface finishing to prevent excessive loss of moisture in order to minimize the potential for developing drying shrinkage cracks during the hydration process. The reactive blocks continued to be cured within its steel formwork for 7 days, after which the formwork was removed. The plywood inserts (which secured the surface mounted targets prior to casting) were also removed.

### 2.6.2 Long-Term Curing

After the initial curing period and removal of the formwork described above, the specimens were subjected to a five-phase curing regime as follows (note that in the remainder of this chapter, time is calculated relative to the date of concrete placement of block ASR 3, which was March 21, 2017):

**Phase 1:** The reactive block specimens were continually covered with burlap and plastic sheets after removal of the steel formwork seven days after the placement of concrete (Figure 2-18). Water was sprayed on the burlap on a daily basis. Wetting of the burlap continued for 106 days after casting. During this period, the environmental chamber was under ambient conditions (temperature of about 75 °F to 80 °F and relative humidity (RH) in the range of 50 % to 75 %).



Figure 2–18. Phase 1 of curing of reactive block specimens

**Phase 2:** The block specimens were uncovered and conditioned to an RH of about 75 % and a temperature of about 75 °F to 80 °F until 180 days after casting (Figure 2-19). Phase 2 allowed (1) the specimen's cover concrete to re-equilibrate after undergoing potentially significant drying between periods of rewetting and (2) a smooth transition in the environmental conditions and as a result, the alkali-silica reaction (ASR) expansion to minimize the effects of creep of the newly cast concrete on the performance of the blocks.



**Figure 2–19. Phase 2 of curing of reactive block specimens**

**Phase 3:** Between 180 days and 470 days after concrete placement, the RH was increased to the range of 95 % to 100 %, which allowed the ASR expansion to accelerate. During this phase, the ambient temperature in the chamber was maintained between 75 °F and 80 °F (Figure 2-20).



**Figure 2–20. Phase 3 of curing of reactive block specimens**

**Phase 4:** The RH in the chamber was kept between 95 % and 100 %, but the temperature was increased to the level of 100 °F to 110 °F to further accelerate the ASR expansion. This phase continued between 470 days and 700 days.

**Phase 5:** After 700 days, the expansion of the blocks had for the most part plateaued (see Section 3.2), the environmental chamber was returned to ambient conditions (RH in the range of 50 % to 75 % and temperature in the range of 75 °F to 90 °F).

## **2.7 NIST TRIAXIAL PRESSURE VESSEL**

A unique feature of the experimental plan for this Task 1 study is the testing of compressive strength of ASR-affected concrete under triaxial compressive stress condition, in addition to the conventional uniaxial compressive test. Triaxial compression test allows the quantification of the effects of different degrees of confinement on the compressive strength of concrete affected by ASR. In this test, radial and axial compressive stresses were applied simultaneously to the concrete core sample and thus, this test simulates more realistically the confinement on the concrete cores being tested (confined radially by pressure resulting from the restraint to expansion provided by the steel reinforcement). For this purpose, a Triaxial Pressure Vessel (TPV) was designed and fabricated at NIST to provide a specified radial pressure (through the confinement of hydraulic fluid) to a concrete core specimen while loading is applied in the longitudinal direction and measurements of its mechanical response are recorded. A rendering of the device and its cross section are shown in Figure 2-21, while Figure 2-22 shows the entire system (TPV with hydraulic power unit and controls) situated in a nominal capacity 220 kip closed-loop servohydraulic load frame.

The NIST TPV was designed for a radial confinement pressure of up to 2300 psi. A feedback control system was developed to ensure that the specified pressure was maintained while the specimen was loaded longitudinally through the servohydraulic load frame. The results of TPV tests are described in Section 3.5 of Chapter 3.



(a) (b)  
Figure 2–21. (a) Triaxial pressure vessel and (b) cross section of triaxial pressure vessel with a prepared cored concrete specimen

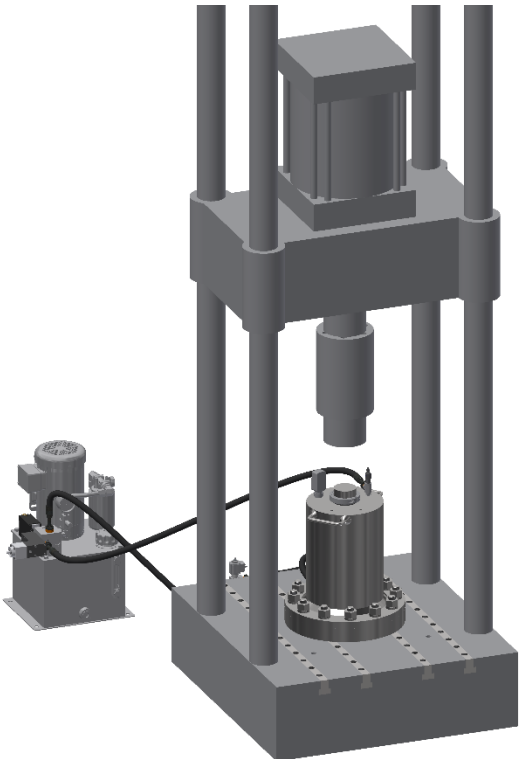


Figure 2–22. Triaxial pressure vessel and hydraulic power unit and controls situated in 220 kip servohydraulic load frame

This page intentionally left blank.

## Chapter 3

# MEASUREMENT AND DATA ANALYSIS

---

---

This chapter presents (1) data on temperature and relative humidity inside the NIST environmental chamber, which characterized the curing conditions of the four block specimens, as well as corresponding temperature histories and relative humidity inside a typical block specimen (Section 3.1); (2) data on ASR-induced strain development in the reinforcements and in the concrete of the block specimens (Section 3.2); (3) data on measurements of surface expansion and crack development on the three reactive block specimens (Section 3.3); (4) results on mechanical properties of ASR-affected concrete obtained using conventional standardized uniaxial compression testing (Section 3.4); and (5) results on concrete's compressive strength under triaxial compressive stress condition obtained using the NIST TPV test apparatus (Section 3.5). These measurements and test results provided basis for the findings and conclusions described in Chapter 4.

### 3.1 ENVIRONMENTAL CONDITIONS

The NIST environmental chamber was equipped with a heating system capable of achieving a temperature of 110 °F and two steam humidifiers capable of achieving a relative humidity approaching 100 %. Thermocouples and relative humidity sensors were located around the chamber to measure the temperature and humidity for the duration of the test program. By and large, the environmental conditions in the chamber were controlled in accordance with the five curing phases described in Section 2.6. Periodically, when measurements needed to be taken or core samples needed to be extracted from the block specimens, requiring staff to be present in the chamber, the temperature and relative humidity in the chamber were then reduced to facilitate appropriate working conditions for staff conducting these operations.

Figure 3-1 shows the measured temperatures based on the thermocouples that were installed around the environmental chamber. The five curing phases, which are delineated by red solid vertical lines, are annotated on the plot. The oscillations in recorded temperatures, especially those during Phases 3 and 4, were a result of shutting down the environmental controls to allow work to be performed on the blocks (e.g., coring, crack mapping), regular maintenance and inspection, etc., as discussed above.

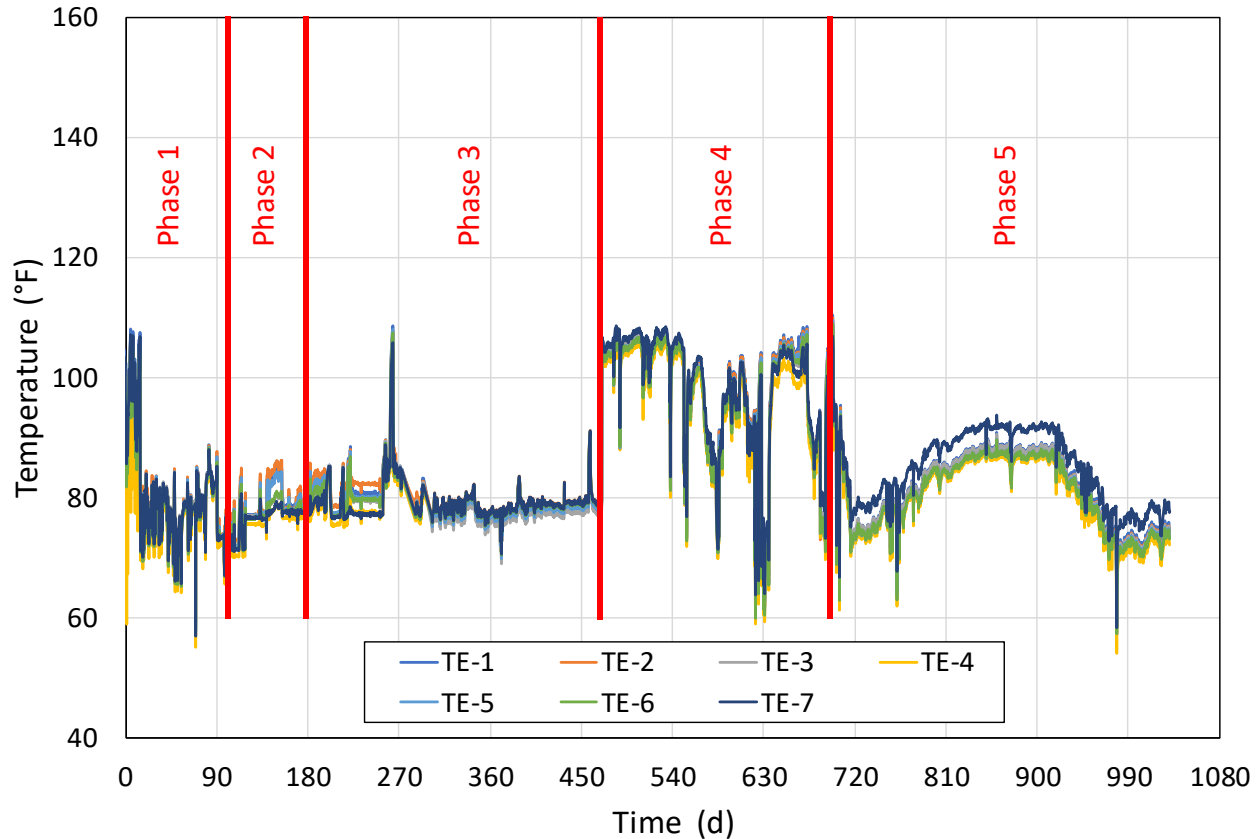


**Figure 3-1. Temperature histories inside the environmental chamber**

Figure 3-2 shows the temperature histories inside the control block. For locations of the thermocouples on this figure, the readers are referred to Section 2.3. Figure 3-2 shows that the block's internal temperature-time histories followed a pattern similar to that of the temperatures measured inside the environmental chamber, but with some time-lag (due to the concrete thermal mass), and with less oscillations. Note also that the initial spike in the temperatures around 80 days (of reactive block ASR 3, which was cast more than two months ahead of the control block, see Section 2.4.2) was due to the heat of hydration, immediately after casting the control block.

The relative humidity was monitored over time using the iButtons inserted in the holes in the blocks (Section 2.3.3). At no point during curing Phases 3 and 4 was the RH measured and found to be less than 95 %. This indicates that sufficient internal moisture was present to initiate and fuel unimpeded formation of the ASR gel in the reactive blocks.

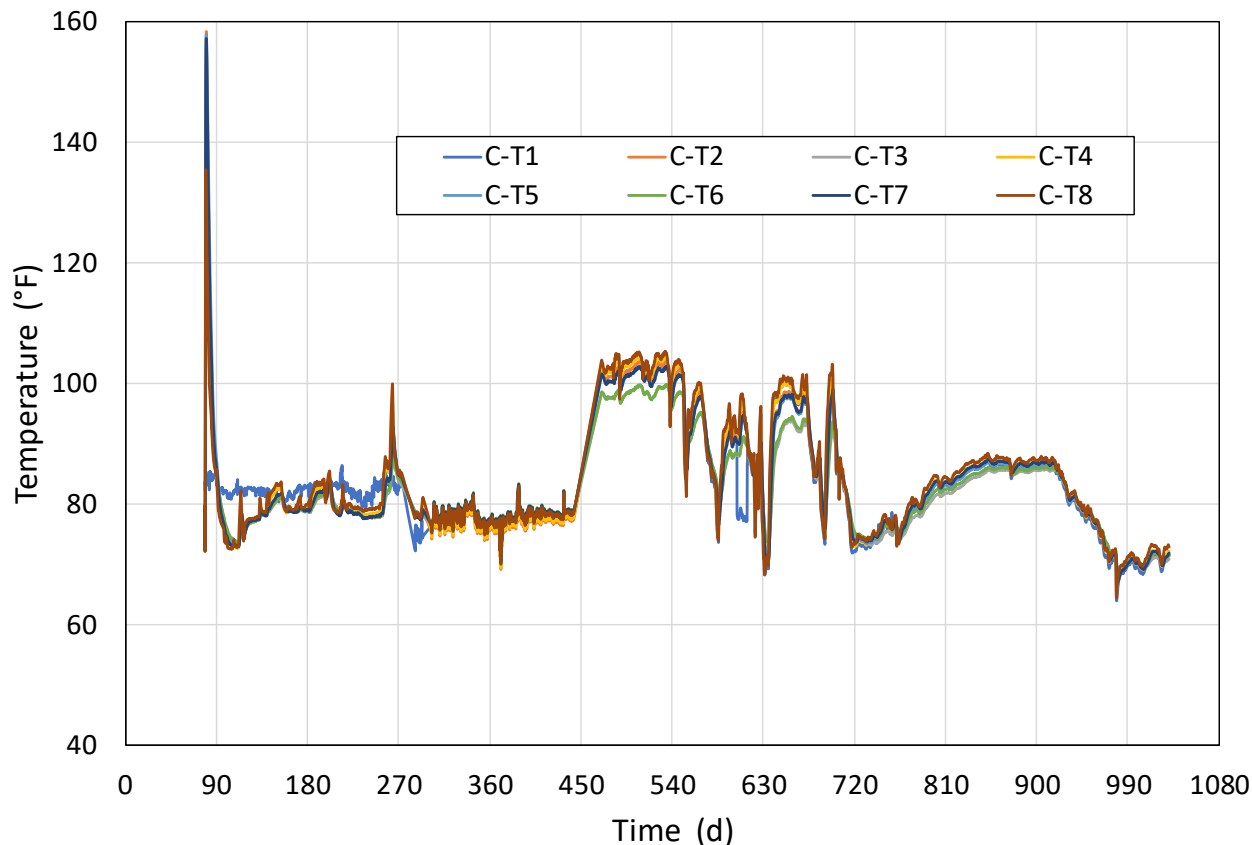


Figure 3–2. Measured temperatures inside the control block

## 3.2 STRAIN-TIME HISTORIES

### 3.2.1 Strains on Reinforcing Bars

Strain development on the reinforcing bars embedded in the blocks was continually monitored using the strain gages installed on the bars' surfaces (Section 2.3.1). Strain data were automatically recorded every 12 minutes on average throughout the entire duration of Task 1. The post-processing of the strain data consisted of two tasks:

- (1) Averaging: To both reduce the amount of data for plotting and the high-frequency noise in the data, every 11 scans were averaged to produce a single strain datapoint, resulting in one strain reading per gage every 2.2 hours.
- (2) Stitching: Data recording was periodically stopped and restarted to allow for system maintenance, or disconnection of gages that had malfunctioned. To ensure that strain data was continuous, the average top three strain values from the new scan (which generally started from zero strain values) were made equivalent to the average of the last three strain values from the previous scan. This resulted in continuous strain time-histories, without discontinuity due to the DAQ stoppages.

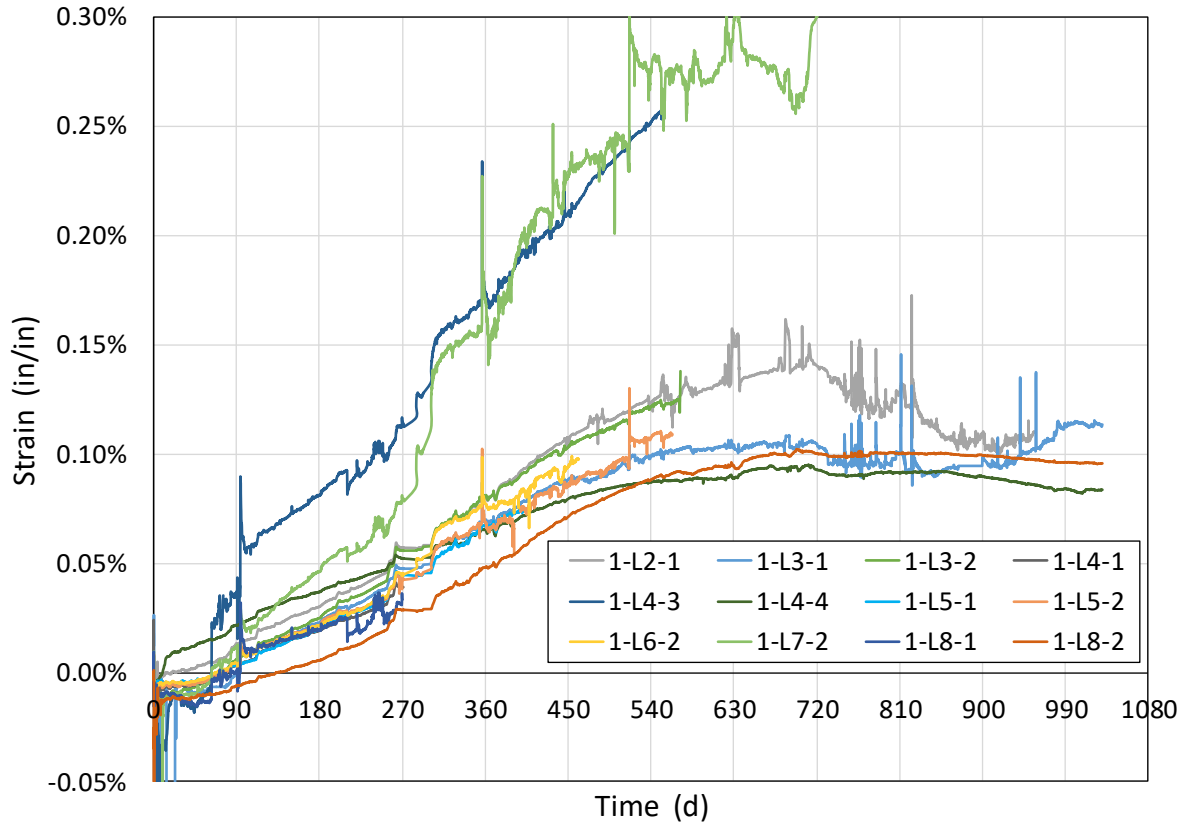
In addition, visual inspection of the time-history of each strain gage measurement was also conducted to ensure that the gage produced meaningful data. Gages whose strain data showed erratic behavior (e.g., sudden upward or downward jumps, discontinuity, or behavior not

consistent with surrounding gages) were removed from the plots starting from the onset of erratic behavior.

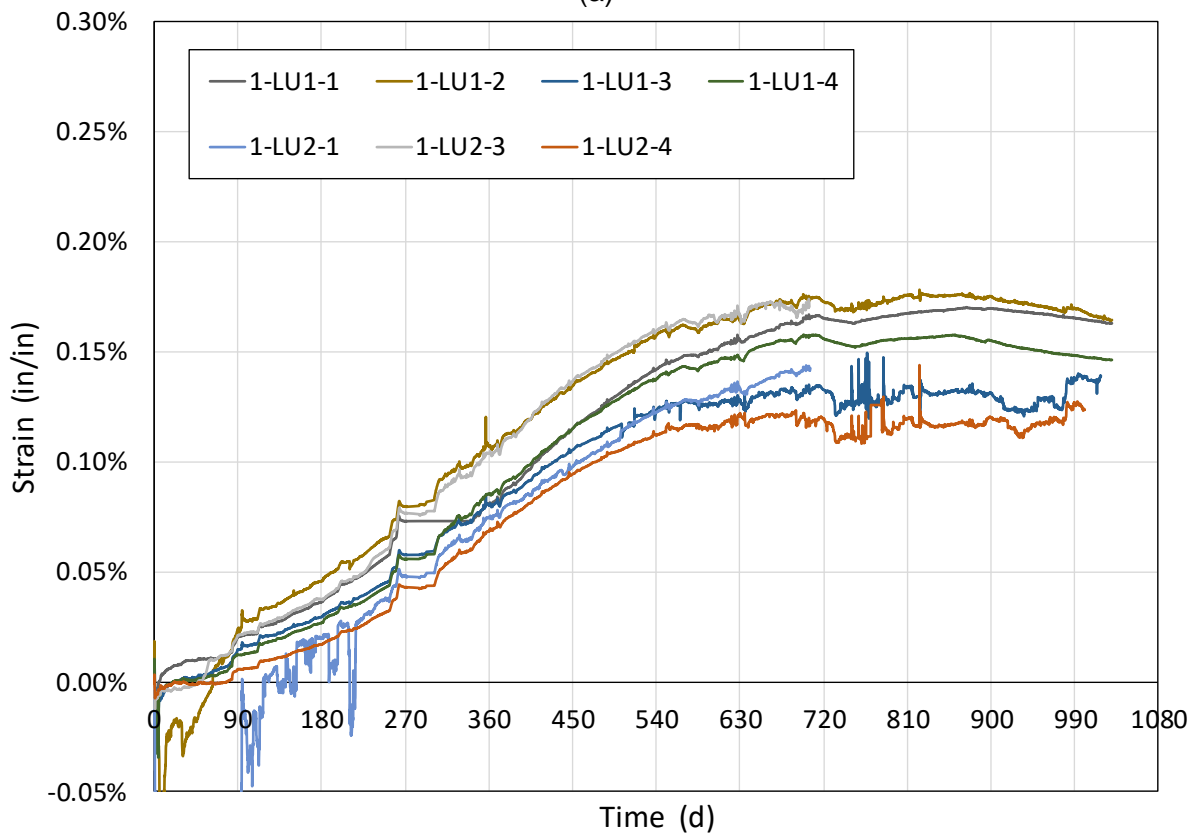
The measured ASR-induced strain developments in the reinforcing bars of the three reactive block specimens are shown in the Figures 3-3 to 3-11 below as follows:

- Figures 3-3, 3-6, and 3-9 show strain development for confinement Region 1 (mid-confinement) of reactive blocks ASR 1, ASR 2, and ASR 3, respectively, for the: (a) longitudinal bars, (b) top corner bars, (c) bottom corner bars, (d) vertical legs of stirrups, (e) top horizontal leg of stirrups, and (f) bottom horizontal leg of stirrups.
- Figures 3-4, 3-7, and 3-10 show strain development for Region 2 (no-confinement) of reactive blocks ASR 1, ASR 2, and ASR 3, respectively, for the top and bottom corner longitudinal reinforcing bars.
- Figures 3-5, 3-8, and 3-11 show strain development for confinement Region 3 (high-confinement) of blocks ASR 1, ASR 2, and ASR 3, respectively, for the: (a) longitudinal bars, (b) top corner bars, (c) bottom corner bars, (d) vertical legs of stirrups, (e) top horizontal leg of stirrups, (f) bottom horizontal leg of stirrups, and (g) cross ties.

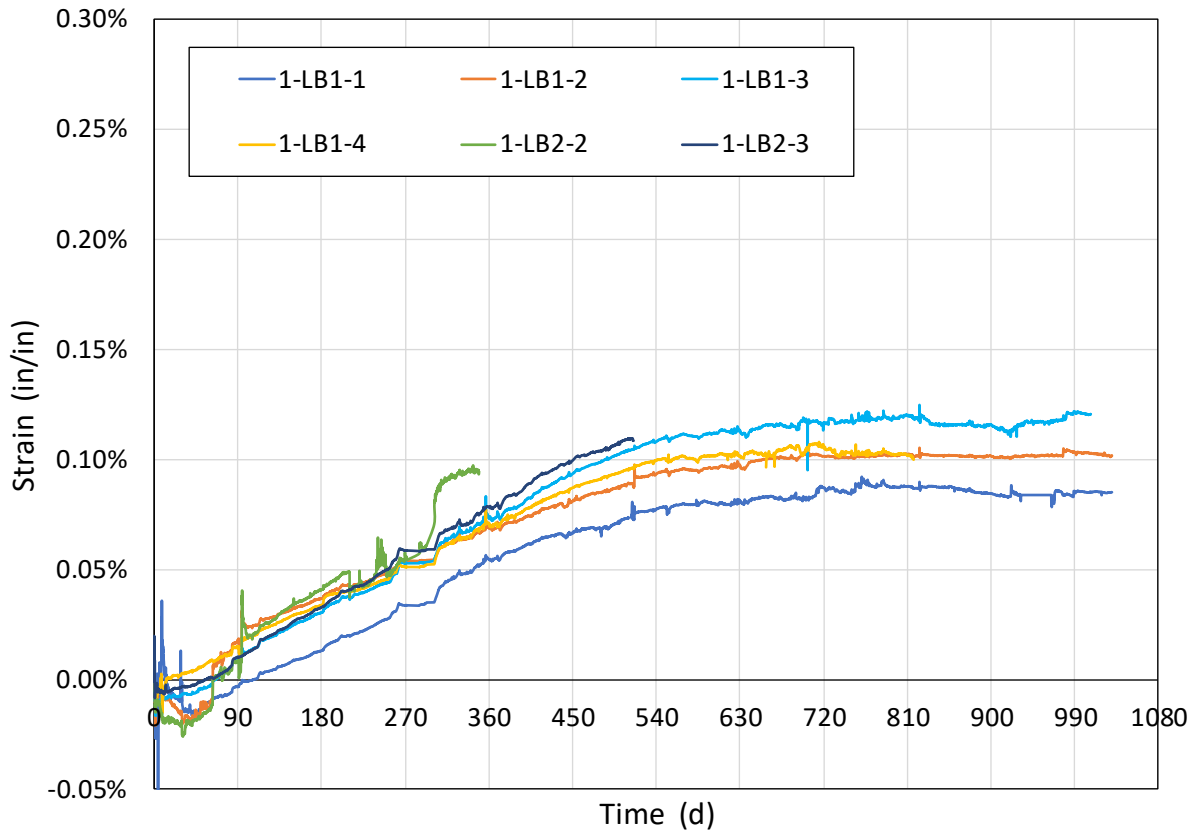
In all plots, positive strain values signify tensile strains (expansion), while negative strain values signify compressive strains (shrinkage). The location and nomenclature of the strain gages in the three reactive blocks are shown in Figure 2-4 and Appendix A.



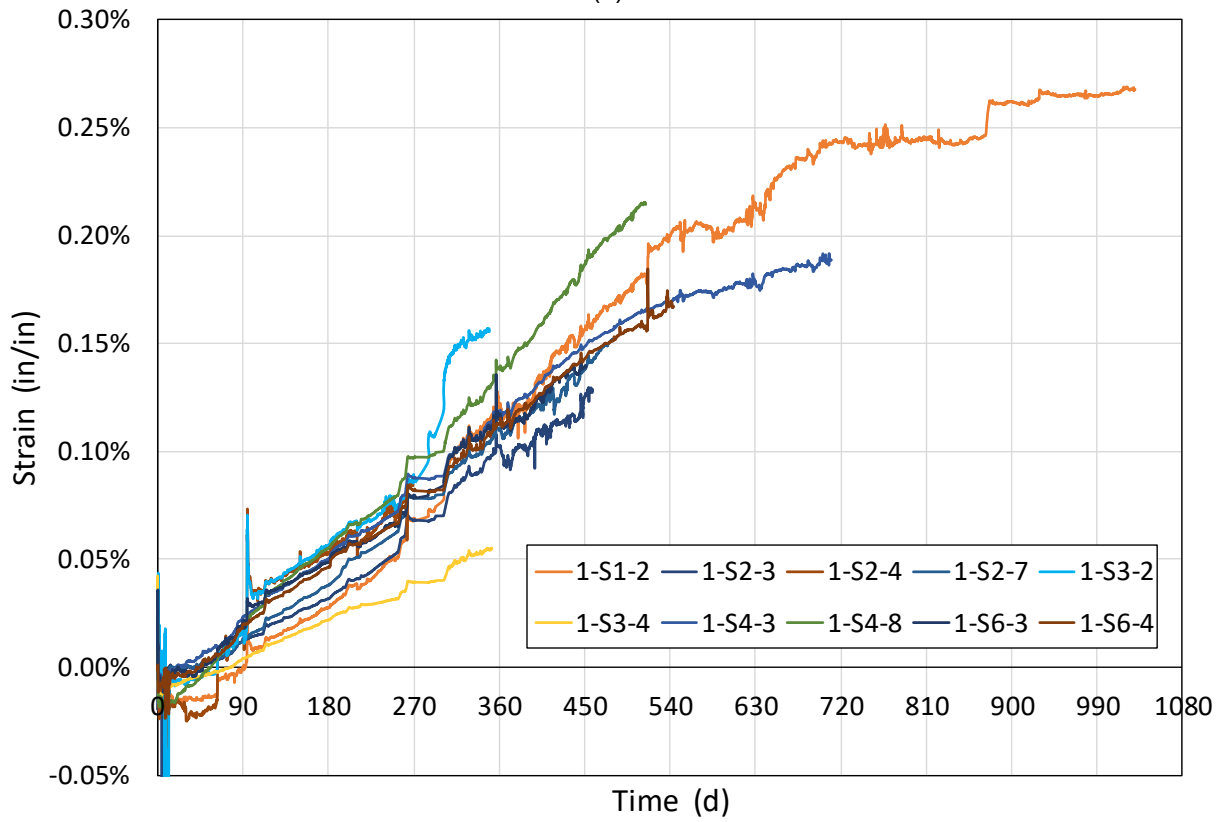
(a)



(b)



(c)



(d)

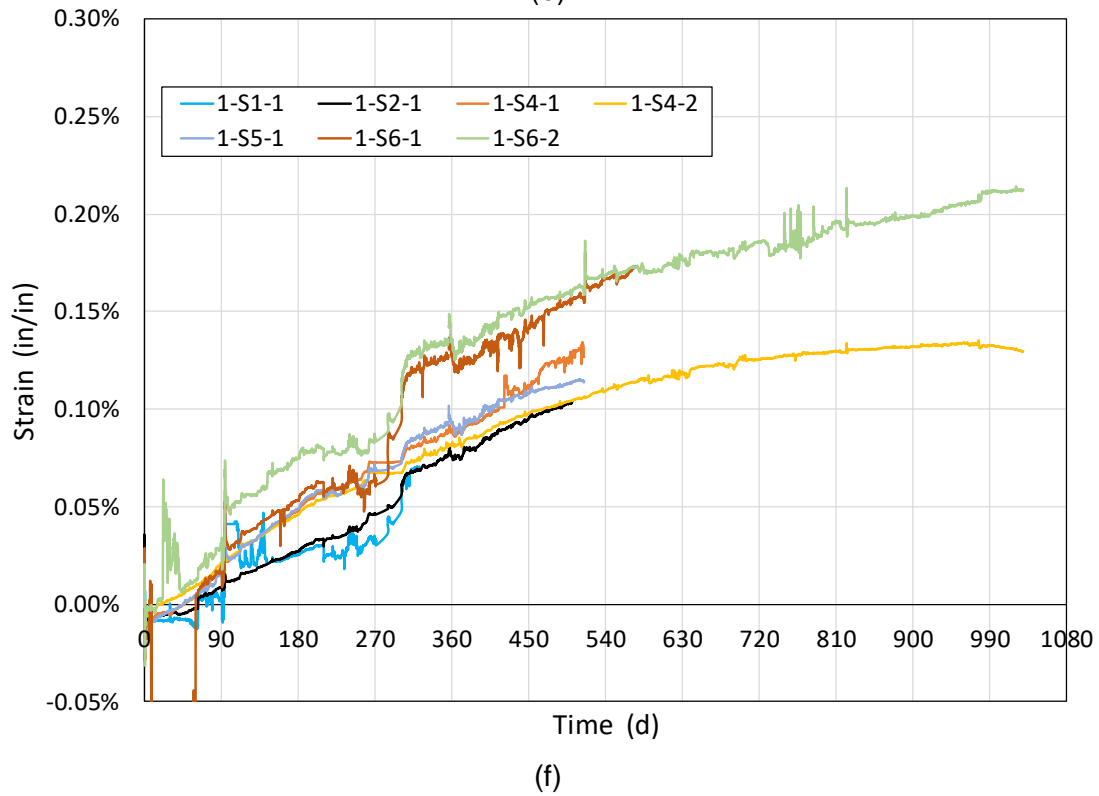
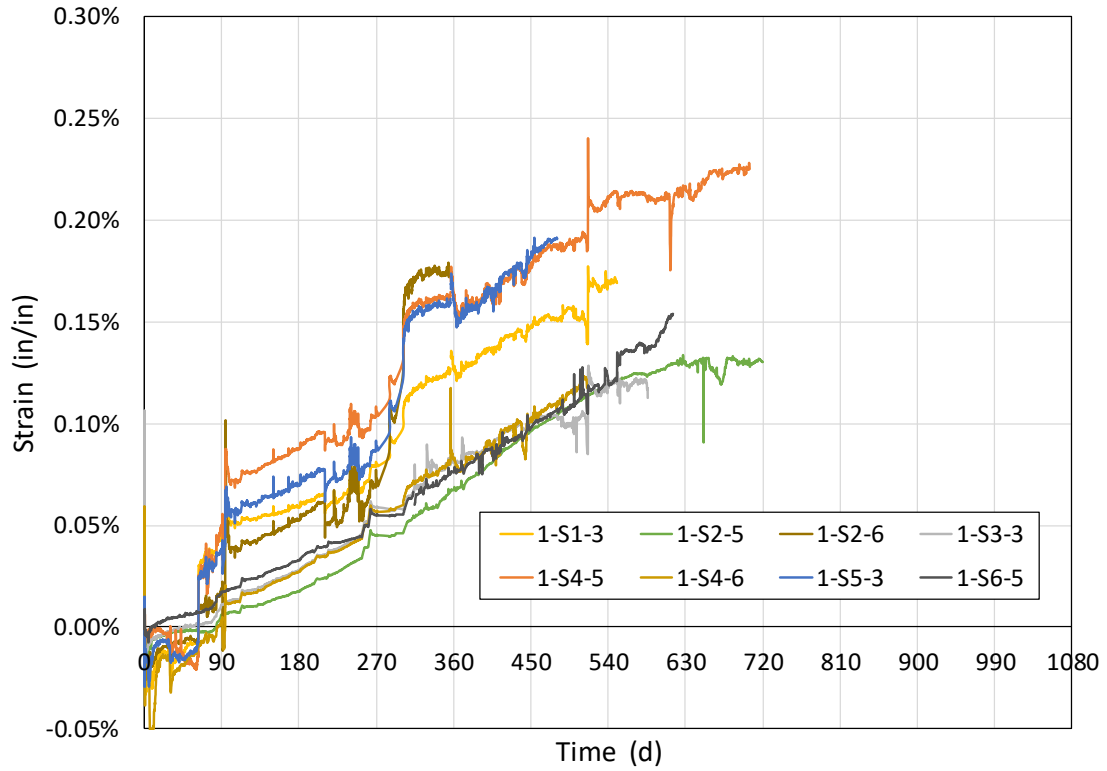


**Figure 3–3. Measured strains on reinforcing bars of Region 1 of block ASR 1: (a) longitudinal bars, (b) top corner bars, (c) bottom corner bars, (d) vertical legs of stirrups, (e) top horizontal leg of stirrups, and (f) bottom horizontal leg of stirrups**

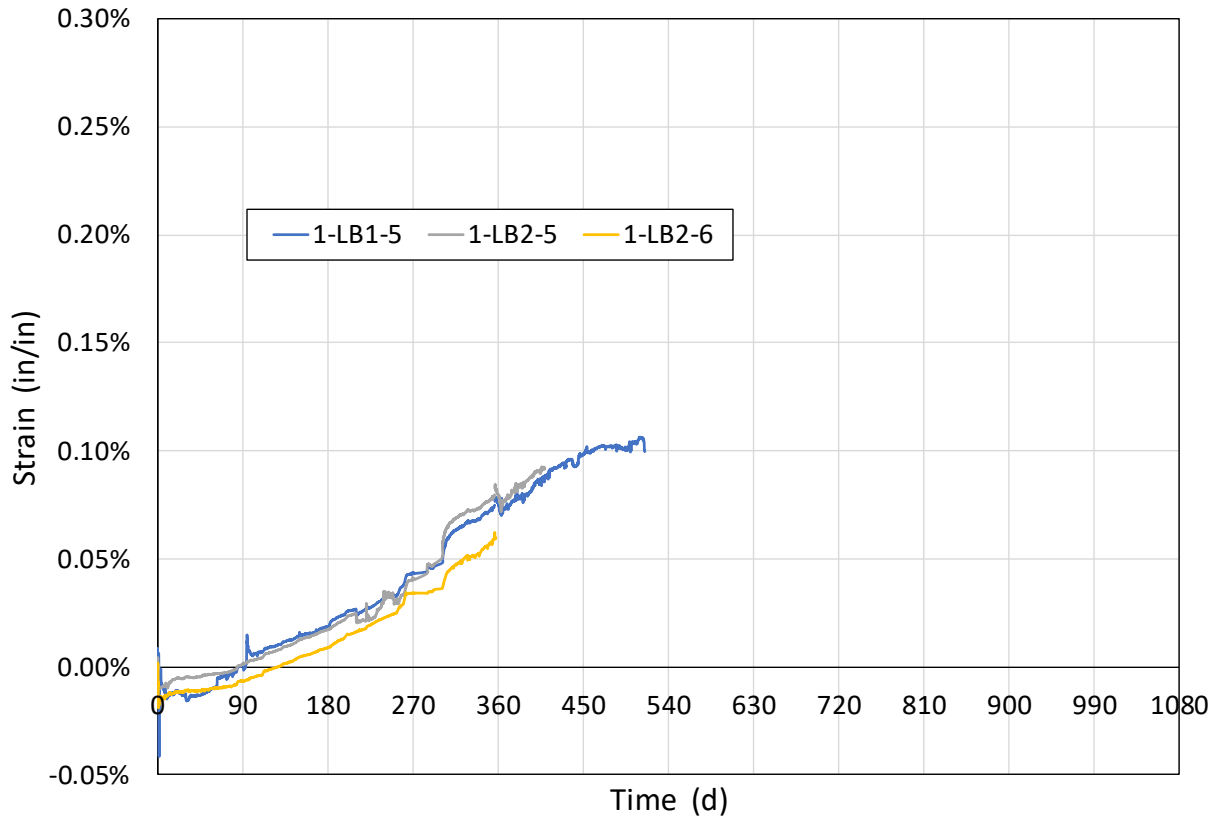
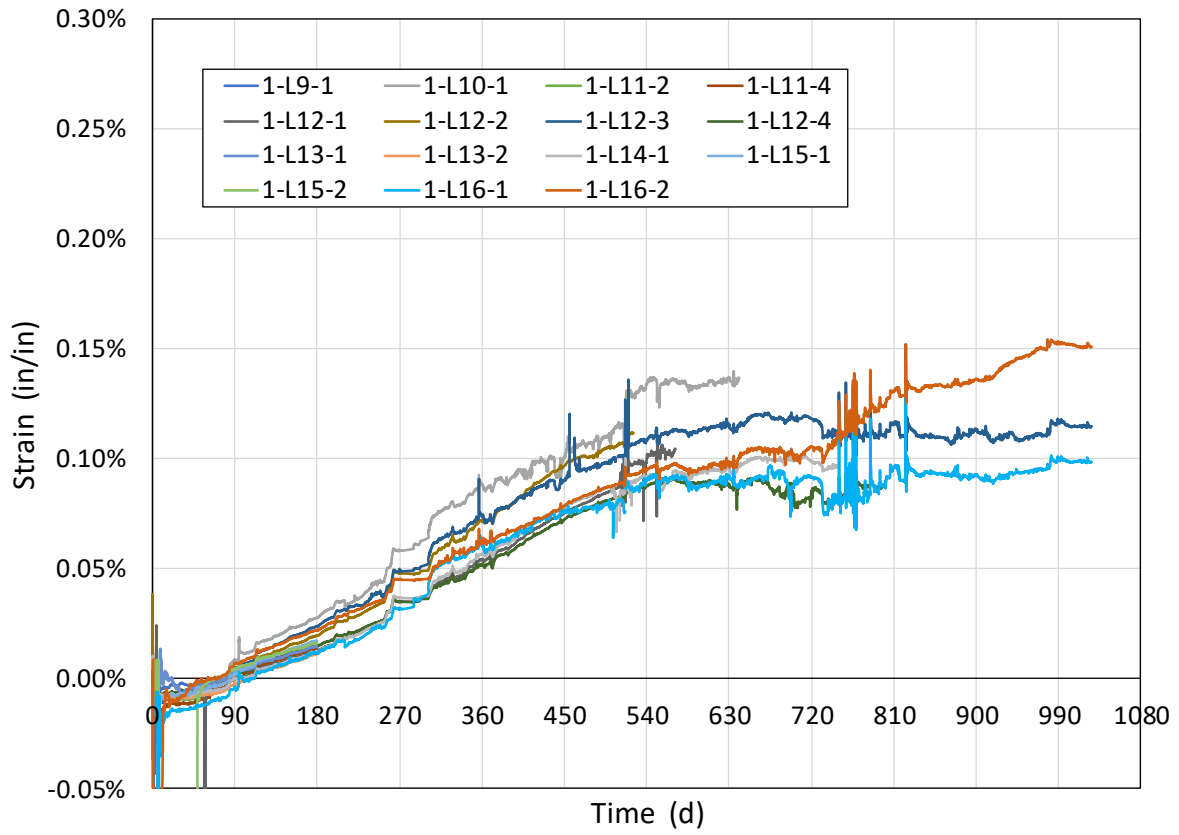
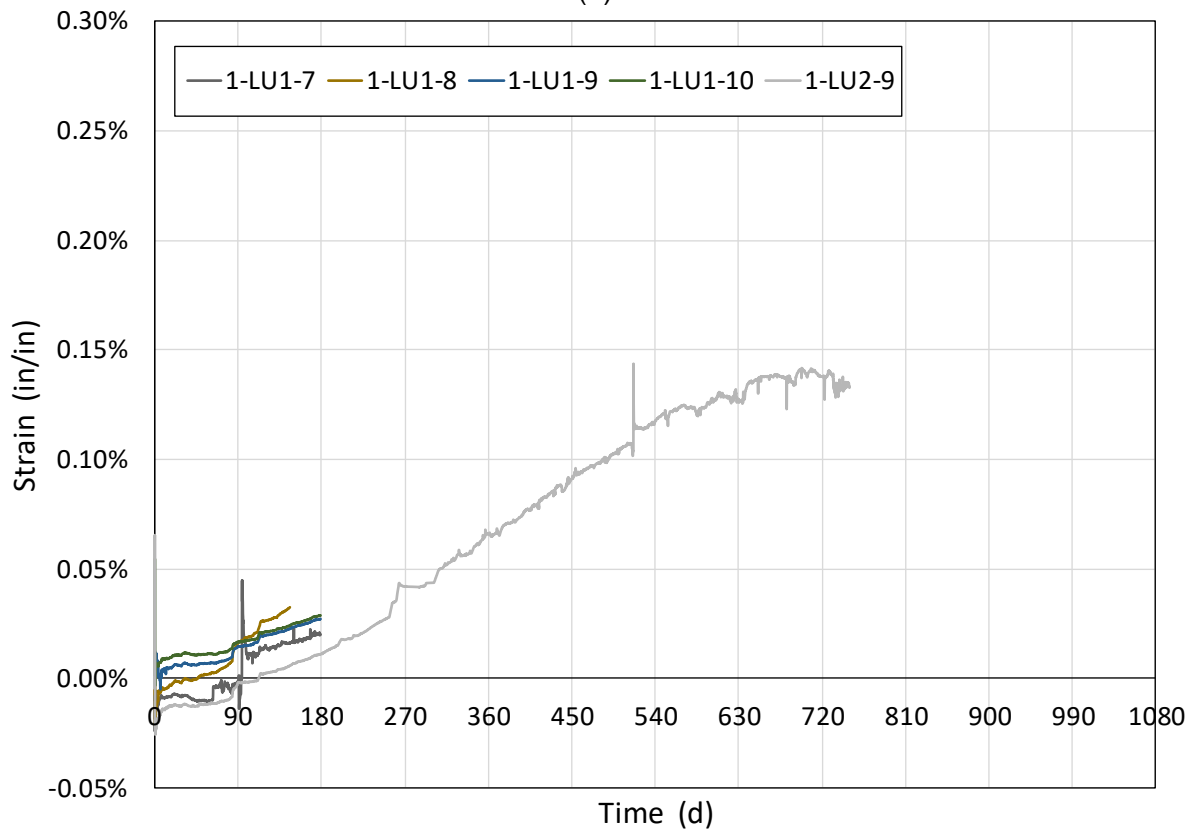


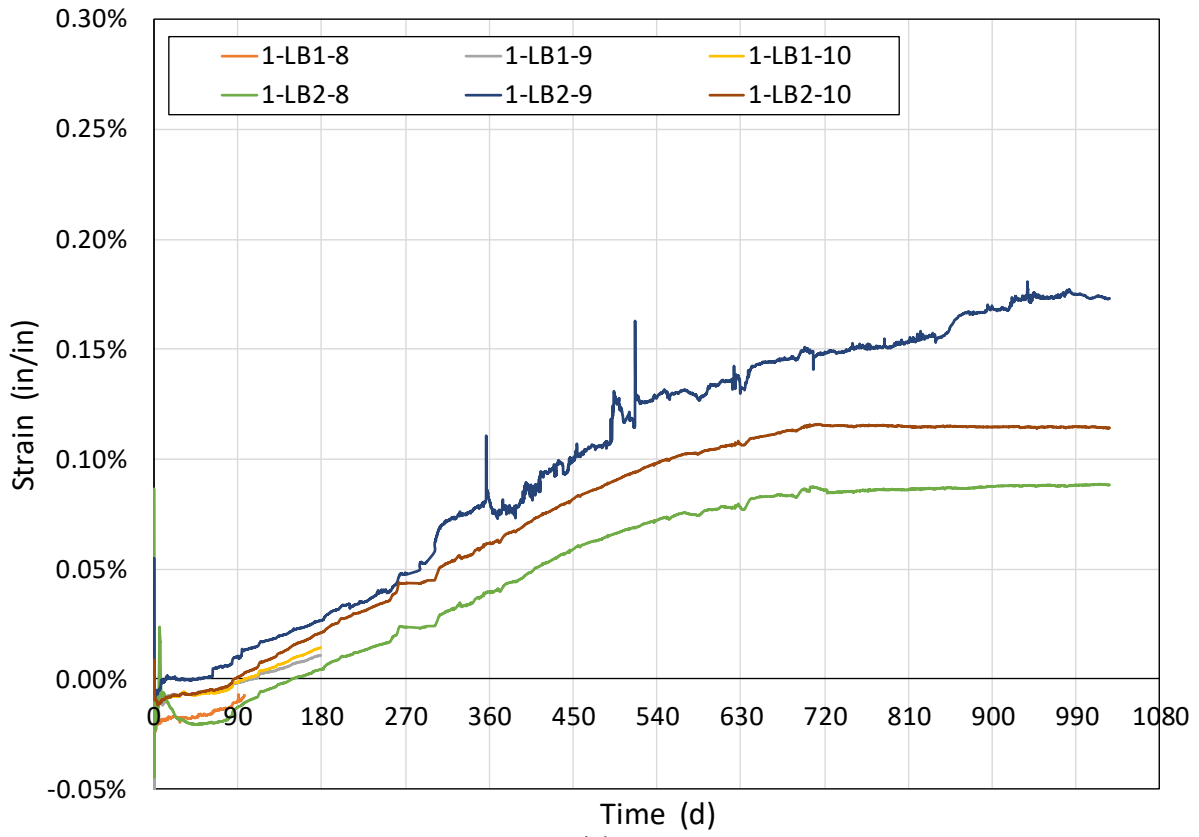
Figure 3–4. Measured strains on corner reinforcing bars of Region 2 of block ASR 1



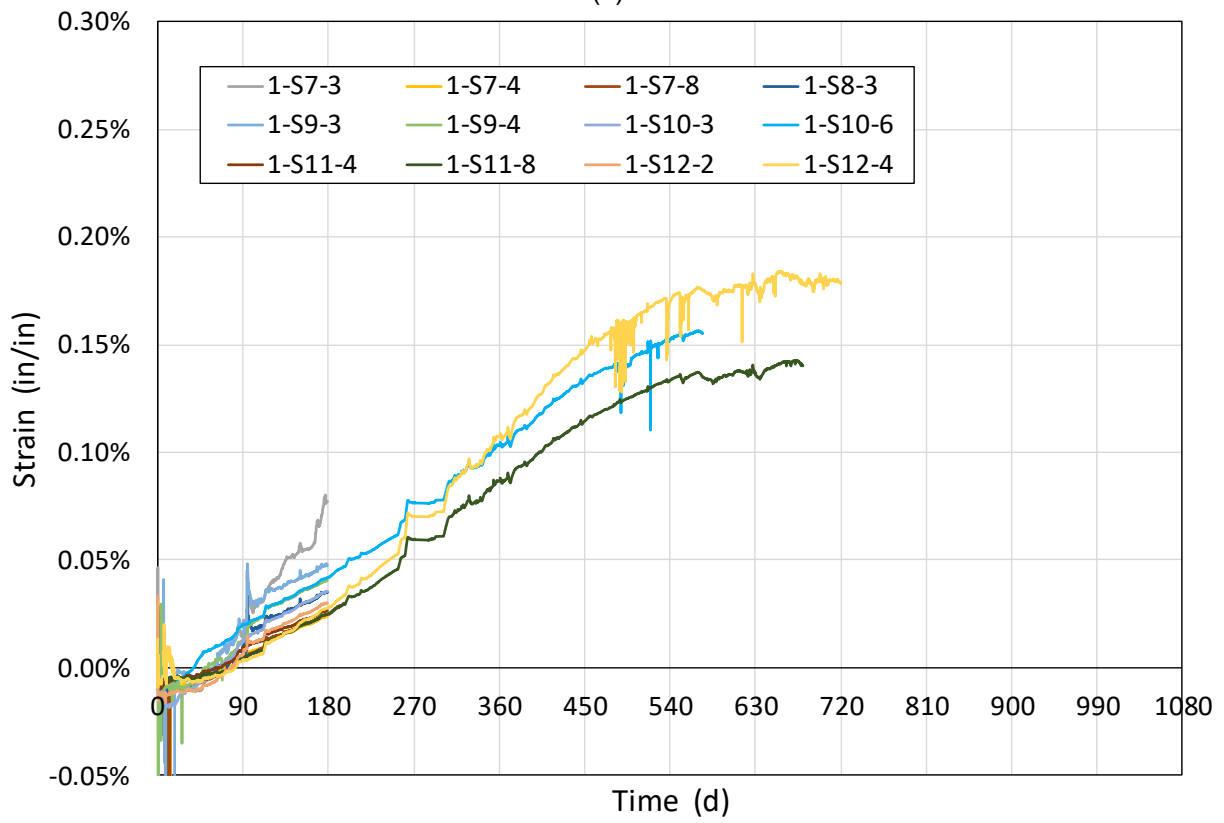
(a)



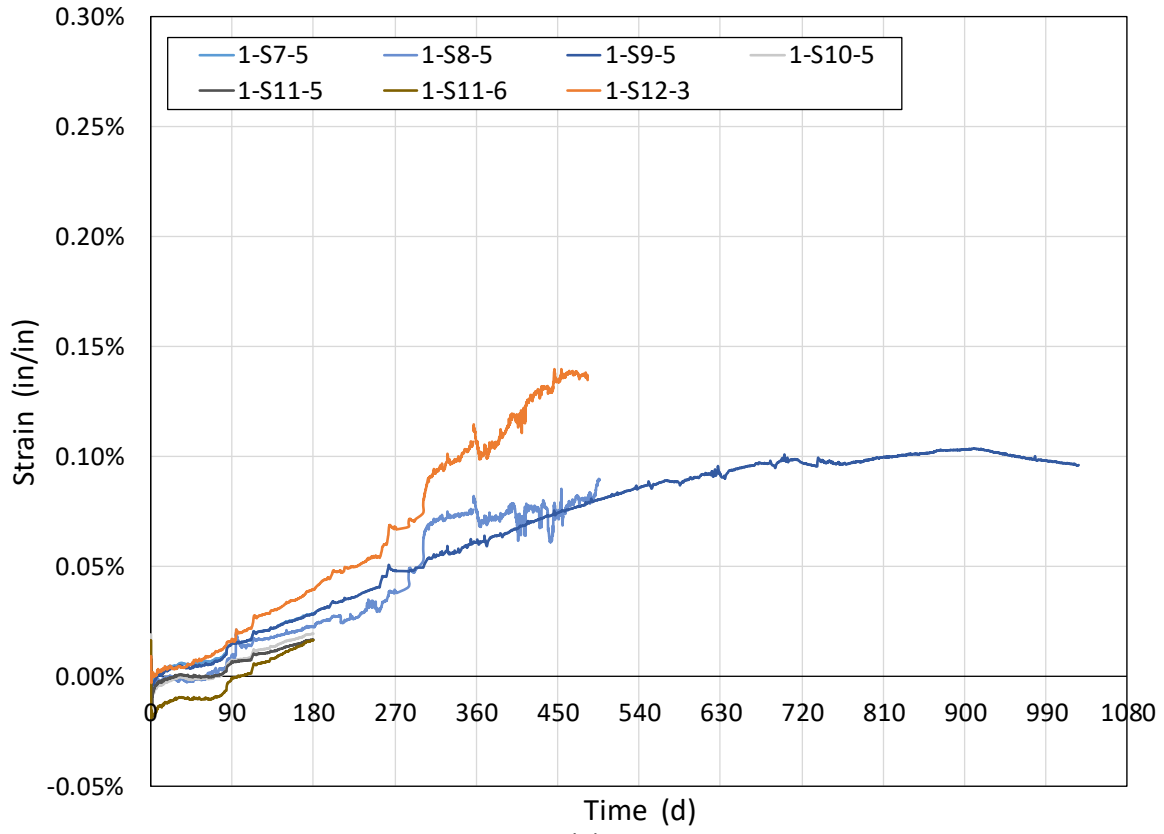
(b)



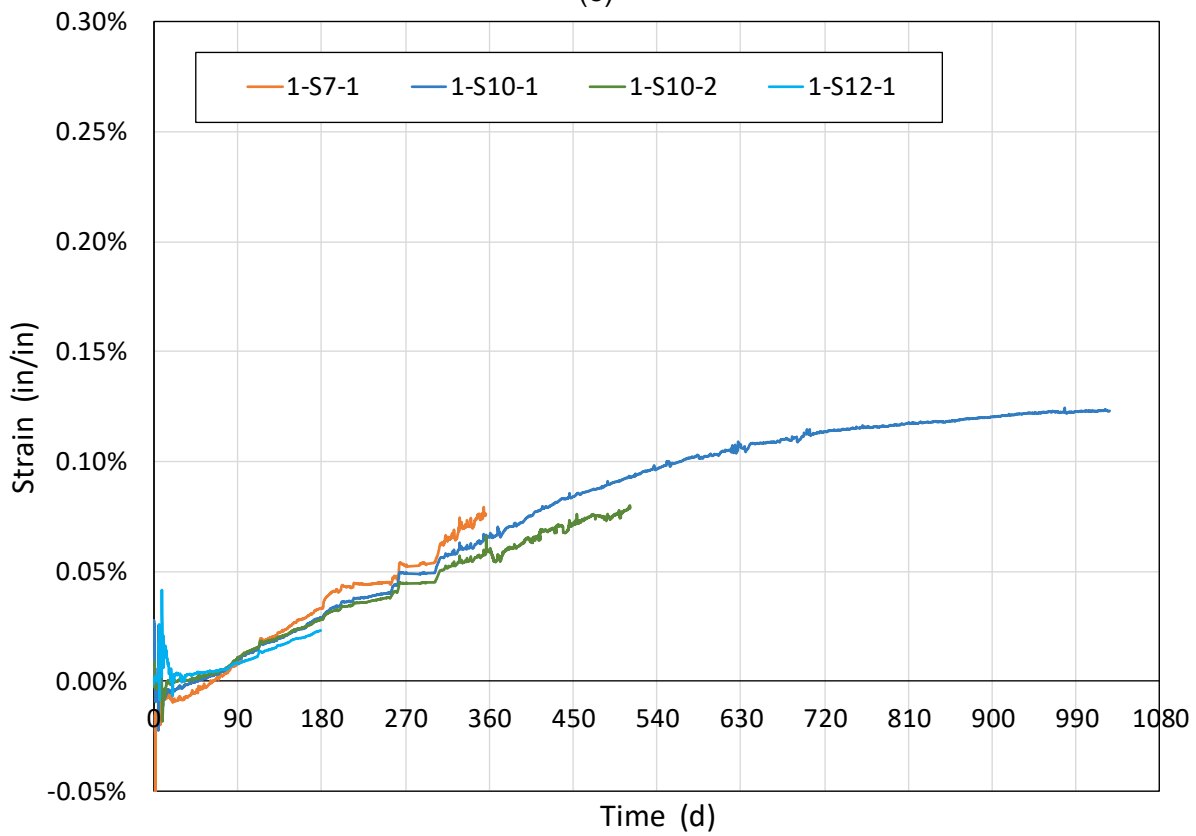
(c)



(d)



(e)



(f)

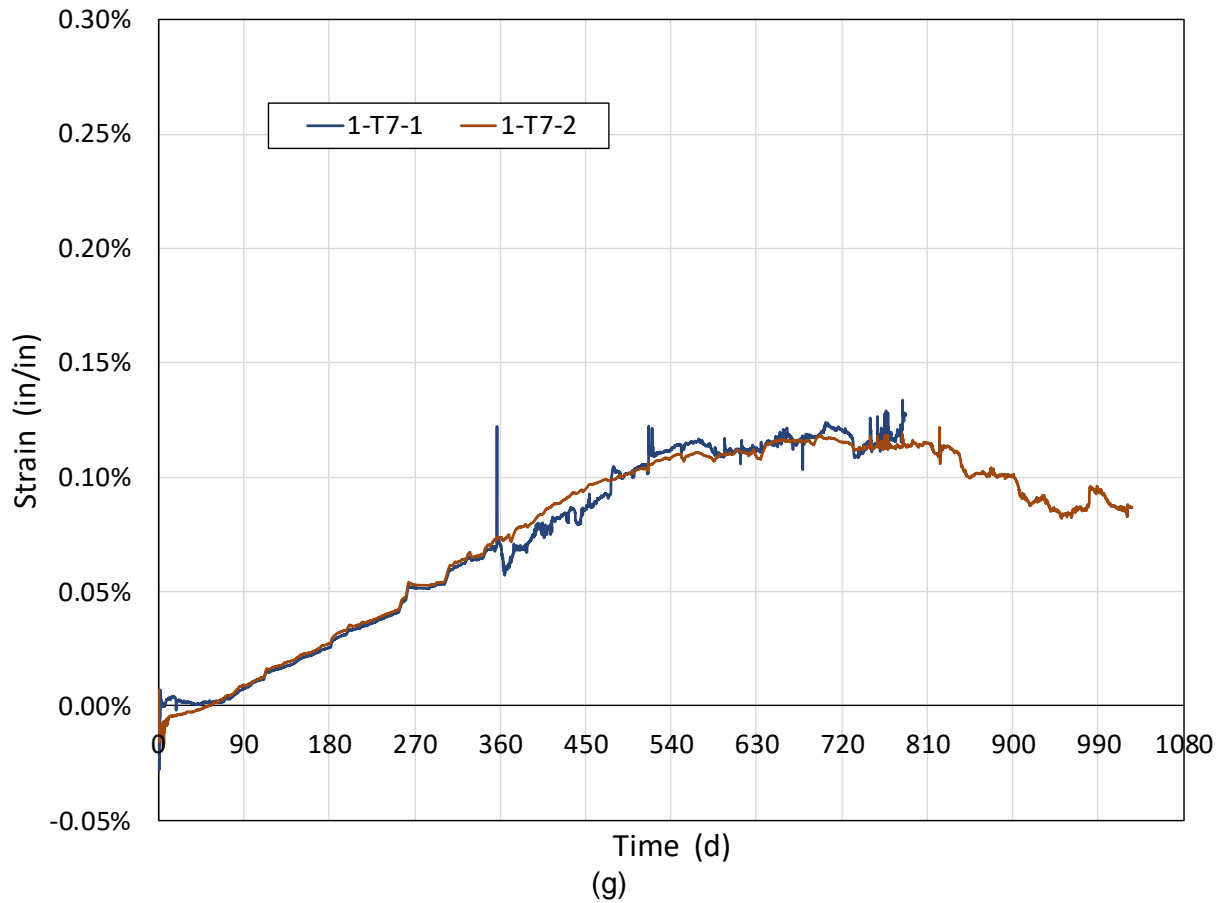
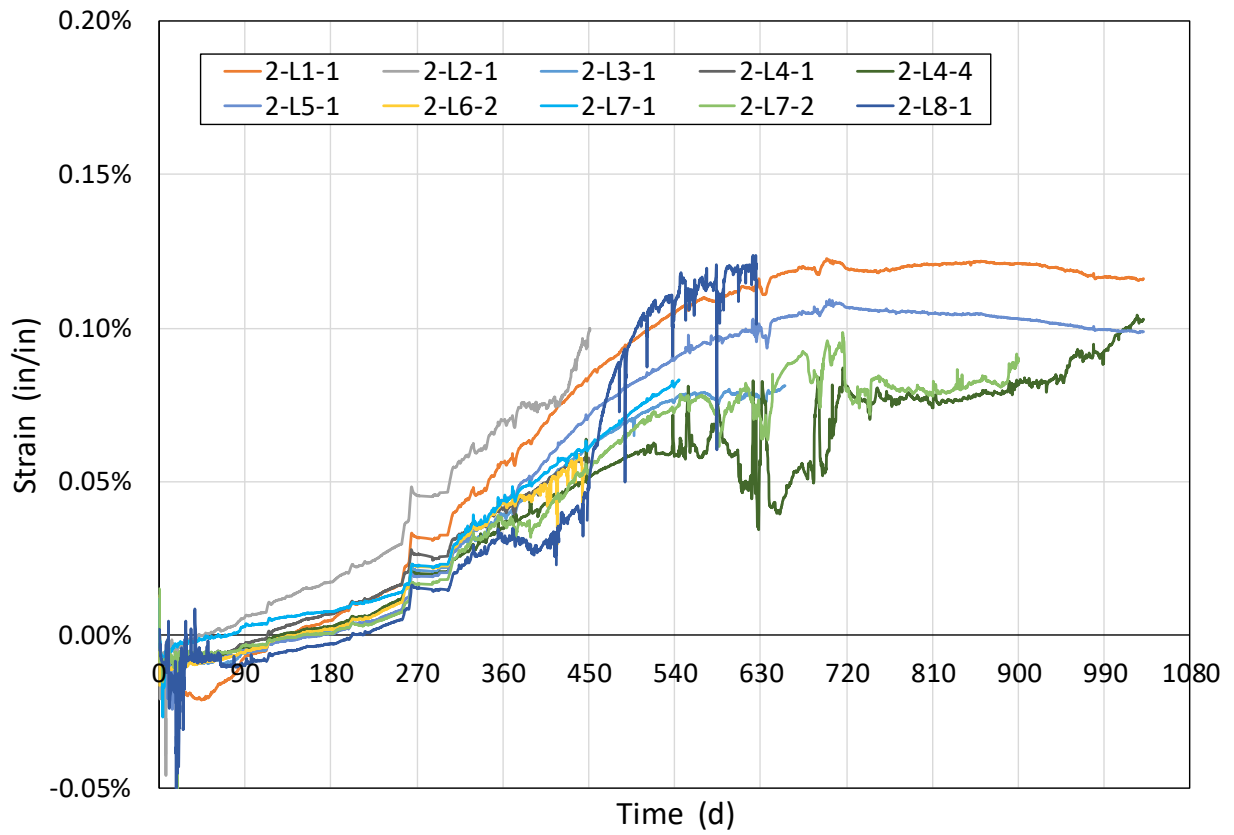
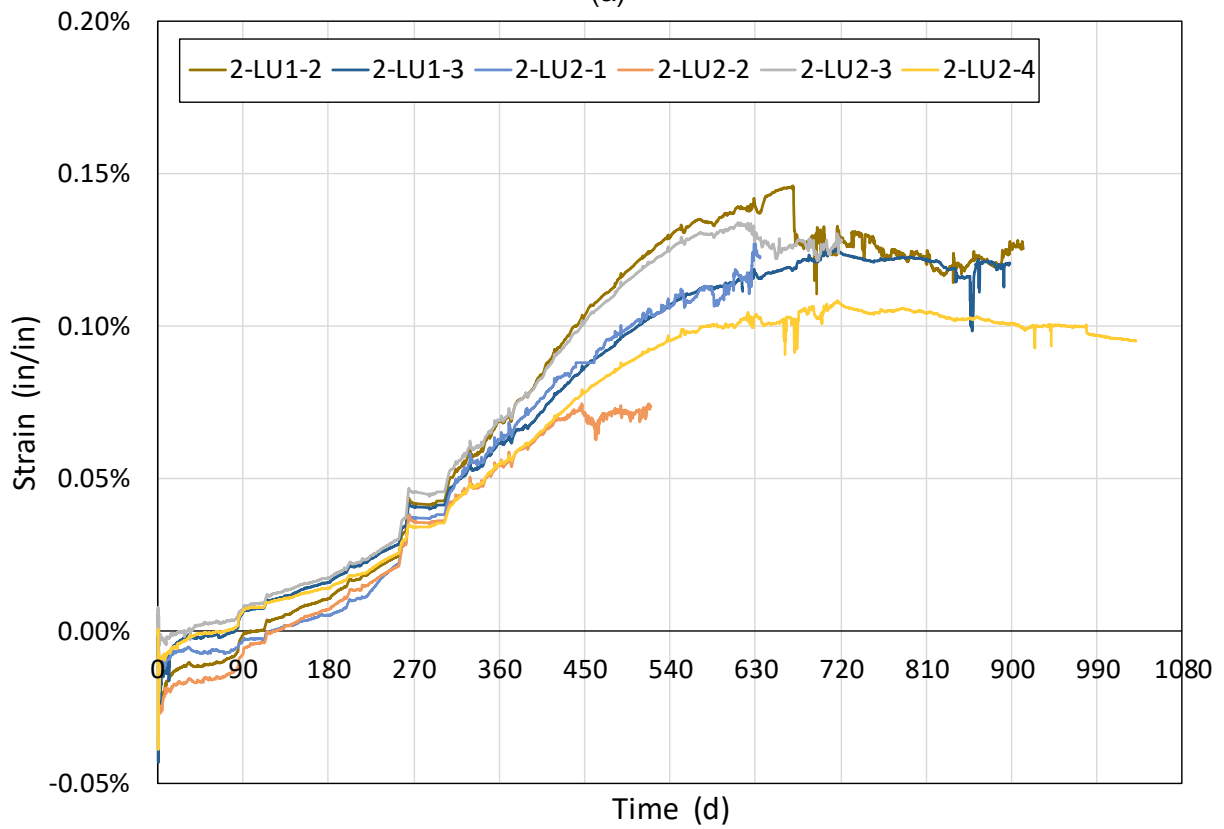


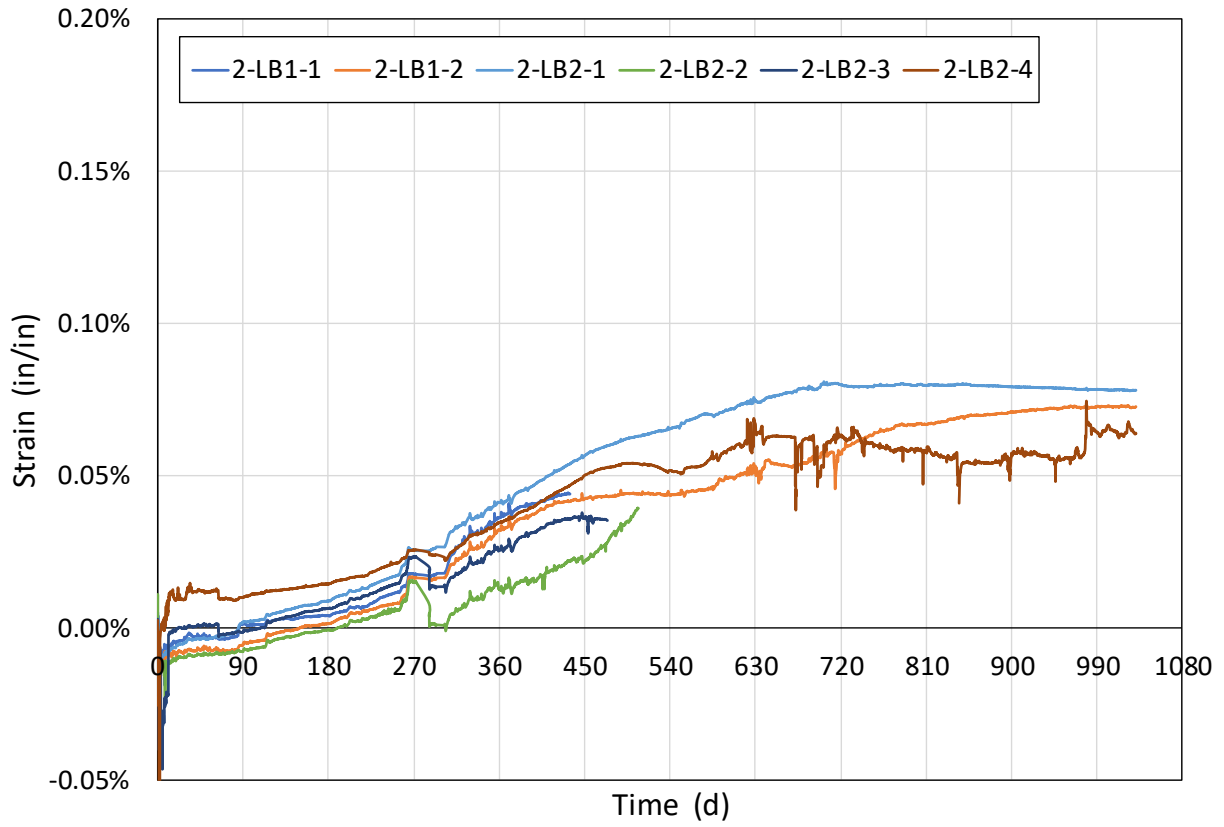
**Figure 3-5. Measured strains on reinforcing bars of Region 3 of block ASR 1: (a) longitudinal bars, (b) top corner bars, (c) bottom corner bars, (d) vertical legs of stirrups, (e) top horizontal leg of stirrups, (f) bottom horizontal leg of stirrups, and (g) cross ties**



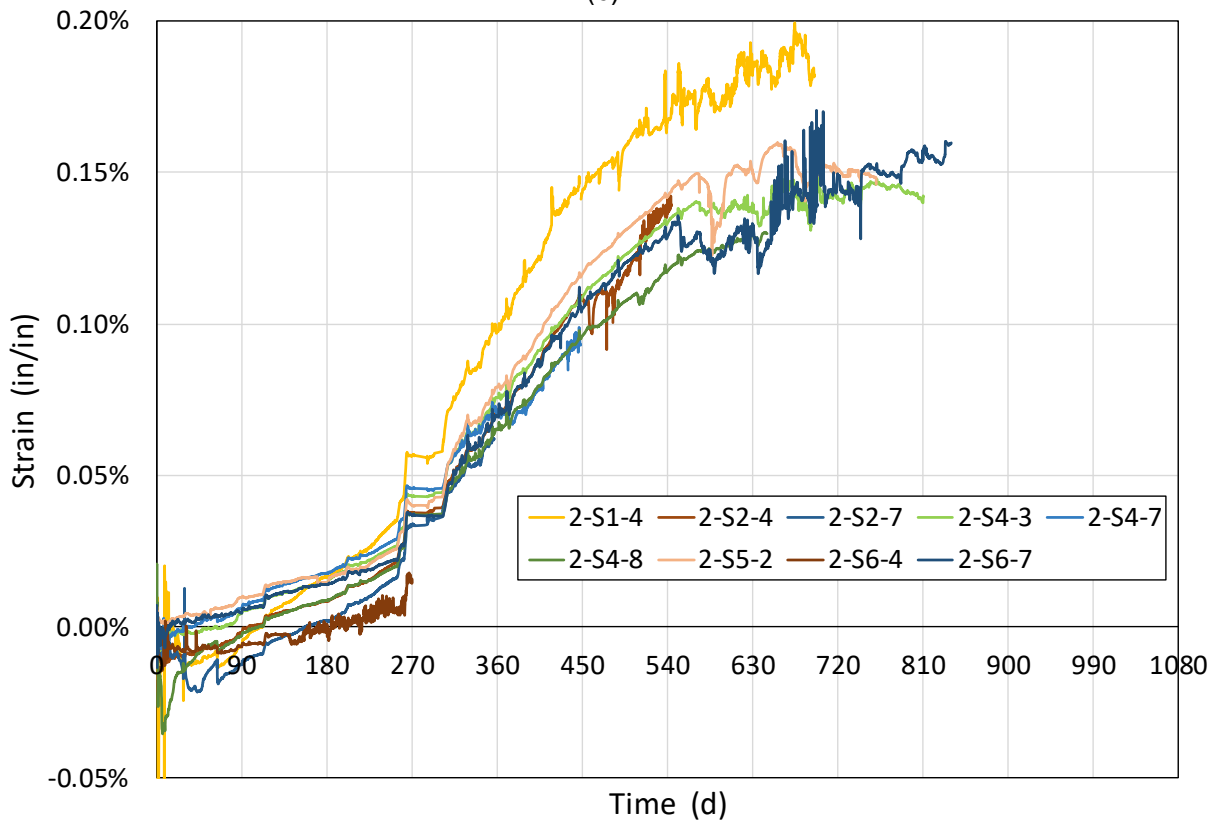
(a)



(b)



(c)



(d)

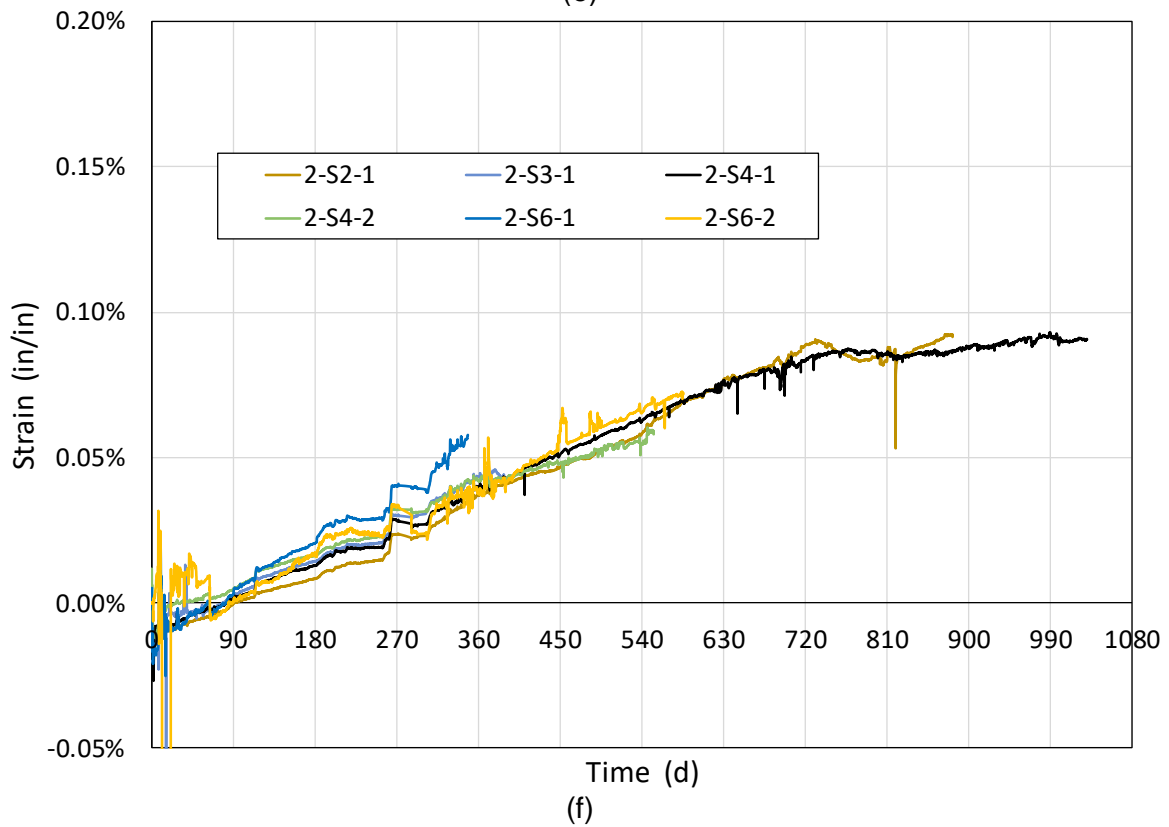
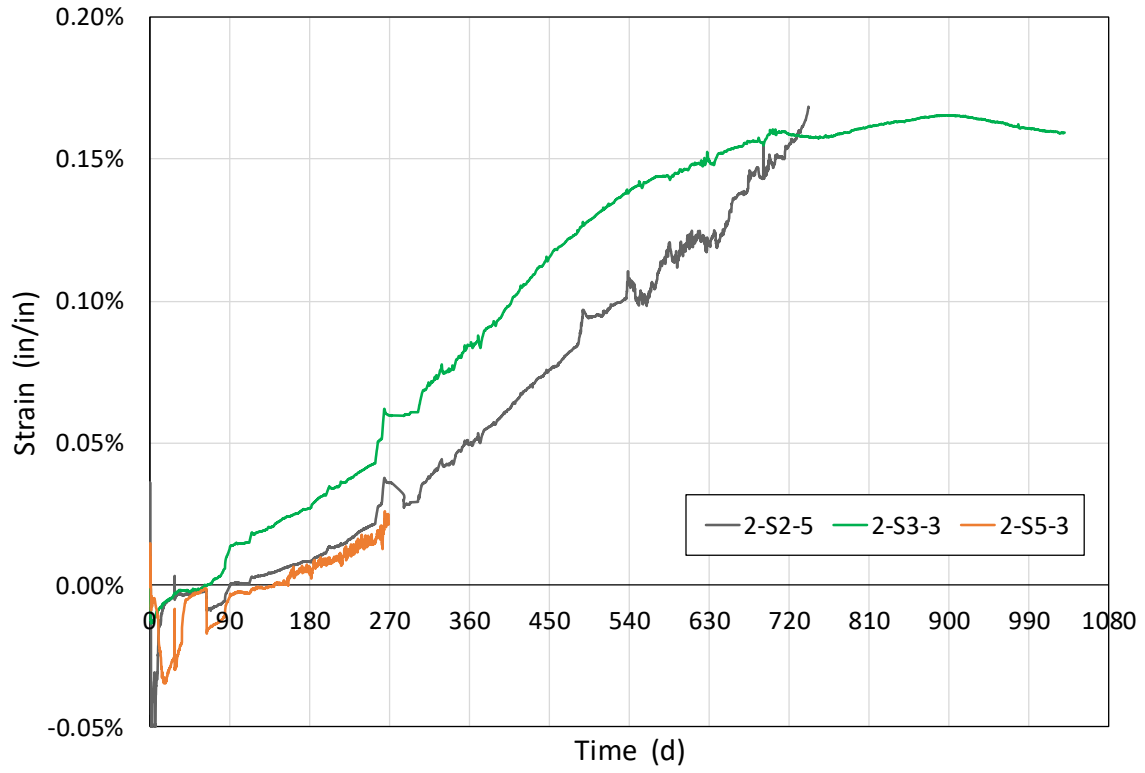


**Figure 3–6. Measured strains on reinforcing bars of Region 1 of block ASR 2: (a) longitudinal bars, (b) top corner bars, (c) bottom corner bars, (d) vertical legs of stirrups, (e) top horizontal leg of stirrups, and (f) bottom horizontal leg of stirrups**

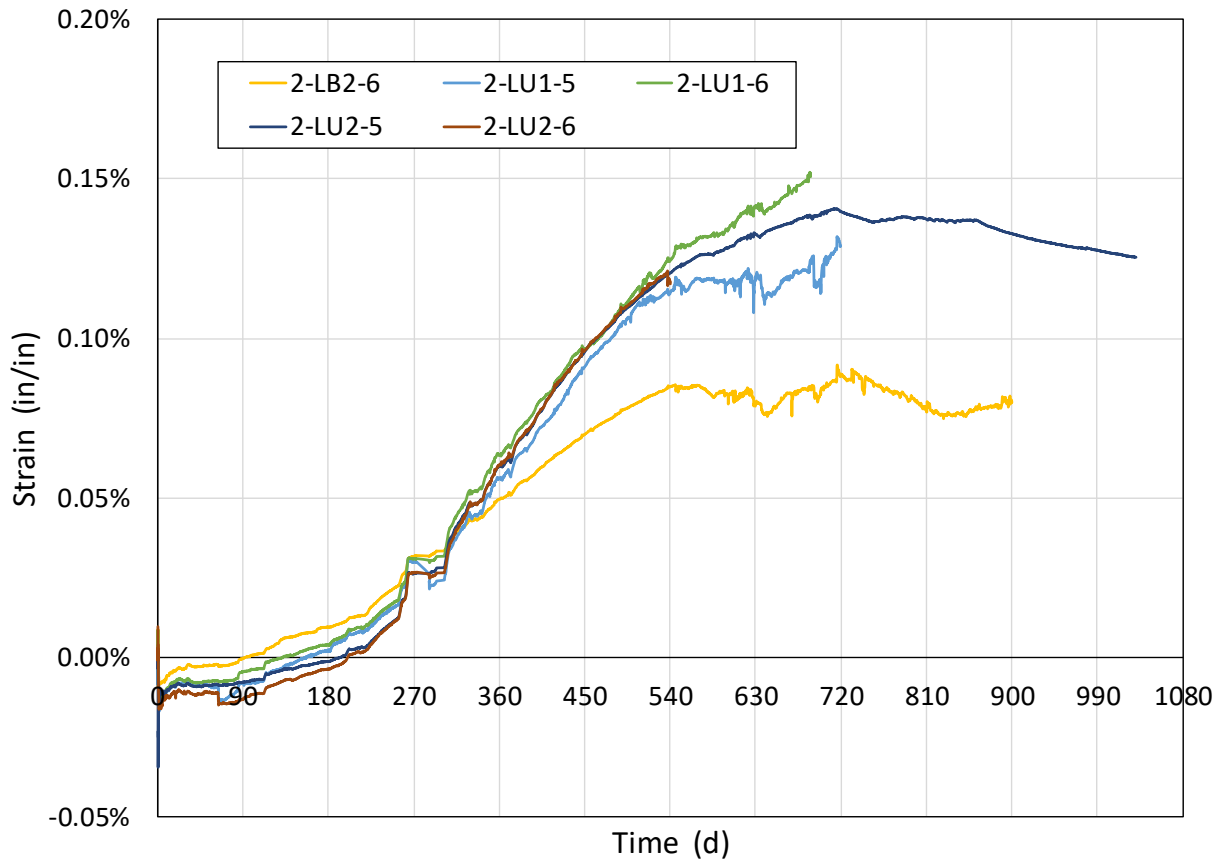
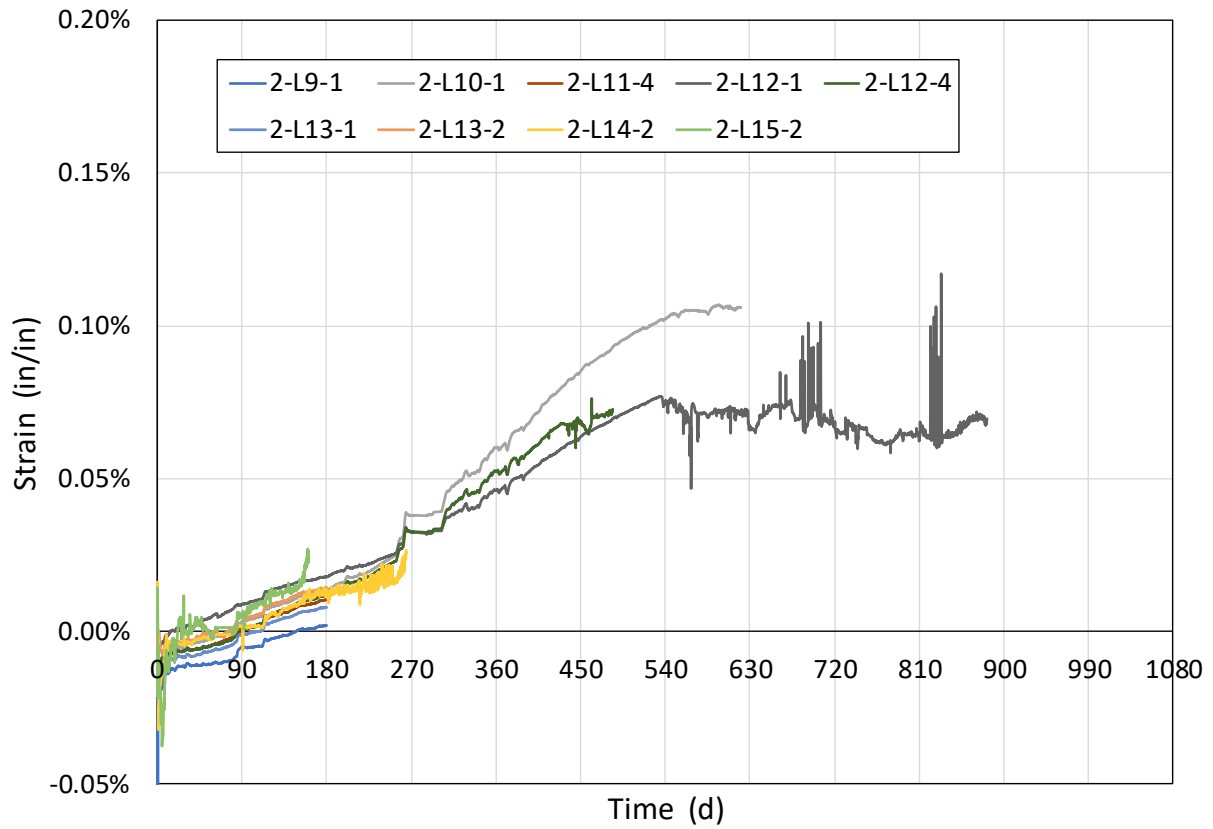
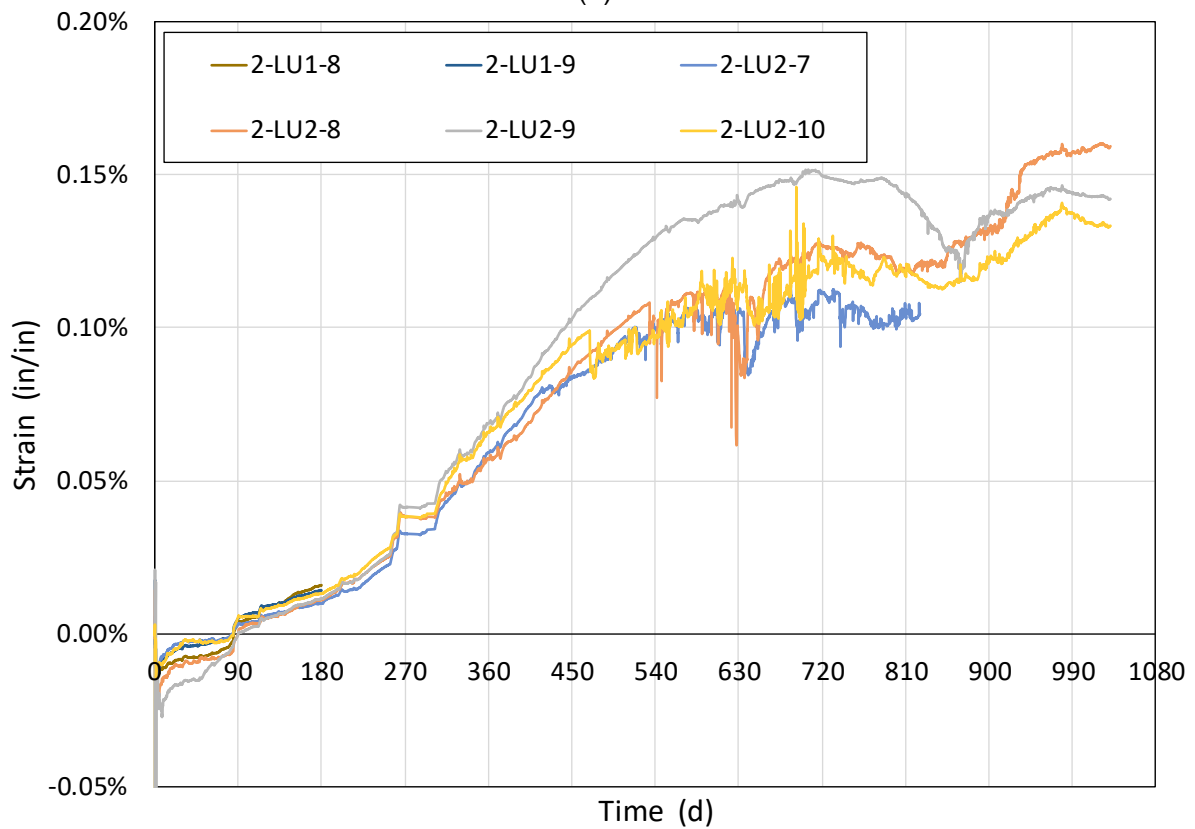


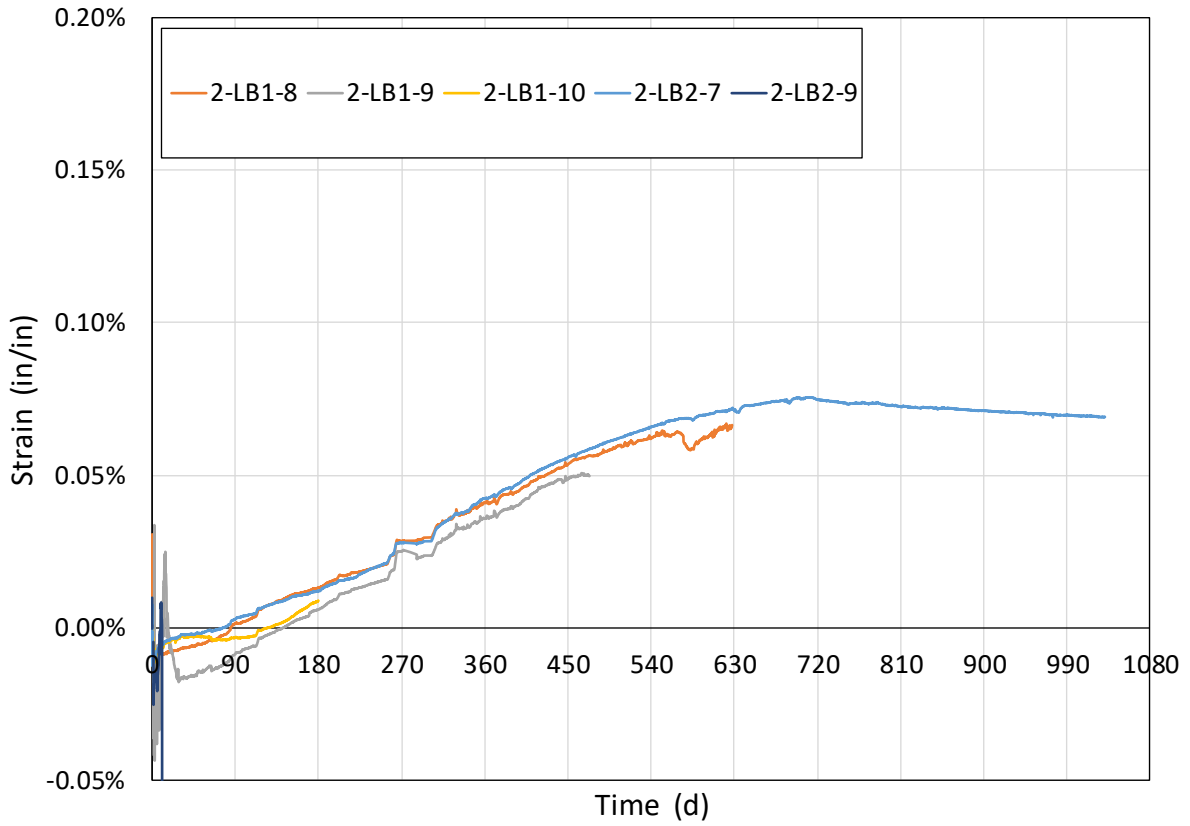
Figure 3–7. Measured strains on corner reinforcing bars of Region 2 of block ASR 2



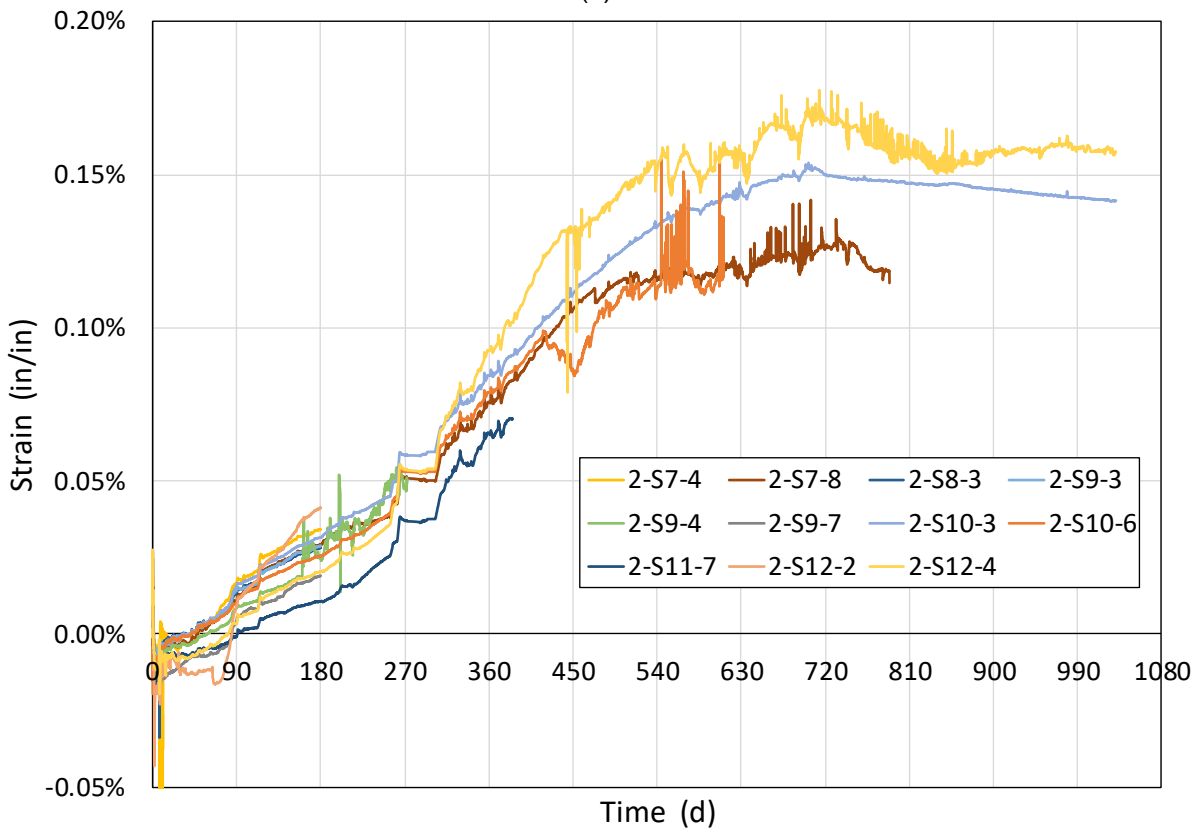
(a)



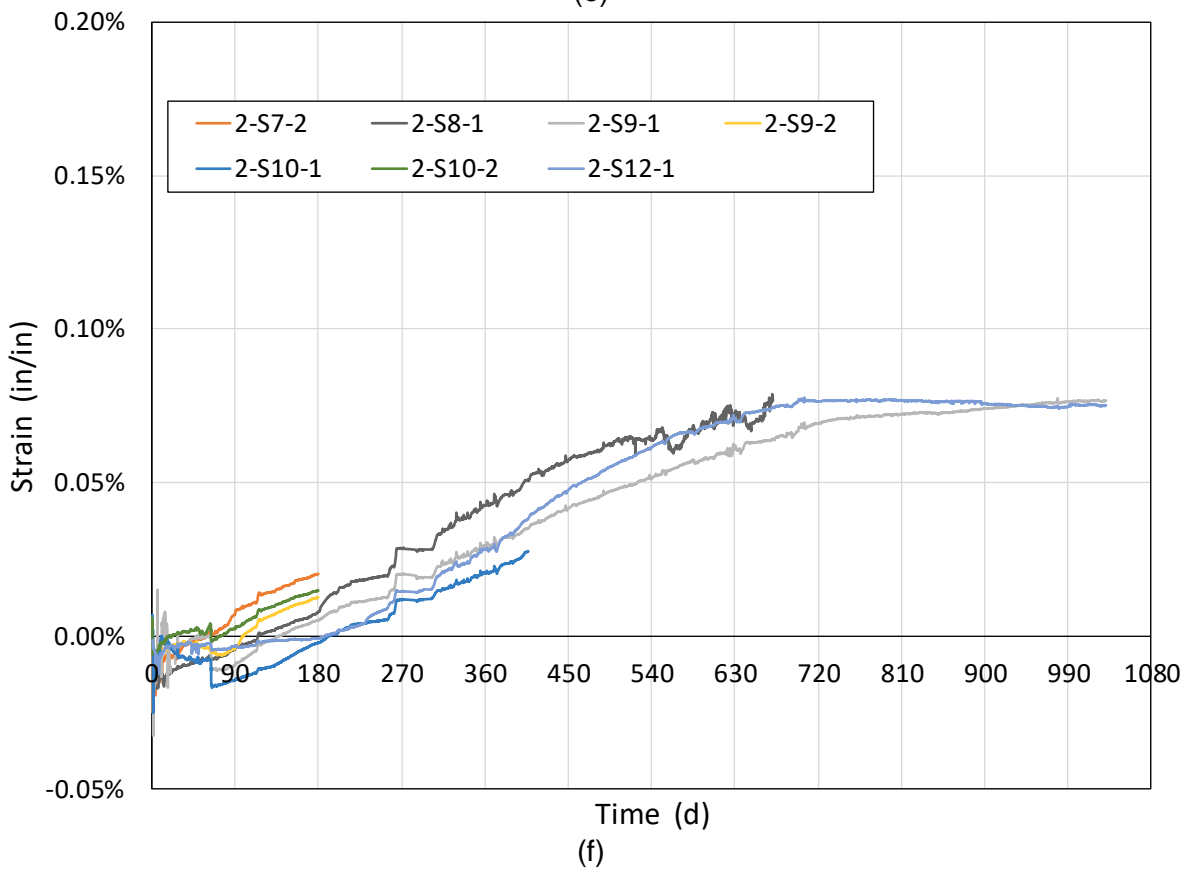
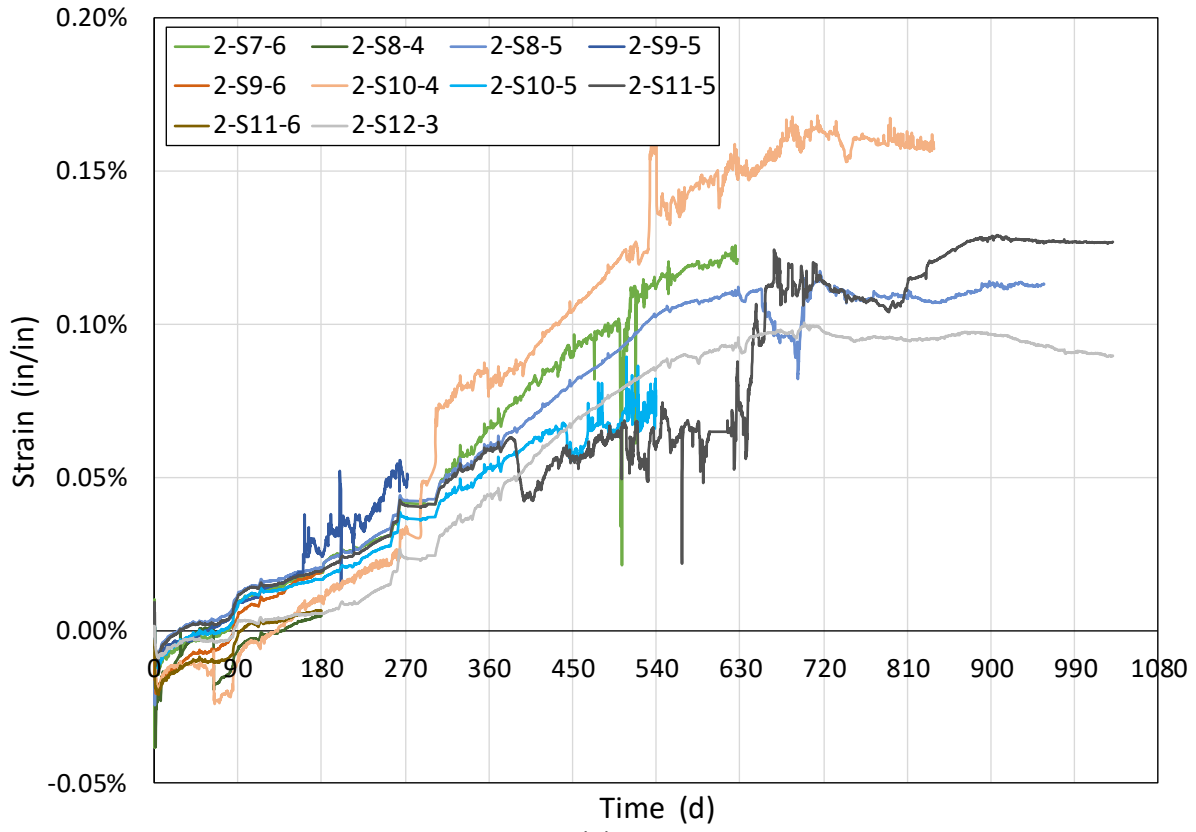
(b)



(c)



(d)



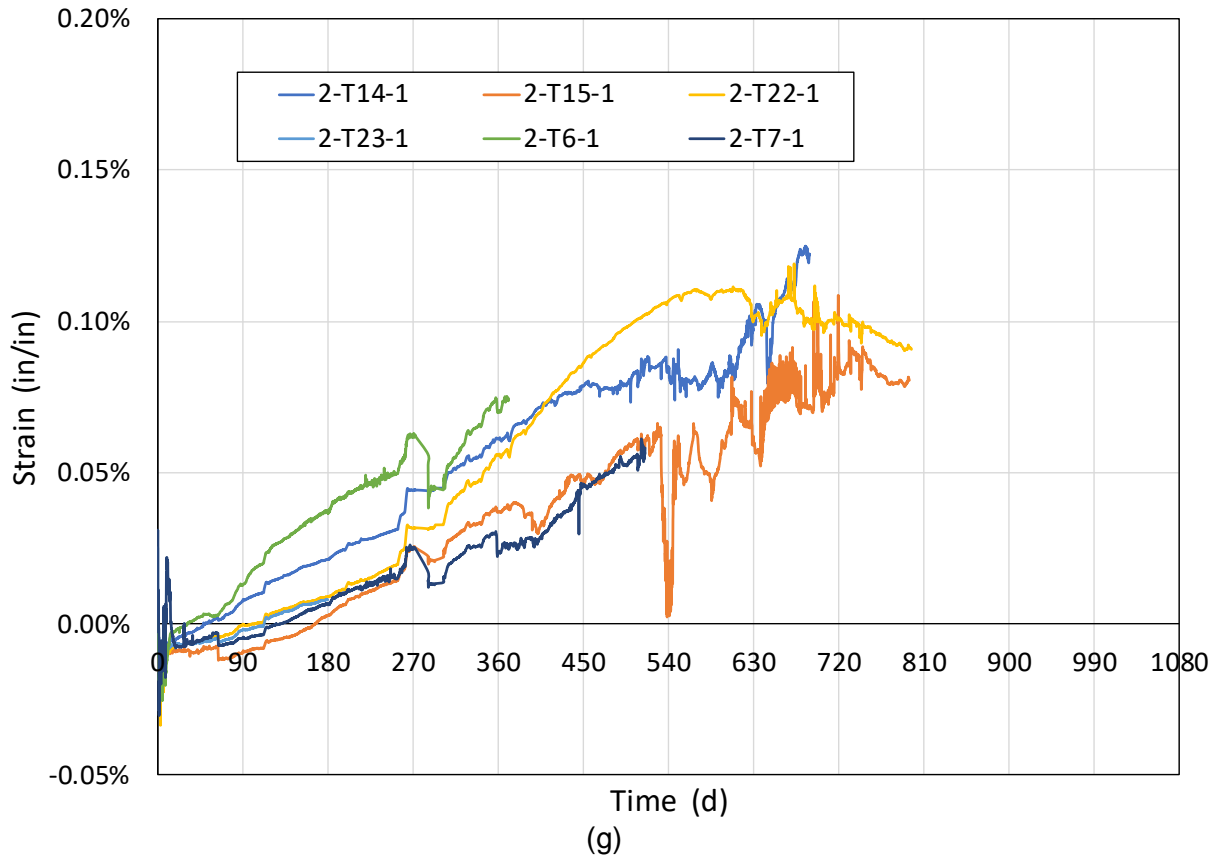
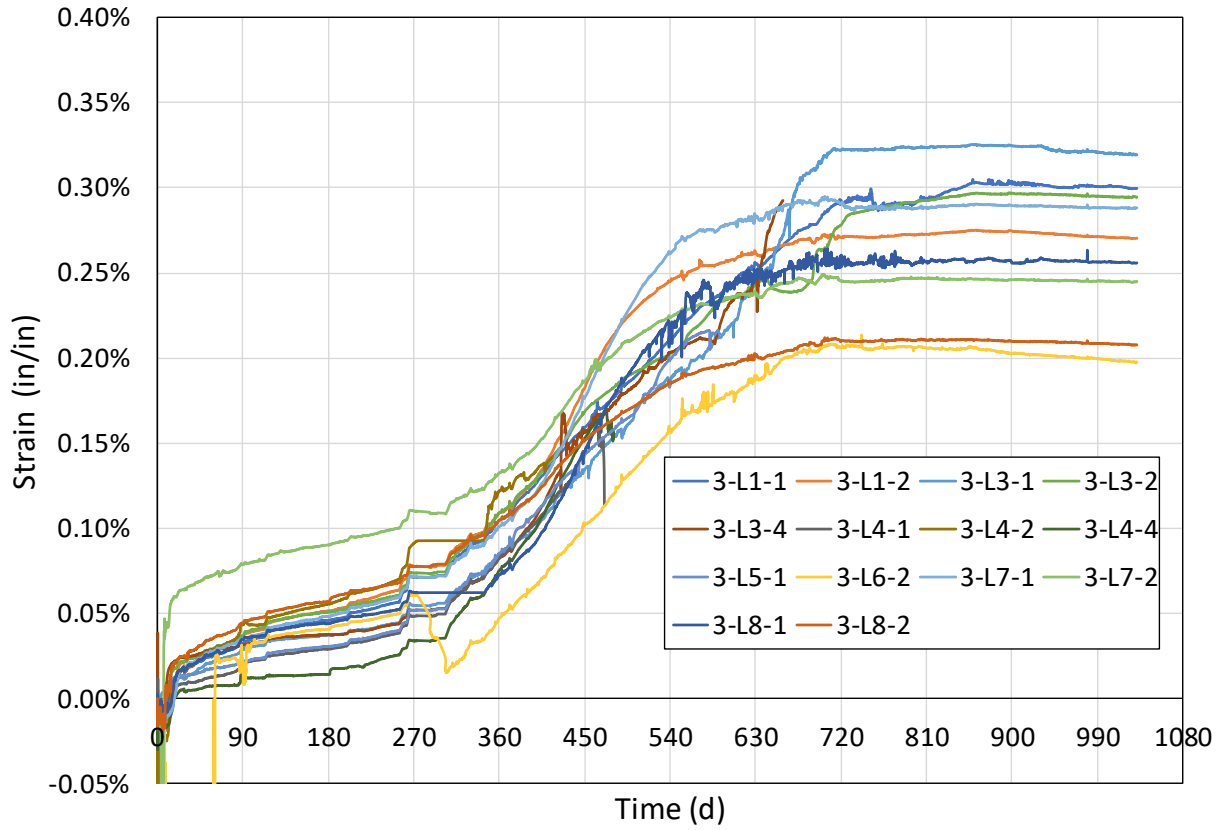
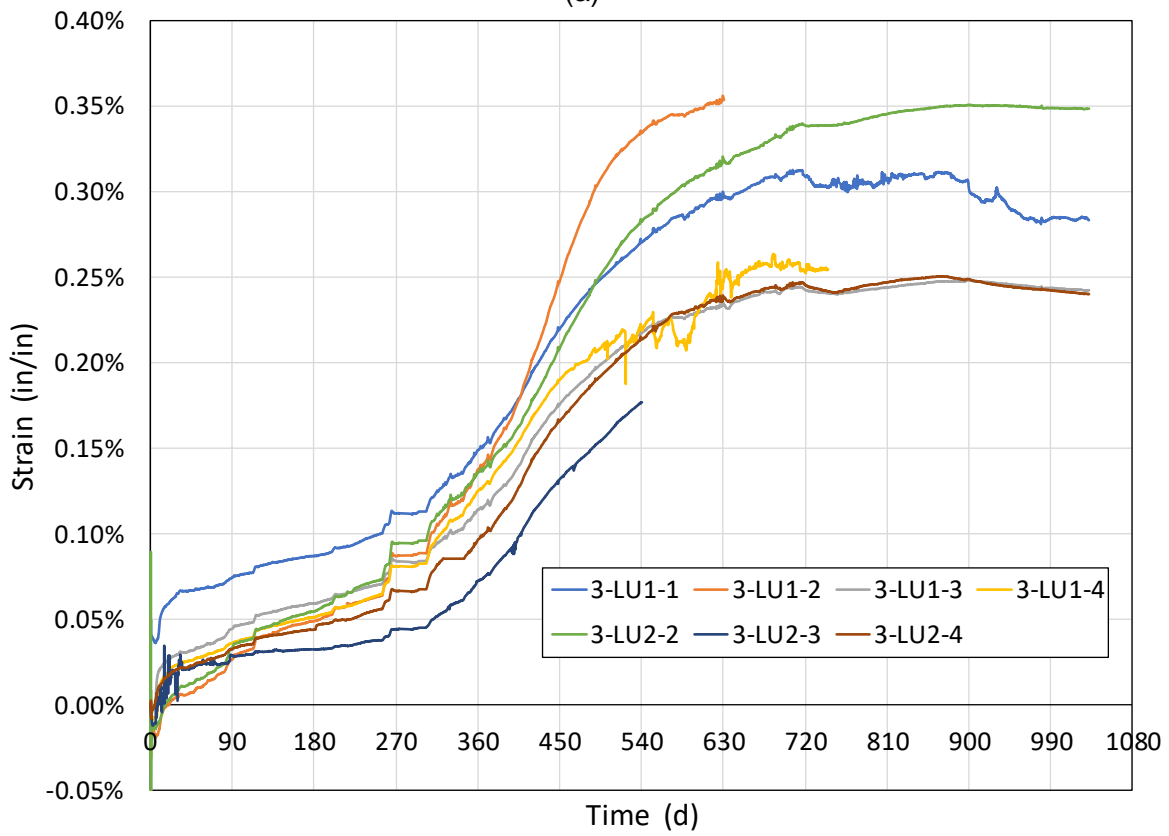


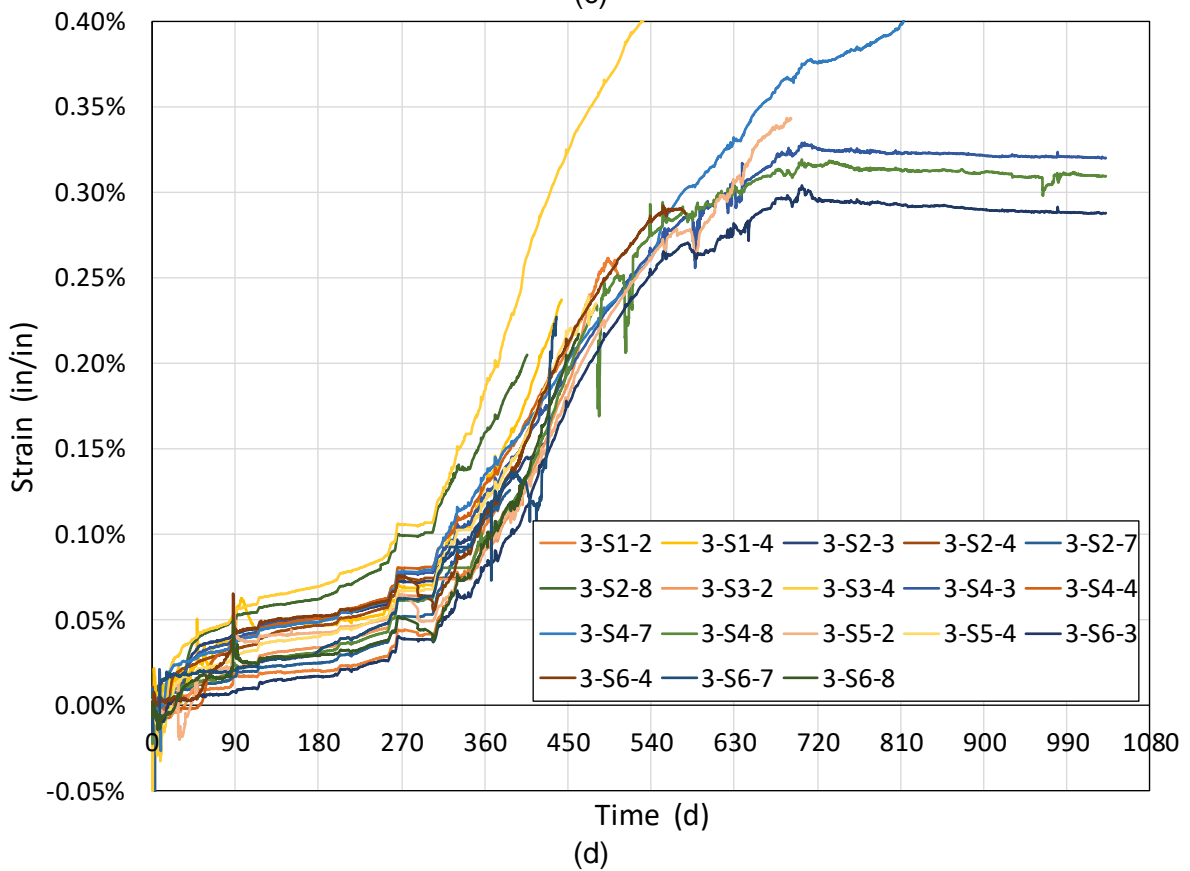
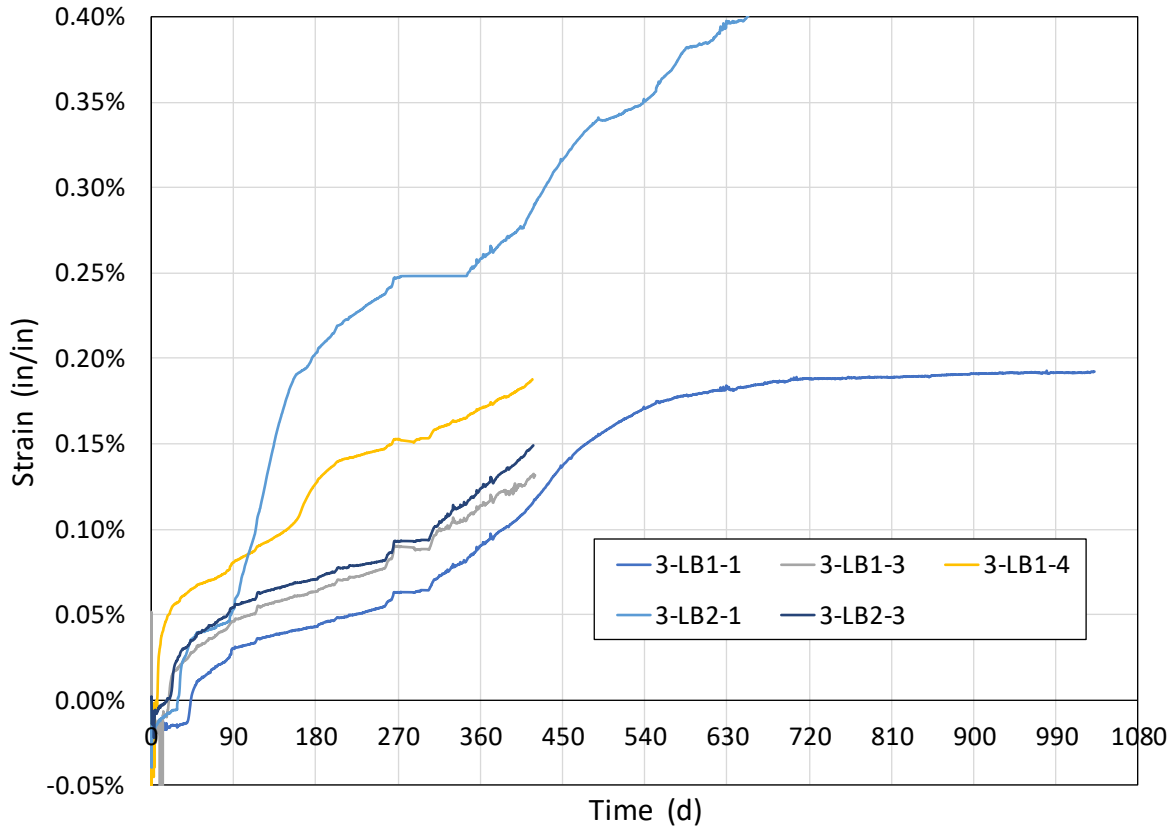
**Figure 3–8. Measured strains on reinforcing bars of Region 3 of block ASR 2: (a) longitudinal bars, (b) top corner bars, (c) bottom corner bars, (d) vertical legs of stirrups, (e) top horizontal leg of stirrups, (f) bottom horizontal leg of stirrups, and (g) cross ties**



(a)



(b)



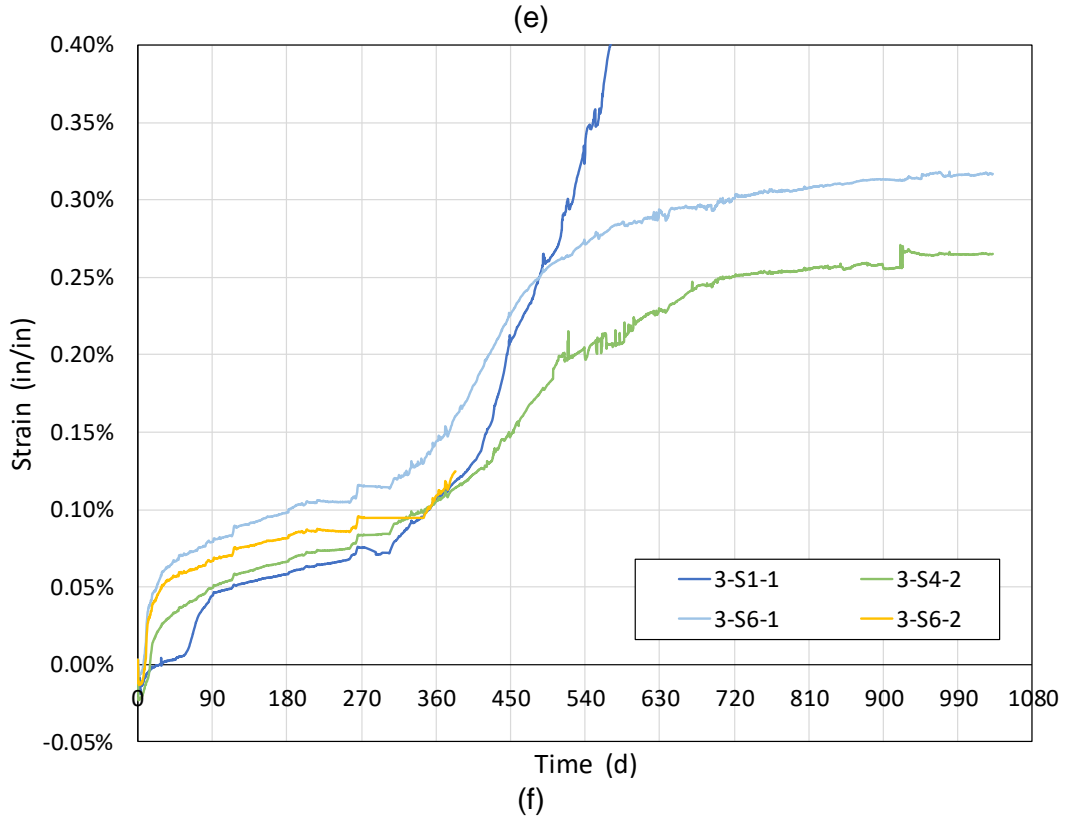
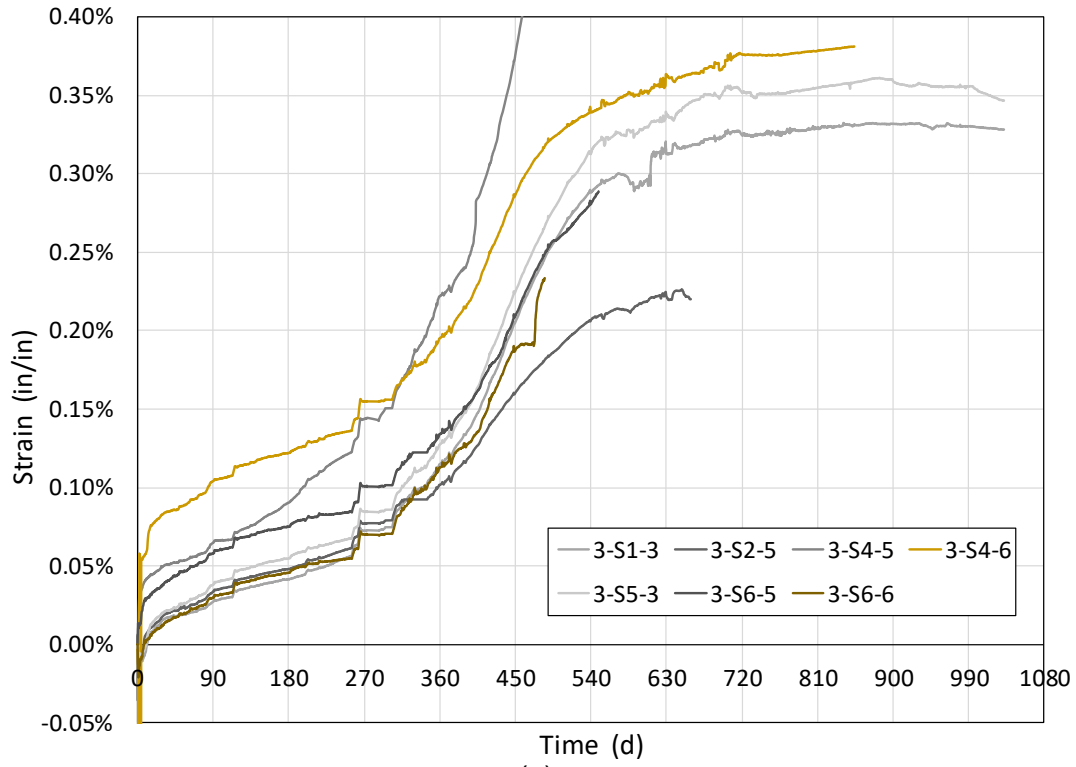


**Figure 3–9. Measured strains on reinforcing bars of Region 1 of block ASR 3: (a) longitudinal bars, (b) top corner bars, (c) bottom corner bars, (d) vertical legs of stirrups, (e) top horizontal leg of stirrups, and (f) bottom horizontal leg of stirrups**

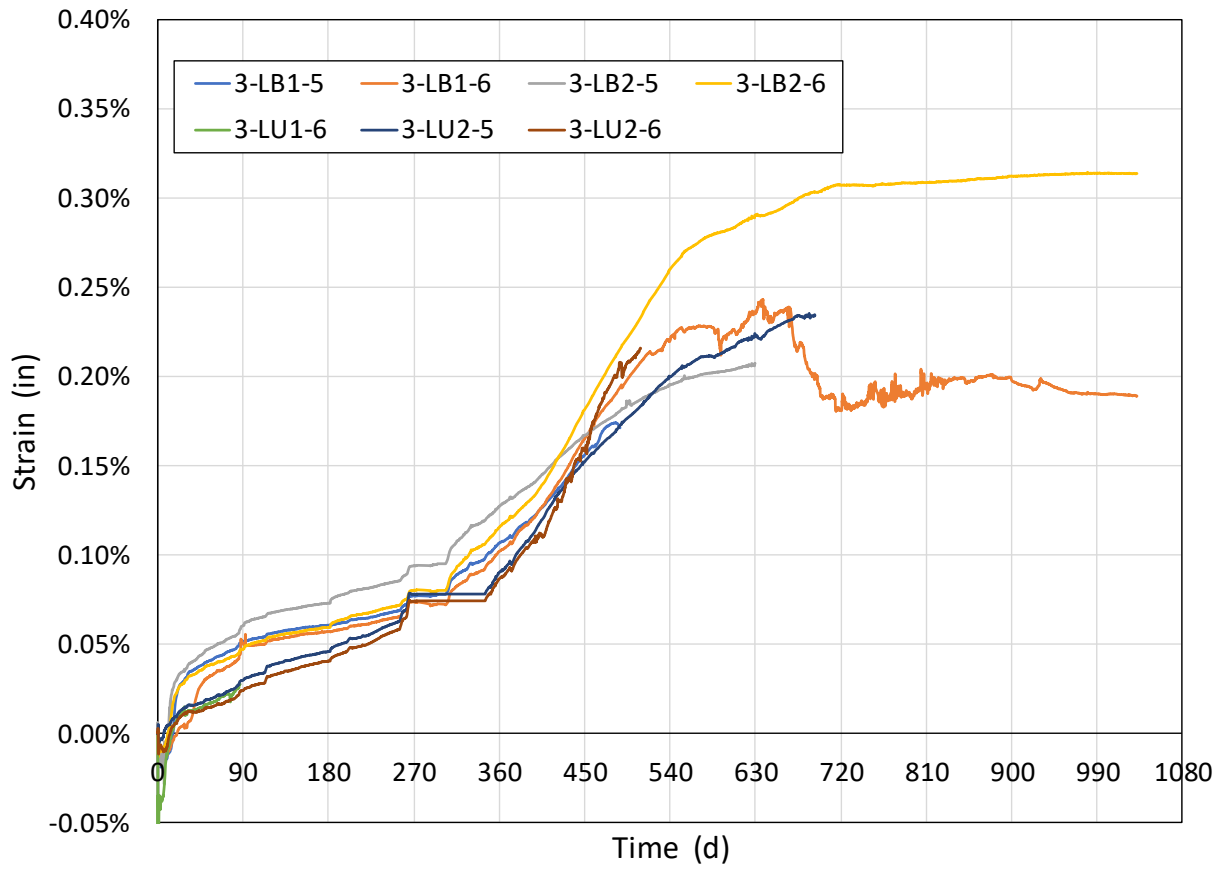
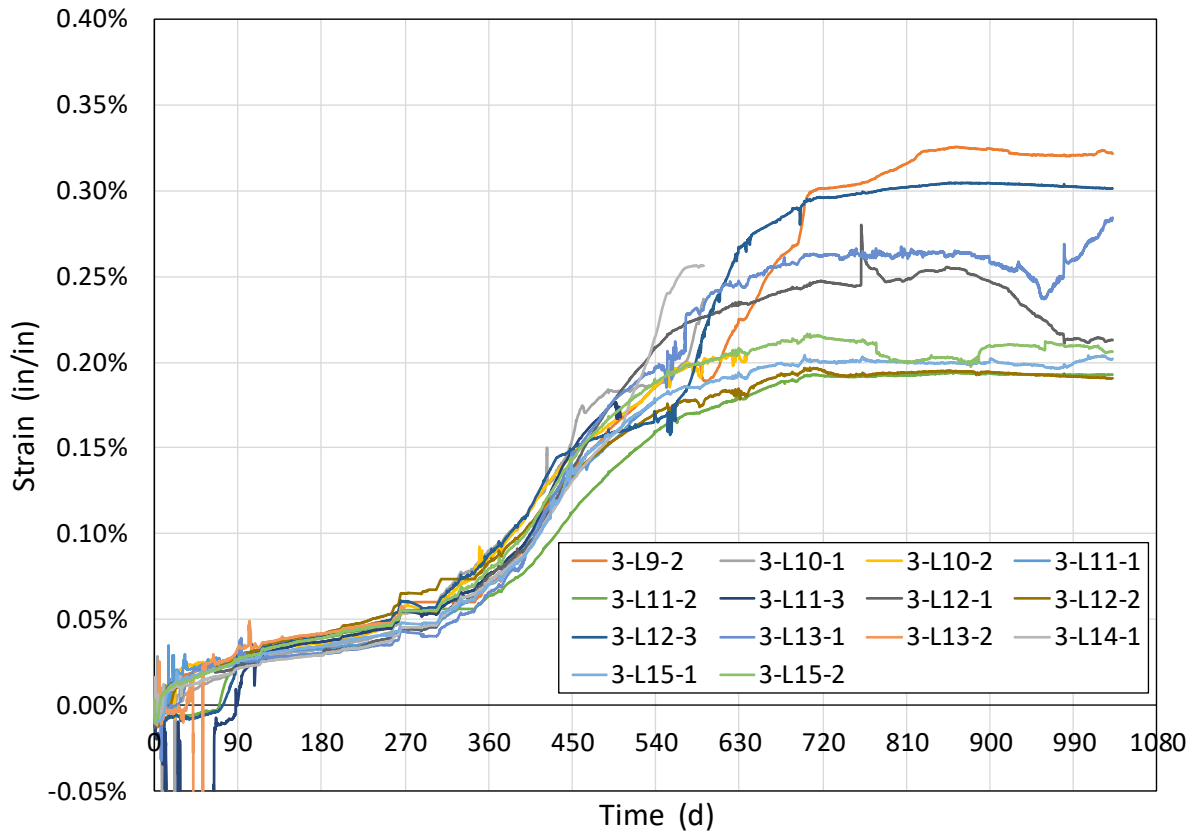
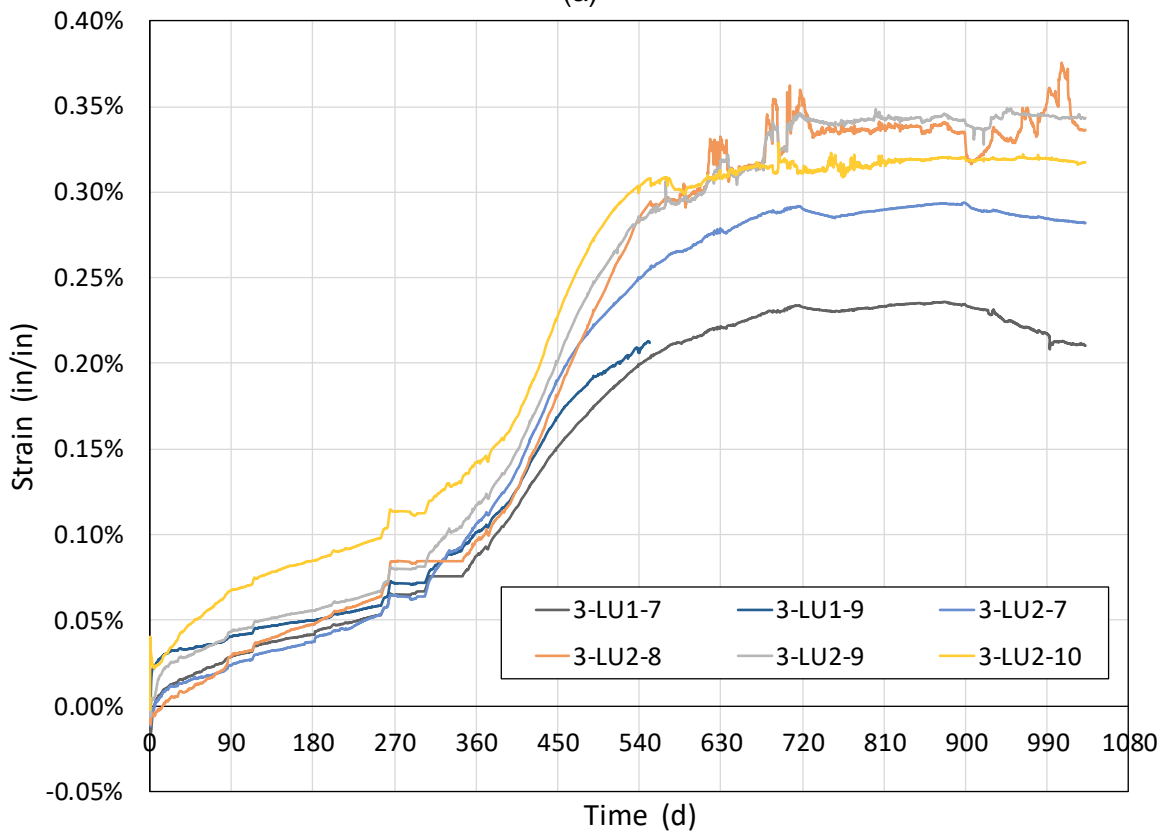


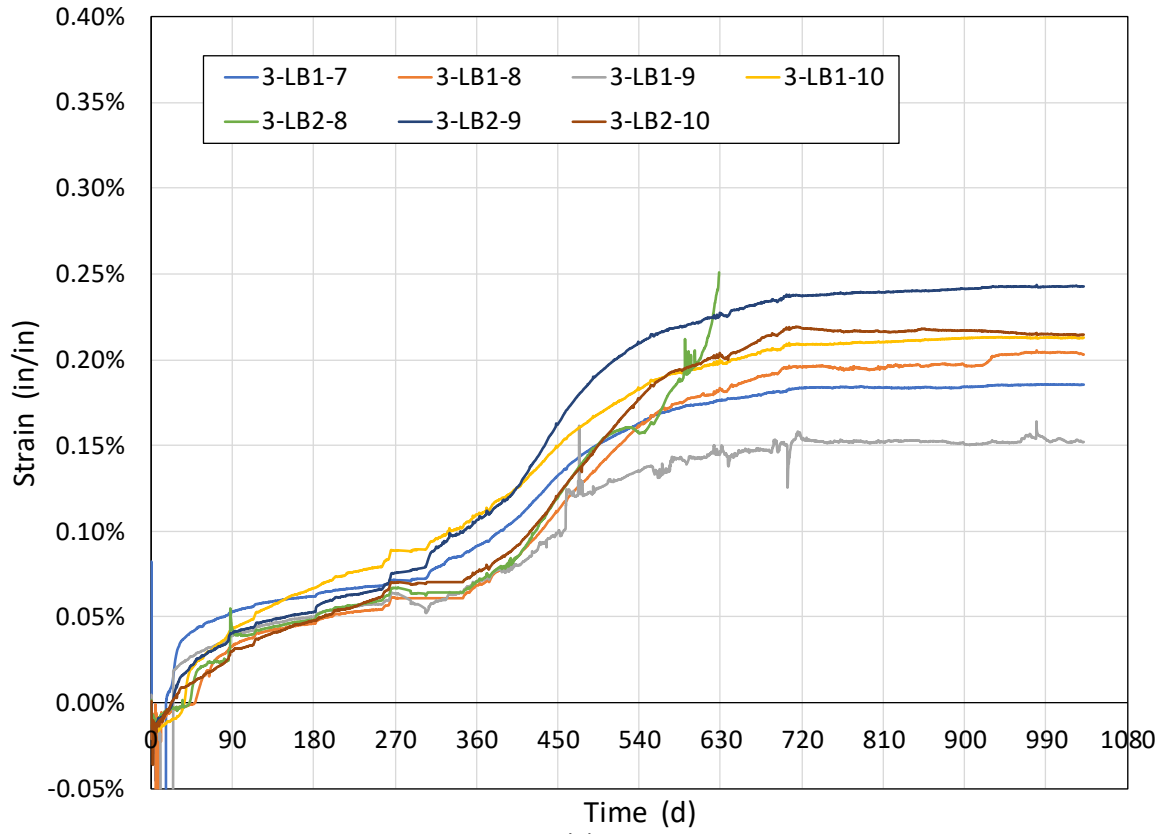
Figure 3–10. Measured strains on corner reinforcing bars of Region 2 of block ASR 3



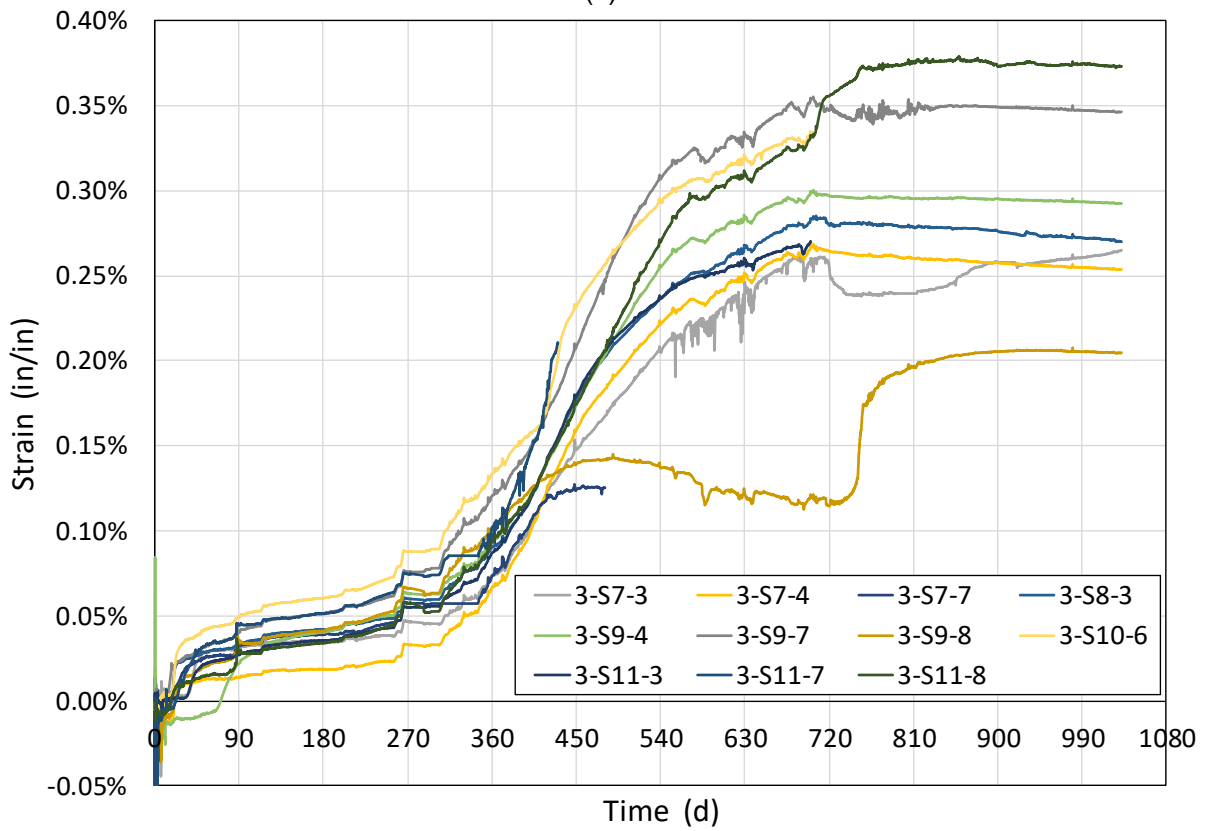
(a)



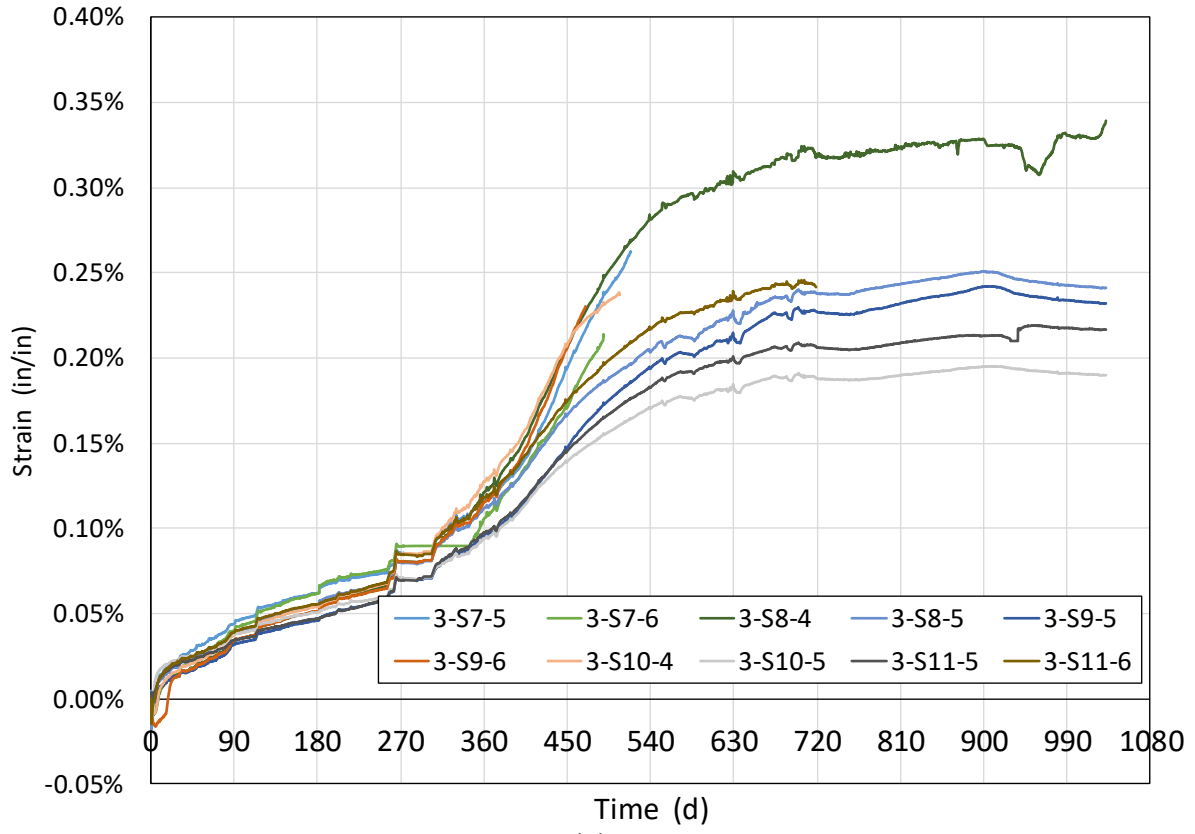
(b)



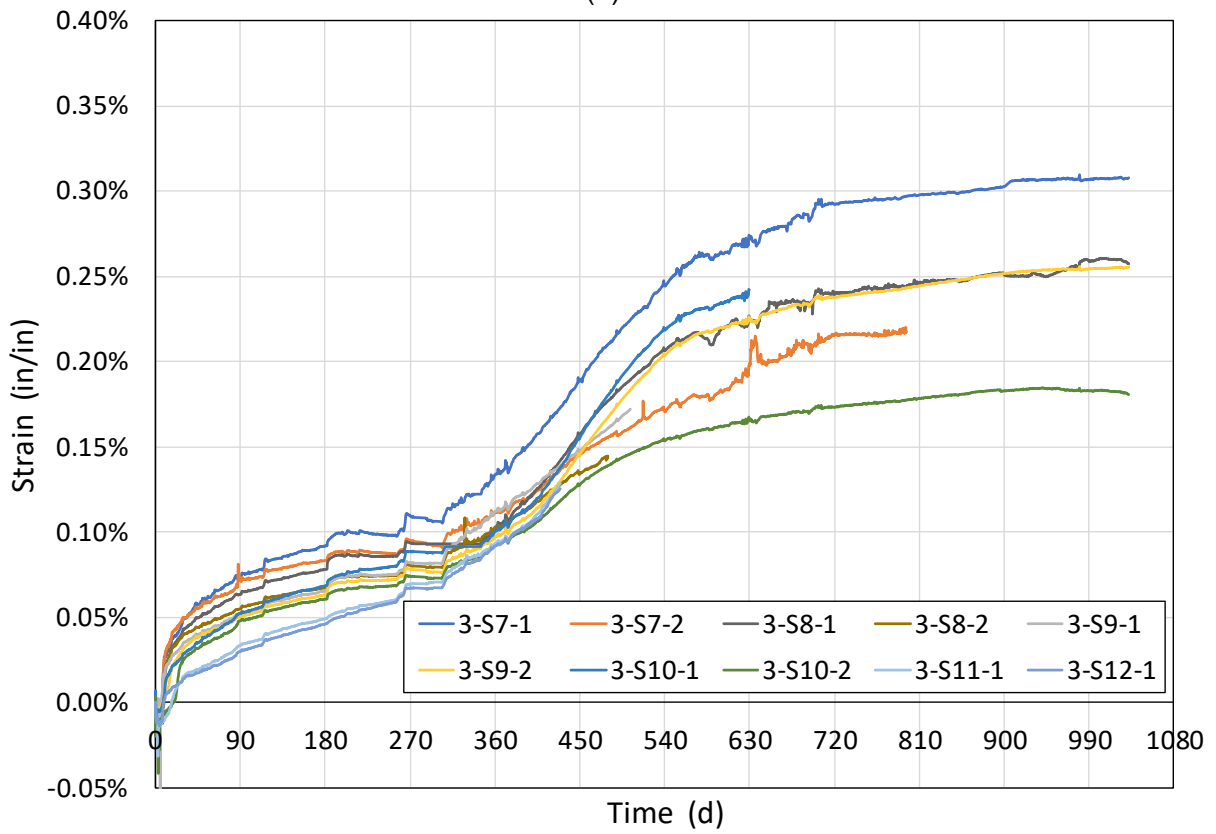
(c)



(d)



(e)



(f)

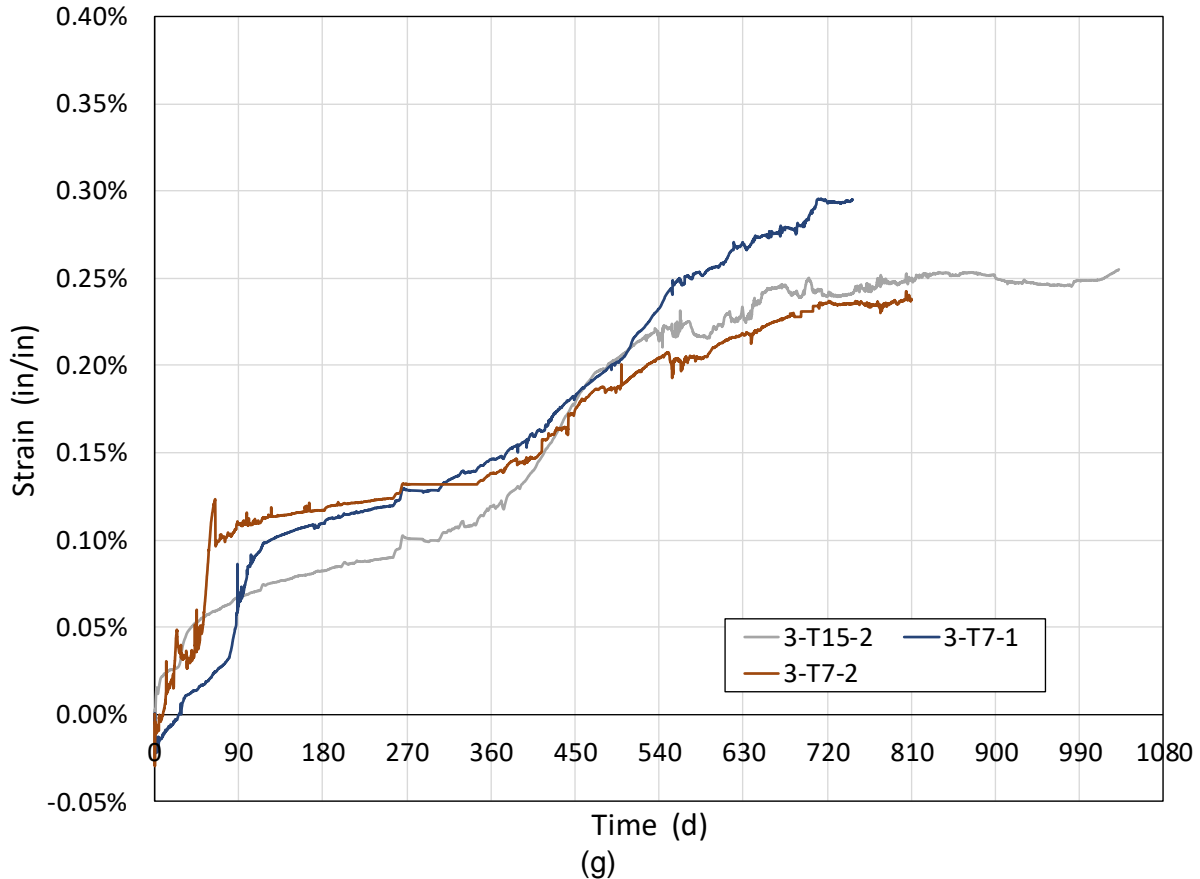


**Figure 3–11. Measured strains on reinforcing bars of Region 3 of block ASR 3: (a) longitudinal bars, (b) top corner bars, (c) bottom corner bars, (d) vertical legs of stirrups, (e) top horizontal leg of stirrups, (f) bottom horizontal leg of stirrups, and (g) cross ties**

As is normal in instrumentation using strain gages embedded in concrete, several strain gages were damaged and lost during concrete placement operation, and several others malfunctioned (loss of moisture protection causing short circuit or loss of bonding due to large strain) over the duration of this study. Gages that malfunctioned can be recognized in the figures by their incomplete data through the more than 1000 days of measurement. Despite these lost gages, due to the large redundancy in the layout of the strain gages, strain data of the surviving gages were sufficient to capture the strain distribution in all blocks. Based on the observed evolution of strain shown in Figures 3-3 to 3-11, the following general observations were made:

- Strain data for all blocks showed an initial shrinkage characterized by negative strain values, which is typical of the concrete hydration and hardening process. Negative strains lasted for up to 90 days, particularly for blocks ASR 1 and ASR 2. With the start of the ASR reaction, the strains became positive, signifying an ASR-induced axial elongation of the reinforcing bars. Strain gages on the reinforcing bars of block ASR 3, the most reactive of the three reactive specimens, were the first to switch signs from negative (shrinkage) to positive (expansion).
- The influence of the curing conditions on ASR-induced concrete expansion is clearly evident as shown in the strain-time histories of the reinforcing bars. The strains “took off”

(i.e., the rate of accumulation of strains rapidly increased) after 180 days following the start of curing Phase 3 (RH in excess of 95 % and temperature of 75 °F to 80 °F). Strains had an even higher rate of increase during Phase 4 of curing (RH in excess of 95 % and temperature of 100 °F to 110 °F).

- Measured strains on the reinforcing bars of the three reactive blocks show a general trend of plateauing (flattening) between 630 days and 720 days, signifying that the ASR expansion has reached its ultimate value and that the expansion has stopped.
- While the cross section of the blocks was symmetric around the vertical axis, no symmetry was observed in the measured strains for the three reactive blocks. Compare for example the strains on the odd-numbered longitudinal bars with those on their even-numbered counterparts, and a large discrepancy would be observed. Similarly, a comparison of the strains on both vertical legs of the stirrups would reveal a lack of symmetry in the measured strains. This may be attributed to (1) a non-uniform ASR expansion and (2) to a lesser extent the effects of uneven, unsymmetrical extraction of the core samples from the block specimens.
- In general, for a given block, the strains in the intermediate confinement Region 1 were slightly larger than those in the heavy confinement Region 3. Compare for example plots (a), (b), (d), (e), and (f) in Figure 3-3 with their counterparts in Figure 3-5. This trend is consistent across the reactive blocks and was expected due to the larger confinement in Region 3 compared with Region 1.
- In general, for a given block and a given Region, the strains on the bottom reinforcing bars were smaller than those on bars located at higher elevation. Compare for example plots (b) for top corner bars with plots (c) for bottom corner bars or plots (e) for stirrups' top leg versus plots (f) for stirrups' bottom leg. This may be due to the friction provided by the ground and/or the larger compaction and overburden pressure on the lower portion of the block, which may have resulted in more restraint and lesser expansion at lower elevation (ACI 207.2R-07, 2007).
- A comparison of the strains in the three blocks indicated that block ASR 3 exhibited the largest expansion of all reactive blocks. Blocks ASR 1 and ASR 2 had somewhat similar expansion values.
- Examination of the strains on the reinforcing bars in the three reactive blocks revealed that the majority of the bars in the highest reactive block ASR 3 had yielded at some point during the duration of Task 1 with strains in excess of their yield strain of typically 0.20 % to 0.23 %. A few reinforcing bars in least reactive block ASR 1 had experienced yielding, while it does not seem that the reinforcing bars in the intermediate reactive block ASR 2 had experienced any yielding.

It is important to note that the measured strains on the reinforcing bars do not represent the unconfined (free) ASR expansion of concrete, but rather the structural response to the ASR-induced expansion at the locations of the reinforcement, with inherent accounting for confinement effects, stress condition and structural deformations, and possible degradation of bond between the concrete and the reinforcement (bond-slip behavior).

For the control block, Figure 3-12 shows the strain development on the reinforcing bars (strain gage locations and nomenclature are shown in Figure 2-5 and Appendix A). The figure shows an

initial shrinkage characterized by negative strain values of up to 0.05 %, which is typical of the concrete hydration and hardening process. Negative strains lasted for a long period of time and later switched to slight expansion with strains of no more than 0.025 %.

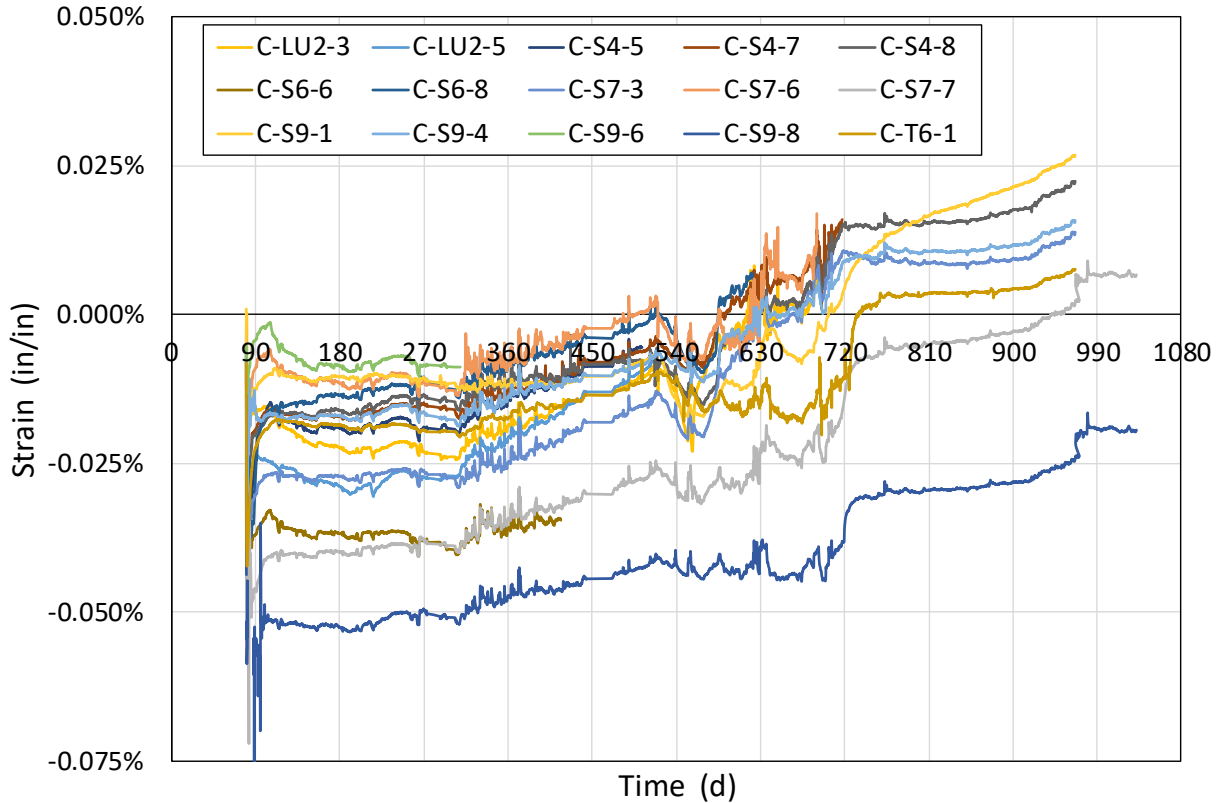


Figure 3–12. Measured strains on reinforcing bars for the control block

### 3.2.2 Strains in Concrete

Strain development in concrete at the center of the blocks was continually monitored and recorded using the tri-directional concrete strain transducers (see Section 2.3.2). Similar to strain gage data on reinforcing bars, concrete strain data were automatically recorded every 12 minutes on average throughout the duration of this study. The post-processing of the concrete strain data followed the same procedure as that described for the reinforcing bars' strain data, i.e., averaging, stitching, and visual inspection to eliminate erratic data. In addition, a correction for 80 days of missing data was applied. Between 265 days and 345 days after casting of reactive block ASR 3, the data acquisition cards for all full-bridge strain transducers malfunctioned and data was subsequently not recorded. Despite attempts to fix the issue, data were missed for these 80 days until the problem was resolved. To correct for the missing data, the rate of the strain development just prior to the missing data ( $r_1$ ) and immediately after fixing the problem ( $r_2$ ) were estimated for each gage. It was assumed that the rate  $r_1$  was constant for the first 25 days (265 days to 290 days) and rate  $r_2$  was constant for the last 25 days (320 days to 345 days). For the middle 30 days (290 days to 320 days), a constant rate of  $(r_1 + r_2) / 2$  was used. This data correction resulted in a smooth strain development for the 80-days period of missing data.

Figures 3-13, 3-14, and 3-15 show the evolution of the strains at the center of the three reactive blocks ASR 1, ASR 2, and ASR 3, respectively. Strain transducer locations in the three reactive block specimens and nomenclature are shown in Figure 2-4. In all plots, positive and negative strain values signify tensile strains (expansion) and compressive strains (shrinkage), respectively. Strain transducers inside the control block did not show any significant expansions and their data is not shown.

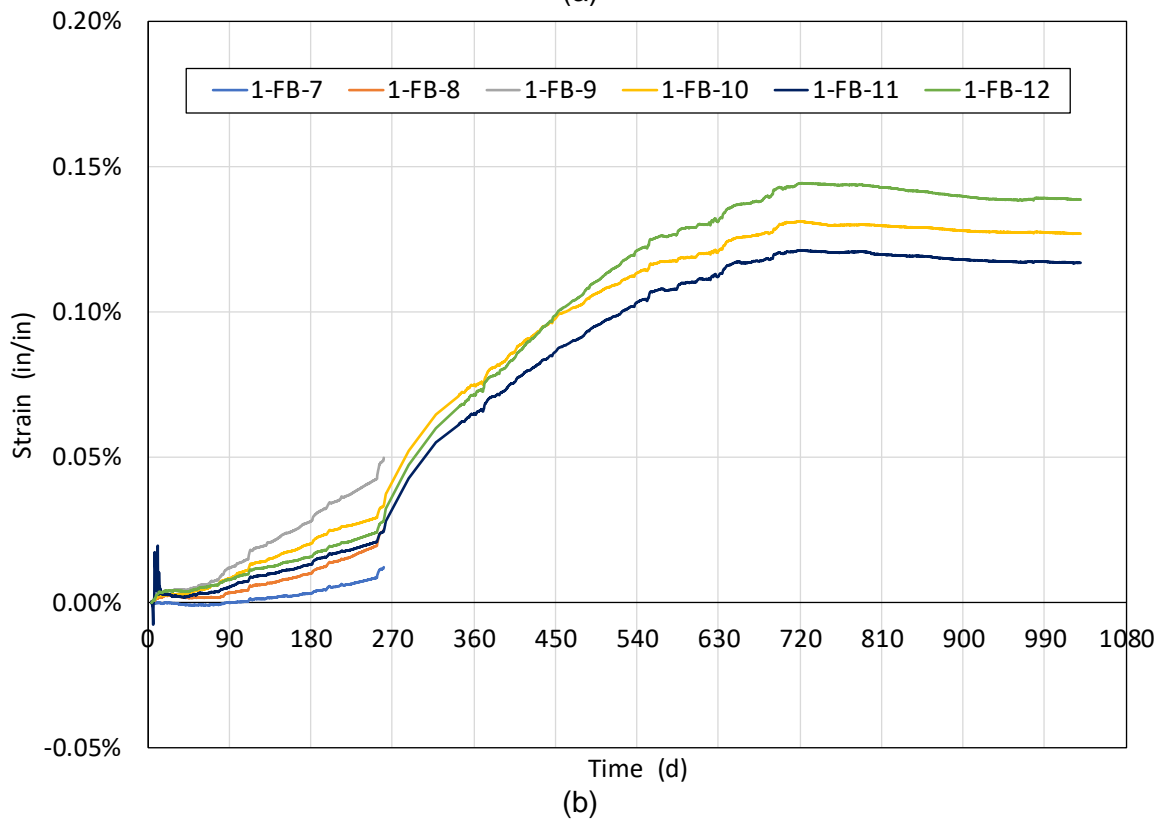
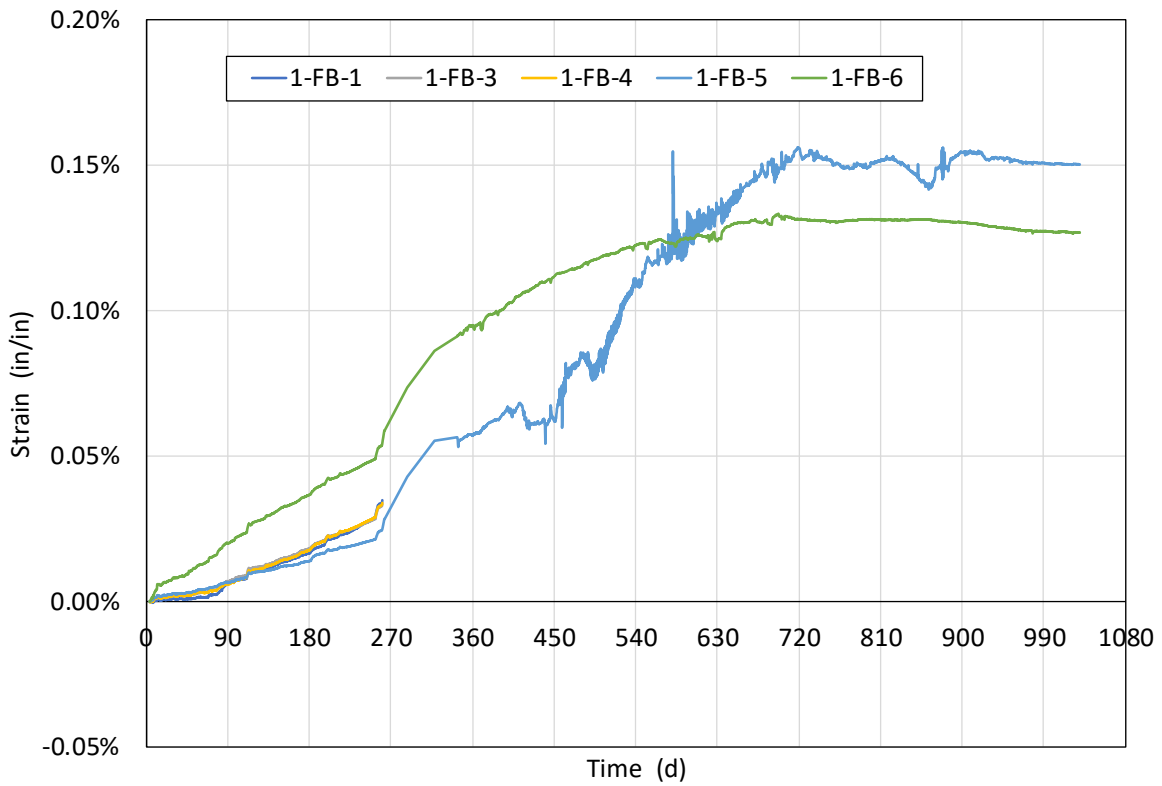
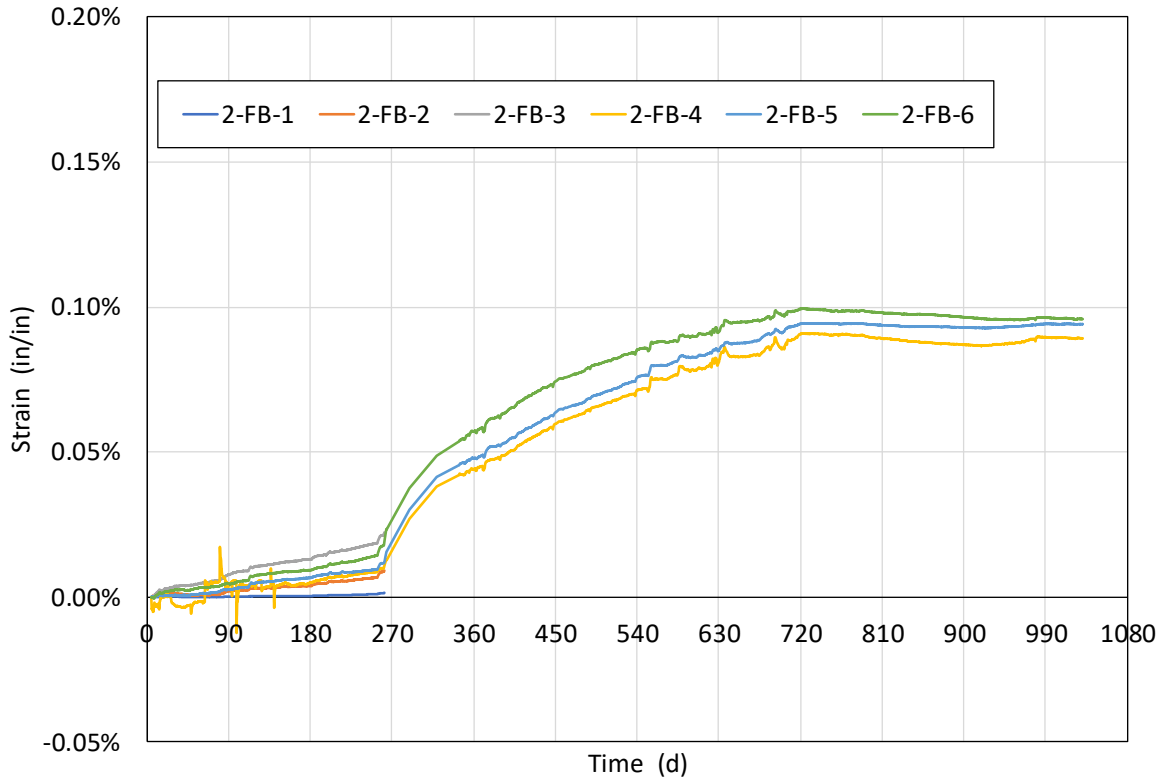
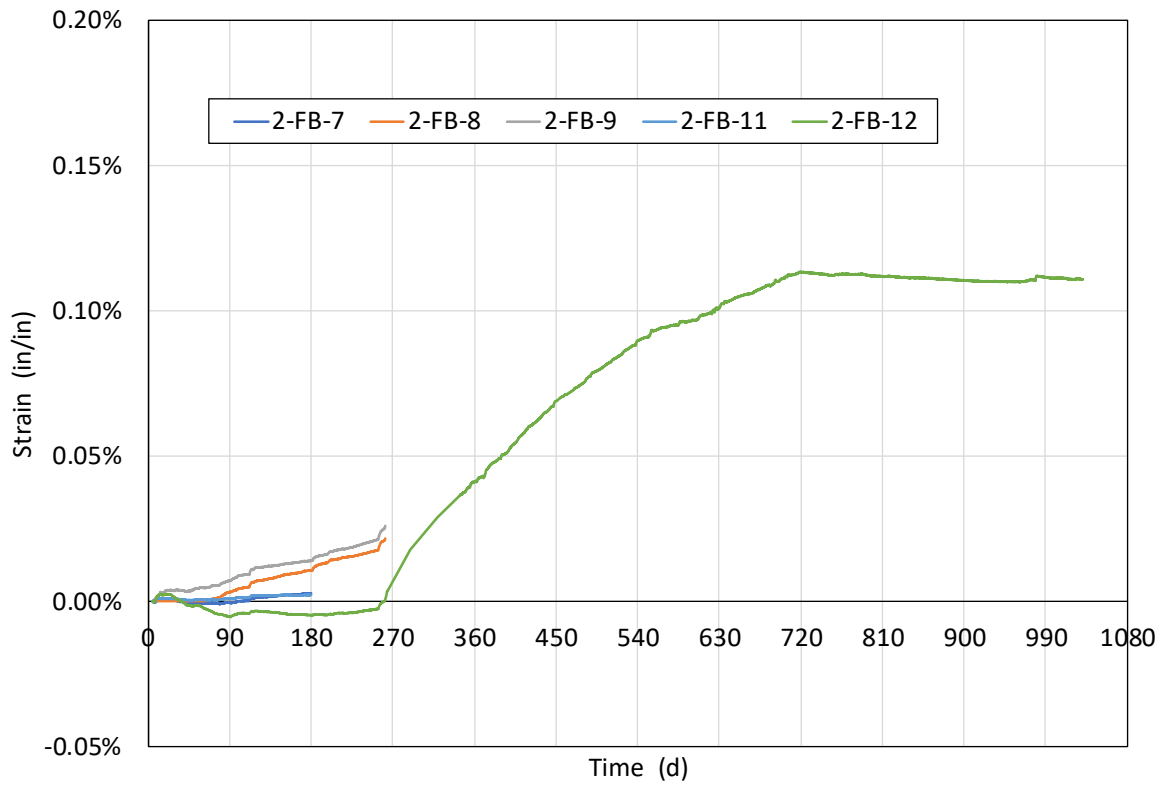


Figure 3–13. Measured strains at the core of block ASR 1: (a) Region 1, and (b) Region 2

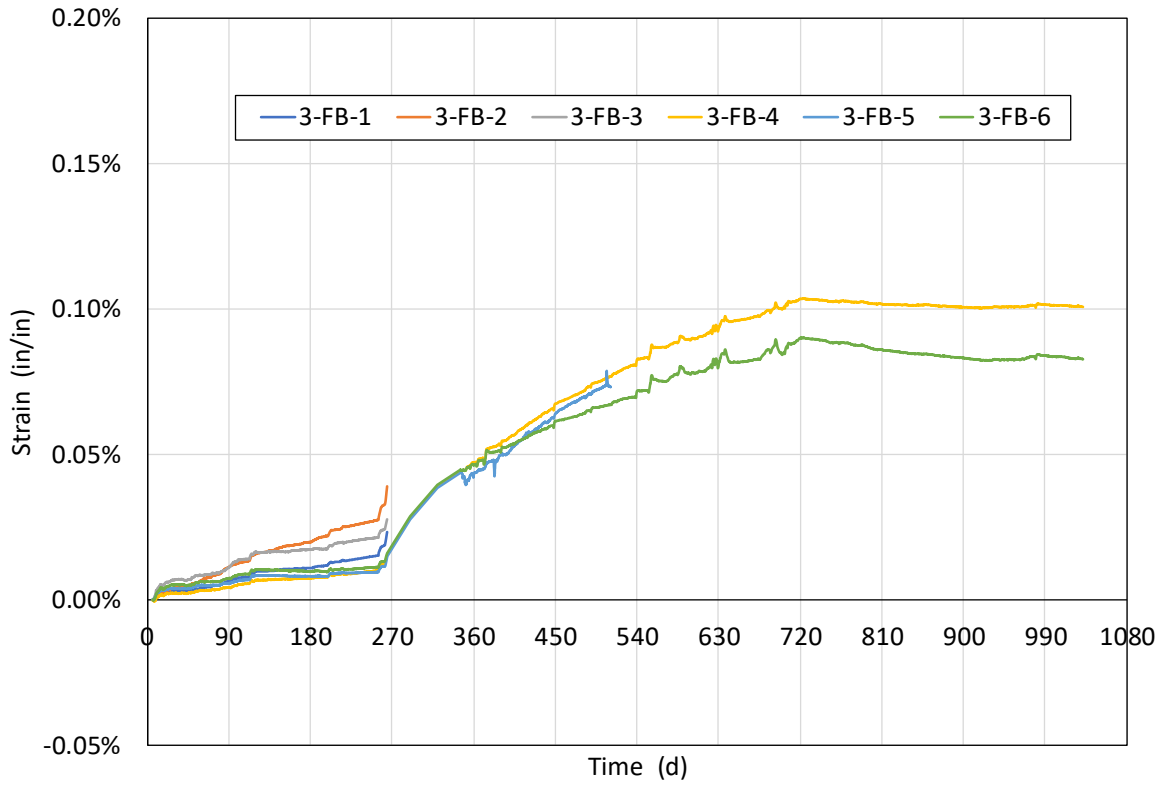


(a)

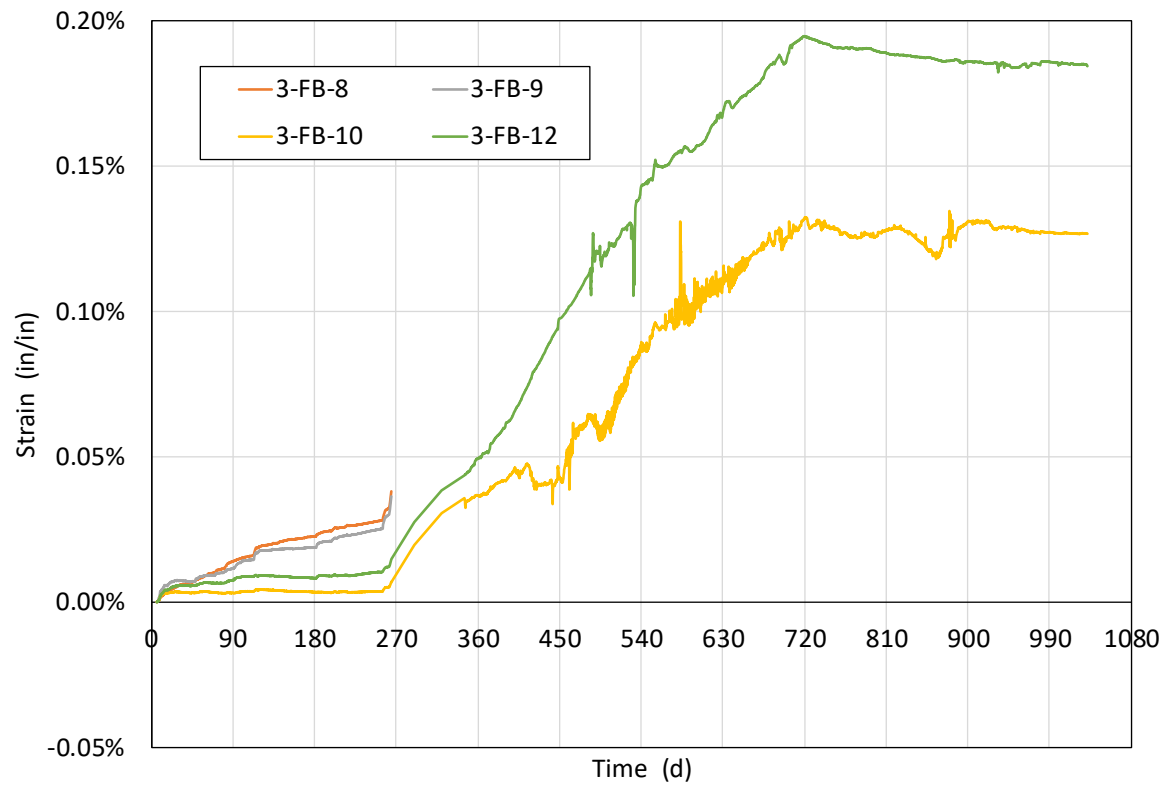


(b)

Figure 3-14. Measured strains at the core of block ASR 2: (a) Region 1, and (b) Region 2



(a)



(b)

Figure 3-15. Measured strains at the core of block ASR 3: (a) Region 1, and (b) Region 2

Based on the concrete strain development data shown in Figures 3-13 to 3-15, the following general observations can be made:

- Several tri-directional strain transducers were lost during concrete placement and others malfunctioned over the duration of this study. Transducers that malfunctioned can be recognized in the figures from their incomplete data through the more than 1000 days of measurement. In particular, no data was available for the heavy confinement Region 3 of all three reactive block specimens. Despite the lost transducers, strain data of the surviving gages were sufficient to capture the ASR-induced strain development at the center of the blocks, especially for the no-confinement Region 2, which is essential for studying the unconfined ASR-induced concrete expansion of the blocks.
- The concrete strains “took off” (i.e., the rate of accumulation of strains increased) after 250 days from concrete casting; about two months after the start of curing Phase 3 (RH in excess of 95 % and temperature of 75 °F to 80 °F), showing evidence of increased concrete reactivity with increased availability of moisture.
- Measured strains in the concrete of the three reactive blocks show a general trend of plateauing (flattening) between 630 days and 720 days, signifying that the ASR expansion has reached its ultimate value and that the expansion has stopped.
- In general, for a given block, the concrete strains in Region 2 were larger than those in Region 1. This is consistent and to be expected since Region 2 had virtually no confinement compared with intermediate confinement in Region 1.
- A comparison of the strains in the three reactive blocks indicate that the highest reactive block ASR 3 experienced the largest expansion of all reactive blocks, which is as expected. Blocks ASR 1 and ASR 2 had somewhat similar expansion values. This is also consistent with ASR-induced strain developments on the reinforcing bars of the reactive block specimens, observed in Section 3.2.1.

In addition, a large discrepancy was observed between the measured strains in concrete at the core of the blocks and the measured strains on the reinforcing bars, which were located close to the exterior of the blocks (just inside the concrete cover). For example, for Region 1 in block ASR 1, the reinforcing bars have peak strains (after strains had plateaued) in excess of 0.20 % (plots (a), (d), (e), and (f) in Figure 3-3) while the peak concrete strains in Figure 3-13(a) were in the range of 0.13 % to 0.15 %. Also, Figures 3-9 and 3-10 for Regions 1 and 2, respectively, of block ASR 3 show peak strains on the reinforcing bars of more than 0.25 % (some reached strain values in excess of 0.35 %), while Figure 3-15 shows concrete strains of about 0.09 % and 0.10 % for Region 1 and 0.13 % and 0.19 % for Region 2 of the same block. This shows that the strains close to the exterior of the blocks were much larger than those at the center. A similar observation in Section 3.3 using surface expansion measurements for Region 2 showed that the surfaces of the blocks in the absence of reinforcing bars had much higher strains than those measured at the center of the three reactive blocks.

This differential expansion between locations near the specimen's surface and its center is consistent with observation made by Bamforth *et al.* (1992) who studied the performance of standard prisms and unreinforced blocks cast with ASR reactive concrete mixtures to examine the effects of scale. In their study, blocks of sizes 79 in × 39 in × 39 in, 39 in × 20 in × 20 in, and 20 in × 10 in × 10 in were kept in a chamber at a temperature of 100 °F and intermittently sprayed with water. Internal strains were measured using embedded vibrating wire gages, while surface

strains were measured with demountable mechanical strain gage (DEMEC). The results showed that the ASR expansions in the blocks were much less than those in the standard prisms. Furthermore, the expansion was largest at the surface, where after one year of curing of the 39 in  $\times$  20 in  $\times$  20 in block, the surface expansion was measured to be about 0.16 %, while the expansions at about 2 in from the surface and at the center of the block (about 10 in deep) were about 0.10 % and 0.075 %, respectively (see Figures 4 and 5 of Bamforth *et al.*, 1992). The authors attributed this non-uniform expansion field to the fact that the surface of the block had a preferential access to water compared with the center of the block, which resulted in a higher expansion at the surface.

Another study by Bracci *et al.* (2012) that examined the performance of lap splices in columns affected by ASR using 16 large-scale column specimens that were cured outdoors. The specimens had a cross section of 2 ft  $\times$  4 ft and were equipped with external DEMECs for measuring surface strain, strain gages on reinforcing bars, and concrete strain transducers (similar to those used in this study, see Chapter 2). The KM gages measured the strains in the concrete cover and the concrete core and were located, respectively, 1 in and 3 in from the surface of the specimen. The strain measurements during expansion consistently showed a strain gradient where the surface strains were the largest and the concrete core were the smallest, despite the small distance between the three measurements. For different measurements, the average ratio of the concrete cover strains and concrete core strains to the surface strains were, respectively, 61 % and 51 %, 63 % and 55 %, and 53 % and 48 %. This indicates that the concrete core strains were consistently smaller than the concrete cover strains.

The above observation and discussion highlight one of the challenges associated with evaluation of large ASR-affected concrete structures, where the unconfined expansion is not a single-value, but in reality, an expansion field that can be largely affected by the size, exposure to humidity, and the potential for alkali leaching. While previous studies provided the mechanical properties of ASR-affected concrete as a function of expansion based on measurements taken from standard prisms, this study will attempt to provide the mechanical properties of the structure or element as a function of the measured expansion field as will be presented in Section 3.4.

### 3.3 SURFACE EXPANSION AND CRACK MAPPING

Two procedures were used to evaluate ASR-induced surface cracking and expansion of the reactive block specimens. These included: (1) using a laser tracker for evaluation of surface expansion of all vertical faces of the block specimens, and (2) using a handheld optical microscope with 20 $\times$  optical magnification for surface crack mapping, and a high-precision caliper for surface expansion determination on a 2 ft  $\times$  2 ft grid on each region of each vertical face of the blocks. Attempts were made to correlate the surface cracking and expansion with measured internal strains, and a summary is presented in Section 3.3.3. No visible surficial cracking was observed on the control block, and as a result, it was not included in this study.

Table 3-1 shows the sequence and dates for measurements of both procedures.

**Table 3–1. History of surface expansion and crack mapping measurements**

<b>Laser Measurement</b>			
	ASR 1	ASR 2	ASR 3
Original Measurement	April 13, 2017, April 17, 2017	April 13, 2017	April 6-7, 2017
2019 Measurement	October 9-11, 2019	October 7, 2019, October 9, 2019	October 4, 2019, October 11, 2019
<b>Crack Mapping and Caliper Measurement</b>			
	ASR 1	ASR 2	ASR 3
Original Measurement (caliper measurement)	April 10, 2017	April 7, 2017	April 6, 2017
Second Measurement (caliper measurement)	May 19, 2017	May 18, 2017	May 17, 2017
2018 Measurement	September 27, 2018	September 25, 2018	September 29, 2018
2019 Measurement	October 7-8, 2019	October 22, 2019, October 29, 2019	October 8, 2019, October 22, 2019

### 3.3.1 Surface Expansion Measurements Using A Laser Tracker

#### 3.3.1.1 Procedure

An Automated Precision Inc. (API) Tracker 3 (Figure 3-16) was used to scan all target points on the surfaces of the reactive blocks. As mentioned in Chapter 2, 280 targets were embedded on the exterior faces of each block specimen to allow measurements of their x-, y-, and z-coordinates over time. The process for laser scanning of these targets consisted of the following steps:



**Figure 3-16. Automated Precision Inc. (API) Tracker 3 used in surface expansion measurements**

- Calibrations: Prior to scanning the surfaces of the reactive blocks, the laser tracker was compensated. The purpose of this step was to conduct several checks prior to each scan to ensure that the tracker is working within the device's nominal specifications. These calibrations included: absolute distance meter linear calibration, quick linear volumetric calibration, and front-back sight check (see <https://apisensor.com/api-services/laser-tracker-calibration/>).
- Target measurement: Measurement of the reference targets and the targets on the surfaces of the blocks was conducted using a 1.5 in spherically mounted retroreflector (SMR), Figure 3-17(a), that was placed into a 1.5 in SMR holder, Figure 3-17(b). The holder, in turn, was tightened into either the reference targets or the targets on the exterior of the blocks. For each target on the blocks and each reference target, five measurements were taken, where each measurement was the average of 50 readings. The average of these five measurements was used for subsequent analysis.



**Figure 3-17. (a) 1.5 in laser tracker SMR, (b) 1.5 in SMR holder used in surface expansion measurements (both from <https://www.metrologyworks.com/>)**

Sources of uncertainty included measurement uncertainty of the laser tracker, mounting of the SMR holder, placement of the SMR in the SMR holder, movement of the reference targets, registration error, and the environmental conditions. For the measurements in this study, the uncertainty from the laser tracker was 0.00056826 in. To quantify the uncertainty of the mounting of the SMR holder and the placement of the SMR in the SMR holder, a set of measurements, by two operators, were made on a large practice concrete specimen that contained identical targets installed the same way as for the block specimens in this study. The standard uncertainty from these two sources was 0.00028526 in (mounting of the SMR holder) and 0.000324106 in (placement of the SMR in the SMR holder). The expanded uncertainty was determined to be 0.00142736 in using a coverage factor  $k=2$  (see Section 3.4.2). This expanded uncertainty corresponds to 133 microstrain for a 10.75 in strain gage length and 98 microstrain for a 14.75 in strain gage length. To minimize the errors from the environmental conditions, the controls for the heating and humidifier systems in the environmental chambers were turned off for at least three days prior to taking the measurements, and the tracker was placed in the chamber for at least 24 hours after the temperature and humidity in the chamber was at ambient conditions.

### 3.3.1.2 Laser Tracker Locations

Since the reference targets and the targets on the exterior of the blocks had to be within the line of sight of the laser tracker, six different locations were selected for the laser tracker as shown in Figure 3-18 as follows (each location used six reference targets):

- Location 1: For the west and south faces of block ASR 1. Location 1 used Reference Targets (RTs) 3, 4, 10, 11, 22, and 23.
- Location 2: For the east and north faces of block ASR 1. Location 2 used Reference Targets (RTs) 5, 6, 19, 20, 21, and 16.
- Location 3: For the east and south faces of block ASR 2. Location 3 used Reference Targets (RTs) 5, 6, 19, 20, 21, and 16.
- Location 4: For the west and north faces of block ASR 2 and the east and north faces of block ASR 3. Location 4 used Reference Targets (RTs) 6, 7, 8, 13, 22, and 23.
- Location 5: For the west face of block ASR 3. Location 5 used Reference Targets (RTs) 3, 4, 6, 8, 16, and 20.
- Location 6: For the south face of block ASR 3. Location 6 used Reference Targets (RTs) 1, 2, 3, 4, 11, and 12.

The location of the laser tracker for the second laser measurement (October 2019) remained within close proximity to that from the original measurement (April 2017). The reference targets were used to transform the measurements from the second measurement to those obtained in the original scan.

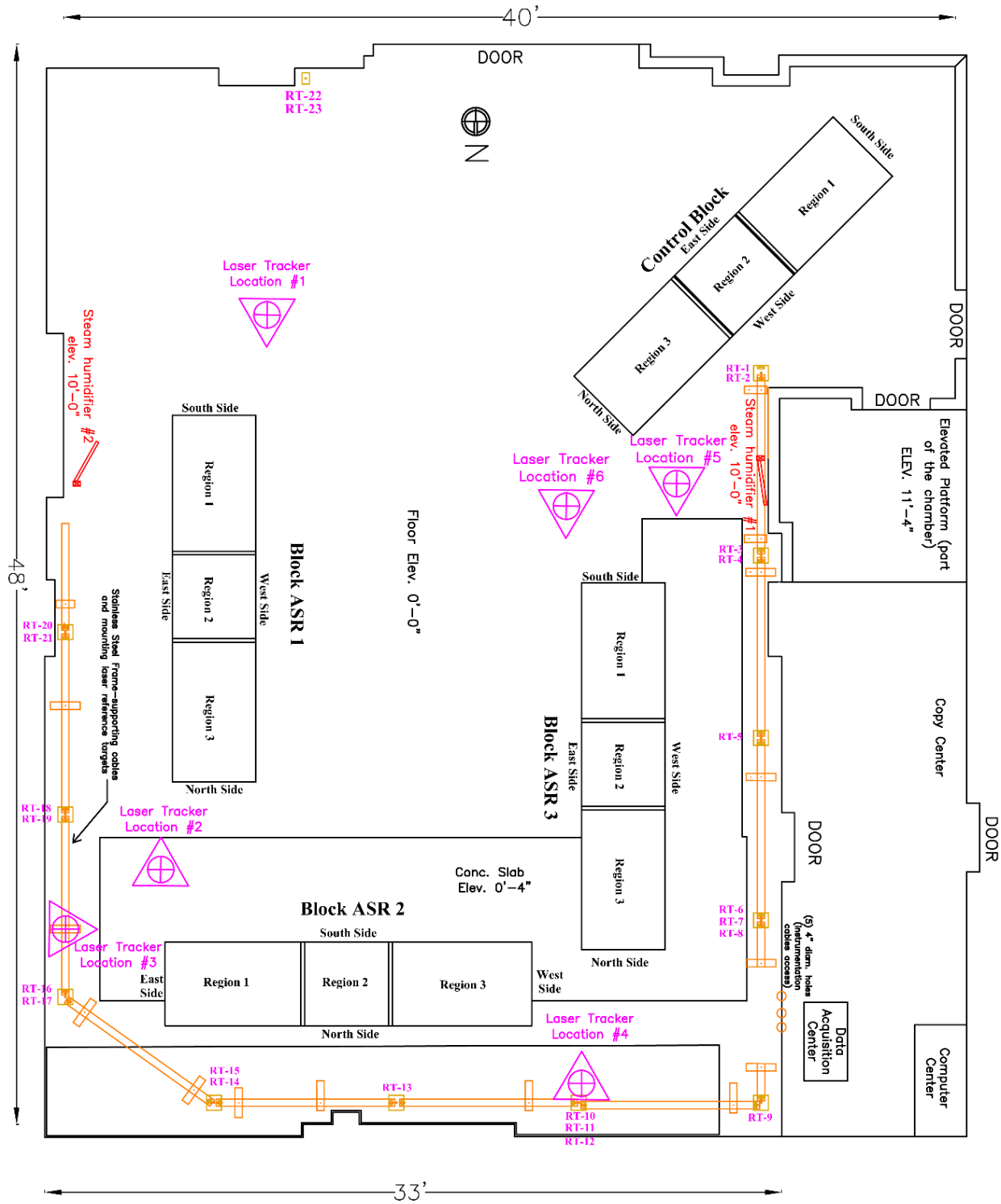


Figure 3-18. Plan view of environmental chamber showing locations of laser tracker for scanning of surfaces of reactive blocks

### 3.3.1.3 Registration of the Second Scan to the Original Scan

A MATLAB program was used to register the coordinates from the second scan to the coordinate system from the original scan. This process required the use of three reference targets from both scans. To determine the best three reference targets (out of the six available reference targets) to be used, the following procedure was used:

- Three reference targets were arbitrarily chosen to determine the transformation matrix (translation and rotation) to register the coordinates from the second scan to the original scan. The translation and rotation were then applied to the remaining reference targets from the second scan that were not used in the registration process. The differences between the transformed x-, y-, and z-coordinates for these reference targets and the corresponding targets in the original were then calculated. These differences are called the target registration error (TRE).
- The above process was repeated for all possible combinations of reference targets, and the errors were calculated for each combination.
- The combination of three reference targets that resulted in the minimum root mean square (RMS) of the TRE was used to transform the measurements from the second scan to the original scan.

The above procedure produced the transformation matrix that was used for each scan.

### 3.3.1.4 Average Surface Strains

Average surface strains (or normalized displacements after surficial cracking occurred, but treated here equivalently as simply strain for the sake of comparisons with strain measurements) on the surfaces of the three reactive blocks were calculated using two procedures: (a) average surface strains between neighboring targets and (b) average surface strains along an entire line of targets in a given region. For both procedures, average surface strains were calculated separately for each direction; vertical and horizontal.

(a) Average surface strains between neighboring targets: Average surface strains were calculated by computing the horizontal and vertical length between neighboring targets from the original,  $l_0$ , and second,  $l_2$ , scans. The average strains were thus calculated, for each direction separately, as  $\epsilon_{avg.} = (l_2 - l_0) / l_0$ . The average surface strains between the targets are presented in Figures B-1, B-2, and B-3 of Appendix B for reactive blocks ASR 1, ASR 2, and ASR 3, respectively. The figures also show the measured strain on the reinforcing bar closest to the space between neighboring targets on the date the second laser scanning was conducted, when available.

For Figures B-1 and B-3 for blocks ASR 1 and ASR 3, plots (a) and (c) show, respectively, the average horizontal surface strains for the east and west faces. Plots (b) and (d) show, respectively, the average vertical strains for the east and west faces of the blocks, while plots (e) and (f) show, respectively, the average horizontal and vertical strains of the ends of the blocks. For Figure B-2 for block ASR 2, plots (a) and (c) show, respectively, the average horizontal surface strains for the north and south faces. Plots (b) and (d) show, respectively, the average vertical strains for the north and south faces of the block, while plots (e) and (f) show, respectively, the average horizontal and vertical strains of the ends of the block.

(b) Average surface strains along an entire line of targets: The three figures, B-1 to B-3, show a wide variation of the average surface strains calculated between neighboring targets, making it difficult to study the strain patterns on the exterior of the blocks. As a result, another set of average surface expansion was developed by calculating the average strain along an entire horizontal and vertical line of targets on each of the three regions in each block in lieu of the average strain

between neighboring targets. The average strains along each line are shown in Figures B-4, B-5, and B-6 of Appendix B for reactive blocks ASR 1, ASR 2, and ASR 3, respectively.

For Figures B-4 and B-6 for blocks ASR 1 and ASR 3, plots (a) and (c) show, respectively, the average horizontal surface strains for the east and west faces, while plots (b) and (d) show, respectively, the average vertical strains for the east and west faces of the blocks. Similarly, for Figure B-5 for block ASR 2, plots (a) and (c) show, respectively, the average horizontal surface strains for the north and south faces, while plots (b) and (d) show, respectively, the average vertical strains for the north and south faces of the block.

The following observations can be drawn from Figures B-4 to B-6:

- As expected and similar to the strain measurements on the reinforcement (near surface) shown in Section 3.2, a comparison of the average surface strains in the three blocks indicated that block ASR 3 exhibited the largest surface expansion of all blocks. Blocks ASR 1 and ASR 2 had somewhat similar average surface expansion values.
- In general, for a given block, the calculated surface strains in Region 1 were slightly larger than those in Region 3. This is again consistent with observations from the measured strains on reinforcing bars and is to be expected due to the larger confinement in Region 3 compared with Region 1. In addition, surface strains in the no-confinement Region 2 (minimum longitudinal reinforcement and no transverse reinforcement) were higher than those in Regions 1 and 3, also as expected.
- In general, for a given block and a given region, the horizontal surface strains at the bottom were smaller than those at higher elevations. This is likely due to the friction provided by the ground which restrained the expansion of lower portion and/or the larger compaction and overburden pressure on the lower portion of the block which may have resulted in less expansion.

### 3.3.1.5 Comparison of Reinforcing Bar Strains and Average Surface Strains

The purpose of this section is to compare the average surface strains calculated in Section 3.3.1.4 based on the laser measurements and the strains measured on the reinforcing bars closest to and in the same direction as the calculated surface strain. Measured strains on reinforcing bars in these comparisons were taken from the same date of the second laser measurement. The average surface strains between neighboring targets (Procedure (a) above) were compared with the strain measurement on the closest reinforcing bars. The average surface strains along an entire line of targets (Procedure (b) above) were compared with the average strain measurements on all reinforcing bars closest to the line of targets. The objective of these comparisons was to examine the effectiveness and accuracy of measuring surface strains in estimating the internal strains in ASR-affected reinforced concrete structures.

Figure 3-19 shows a comparison of the average surface strains between neighboring targets (based on Figures B-1 to B-3), Procedure (a), and measured strains on reinforcing bars closest to the spacing between two targets (reinforcing bar strains were also shown in Figures B-1 to B-3) for the three reactive blocks. In Figure 3-19, the reinforcing bar strains are plotted on the horizontal axis while the average surface strains are plotted on the vertical axis. The figure indicates that for blocks ASR 1 and ASR 2 (reinforcing bar strains at or less than 0.15 %), there was a better correlation between the average surface strains and the corresponding reinforcing bar strains compared with block ASR 3 (reinforcing bar strains between 0.15 % and 0.35 %). Table 3-2 presents the statistics of the ratio of the average measured strains between neighboring targets and the corresponding measured strains on reinforcing bars. The table shows that the

average ratio for blocks ASR 1 and ASR 2 was 1.29 and 1.06, respectively. For block ASR 3, that ratio was 0.39. The large coefficient of variation, especially for blocks ASR 2 (82 %) and ASR 3 (73 %), is indicative of the large scatter in the data.

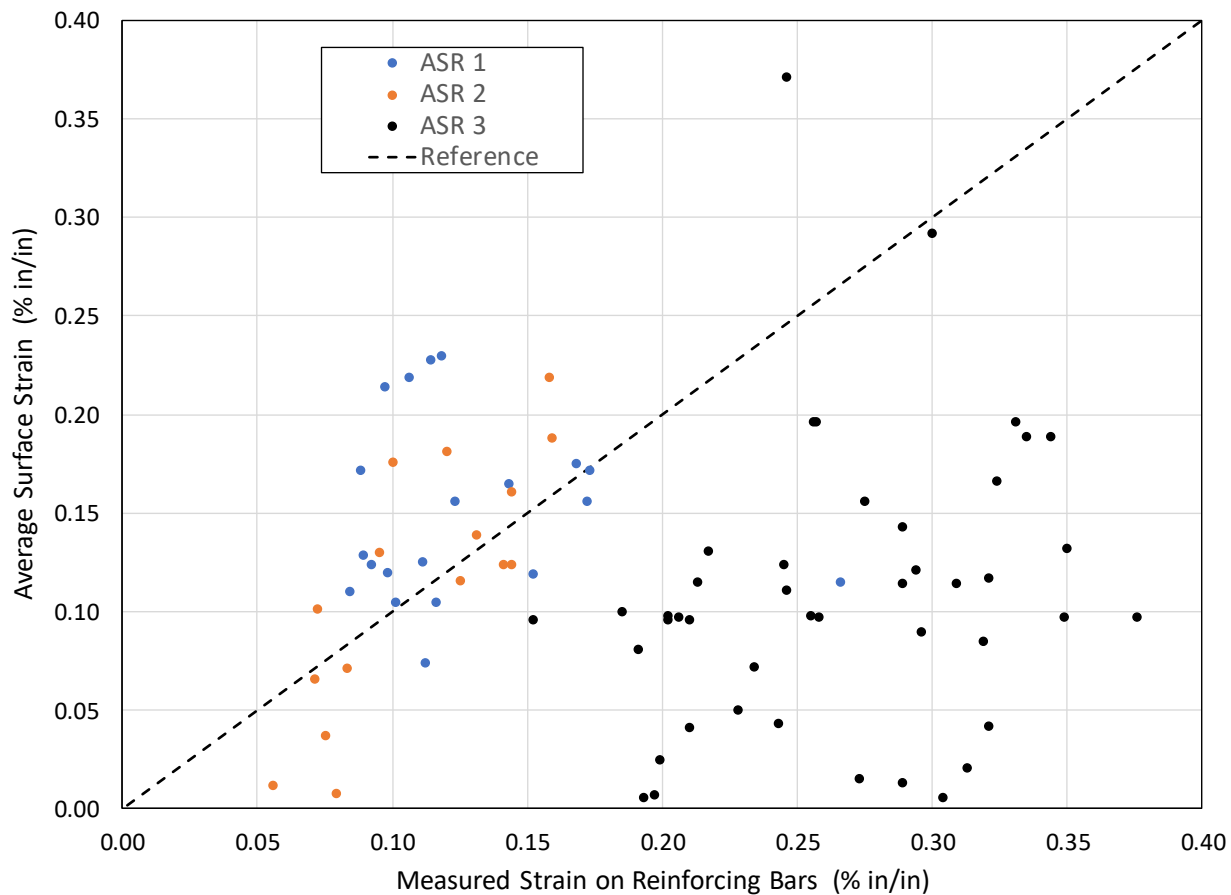


**Figure 3-19. Average surface strains using laser measurements between neighboring targets versus measured strains on corresponding reinforcing bars**

**Table 3–2. Statistics of the ratio of the average measured strains using laser measurements between neighboring targets to the corresponding measured strains or reinforcing bars**

	ASR 1	ASR 2	ASR 3
Average	1.29	1.06	0.39
Standard Deviation	0.5	0.87	0.29
Coefficient of Variation	0.39	0.82	0.73

Better correlation was obtained between the average surface strains along target lines (based on Figures B-4 to B-6), Procedure (b), and the average of the measured strains on reinforcing bars closest to the same target line. Figure 3-20 shows a comparison of the average surface strains along target lines for the blocks and the averaged measured strains on reinforcing bars closest to the target line for the three reactive blocks. The figure shows better correlation between the

average surface strains and the corresponding average reinforcing bar strains for blocks ASR 1 and ASR 2 with strains at or less than 0.15 %. The better correlation here is attributed to the less variability in the averaged surface strains along target lines compared with the strains calculated between neighboring targets. For block ASR 3 with higher reinforcing bar strains, the correlation between the two sets of strains was still weak, with the strains in the reinforcing bars significantly higher than those from the average surface strains. Table 3-3 presents the statistics of the ratio of the average measured strains along target lines and the corresponding measured strains on reinforcing bars. The table shows that the average ratio for blocks ASR 1 and ASR 2 was 1.00 and 1.05, respectively. For block ASR 3, that average ratio was 0.46, reflecting the large difference between the surface strains and the reinforcing bar strains for this block. The coefficients of variation for the three blocks were much lower than those based on the surface strains between two neighboring targets, reflecting the lesser scatter in the data.

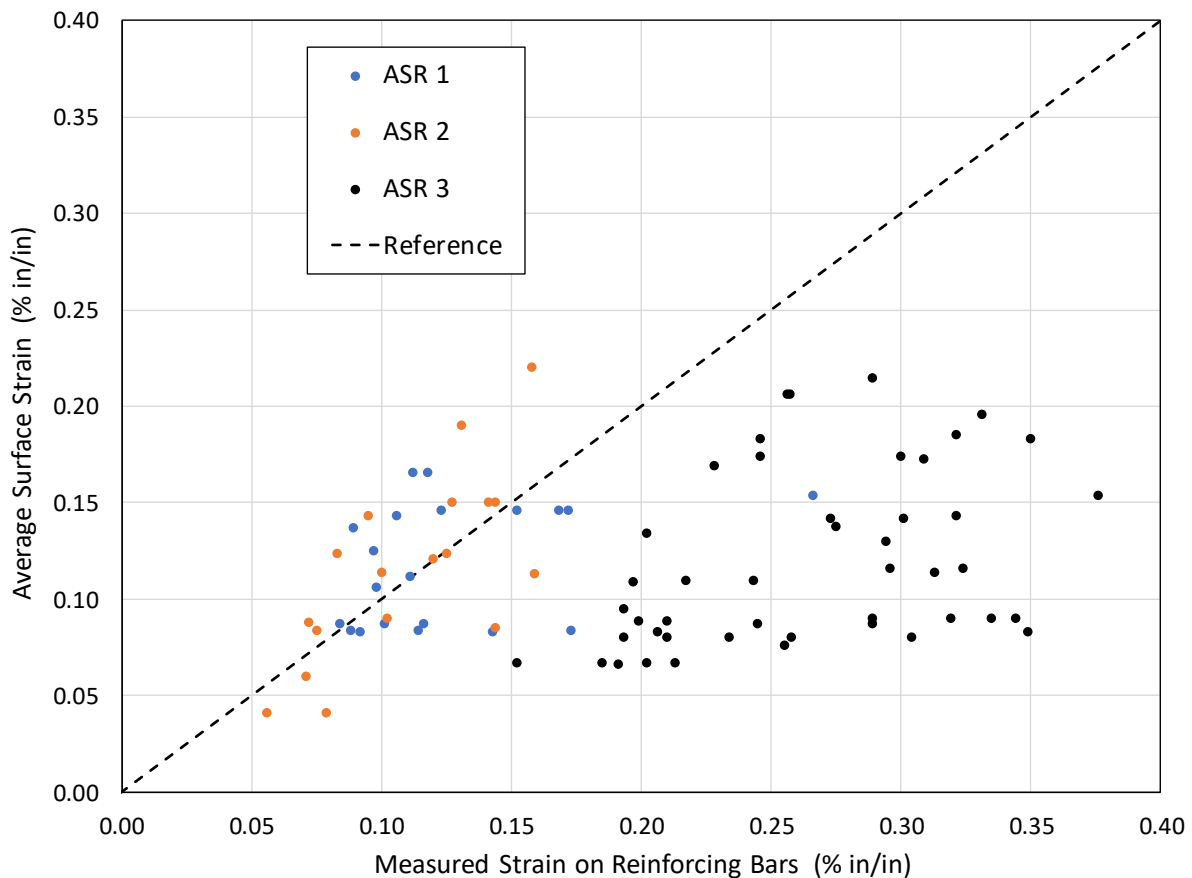


**Figure 3-20. Average surface strains using laser measurements along target lines versus average measured strains on corresponding reinforcing bars**

**Table 3–3. Statistics of the ratio of the average measured strains along target lines and the corresponding average measured strains on reinforcing bars**

	ASR 1	ASR 2	ASR 3
Average	1.00	1.05	0.46
Standard Deviation	0.30	0.30	0.15
Coefficient of Variation	0.30	0.29	0.34

Figure 3-21 superposes to the data in Figure 3-20 the mean value of the ratio of average surface strains along target lines (Table 3-3) to the average reinforcing bar strains, along with the upper and lower limits estimated as the mean  $\pm$  standard deviation from Table 3-3. As the figure shows, the mean and the two bounds were calculated in two segments: a linear segment corresponding to the data for blocks ASR 1 and ASR 2, and a constant segment corresponding to the data for block ASR 3. As the figure indicates, the majority of the measured data points were within the upper and lower bounds.

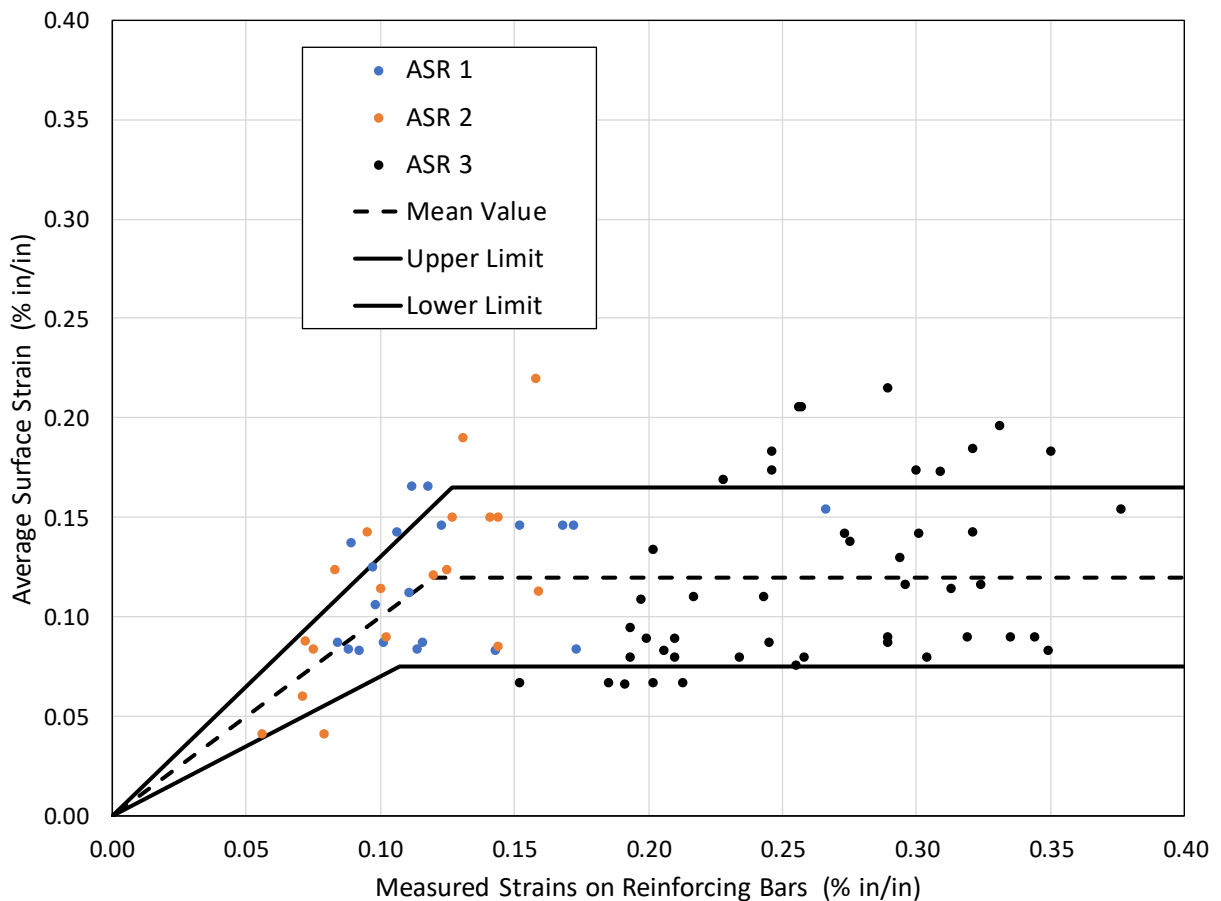


**Figure 3-21. Mean value and upper and lower bounds for average surface strains using laser measurements along target lines versus measured strains on corresponding reinforcing bars**

### 3.3.1.6 Estimation of Unconfined (Free) ASR Surface Expansions

While the concrete prisms (Feldman *et al.*, 2020) provide information on the progress of the unconfined (free) ASR strains, this information cannot be directly used to estimate the time-history of the unconfined ASR expansion for a large structure similar to the block specimens used in this study. In addition, while the strains on the reinforcing bars inside the blocks provide valuable data on the evolution of the ASR expansion, this data represent confined rather than unconfined expansions, as the reinforcing cage provides a certain level of restraint against the expansion.

In this section, the average surface strains in unconfined Region 2 of the three reactive blocks were used to calculate the unconfined ASR surface expansion values at the time of measurement (October 2019). Furthermore, only vertical strains were considered in the calculation since horizontal strains were affected by the four corner longitudinal reinforcing bars and the friction provided by the ground. For that purpose, the average vertical strains in plots (b) and (d) of Figures B-4 to B-6 in Appendix B, Procedure (b), were averaged and were considered as the unconfined ASR surface linear expansion of each block at the time of the second laser measurement. These average values are presented in Table 3-4. As has been observed repeatedly with the reinforcing bar strain data and the average surface strain data, the average unconfined ASR surface strain for block ASR 3 was larger than that for blocks ASR 1 and ASR 2, while the unconfined strains for blocks ASR 1 and ASR 2 were somewhat similar. As was mentioned in Section 3.2, large differences were observed between the average unconfined surface strains in Region 2 and the measured strains at the center of Region 2 for all blocks, indicating that the ASR expansion is a complex field, rather than a single value.

**Table 3–4. Average vertical surface strains in Region 2 of the three reactive blocks (% in/in)**

	ASR 1	ASR 2	ASR 3
Average	0.261	0.247	0.347
Standard Deviation	0.022	0.059	0.034
Coefficient of Variation	0.083	0.237	0.098

### 3.3.2 Surface Crack Mapping and Expansion Using Cracking Index Method

Surface crack mapping is typically carried out to quantify the degree of surface cracking due to internal crack development and damage of concrete members. The crack mapping process includes measurement and summation of crack widths along a set of orthogonal lines drawn on the surface of a concrete member, which is known as the cracking indexing. The crack index (CI) method was developed and is used extensively by the Federal Highway Administration (FHWA), see Fournier *et al.* (2010). The CI method is considered as a measure of the extent of surface damage to the concrete due to ASR; the higher the CI values, the higher the extent of damage on the concrete element under investigation.

The purpose of this section is to determine if there is any correlation between the CI and the surface and internal strains on ASR-affected concrete structure. To that end, a 2 x 2 grid was drawn on the exterior faces of all reactive blocks for measuring crack widths. Figure 3-22 shows the grid drawn on the surface of block ASR 3. As shown in the figure, the vertical and horizontal lines of the grid were aligned with the targets installed on the surface prior to concrete placement

(see Chapter 2) with a length between targets of 10.75 in (Figure 2-8). The number and width of cracks were measured along the grid lines. The process can be outlined as follows:

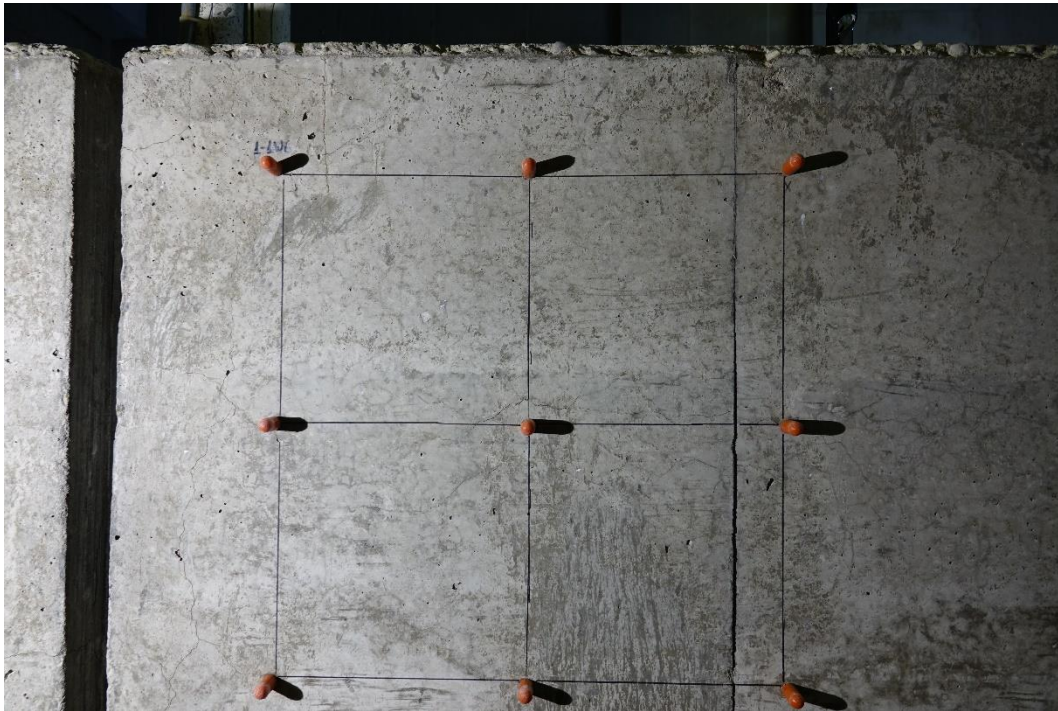


**Figure 3-22. Grid used for measurement of surface cracking using an optical microscope and surface expansion using a high-precision caliper**

- Identify the location of the grid as the area with the most intense cracking and least number of extracted cores for a given confinement region. For that purpose, eight grids consisting of three horizontal and three vertical lines each (Figure 3-22) were identified for each reactive block (one grid for each confinement region on each face, along with the two ends of the block).
- The cracking pattern was documented for each grid using high-resolution camera.
- Each line on the grid was scanned using a handheld optical microscope with 20 $\times$  optical magnification that measured crack widths with high accuracy. Note that the microscope provided measurements of crack widths down to 0.1 mm. However, there were many instances where smaller crack width was detected. In these instances, “eyeballing” was used to approximate the crack width (e.g., 0.07 mm).
- The CI was calculated for each direction and for each grid line as the summation of all crack widths along a given grid line and then dividing by the original length of the line.
- The vertical and horizontal distances between the targets defining each grid were measured using a high-precision caliper with an accuracy of  $\pm 0.001$  in. These measurements were compared with original measurements taken two weeks after concrete placement to provide data on the displacements that took place between these targets and as a result, the average surface strains between two neighboring targets.

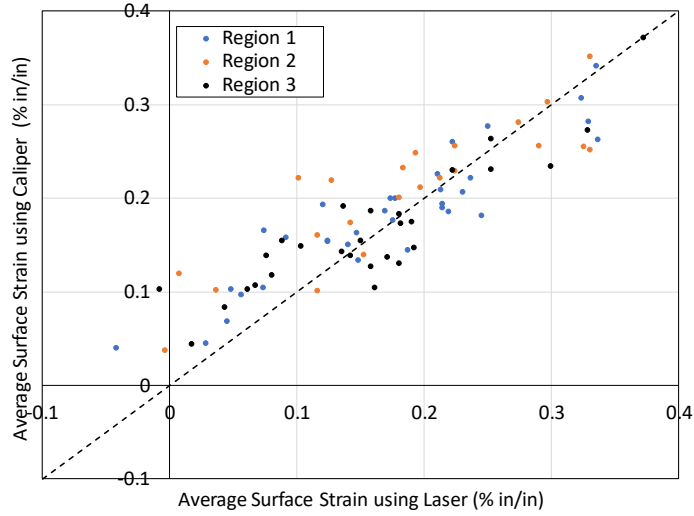
As shown in Table 3-1, the process was performed twice: September 2018 and October 2019. The results presented in this section were based on the October 2019 measurement to allow comparisons with the laser measurements (Section 3.3.1). Findings from the September 2018 measurement were consistent with those from October 2019, and thus, results from the September 2018 measurement are not shown here for brevity.

The average surface strains between the neighboring targets using calipers (in red) and the cracking index (in green) are presented in Figures C-1, C-2, and C-3 in Appendix C for reactive blocks ASR 1, ASR 2, and ASR 3, respectively along with the average surface strains based on laser measurements (in blue) and measured strain on the reinforcing bar closest to the space between neighboring targets on the dates the laser scanning was conducted, when available (in black). For Figures C-1 and C-3 for blocks ASR 1 and ASR 3, plots (a) and (b) show, respectively, the results for the east and west faces, while plot (c) shows the results for the north and south ends of the blocks. For Figure C-2 for block ASR 2, plots (a) and (b) show, respectively, the results for the north and south faces, while plot (c) shown the results for the east and west ends of the block.

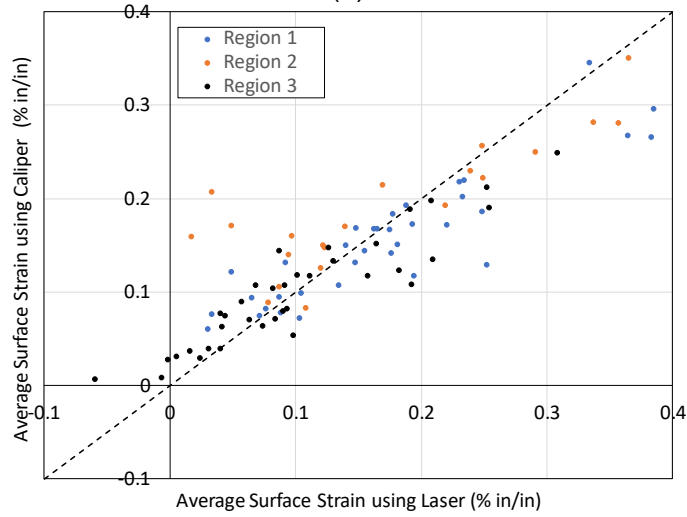
Due to the scarcity of data from strains on reinforcing bars corresponding to the grids on the surfaces of the blocks, comparisons are provided to examine correlation between the average strains using the caliper measurements and those based on laser measurements. These comparisons are shown in Figure 3-23 for the three reactive blocks. Different colors are used to differentiate between the different regions of each block. The figure shows that in general, surface expansion measurements using the laser tracker were consistent with those using the caliper. Some inconsistencies do exist due likely to human error in using hand-held caliper, small differences in dates of measurements, and slightly different gage length (center to center of targets for laser measurement and out to out for caliper measurement). Table 3-5 presents for the three reactive blocks, the statistics of the ratio of the average measured surface strain between neighboring targets using the high-precision caliper to that using the laser tracker.

**Table 3–5. Statistics of the ratio of the average measured strains between targets using Caliper measurement and the corresponding average strains using laser tracker**

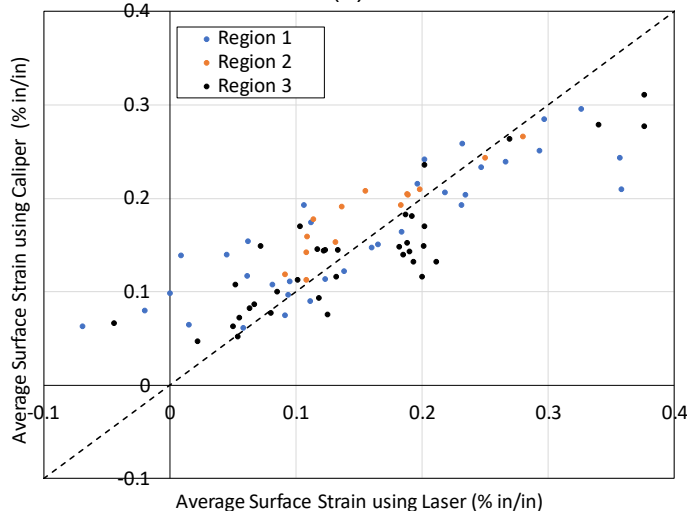
	ASR 1	ASR 2	ASR 3
Average	1.02	0.94	0.99
Standard Deviation	0.27	0.20	0.27
Coefficient of Variation	0.26	0.22	0.27



(a)



(b)



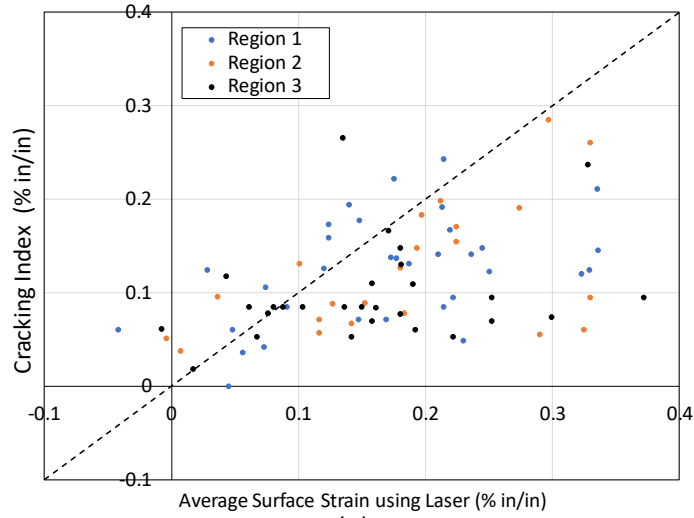
(c)

**Figure 3-23. Average surface strains using caliper measurements versus average surface strains using laser measurements for blocks (a) ASR 1, (b) ASR 2, and (c) ASR 3**

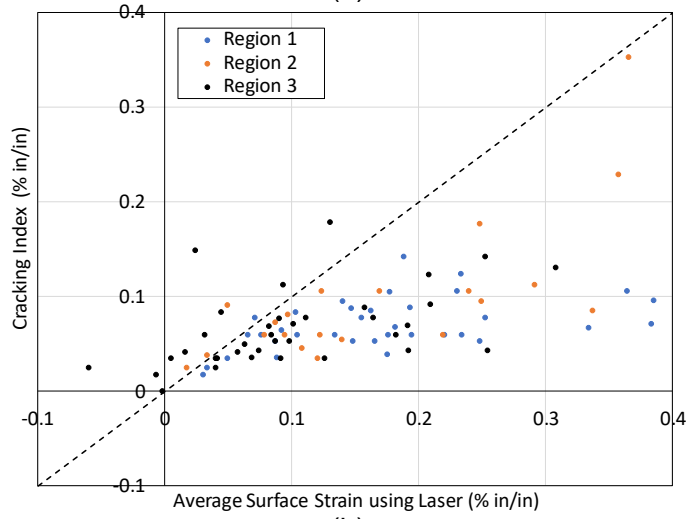
Another comparison is presented to examine the correlation between the calculated CI and the average surface strains along the same grid line using the laser measurements. The comparison is shown in Figure 3-24 for the three reactive blocks. Different colors are used to differentiate between the different regions of each block. The figure indicates that the cracking index method yielded results that were not consistent with the surface expansion measurements, probably due to the inability of the CI method to capture the expansions. In addition, comparing the cracking index in Figures C-1 to C-3 in Appendix C with the strains measured on neighboring reinforcing bars shows a poor correlation. It should be noted also that the method, being based largely on visual measurement, are subject to measurement errors. Table 3-6 presents for the three reactive blocks, the statistics of the ratio of the CI to the average surface strain using the laser tracker. Two observations can be gleaned from the table. First, the average ratio of the CI to the surface strain is consistently less than unity indicating that the CI results are smaller than the surface strains. Second, there is a large scatter in the data resulting in a coefficient of variation for the ratio of about 50 %. Similar observations were also made by Bracci *et al.* (2012) who found that the CI data were highly scattered and converged to about 50 % of the surface strain.

**Table 3–6. Statistics of the ratio of the cracking index to the corresponding average measured strains between neighboring targets using laser tracker**

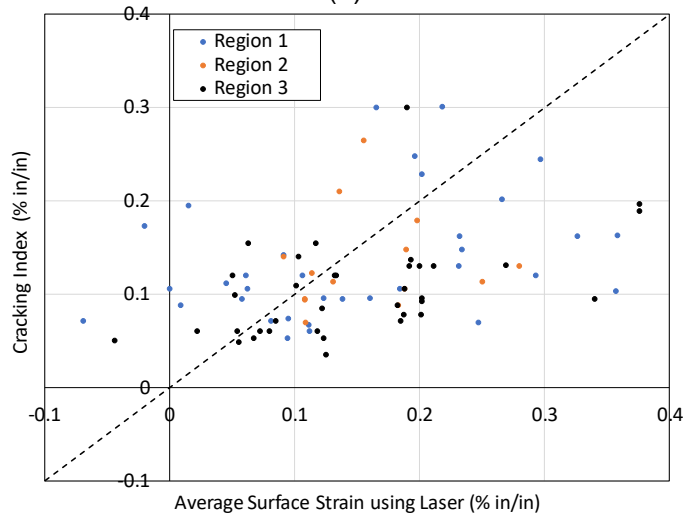
	ASR 1	ASR 2	ASR 3
Average	0.68	0.58	0.78
Standard Deviation	0.37	0.31	0.38
Coefficient of Variation	0.54	0.53	0.49



(a)



(b)



(c)

**Figure 3-24. Cracking Index versus average surface strains using laser measurements for blocks (a) ASR 1, (b) ASR 2, and (c) ASR 3**

### 3.3.3 Summary

- A reasonable correlation was observed between the average surface strains along target lines and the corresponding reinforcing bar strains for blocks ASR 1 and ASR 2 with strains at or less than 0.15 %. The correlation became much poorer for block ASR 3 with strains between 0.15 % and 0.35 % where the average surface strains using laser measurements along target lines were smaller than the average measured strains on reinforcing bars. This indicates that surface expansion measurements may provide reasonable estimate of strains only at low expansion levels.
- In general, surface expansion measurements using the high-precision caliper were consistent with those using laser measurements. Some inconsistencies do exist due likely to human error, small differences in dates of measurements, and slightly different gage length.
- The CI method yielded results that were not consistent with the surface expansion measurements nor the strain measurements on reinforcing bars, probably due to the inability of the method to properly capture the expansions. The CI values were smaller than the corresponding average surface strains.
- The inability of the surface expansion measurements and the CI method to capture the actual concrete expansion (or strains on reinforcing bars) is likely because the behavior and strains in the concrete cover are different from those within the confining reinforcing bars. The surface expansion measurements and the cracking index method, however, can be useful tools to monitor the evolution of ASR, but not the expansion values.
- Surface expansion measurements indicated the following trends in ASR-induced strain developments on surfaces of the block specimens:
  - Higher strain values over time (increased expansion over time)
  - Lower strains at the bottom of the blocks compared with those at the top due likely to friction with the ground
  - Larger strains in the unconfined regions, with the lowest strains in the highest confined region

## 3.4 MECHANICAL PROPERTIES OF CONCRETE

The section presents the results of mechanical property testing on companion cylinders, prepared during concrete placement of the block specimens, and cores extracted from the specimens as they undergo degradation due to ASR expansion. Section 3.4.1 provides an overview of the mechanical properties test program including the different types of testing conducted, the coring procedure, and the method used for determination of the concrete modulus of elasticity. Section 3.4.2 presents the test results including uniaxial compressive strength, modulus of elasticity, and splitting tensile strength as a function of time, while Section 3.4.3 provides detailed analysis of the test results. Section 3.4.4 presents the mechanical properties of cores as a function of the unconfined expansion of cores. All mechanical property tests were conducted using the 220 kip closed-loop servohydraulic load frame described in Section 2.7.

### 3.4.1 Overview of Mechanical Property Testing Program

For each reactive and control block, 4 in × 8 in and 6 in × 12 in concrete cylinders were prepared to measure concrete mechanical properties over time. Mechanical property testing of the 4 in × 8 in cylinders (compressive strength, modulus of elasticity, and splitting tensile strength) was conducted at 7 days, 14 days, 28 days, 56 days, 91 days, 180 days, and 1 year after the blocks

were cast. The 6 in × 12 in cylinders were tested only at 28 days after casting and only for compressive strength and modulus of elasticity. The companion cylinders were stored in the environmental chamber and were exposed to the same environmental conditions as the block specimens.

Cores were extracted from each block at 28 days, 90 days, 180 days, 1 year, and 1-3/4 year after concrete placement. Concrete cores of 2.75 in diameter were extracted from the blocks by using a cylindrical wet coring bit, which had an outer diameter of 3 in, Figure 3-25. In general, the length of each core ranged from 21 in to 24 in. In most cases, each extracted core yielded three cylindrical core samples for compressive and tensile strength testing. All tests were conducted within 24 hours after extraction of cores to minimize potential damage due to loss of natural confinement. Note, however, that the extracted cores lose their in-situ structural surroundings, and as a result, the tests conducted on them represent testing of isolated cores without their structural context. To prepare the core samples for testing, the cores were cut to appropriate length and the surfaces were ground to create a smooth surface at the top and bottom of each core sample.



**Figure 3–25. Extraction of cores from the blocks**

The mechanical property testing for both the companion cylinders and cores on each date included:

- Compressive Strength and Compressive Modulus of Elasticity (or Compressive Modulus) testing (Figure 3-26): Compressive strength and static modulus of elasticity were determined by testing at least three concrete cylinders for each of these properties in accordance with the ASTM C39 Standard (ASTM C39/C39M-17a, 2017) and the ASTM C469 Standard (ASTM C469/C469M-14, 2014), respectively.



**Figure 3–26. Compressive strength and elastic modulus testing of concrete cylinders**

- Splitting Tensile Strength testing (Figure 3-27): At least three cylinders were tested to determine the splitting tensile strength of the concrete in accordance with the ASTM C496 Standard (ASTM C496/C496M-17, 2017).



**Figure 3–27. Splitting Tensile Strength testing of concrete cylinders**

### 3.4.1.1 Coring Location

Cores were taken periodically over the duration of Task 1 to study the influence of ASR-induced damage on the mechanical properties of concrete. Due to the high density of steel reinforcement in Regions 1 and 3 of the block specimens, it was necessary to clearly define the specific locations for coring to avoid potential damage to the reinforcing bar cage (and subsequent loss of data throughout the duration of testing). The coring plan was designed to avoid the reinforcement and the strain gages mounted on the reinforcement, and the regions with the embedded triaxial concrete strain transducers (indicated by orange rectangles in the figure). For a typical elevation of a reactive block, these potential core locations are shown in Figure 3-28 where centerlines of potential core locations are shown by the red lines.

The cores were taken by anchoring a standard coring stand with a mounted core drill that was required to be flush with the surface of the block. The potential coring locations were therefore limited to the centerlines between two adjacent surface-mounted targets (see Section 2.3.4). A 24 in long and 3 in nominal diameter concrete core barrel was utilized to obtain the longest continuous specimen achievable. The red-hatched regions in Figure 3-28 represent to-scale core holes for reference. In general, the procedure was to start from exterior spaces between adjacent stirrups and to work from the outside toward the inside of a given region of the block over time in order to maximize remaining, undisturbed, fully confined zones.

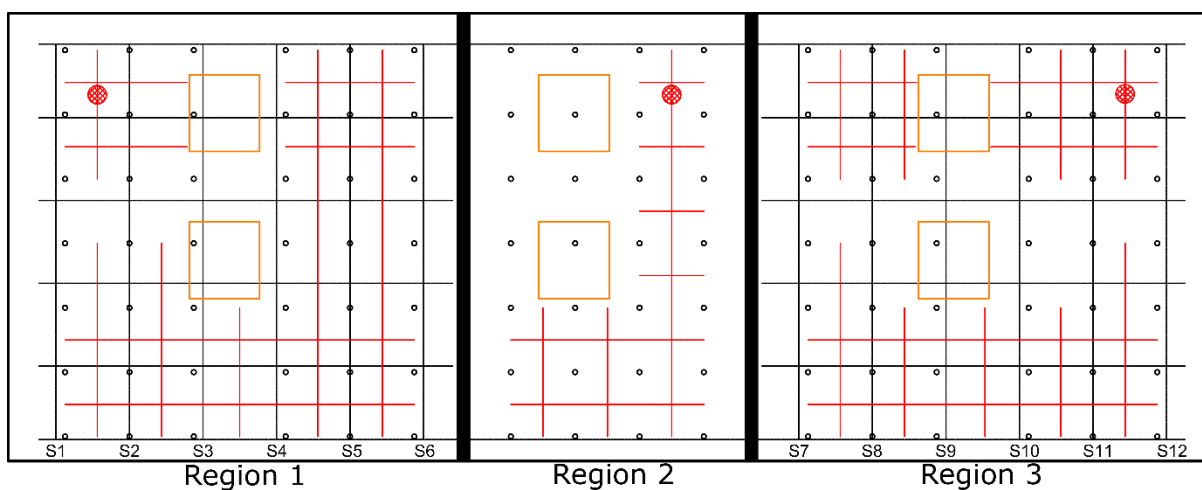


**Figure 3–28. Potential core locations. Centerline of potential core locations indicated by red line, black lines indicate approximate centerline of reinforcement, circles represent surface cast targets, and orange boxes indicate regions with embedded concrete strain transducers**

In addition to the core sampling locations, due to the various confinement conditions it was necessary to consider the effect of depth into the specimen where a single prepared, cored specimen may be taken. To aid understanding, Figure 3-29 schematically shows the various potential levels of confinement provided by the reinforcement in Regions 1 and 3, where dark blue indicates regions of complete effective confinement due to the development of arching action (Mander *et al.*, 1988) while the shaded regions represent partial effective confinement which is dependent on the stiffness and induced tension due to the ASR reaction in the longitudinal reinforcement. From this schematic, it is apparent that two potential regions of interest may be obtained from a single core: a relatively low confined cover region and a partially to completely

confined core region. For the purpose of this study, the standard procedure was to obtain two specimens from the confined region which were alternately utilized to determine the compressive and tensile behaviors. The remaining cover region of the core was utilized to obtain a second compressive test specimen.

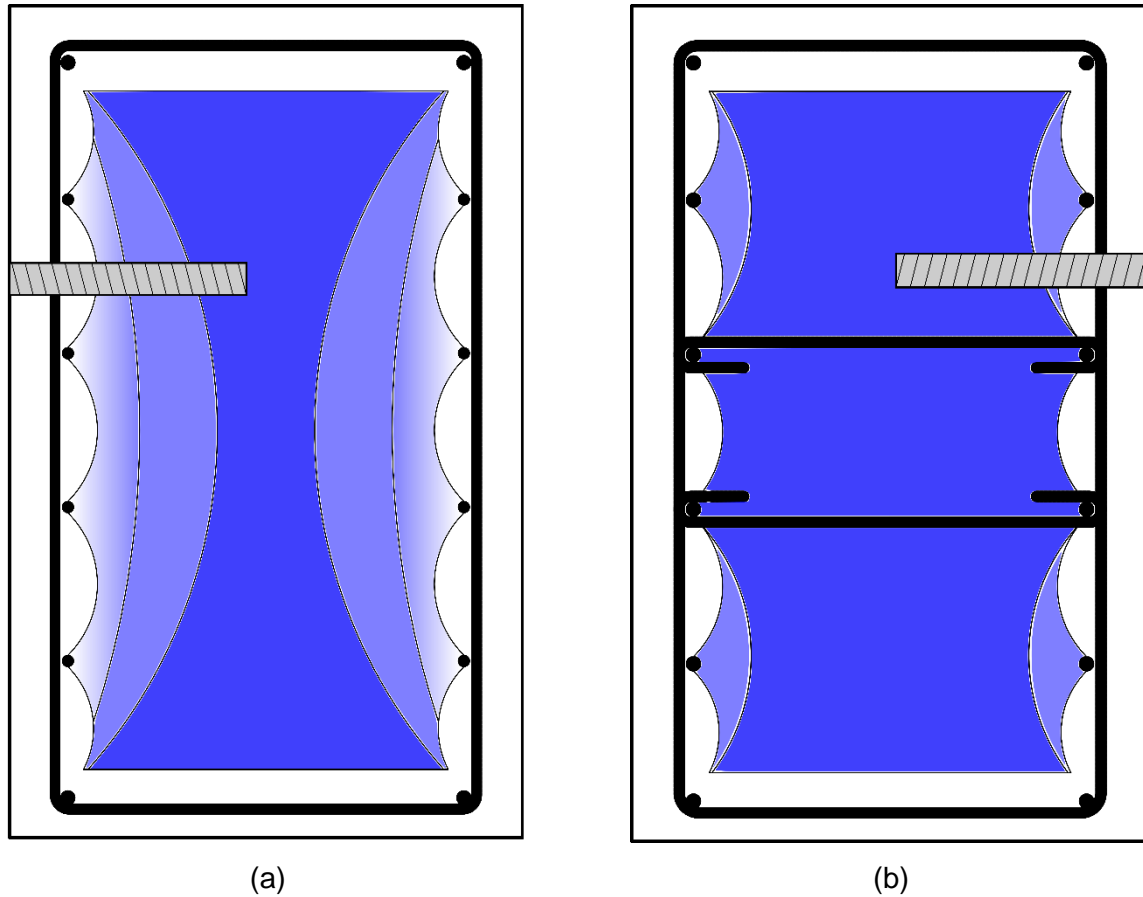


**Figure 3–29. Elevation cross section of idealized confinement zones in (a) Region 1 and (b) Region 3 of the blocks**

To keep track of the location and age of the extracted core specimens, a numbering system for each specimen was devised as shown in Figure 3-30. The numbering system defined the block number (e.g., 2 for block ASR 2), the region number (e.g., 3 for Region 3), the stirrups numbers (for Regions 1 and 3) or vertical line of targets (for Region 2) straddling the core, the block face where the core is extracted (e.g., N for north), height above ground in inches, the age of the block in days at time of coring, and the depth of the specimen prepared from the core where C1 was the deepest.

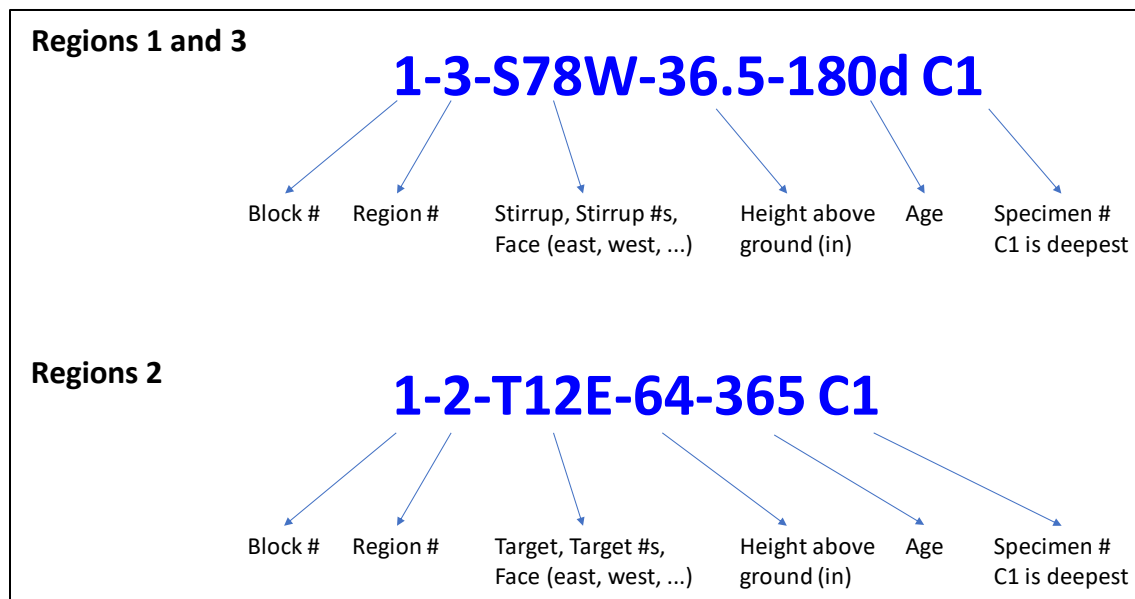


**Figure 3–30. Core specimen numbering system**

#### 3.4.1.2 Calculation of the modulus of elasticity

As previously mentioned, compressive modulus of elasticity testing was conducted in accordance with the procedures and loading rates specified by ASTM C469/469M-14 Standard Test Method for Static Modulus of Elasticity and Poisson's Ratio of Concrete in Compression (ASTM C469/C469M-14, 2014). However, it was recognized that calculation of the modulus of elasticity by the standard's secant stiffness method could not capture the influence of nonlinearity of the compressive stress-strain response observed in the ASR-affected cylinders and core specimens (see Figure 3-31), because it only incorporates information from the stress and strain corresponding to 40 % of ultimate load and the stress corresponding to a longitudinal strain of 0.005 %. As a result, an alternative approach was used in this study. To linearize the response while better capturing the basic features of the nonlinear behavior, the reported values of compressive modulus of elasticity were calculated as the slope obtained from linear regression of the cylinder's stress-strain data up to the stress corresponding to 40 % of ultimate load as shown in Figure 3-31. In the figure, the linear regression lines are shown as dashed lines. In the procedure used herein, the modulus of elasticity was taken as the average of the slopes of the three linear regression lines.

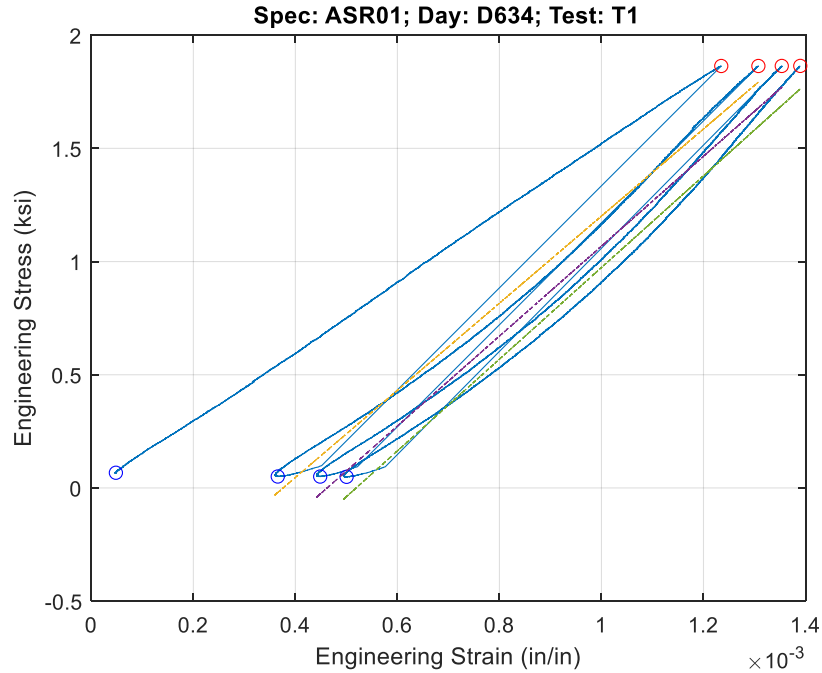


**Figure 3–31. Example of linear regression lines (dashed lines) calculated from each of three cycles of a cylinder’s stress-strain data for a core extracted from block ASR 3 at 634 days. The modulus of elasticity was taken as the average slope of the three linear regression lines**

Figure 3-32 shows a comparison of the modulus of elasticity calculated using ASTM C469/469M-14’s secant stiffness method relative to that calculated using linear regression based on data taken from concrete mixture ASR 3 (see Section 2.1). The comparison showed that defining the modulus as the slope of the linear regression rather than the secant stiffness had a minimal effect on the calculated modulus of elasticity.

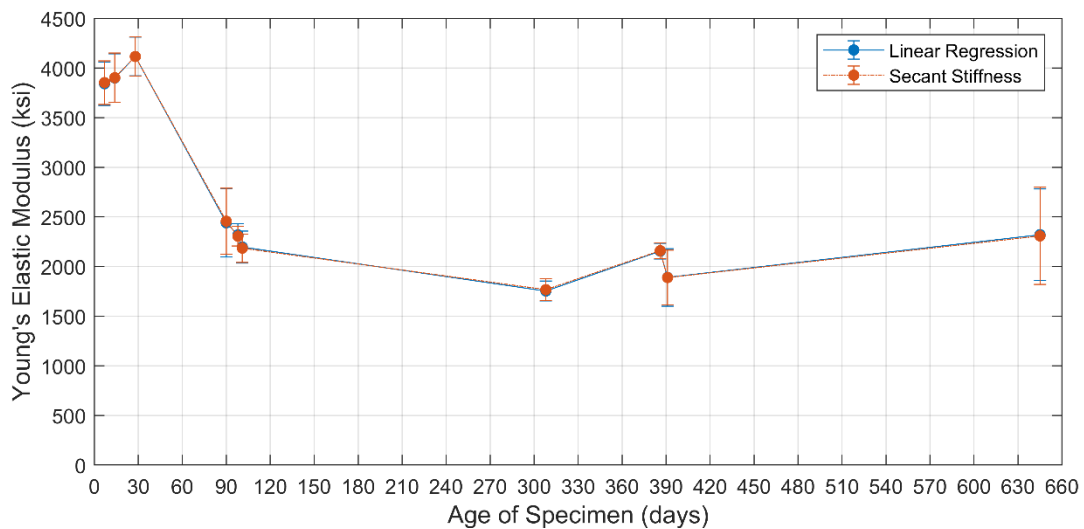


**Figure 3–32. Comparison of the modulus of elasticity values calculated using ASTM C469/469M-14’s secant stiffness method to values calculated using linear regression**

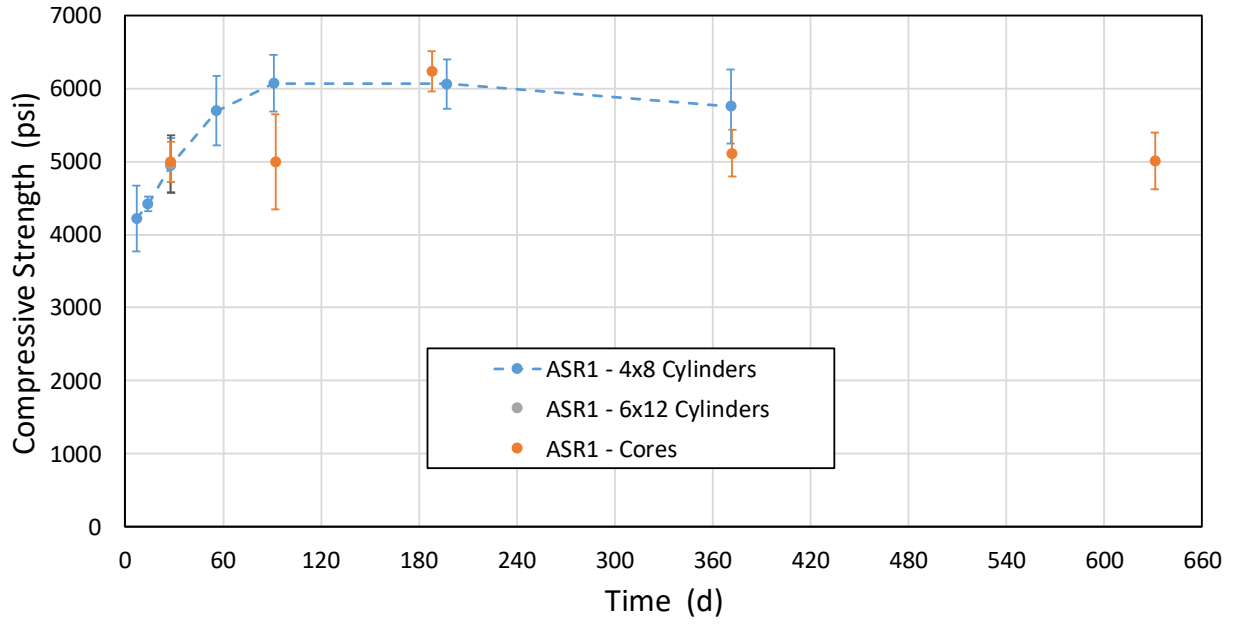
### 3.4.2 Results of mechanical property tests

Each value reported in the sections that follow is denoted by mean value,  $\mu_c$ , which was typically averaged from at least three independent measurements, followed by  $\pm$  uncertainty,  $U$ . Unless otherwise noted, the uncertainty is reported by the expanded uncertainty associated with the mean, which is determined for  $n$  independent measurements by  $U = (k \cdot u_c) / \sqrt{n}$  from the combined standard uncertainty,  $u_c$  (i.e., estimated standard uncertainty in the mean from a Type A uncertainty analysis) with a coverage factor of  $k$  determined by the two-tailed Student's  $t$  distribution at probability  $p = 95\%$  (i.e., at the 95<sup>th</sup> percentile) with  $N = n - 1$  degrees of freedom. Assuming that the unknown true value being measured (for example, the compressive strength, elastic modulus, or tensile strength) is approximately normally distributed with standard deviation  $u_c$ , the reported mean value lies within the interval defined by  $\pm U$  with a level of confidence of exactly 95%. For each plot in this section, filled circular markers correspond to mean values computed from all samples taken from a block on a particular day, and the error bars correspond to  $\mu_c \pm U$ .

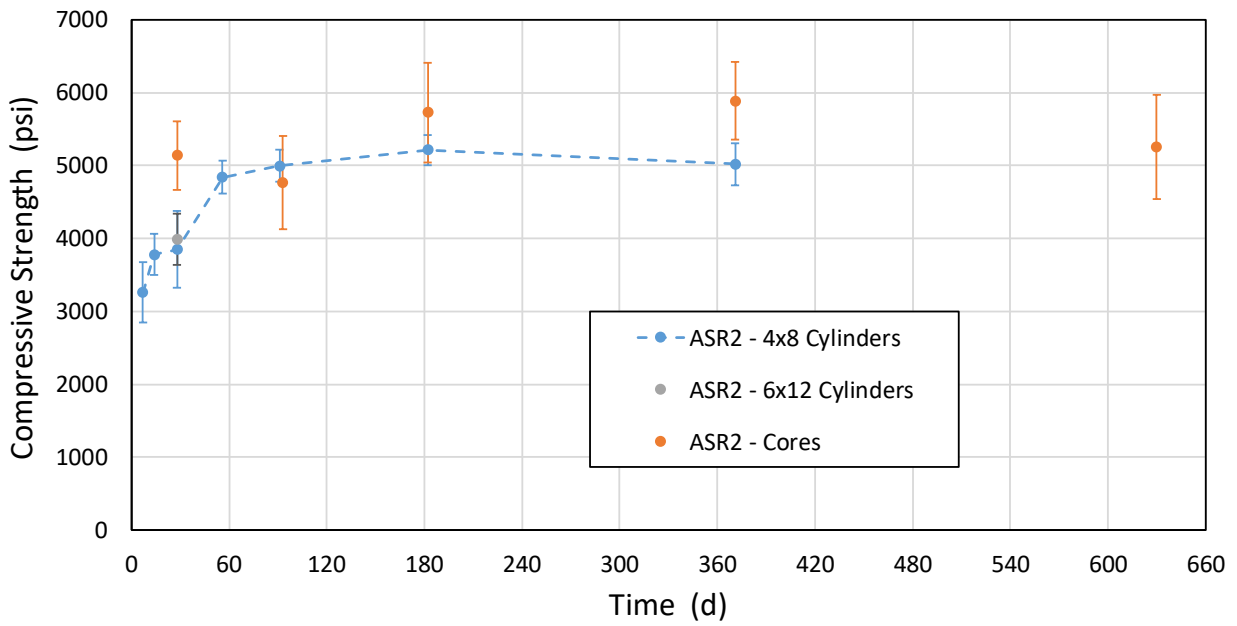
Measurement uncertainties calculated for the structural response parameters, such as stress and strain, are reported in Table D-1 in Appendix D. The measurement uncertainty calculated for stress varied between the 4 in  $\times$  8 in cylinders and 2.75 in  $\times$  6 in cores extracted from the blocks because, while the uncertainty in the measured load is constant, but the areas required to convert the load (e.g., units of kip) to stress (e.g., units of psi) are different. The measurement uncertainty calculated for the strain also varied between the 4 in  $\times$  8 in cylinders and 2.75 in  $\times$  6 in cores because different axial extensometers (with different gage lengths and different expanded uncertainties) were used to measure their displacement response.

#### 3.4.2.1 Compressive Strength

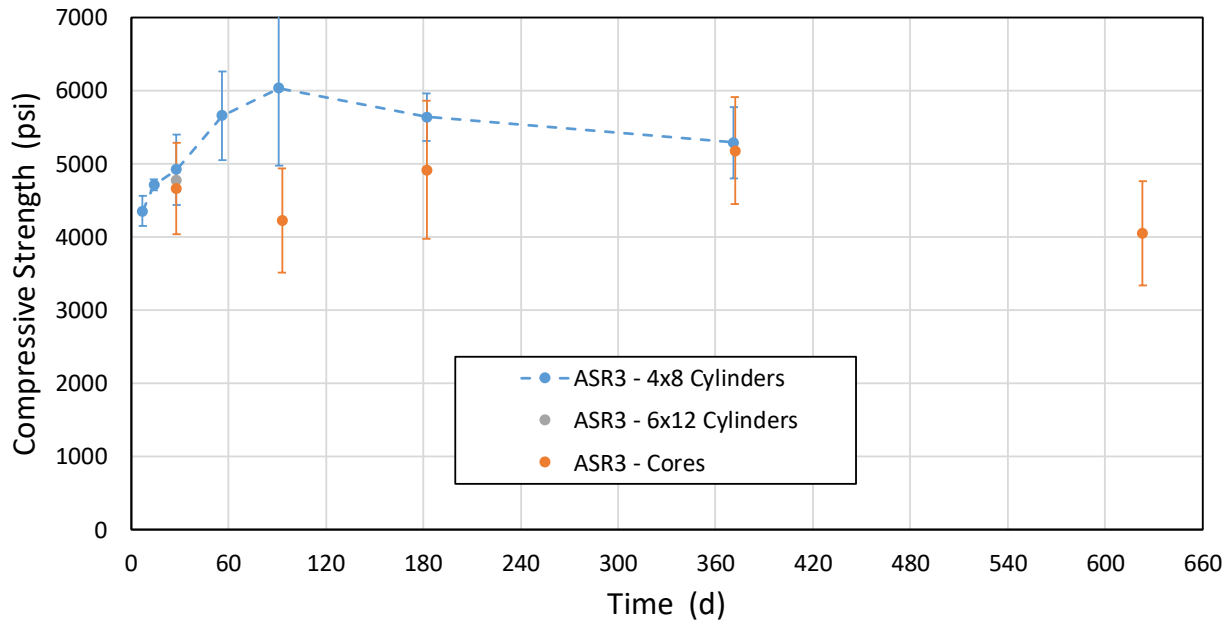
Figure 3-33 presents for all blocks the uniaxial compressive strength results versus time for the concrete cylinders prepared during concrete casting, and core specimens extracted from the blocks. In the figure, plots (a), (b), (c), and (d) show the results for the reactive blocks ASR 1, ASR 2, ASR 3, and the control block, respectively. For the core specimen data, the mean values and uncertainties were calculated from cores extracted from all three regions of each block. In general, the plots show an increase in compressive strength of cylinders and cores at the early stages up to 90 days. Cylinders and cores for all blocks showed an average compressive strength at 28 days of about 5000 psi (the actual strengths ranged from 4920 psi  $\pm$  480 psi to 5020 psi  $\pm$  290 psi), except for block ASR 2 which had an average compressive strength of 3850 psi  $\pm$  530 psi. After 90 days, cylinders from the control block continued to gain strength and reached a compressive strength of 6410 psi  $\pm$  620 psi after 791 days. On the other hand, cylinders and cores from the reactive blocks (ASR 1, ASR 2, and ASR 3) had reduced strengths after 360 days, in comparison to their 28-day compressive strength. Cores extracted from the three reactive specimens showed that block ASR 3 (which exhibited the highest expansion, see Section 3.2) had the largest reduction in compressive strength, with a measured compressive strength of only 4050 psi  $\pm$  710 psi after 626 days. Note that, since the length to diameter ratio for all cylinder and core sizes in this study was larger than 1.75, no size adjustment was needed for the resulting compressive strength per the provisions of the ASTM C39 Standard (ASTM C39/C39M-17a, 2017).



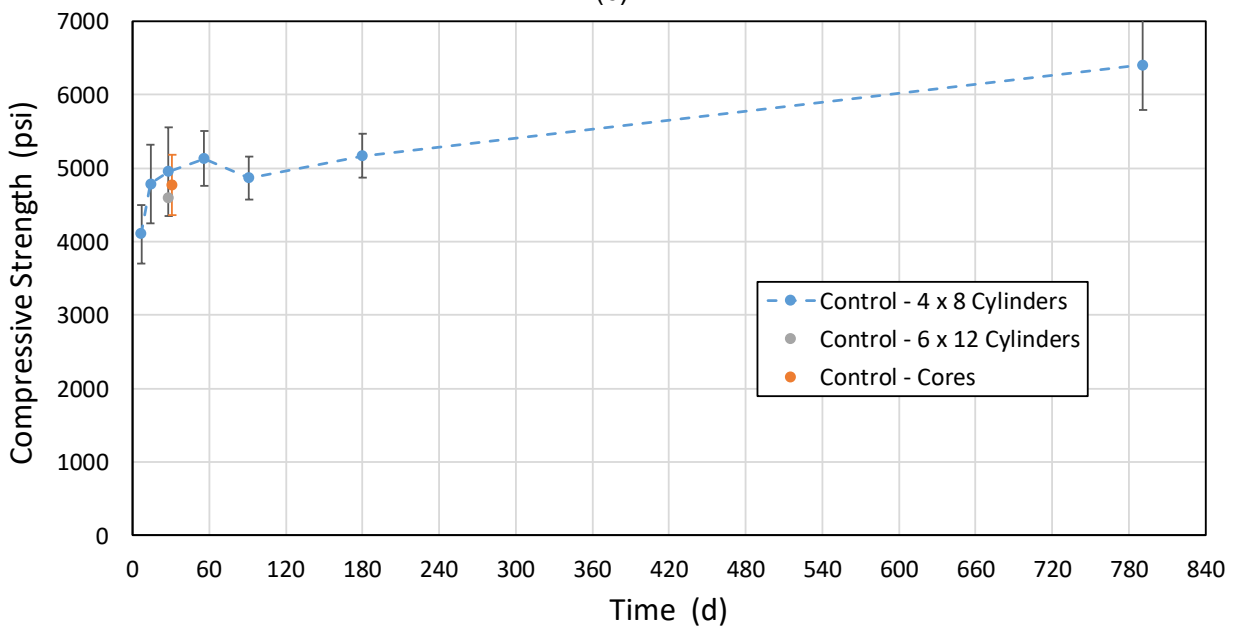
(a)



(b)



(c)



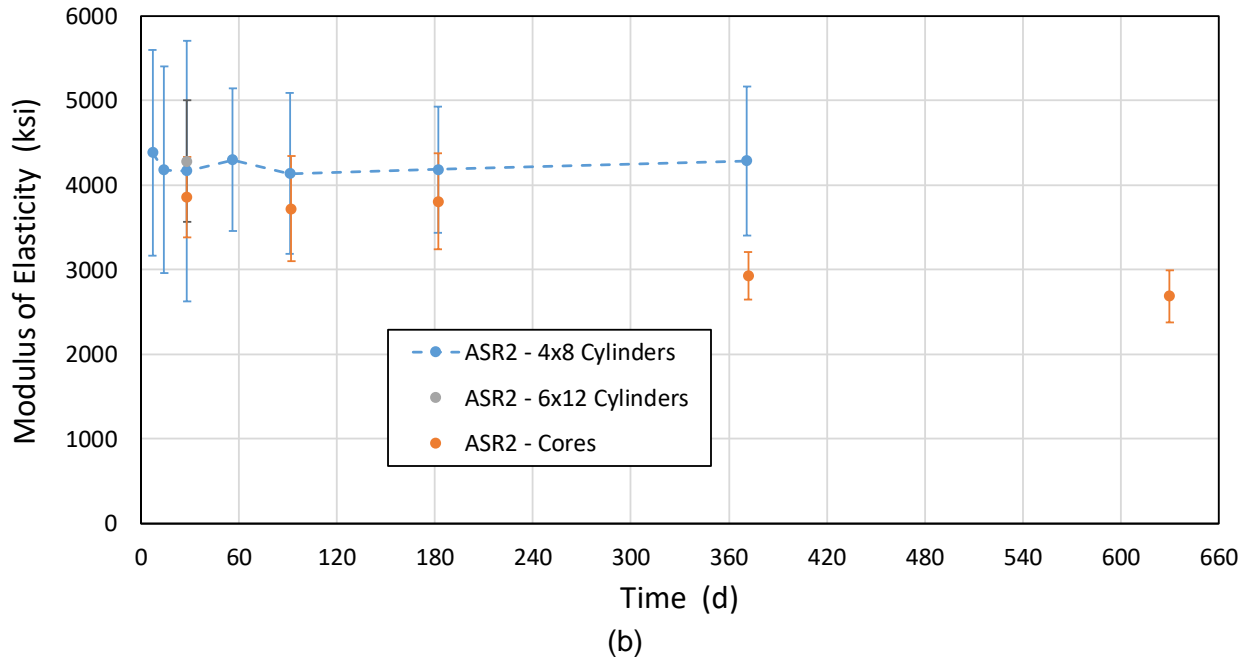
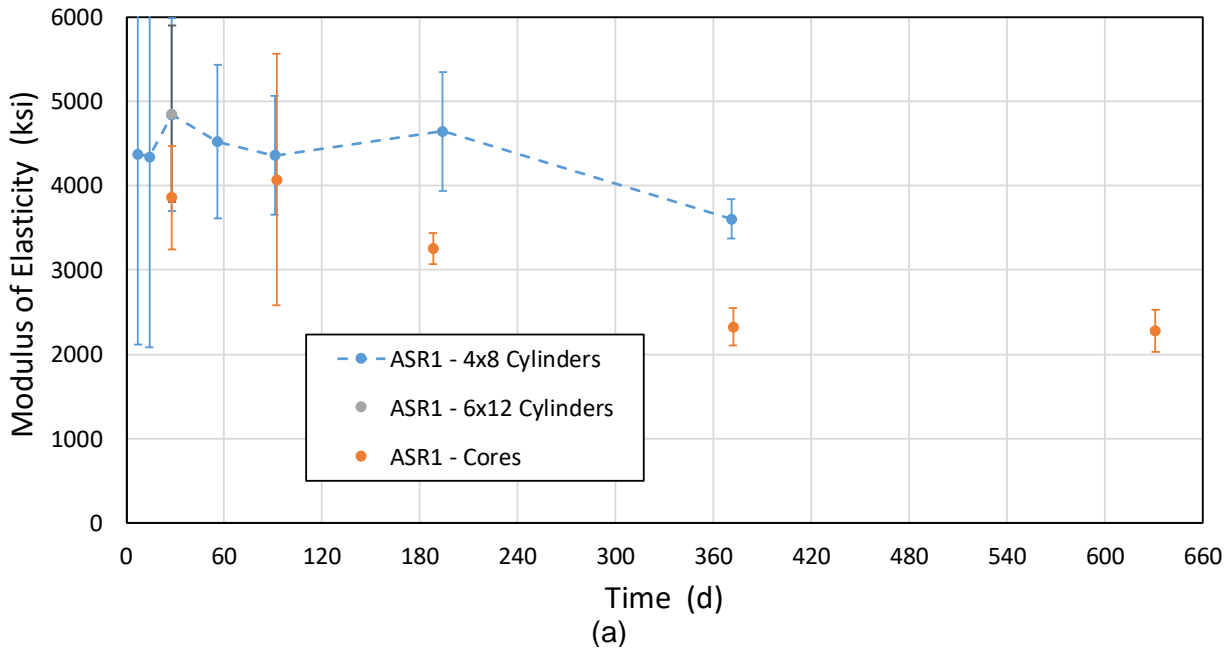
(d)

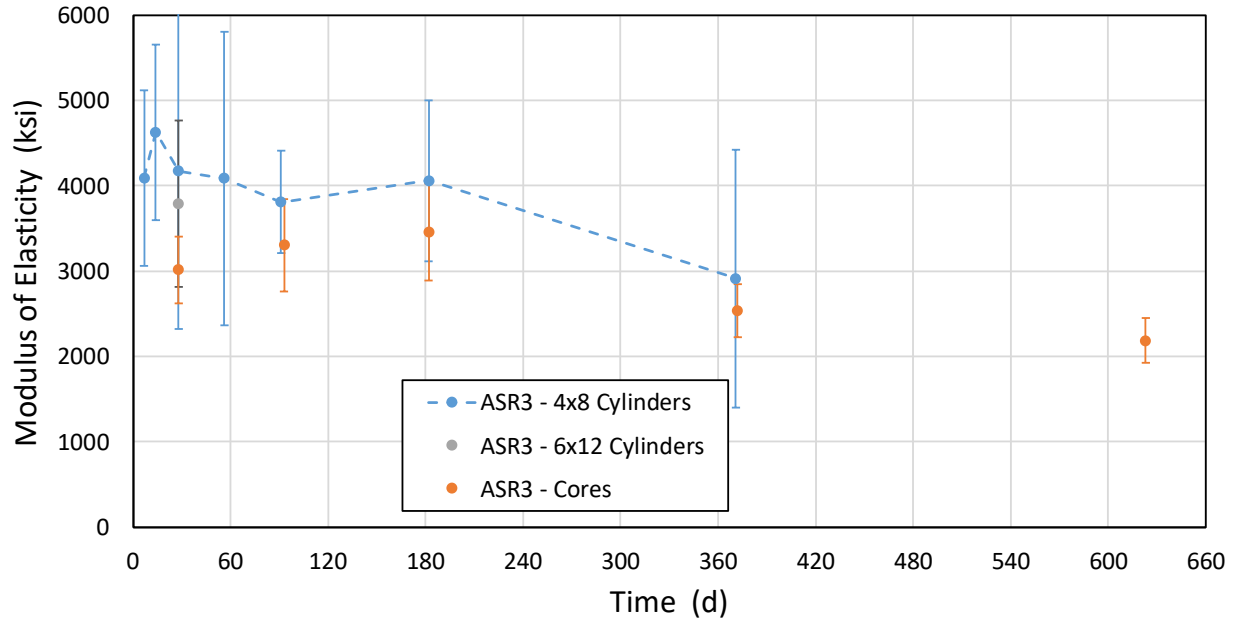
**Figure 3–33. Average compressive strength test results for cylinders and cores from (a) block ASR 1, (b) block ASR 2, (c) block ASR 3, and (d) control block**

### 3.4.2.2 Modulus of elasticity

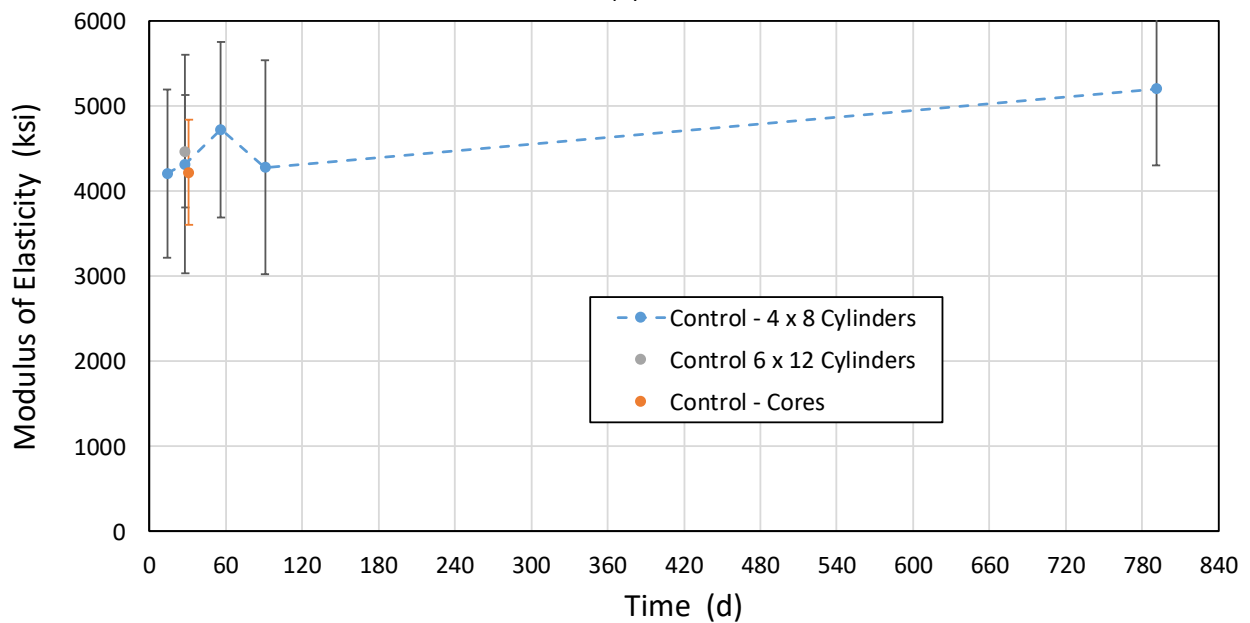
Figure 3-34 presents for all blocks the modulus of elasticity results versus time for the concrete cylinders prepared during concrete casting, and core specimens extracted from the blocks. In the figure, plots (a), (b), (c), and (d) show the results for the ASR 1, ASR 2, ASR 3, and control blocks, respectively. Except for the modulus data at 7 days and 14 days, at which for each block their variances were pooled (by making the assumption that the natural uncertainty did not change between 7 days and 14 days), the error bars represent the mean value ± expanded uncertainty

in the mean,  $U$ . For the core specimen data, the mean values and uncertainties were calculated from cores extracted from all three regions of each block. In general, the modulus of the concrete cylinders for the reactive blocks (ASR 1, ASR 2, and ASR 3) did not significantly vary over the first 180 days, after which reductions in the modulus were observed for block ASR 1 and block ASR 3. Cores extracted from the three reactive blocks showed a consistent reduction in compressive modulus with time, for more than 180 days after casting. For the three reactive blocks, the modulus had an average value in the range of 2180 ksi  $\pm$  260 ksi to 2690 ksi  $\pm$  310 ksi after 630 days, compared with a range of 3010 ksi  $\pm$  390 ksi to 3860 ksi  $\pm$  620 ksi at 28 days. The mean value of the compressive modulus of concrete of the control (non-reactive) block increased from 90 days to 791 days.





(c)



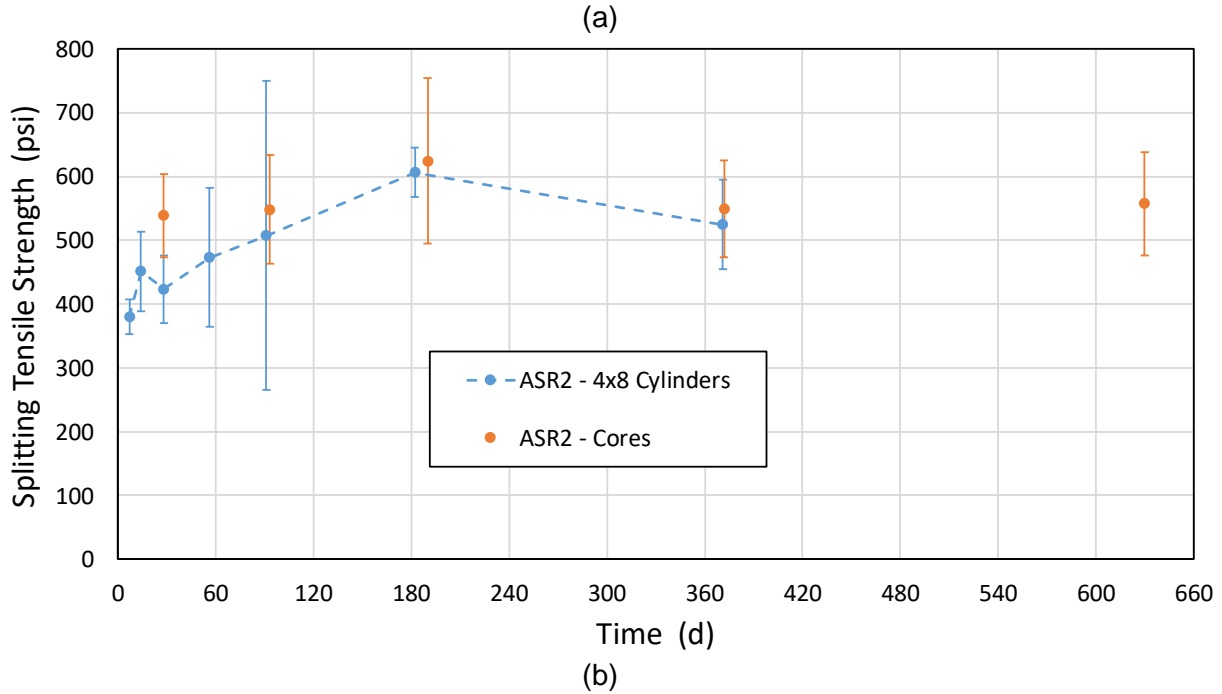
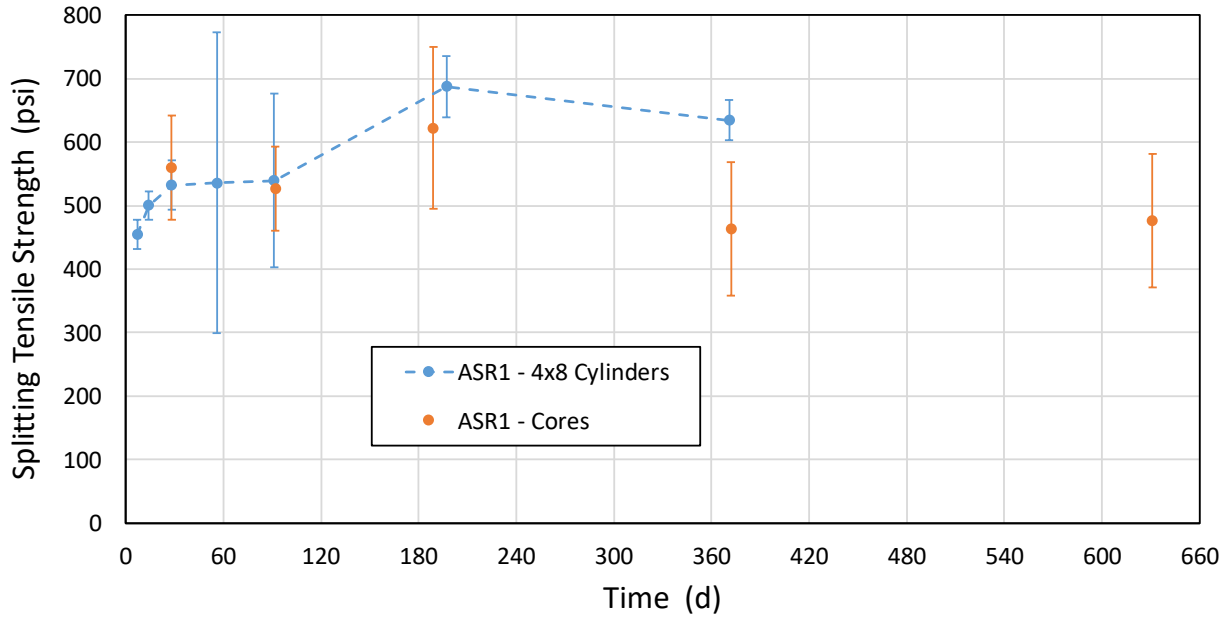
(d)

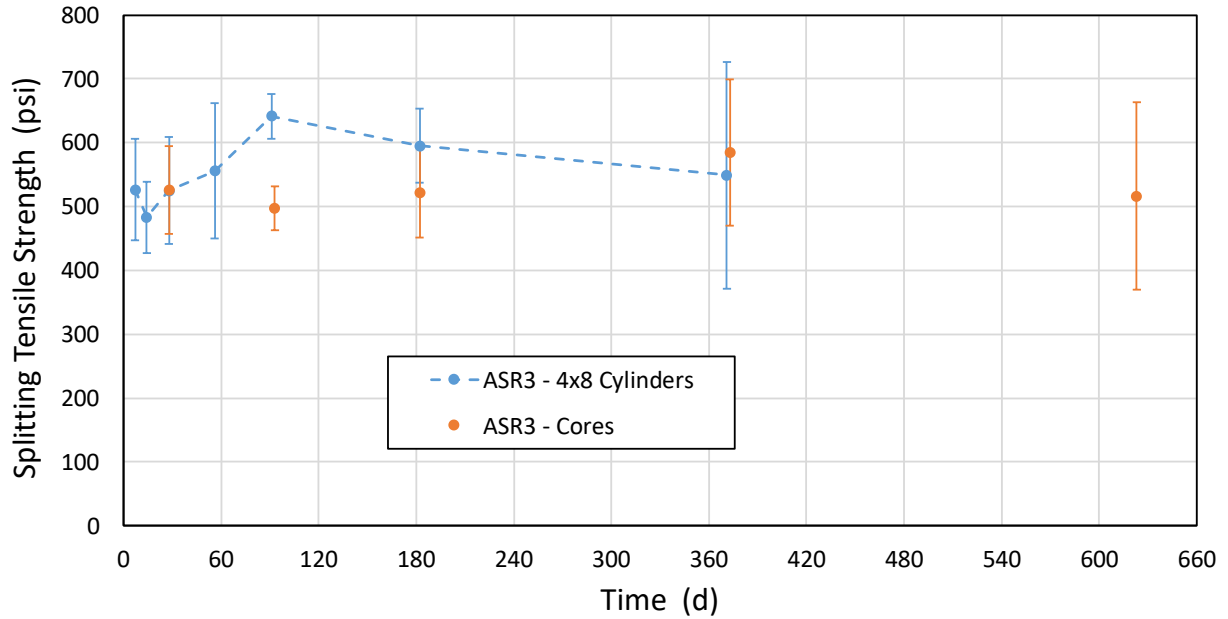
**Figure 3–34. Average modulus of elasticity test results for cylinders and cores from (a) block ASR 1, (b) block ASR 2, (c) block ASR 3, and (d) Control block**

### 3.4.2.3 Splitting tensile strength

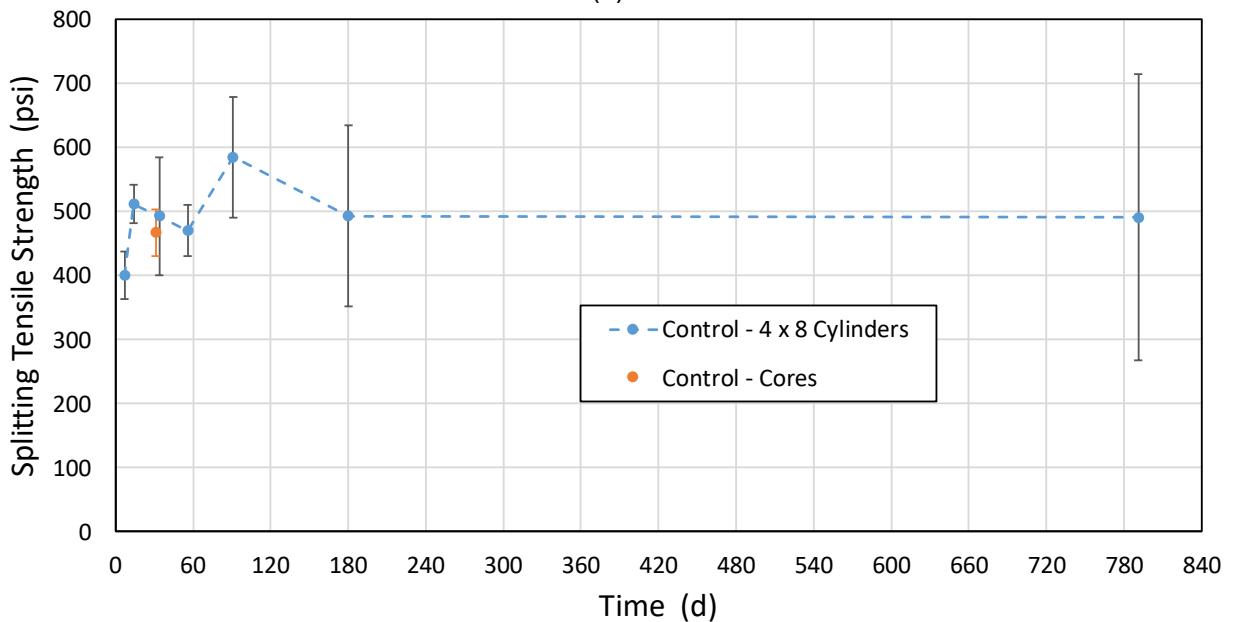
Figure 3-35 presents for all blocks the splitting tensile strength results versus time for the concrete cylinders prepared during concrete casting, and core specimens extracted from the blocks. In the figure, plots (a), (b), (c), and (d) show the results for the reactive blocks ASR 1, ASR 2, ASR 3, and the control block, respectively. The error bars in the plot correspond to the mean value  $\pm$  expanded uncertainty in the mean,  $U$ . For the core specimen data, the mean values and

uncertainties were calculated from cores extracted from all three regions of each block. For reactive blocks ASR 1 and ASR 2, the cylinder and core data showed an increase in mean tensile strength over the first 200 days. Beyond that, slight reductions in the mean tensile strength were observed. For block ASR 3, only a slight variation in mean tensile strength of the cores was observed between 90 days and 623 days, while the cylinders showed a slightly increasing mean tensile strength for the first 90 days, followed by a slight reduction in the tensile strength. The cylinders from the control block had relatively little variation after 56 days, and the mean tensile strength was nearly constant between 180 days and 791 days.





(c)



(d)

**Figure 3–35. Average splitting tensile strength test results for cylinders and cores from (a) block ASR 1, (b) block ASR 2, (c) block ASR 3, and (d) Control block**

### 3.4.3 Analysis of Core Test Results

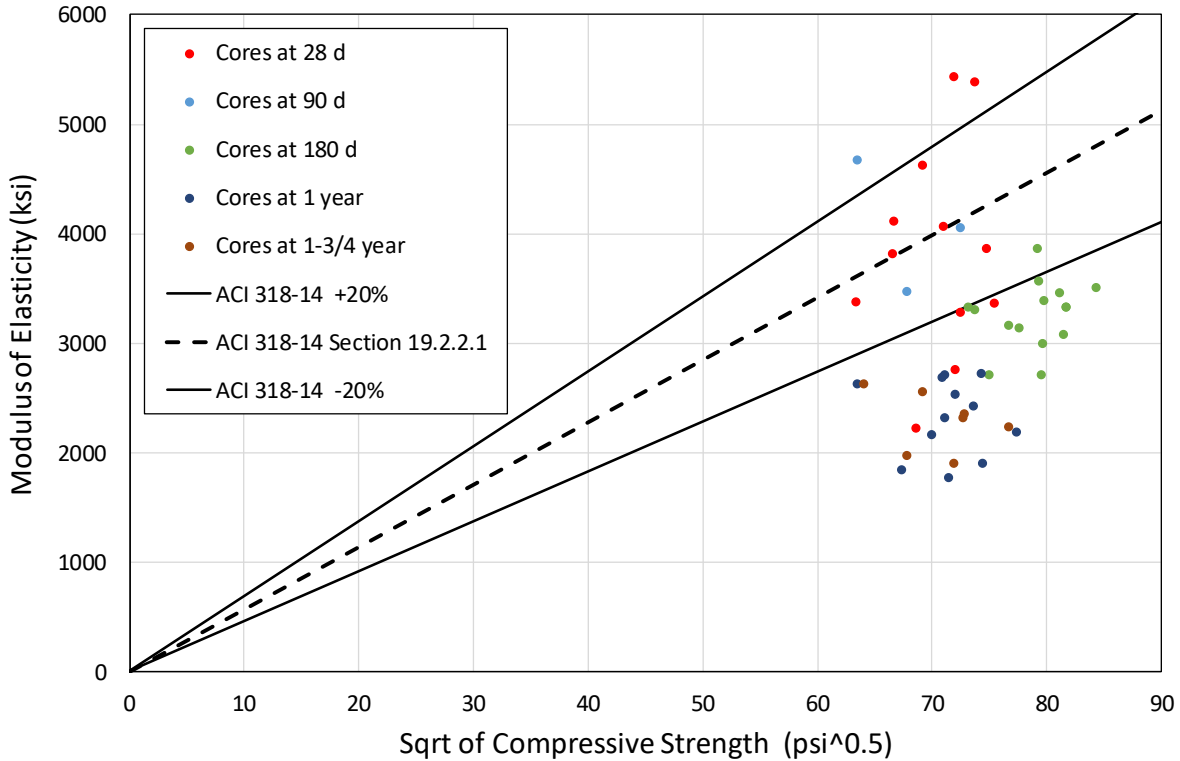
#### 3.4.3.1 Modulus of elasticity-compressive strength relationship

Figure 3-36 shows results of measured compressive modulus of cores versus the square root of the measured compressive strength (circular markers) at various times of reactive blocks ASR 1, ASR 2, and ASR 3. The different marker colors signify different ages of concrete, measured in days after casting. The dashed line in the plots represents the compressive modulus calculated

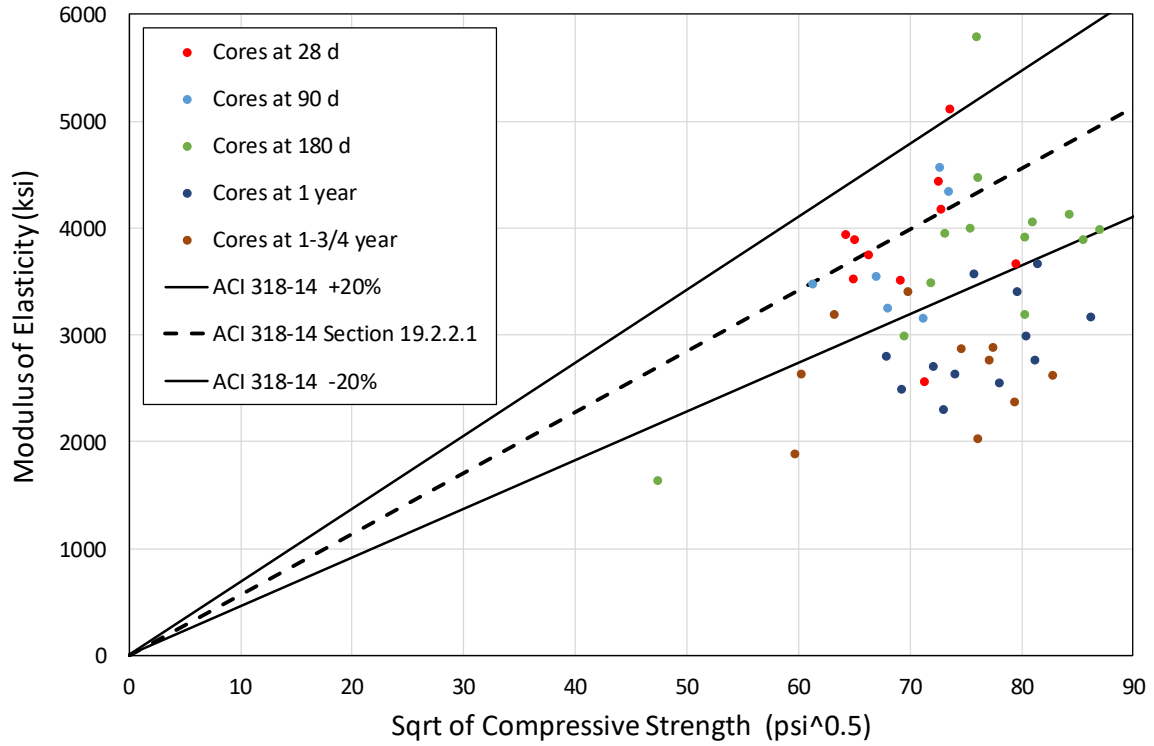
as a function of the concrete compressive strength per ACI 318-14 (Section 19.2.2.1), while the two solid lines represent  $\pm 20\%$  deviations from the ACI equation. Equation 19.2.2.1.b in ACI 318-14 calculates the compressive modulus,  $E_c$ , as a function of the concrete 28-day compressive strength,  $f'_c$ , as:

$$E_c = 57000 \sqrt{f'_c} \quad (\text{in psi})$$

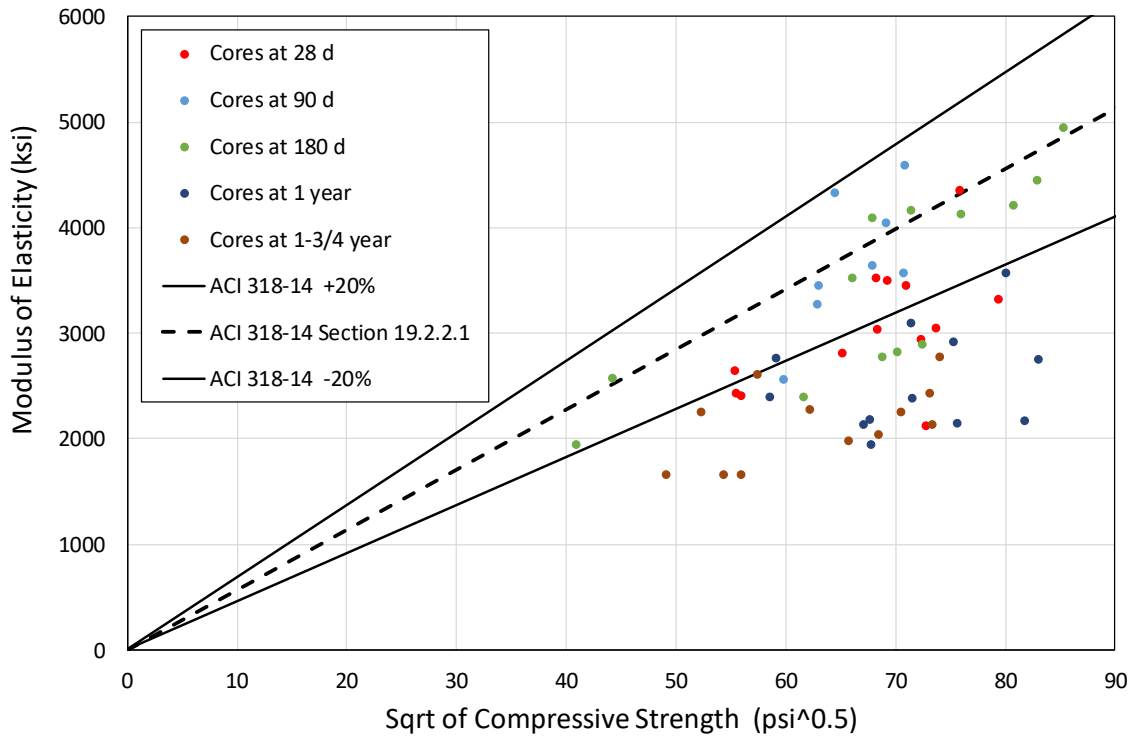
The plots in Figure 3-36 show that, at an early age (i.e., at early stages of ASR reaction), the compressive modulus of the three reactive blocks was, for the most part, within the  $\pm 20\%$  range of the ACI equation. After increased numbers of days (and consequently ASR expansions), the measured compressive modulus of the reactive blocks became significantly lower, on average, than the modulus predicted by the ACI equation. This trend indicates that the compressive modulus degraded faster with ASR expansion than did the concrete compressive strength.



(a)



(b)



(c)

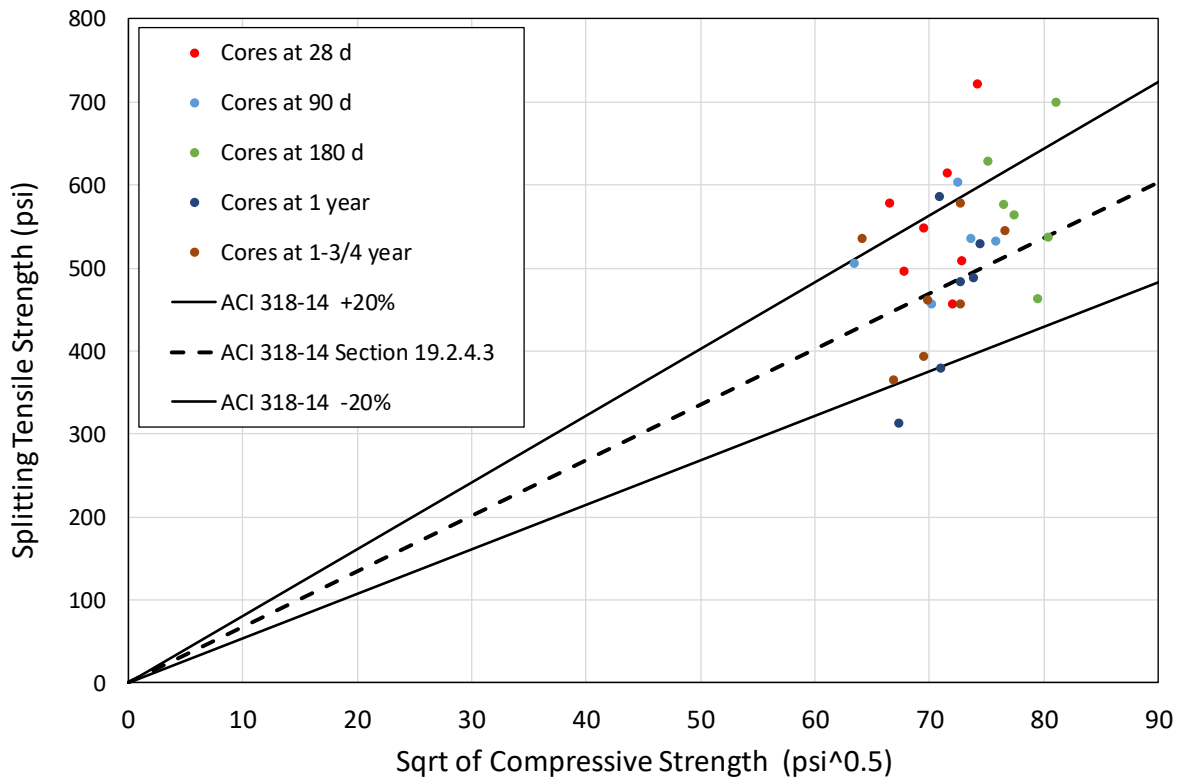
Figure 3-36. Comparison of measured modulus of elasticity and calculated modulus of elasticity based on ACI 318-14 equation for cores extracted from reactive blocks (a) ASR 1, (b) ASR 2, and (c) ASR 3

### 3.4.3.2 Splitting tensile strength-compressive strength relationship

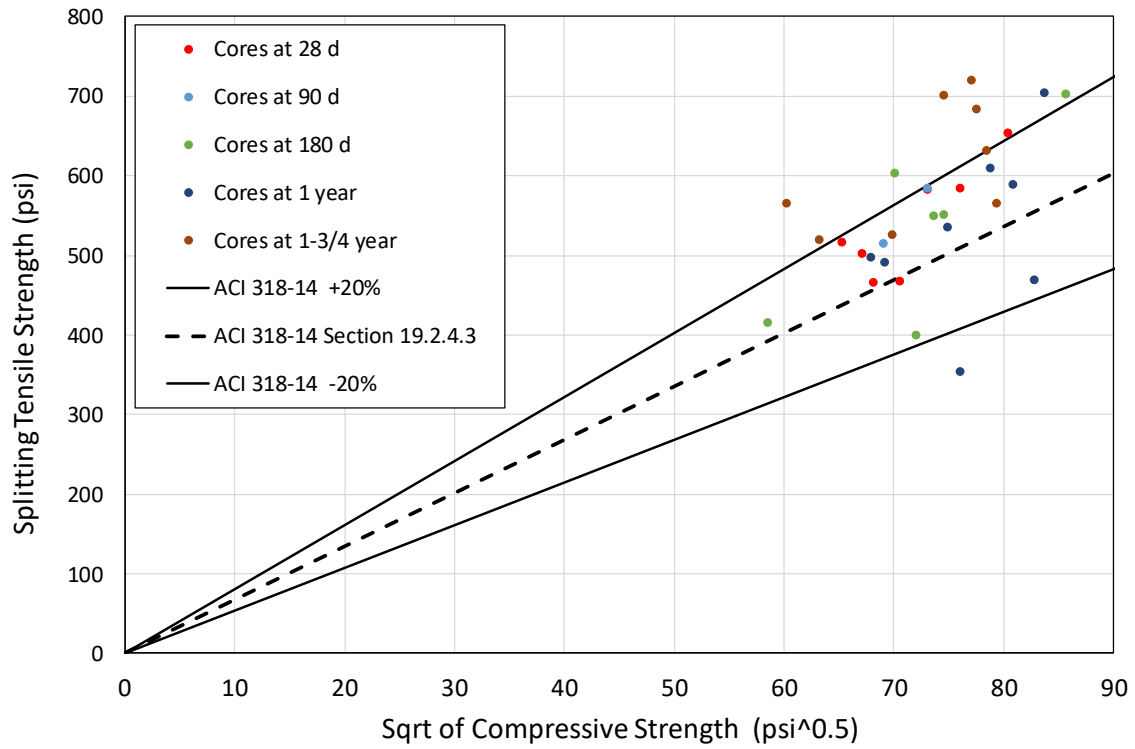
Figure 3-37 shows the measured mean splitting tensile strength of cores versus the square root of the measured mean compressive strength (circular markers) at various ages of the reactive ASR 1, ASR 2, and ASR 3 blocks, measured in days after casting. The different marker colors signify different numbers of days after casting of concrete. The dashed line in the plots presents the splitting tensile strength calculated as a function of the compressive strength of concrete per ACI 318-14 (Section 19.2.4.3), while the two solid lines present  $\pm 20\%$  deviations from the ACI equation. Section 19.2.4.3 of ACI 318-14 calculates the splitting tensile strength,  $f_{ct}$ , as a function of the measured average concrete compressive strength,  $f_{cm}$ , as

$$f_{ct} = 6.7 \sqrt{f_{cm}} \quad (\text{in psi})$$

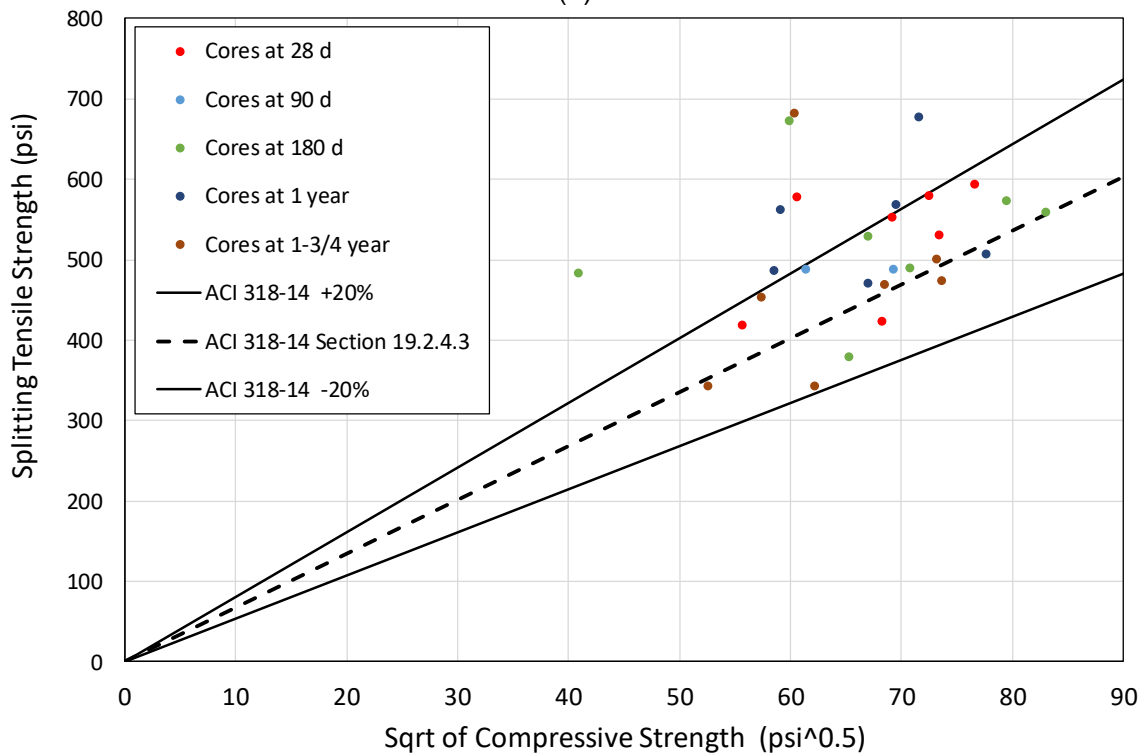
The figure shows that at an early age (at early stages of ASR reaction), the measured splitting tensile strength of the reactive blocks was, for the most part, within the  $\pm 20\%$  range of the ACI equation. After increased numbers of days (and consequently ASR expansions), the measured splitting tensile strength of the blocks became, on average, slightly higher than the ACI equation. However, the large scatter in the data does not permit development of definitive conclusions regarding the effects of ASR on the validity of the ACI splitting tensile strength equation.



(a)



(b)

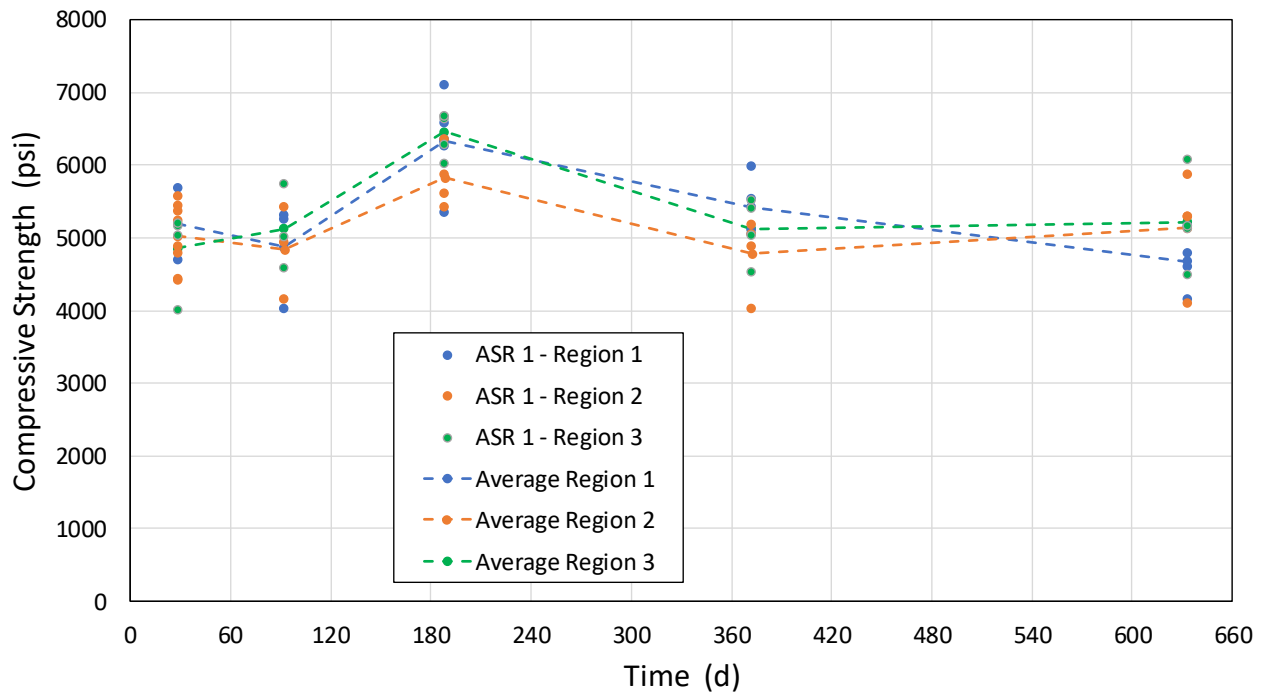


(c)

**Figure 3–37. Comparison of measured splitting tensile strength and calculated tensile strength based on ACI 318-14 equation for cores extracted from reactive blocks (a) ASR 1, (b) ASR 2, and (c) ASR 3**

3.4.3.3 Effect of confinement region

Figure 3-38 shows the measured compressive strength of cores extracted from the three confinement regions (see Chapter 2) in reactive blocks ASR 1, ASR 2, and ASR 3. The compressive strengths of the individual cores are shown as circular markers while the dashed lines connect the mean compressive strength at each day of testing. No discernable trend was found in the data regarding differences in the uniaxial compressive strength of cores extracted from the three different confinement regions of the blocks.



(a)

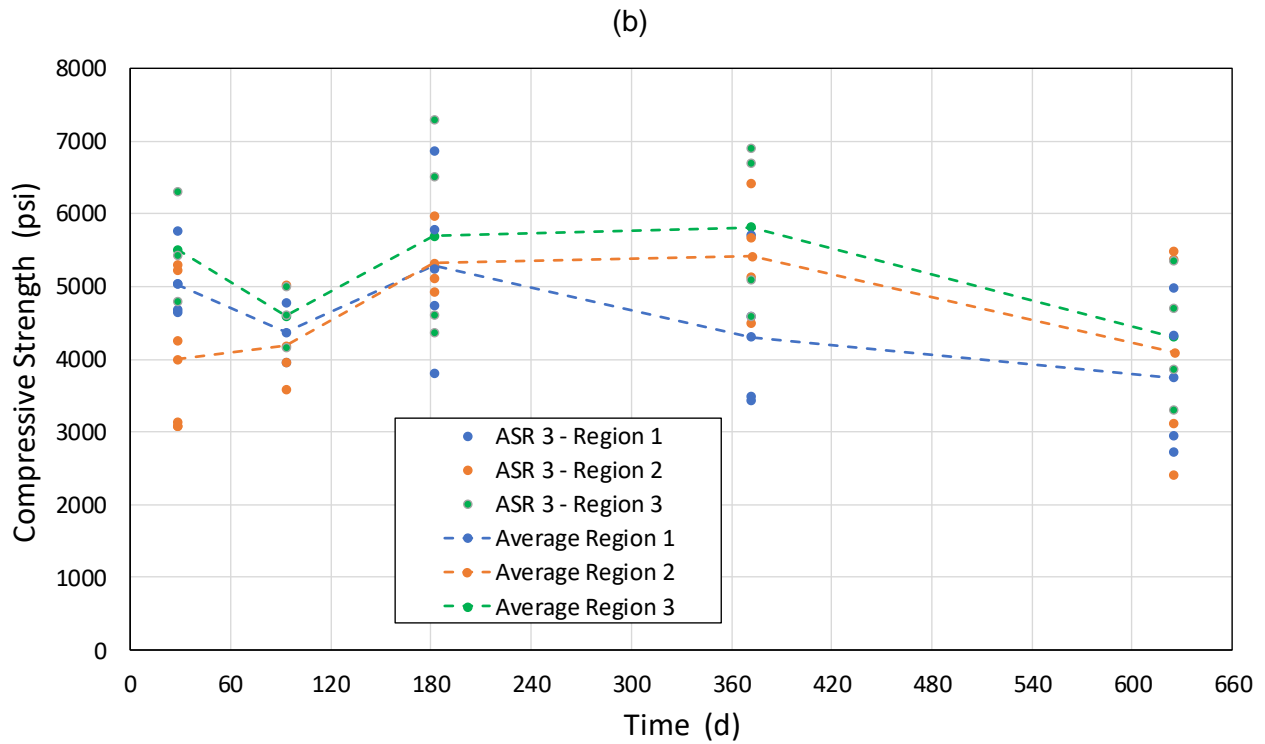
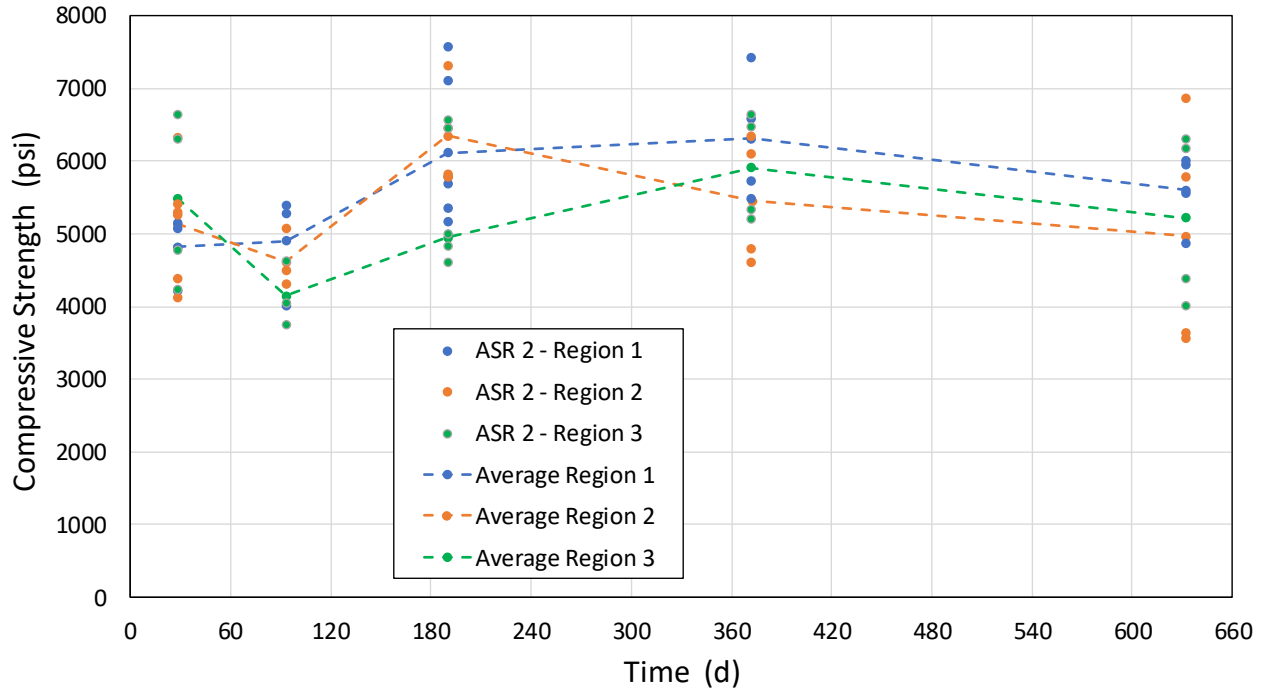
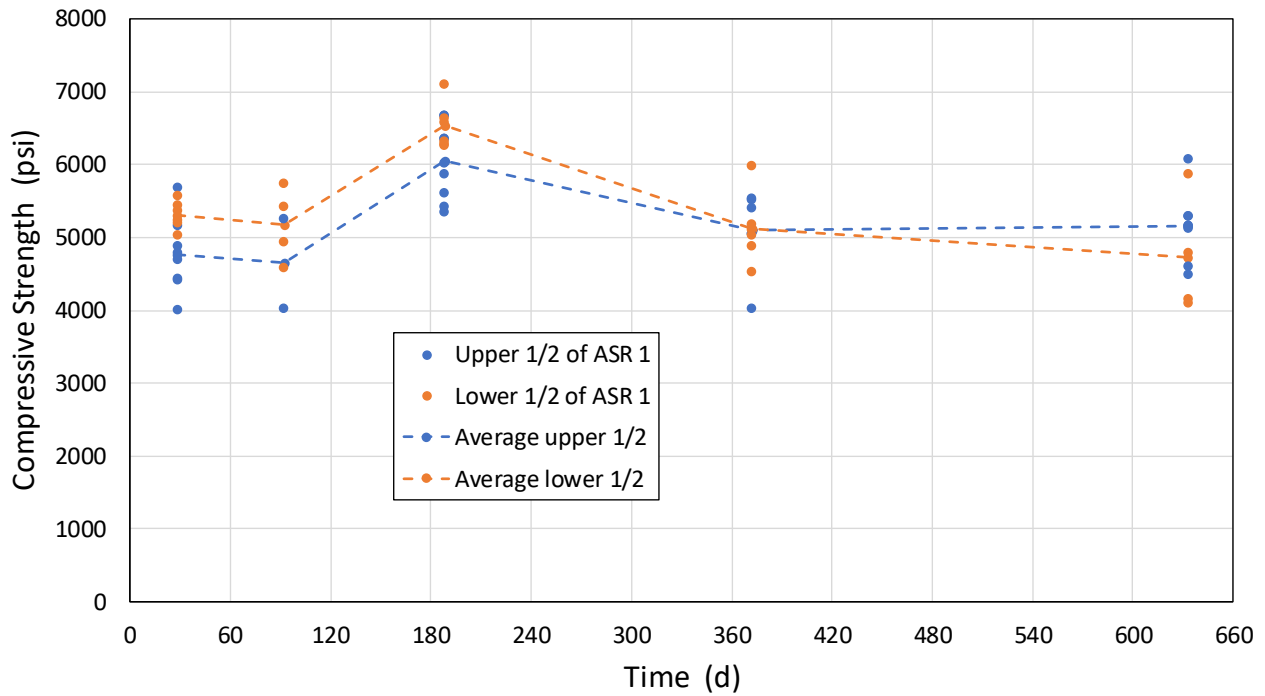


**Figure 3–38. Effect of confinement region on compressive strength of cores extracted from blocks (a) ASR 1, (b) ASR 2, and (c) ASR 3**

### 3.4.3.4 Effect of core location (height)

Figure 3-39 presents measured compressive strength of cores extracted from reactive blocks ASR 1, ASR 2, and ASR 3 in two groups: cores extracted from the lower 34 in of the block (labeled lower 1/2), and cores extracted at heights higher than 34 in (labeled upper 1/2). The compressive strengths of the individual cores are shown as circular markers while the dashed lines connect the mean compressive strength at each day of testing. While for block ASR 3, the average compressive strengths of cores extracted from the lower half of the block were, on average, higher than those extracted from the upper portion, block ASR 2 exhibited the opposite trend. As a result, no systematic trend was found in the data regarding the difference in compressive strength of cores extracted from the lower or upper portions of the blocks.



(a)

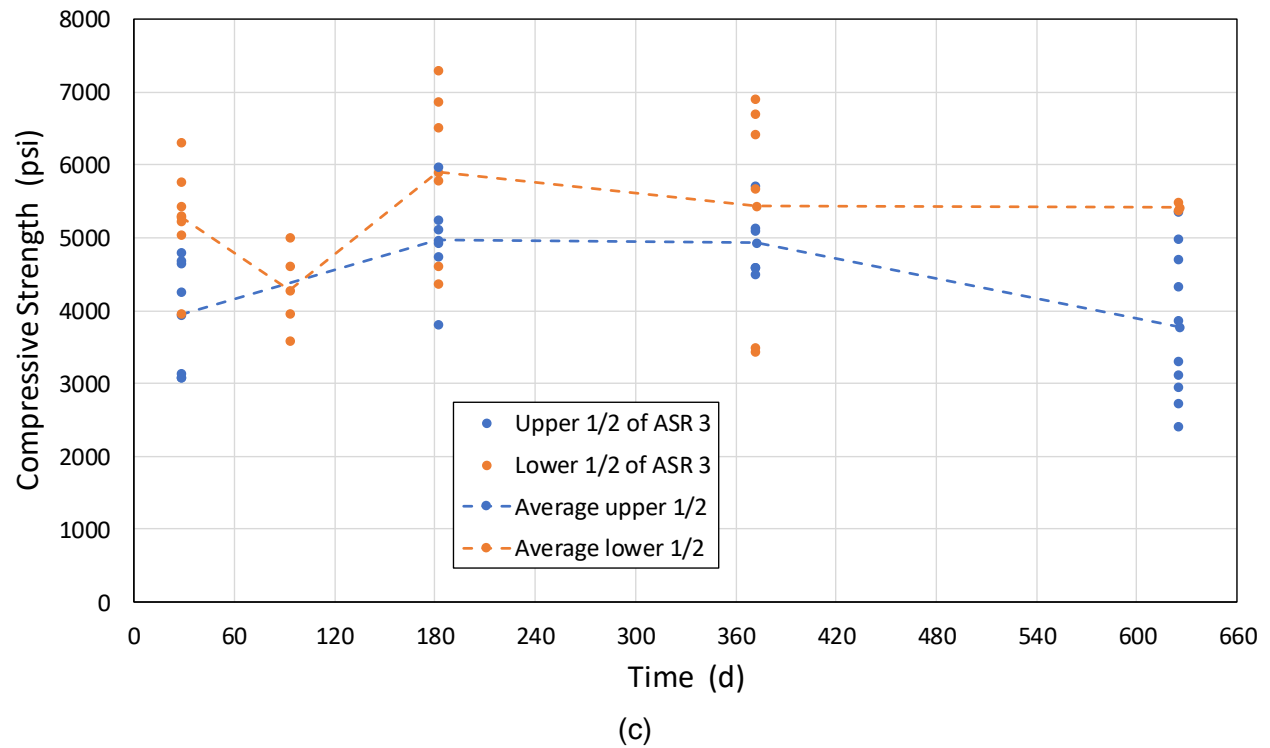
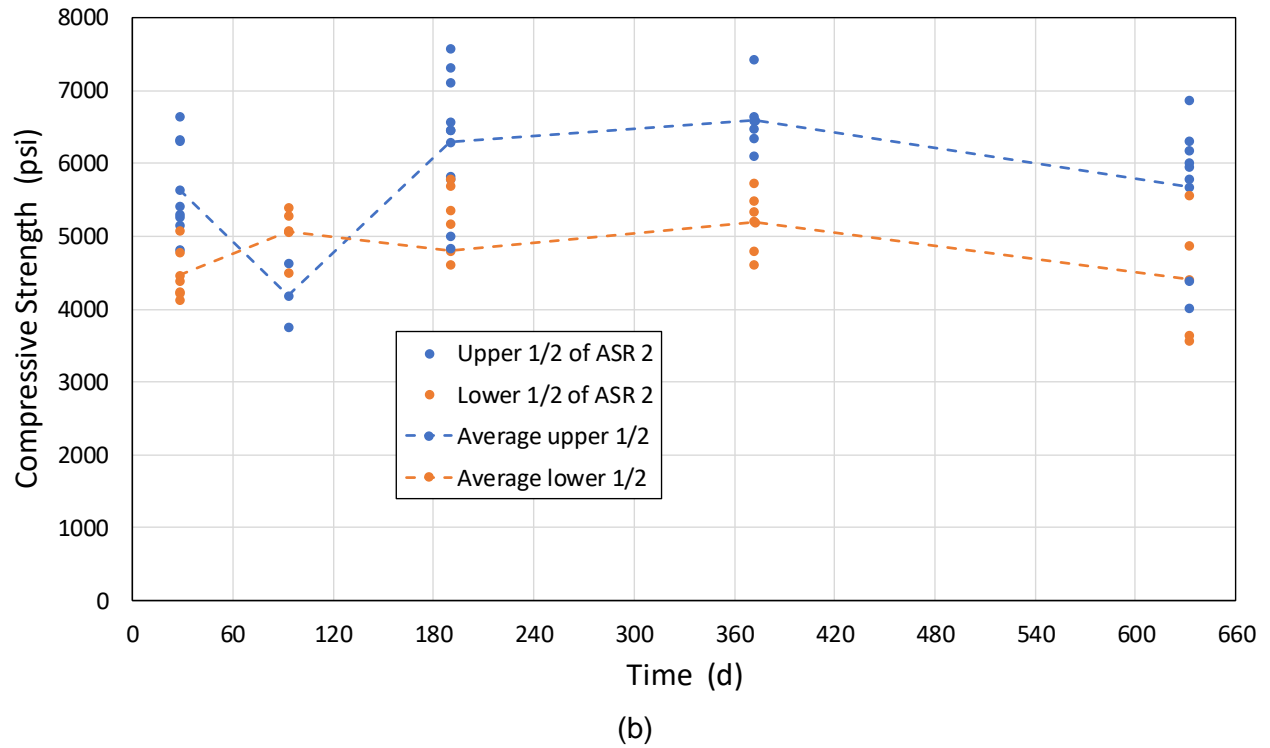


Figure 3–39. Effect of core height on compressive strength of cores extracted from blocks (a) ASR 1, (b) ASR 2, and (c) ASR 3

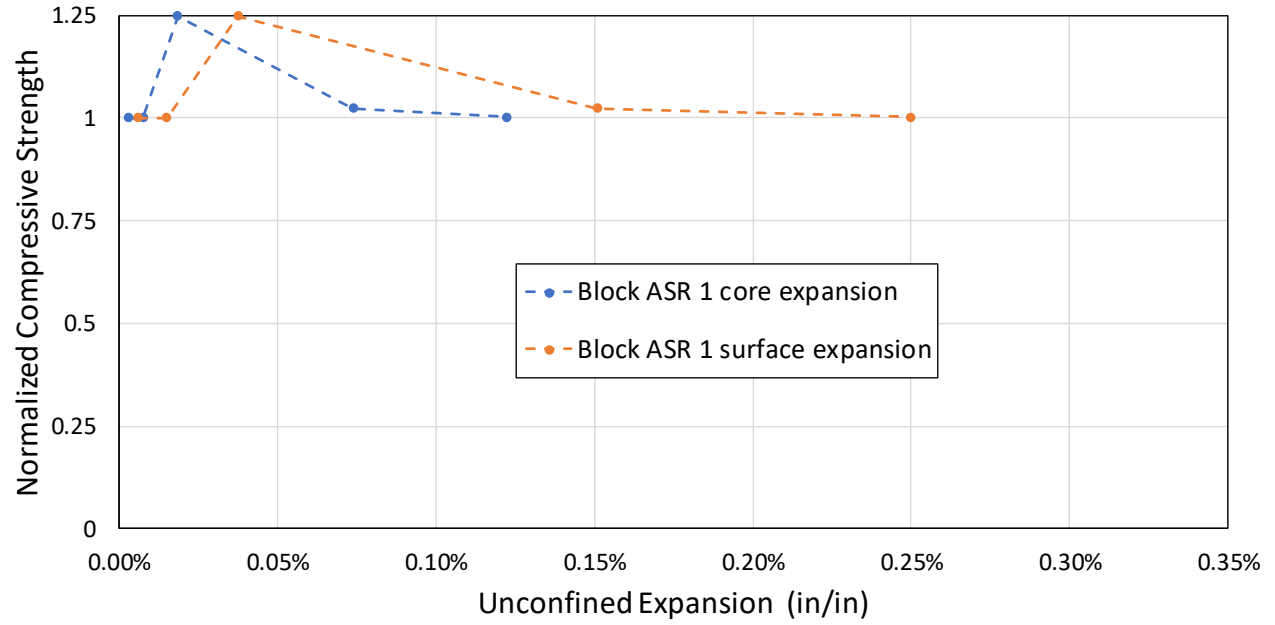
### 3.4.4 Normalized Mechanical Properties

Section 3.4.2 presented the mechanical properties of cores extracted from the reactive blocks versus time. The purpose of this section is to present the mechanical properties of cores as normalized values versus the unconfined ASR expansion of the blocks. As a result, the mean compressive strength, compressive modulus, and splitting tensile strength were normalized by their respective mean 28-days values. As shown in Sections 3.2 and 3.3, the unconfined expansion in the unconfined Region 2 of the reactive blocks was not uniform, but rather an expansion field with largest and smallest expansion at the surface and center of the blocks, respectively. Therefore, the normalized properties are plotted in this section against two unconfined linear expansion values:

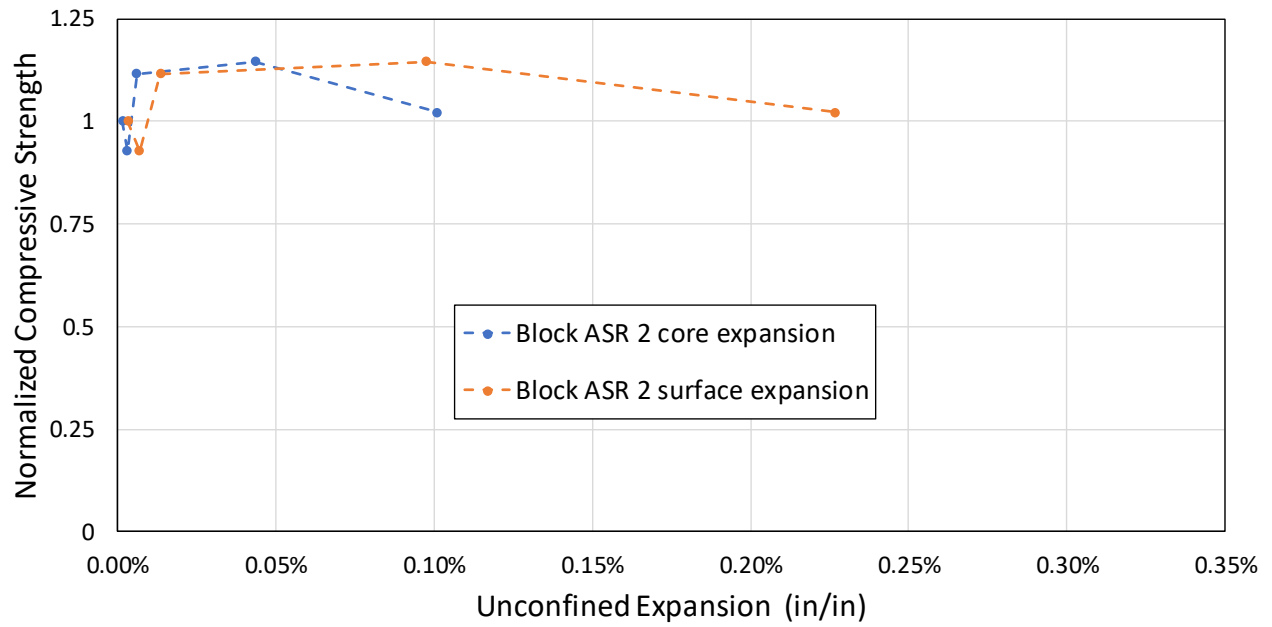
- Concrete strain measurements at the center of Region 2 of each block corresponding to the mechanical property test date. For that purpose, an average of the three strain measurements in three directions was used, see plots (b) in Figures 3-13 to 3-15.
- Surface strain measurements on the exterior faces of Region 2 of the blocks. This was achieved by scaling up the average concrete strain measurements above by the ratio of surface expansion measurement (Table 3.4) to the average concrete strain measurement at the date the surface expansion data were taken.

For the three reactive blocks, the normalized compressive strength, modulus of elasticity, and splitting tensile strength versus the unconfined linear expansion (block center expansion and surface expansion) are presented in Figures 3-40, 3-41, and 3-42, respectively. The figures show the following:

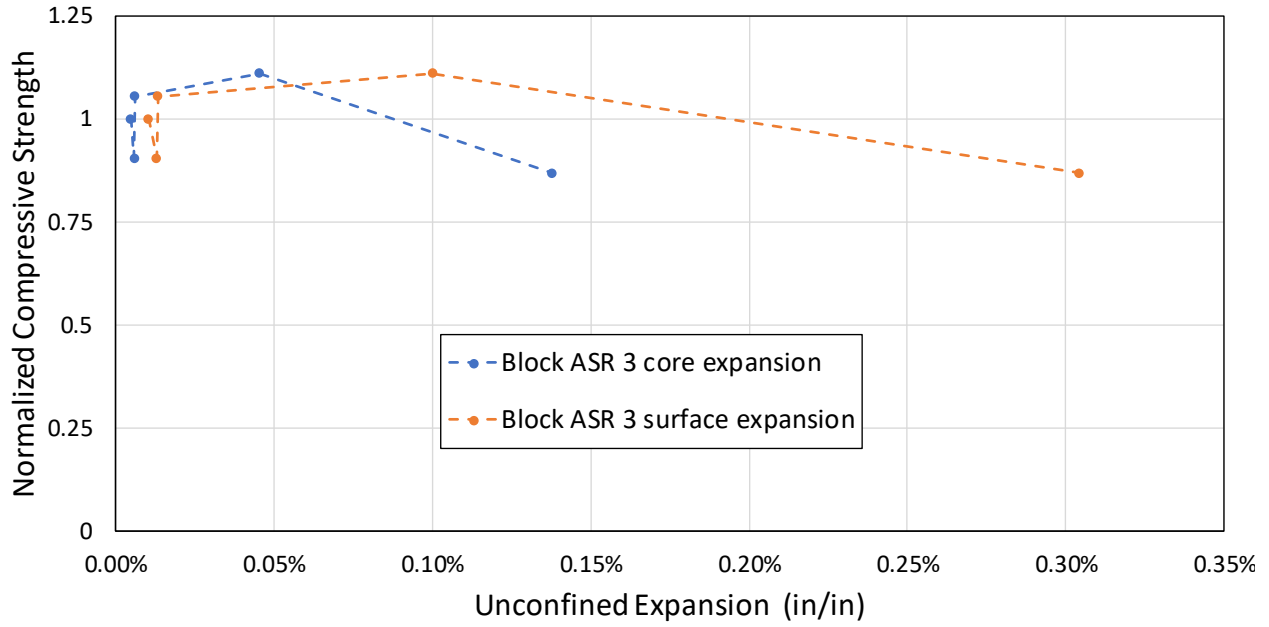
- Except for cores from block ASR 3, no reduction in the uniaxial compressive strength compared with the 28-day compressive strength was observed. Cores from block ASR 3 exhibited a reduction in compressive strength of  $13\% \pm 15\%$  compared with the 28-day strength.
- All reactive blocks showed reductions in the modulus of elasticity of  $28\% \pm 9\%$  to  $41\% \pm 6\%$  compared with the 28-day modulus of elasticity.
- Cores from blocks ASR 2 and ASR 3 showed no reductions in the splitting tensile strength, while those from block ASR 1 exhibited a reduction of  $15\% \pm 13\%$  in the splitting tensile strength compared with the 28-day strength.



(a)

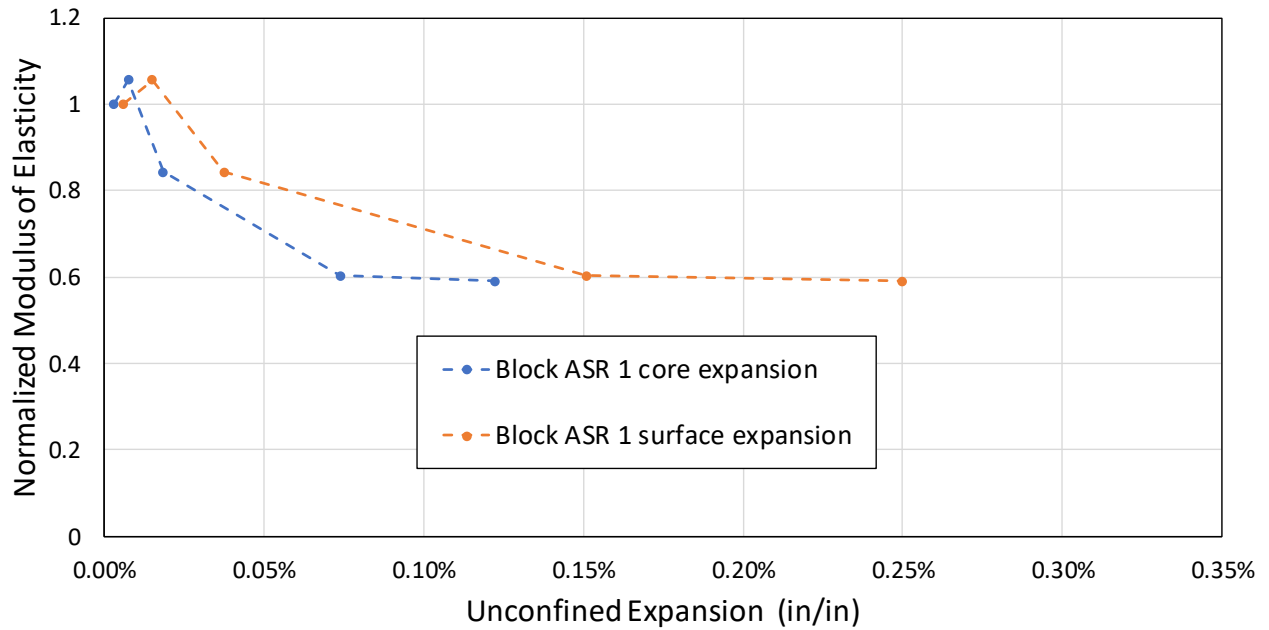


(b)

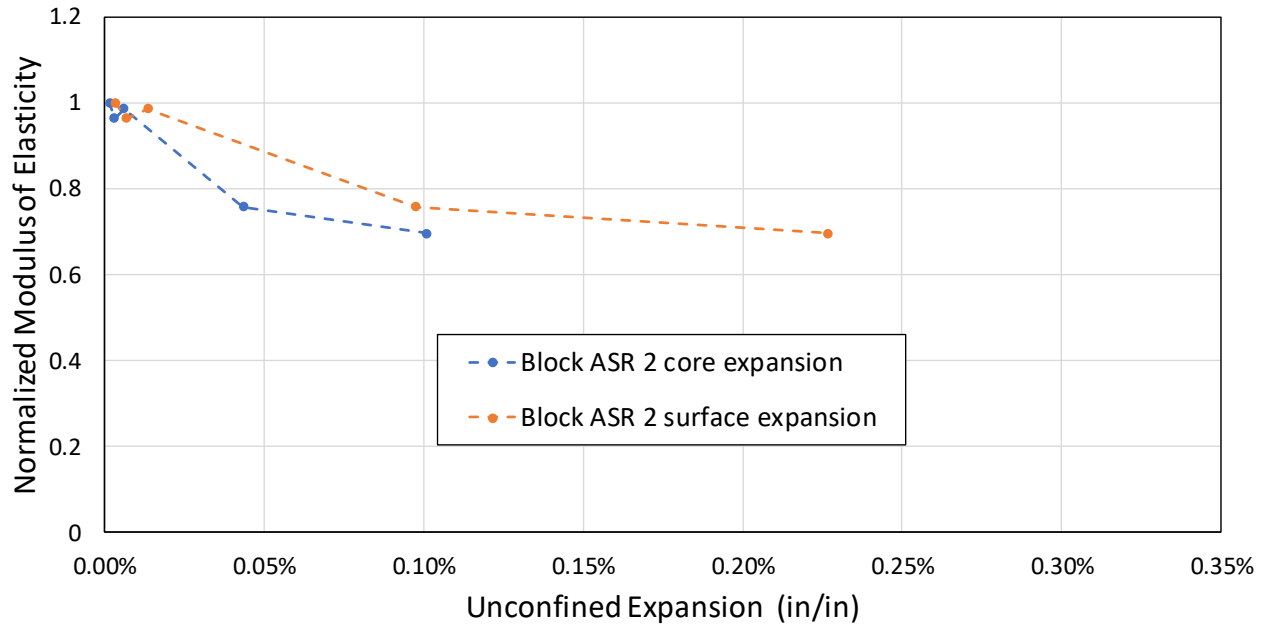


(c)

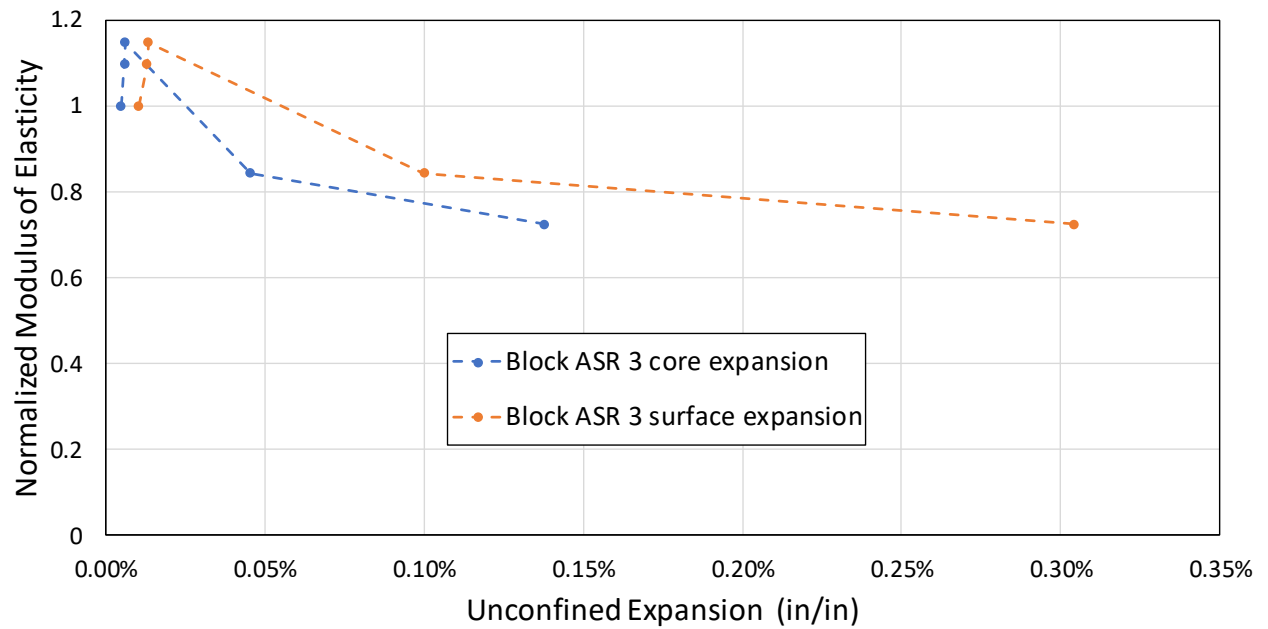
Figure 3–40. Average compressive strength normalized to 28-day compressive strength versus unconfined expansion for cores from (a) ASR 1, (b) ASR 2, and (c) ASR 3 blocks



(a)

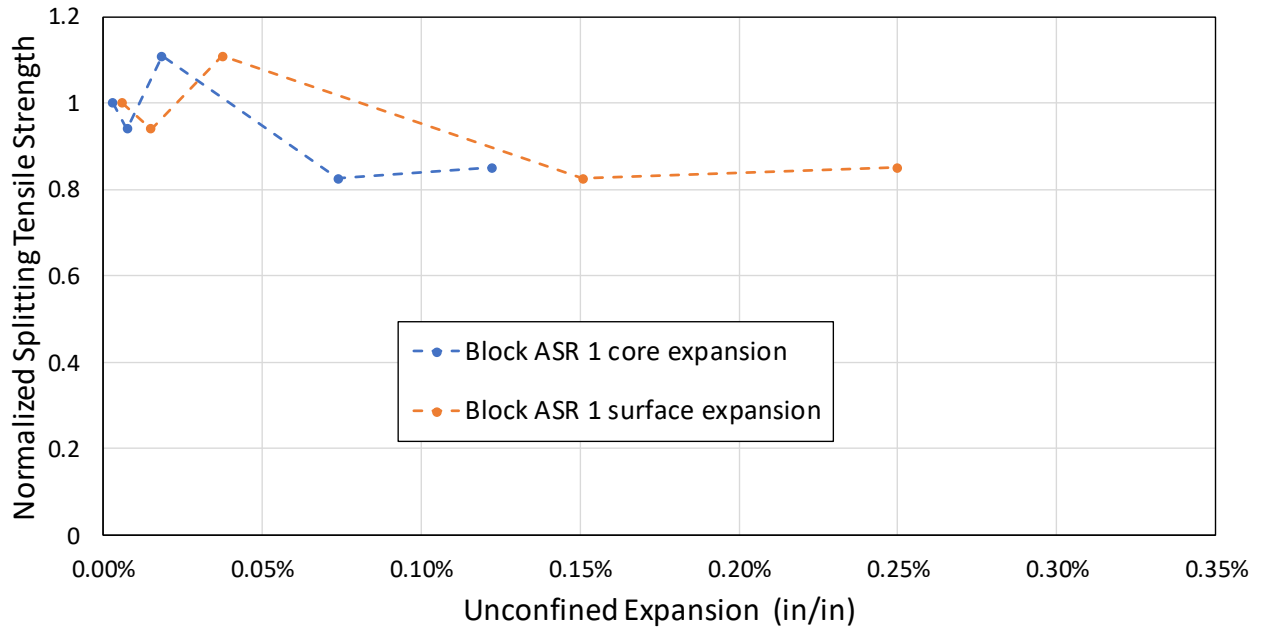


(b)

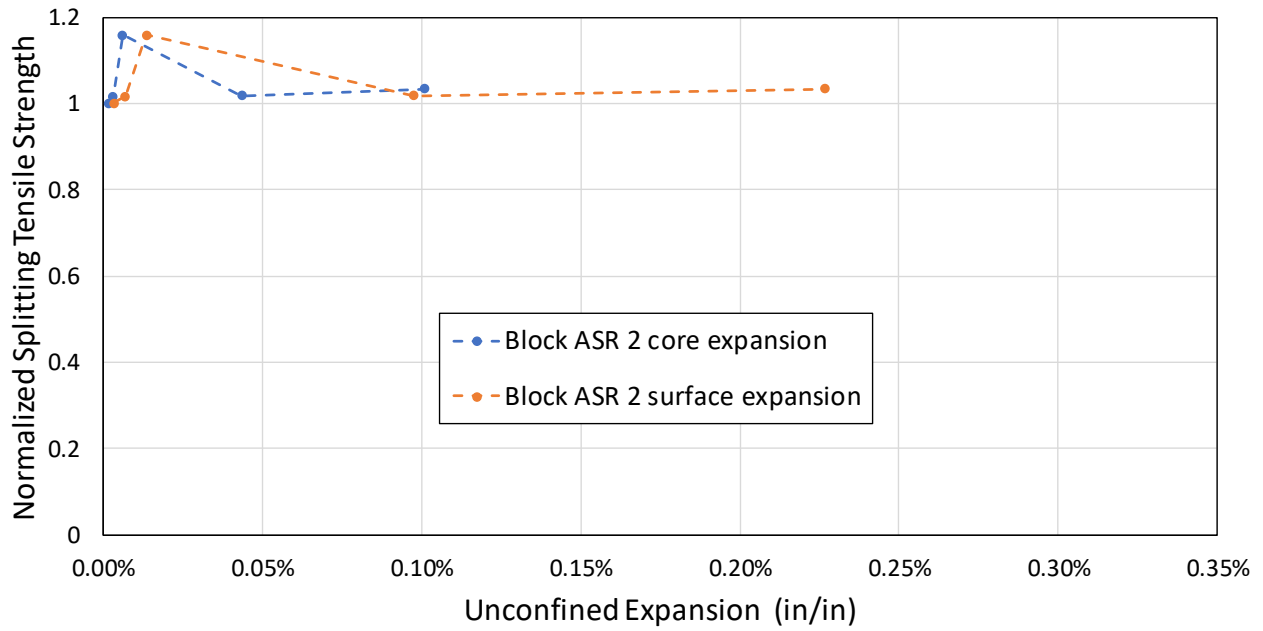


(c)

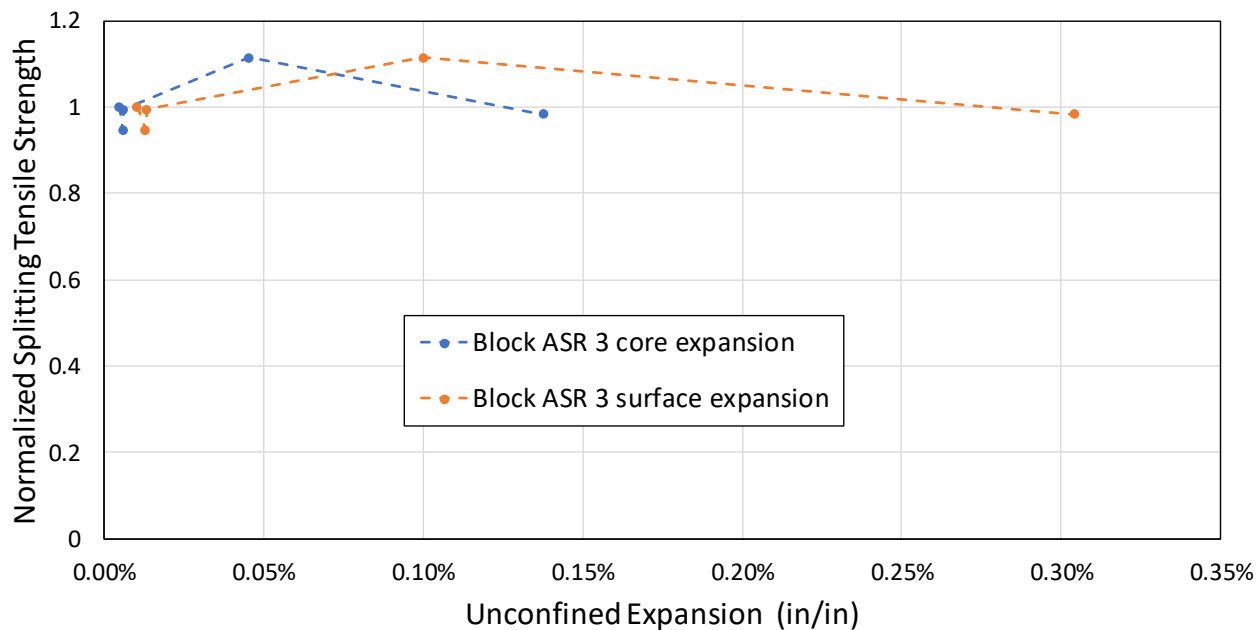
**Figure 3–41. Average modulus of elasticity normalized to 28-day modulus of elasticity versus unconfined expansion for cores from (a) ASR 1, (b) ASR 2, and (c) ASR 3 blocks**



(a)



(b)



(c)

**Figure 3–42. Average splitting tensile strength normalized to 28-day tensile strength versus unconfined expansion for cores from (a) ASR 1, (b) ASR 2, and (c) ASR 3 blocks**

### 3.5 TRIAXIAL TESTING OF CORE SPECIMENS

To evaluate the effects of different degrees of confinement on the compressive strength of ASR-affected concrete, core specimens extracted from the reactive blocks were tested under radial pressure, representative of the confinement provided by the reinforcement cage, while uniaxial loading was applied in the longitudinal direction until loss of strength was observed. Details of the TPV that was designed and fabricated by NIST to conduct the triaxial testing of core specimens was shown in Section 2.7. In the following sections, Section 3.5.1 discusses the amount of confinement pressure that was used in the experiments. Section 3.5.2 outlines the experimental plan for evaluation of the relationship between the confinement pressure and the compressive strength of the ASR-affected concrete, while Section 3.5.3 presents the test procedure and the method used to correct the measured loads to account for friction in the rod seal and pressure from the hydraulic oil inside the TPV. Test results and statistical analysis of these results are provided in Section 3.5.4.

#### 3.5.1 Estimate of confinement pressure

Since the purpose of the triaxial compression testing was to examine the relationship between the confinement pressure and the compressive strength of the cores rather than the compressive strength at a given expansion level, an estimate of the maximum confinement pressure that might have been experienced inside the block specimens was used.

For that purpose, an analysis was conducted for Region 3 of the reactive blocks since it had the highest confinement and as a result, the maximum confinement pressure. For this analysis, the reinforcing bars were assumed to have yielded (with a yield stress of  $f_y = 68$  ksi). The assumption

was supported by the strain measurements on the reinforcing bars in Regions 1 and 3 of block ASR 3 (see Section 3.2.1). The average stresses in the confined area (area bounded by the reinforcing bars),  $\sigma_{avg}$ , in three orthogonal directions were calculated as:

$$\sigma_{avg} = A_s f_y / b_c d_c \quad (3.1)$$

where  $A_s$  is the total area of steel reinforcement at a given cross section and in a given direction, and  $b_c$  and  $d_c$  define the concrete dimensions of the cross section bounded by the reinforcing bars. Using the equation above, the average confinement stresses were calculated as 390 psi in the vertical direction, 350 psi in transverse direction, and 422 psi in the longitudinal direction (see Figure 3-43).

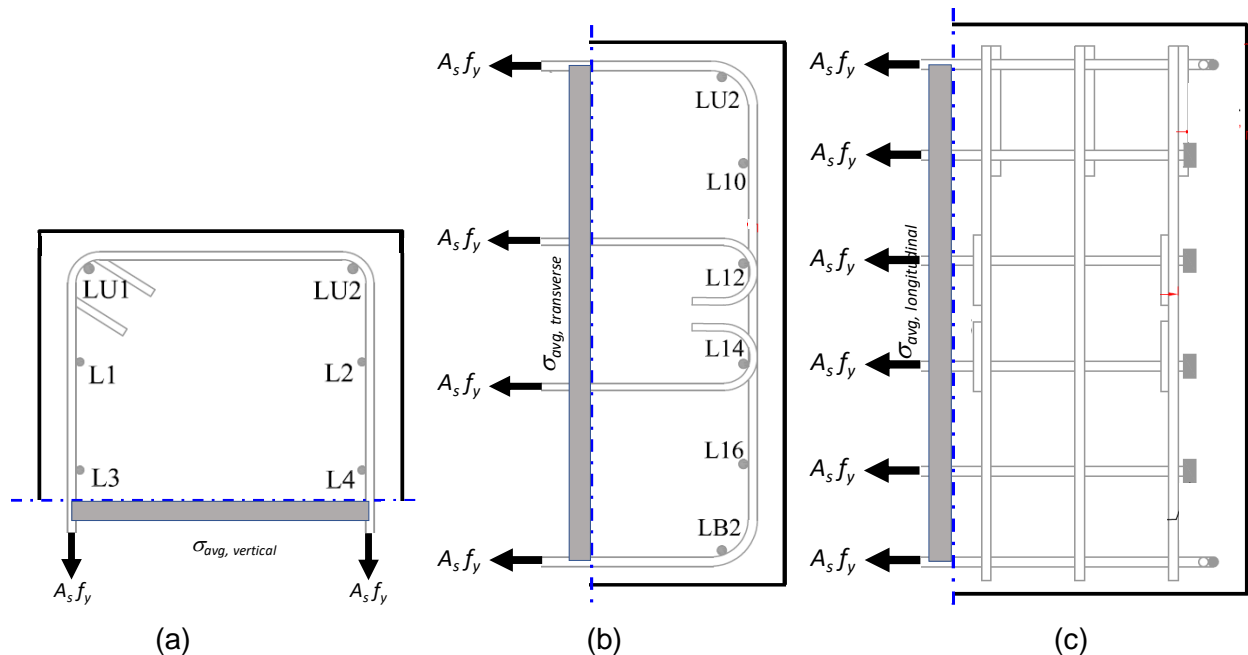


Figure 3-43. Concrete stresses in the (a) vertical, (b) transverse, and (c) longitudinal direction

The average stresses outlined above, however, do not represent the maximum stresses that would be experienced inside the blocks due to stress localizations, especially in areas close to the reinforcing bars. As a result, a maximum confinement pressure of 700 psi was considered in this study to account for potential localizations and to allow for a large range of confinement pressures in determining the compressive strength of confined concrete without the need for extrapolation.

### 3.5.2 Design of TPV experiment

As stated earlier, the purpose of the triaxial compression test was to examine and develop the relationship between the confinement pressure and the in-situ compressive strength of ASR-affected concrete. To achieve that objective, the triaxial compression testing considered the following three variables:

- Confinement pressure: Three levels of radial confinement pressure were used: 0 psi, 350 psi, and 700 psi.

- ASR expansion: Two levels of ASR expansion were considered: (1) cores extracted from low reactive block ASR 1 and (2) cores extracted from high reactive block ASR 3.
- Confinement region: Two levels of confinement were considered: (1) cores extracted from intermediate confinement Region 1 (with volumetric reinforcement ratio  $\rho_v = 0.72\%$ , see Section 2.2) and (2) cores extracted from heavy confinement Region 3 (volumetric reinforcement ratio  $\rho_v = 1.14\%$ ).

Schematically, the variables considered in triaxial compression testing are shown in Figure 3-44.

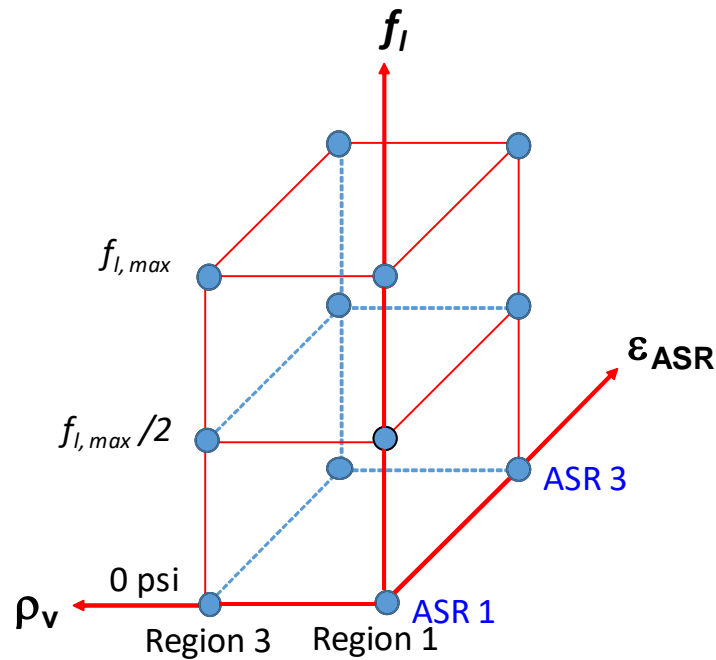


Figure 3-44. Variables considered in the design of experiment

Based on the above discussion, the test matrix for triaxial compression testing of cores, which called for a total of 24 core specimens for statistical evaluation of the above three variables is shown in Table 3-7. Note that for test 1 to 12, the specified radial confinement pressure is 0 psi. This means these tests were actually performed as uniaxial compression tests. Only test 13 to 24, with confinement pressures of 350 psi and 700 psi, were performed using the TPV in conjunction with the servohydraulic load frame.

**Table 3-7. Test matrix for triaxial testing of cores**

<b>Test</b>	<b>Pressure (psi)</b>	<b>Region</b>	<b>Block</b>
1	0	1	ASR 1
2	0	1	ASR 1
3	0	1	ASR 1
4	0	3	ASR 1
5	0	3	ASR 1
6	0	3	ASR 1
7	0	1	ASR 3
8	0	1	ASR 3
9	0	1	ASR 3
10	0	3	ASR 3
11	0	3	ASR 3
12	0	3	ASR 3
13	350	1	ASR 1
14	700	1	ASR 1
15	350	3	ASR 1
16	700	3	ASR 1
17	350	1	ASR 3
18	700	1	ASR 3
19	350	3	ASR 3
20	700	3	ASR 3
21	350	1	ASR 1
22	350	3	ASR 1
23	350	1	ASR 3
24	350	3	ASR 3

### 3.5.3 TPV test procedure and data correction

#### 3.5.3.1 Test procedure

Triaxial testing was conducted on cores extracted from reactive blocks ASR 1 and ASR 3 after 1024 days to 1089 days from concrete placement. At the time of this testing, the expansions in all blocks had plateaued. Similar to the mechanical property testing described in Section 3.4, cores were extracted from Regions 1 and 3 of those blocks. To eliminate the effect of height on

the results, all cores were extracted from mid-height of the blocks. Each core yielded three specimens with the same size as that shown in Section 3.4. The deepest specimen was used for the TPV testing, while the other two specimens were used for uniaxial compression tests per the test matrix in Table 3-7. To prepare and create a smooth surface at the top and bottom of each specimen, the cores were cut and the surfaces were ground.

For testing in the TPV (Test 13 to 24), each core specimen was wrapped with a shrink tube, and O-rings were used at the top and bottom of the specimen to prevent oil leakage into the specimen (Figure 3-45(a)). The specimen was then placed inside the TPV and a metallic screen was installed around the specimen to prevent any debris or fragments from disrupting the flow of the hydraulic oil (Figure 3-45(b)). The bolts at the bottom of the TPV chamber were tightened and placed in the universal testing machine (Figure 3-45(c)). The chamber was then filled with hydraulic oil and pressure inside the TPV was increased to the desired level using a hydraulic pump. At this stage, the loading from the servohydraulic load frame was applied under displacement control at a rate of 0.004 in/min (Figure 3-45(d)). As mentioned in Section 2.7, a feedback control system ensured that the specified pressure was maintained during loading, and as a result, the pressure inside the TPV was maintained within 1 % of the specified pressure during testing. The loading continued until the applied axial load (post-peak) dropped by 10 %, signifying failure or loss of load carrying capacity of the core specimen. At that moment, the test was stopped and the peak load value was used to calculate the compressive strength of the cored specimen. The typical failure of the specimen was characterized by longitudinal cracks that were observed on the perimeter of the specimen (Figure 3-45(e)).



(a)



(b)



(c)



(d)



(e)

**Figure 3-45. Triaxial compression test procedure: (a) specimen was with a shrink tub and O-rings, (b) specimen inside TPV with metallic screen, (c) assembled TPV with bolts tightened, (d) TPV test setup in servohydraulic load frame, and (e) failed specimen**

### 3.5.3.2 Data correction

A schematic of the TPV assembly is shown in Figure 3-46. Compressive loads from the load frame were applied through a piston, which passed through the lid of the TPV chamber, to the concrete specimen. Friction in the rod seal and pressure from the oil in the TPV both contributed to the force measured by the load cell during testing. The pressure in the TPV created axial

stresses in the concrete specimen. Because the concrete core specimen had a smaller diameter than the piston, the load applied to concrete core specimen due to pressure in the chamber was smaller. As a result, a correction to the measured peak force was required to compensate for the forces generated due to friction and oil pressure.

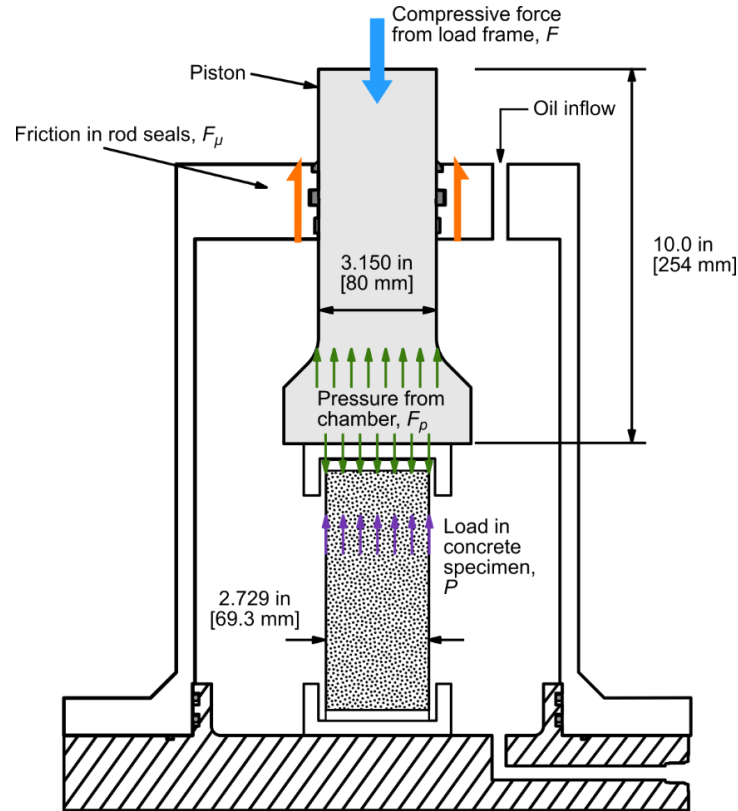


Figure 3-46. Schematic of TPV assembly showing load transfer mechanism

The total force on the concrete cylinder,  $P$ , which is the quantity of interest in these tests, is given by

$$P = F - F_0 - F_\mu - F_p \quad (3.2)$$

where  $F$  is the load measured and recorded by the load cell during testing,  $F_0$  is the offset reading at zero applied load (measured),  $F_\mu$  is the force in the rod seal due to motion of the piston (estimated), and  $F_p = f_l (A_p - A_c)$  is the difference in force applied by the pressure in the TPV due to the different diameters of the piston and concrete core (calculated).  $A_p$  is the area of the piston that passes through the lid of the TPV,  $A_c$  is the area of the concrete cylinder, and as defined before,  $f_l$  is the measured pressure inside the TPV. The uncertainty in the measurement of the force  $F$  is reported in Table D-1 in Appendix D.

In order to estimate the force corrections that needed to be applied, two tests at pressures of 350 psi and 700 psi were performed without a concrete core specimen in the TPV. The force recorded in the actuator included: (1) an initial offset at zero pressure due to both the instrument offset and initial friction, (2) pressure in the chamber reacting against the piston, and (3) friction of the rod seal at the specific pressure tested. Figure 3-47 shows the measured force in the actuator load cell during the two tests. Each test consisted of three phases. The actuator position

was held constant and the chamber pressure was increased to the target pressure value (Pressurization in Figure 3-47). Then, under displacement control, the actuator was displaced downward 0.04 in at a rate of 0.004 in/min (Testing in the figure). This rate corresponded to the displacement rate used during testing of the core specimens (Section 3.5.3.1). After reaching the target displacement, pressure in the chamber was slowly released (Depressurization in the figure). Each test was repeated twice, and the results were similar. Therefore, only one test is shown here, for clarity.

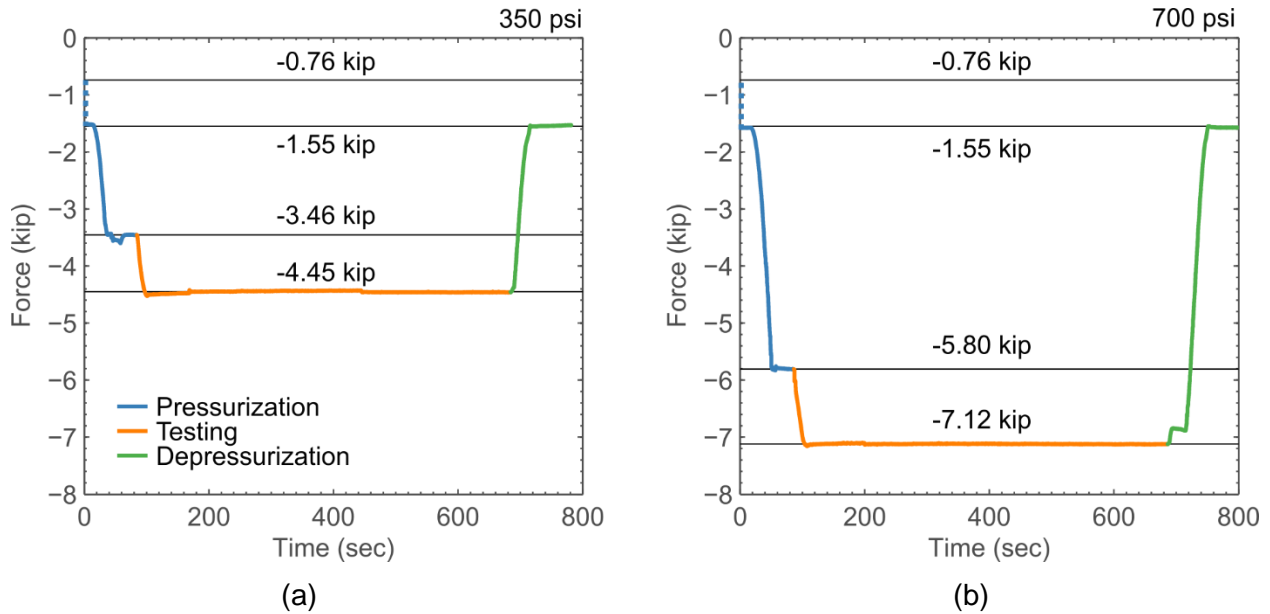


**Figure 3-47. Measured force during pressurized tests without core specimen at pressure of (a) 350 psi and (b) 700 psi**

**Offset load:** The average offset reading, prior to making contact with the TPV piston, was (a negative indicates compression), irrespective of pressure:

$$F_0 = -0.76 \text{ kip}$$

**Friction:** The initial reading after contacting the TPV piston and displacing the piston under zero pressure was

$$F_0 + F_\mu = -1.55 \text{ kip}$$

This value implies a friction value,  $F_\mu = -0.79 \text{ kip}$ . It is assumed that this maximum friction value does not change after pressurization. During the testing phase, the force required to move the piston increased initially. It is presumed that this change in force was caused by the reversal of friction forces in the rod seal, from acting with the actuator during pressurization to against the motion of the actuator during testing.

**TPV pressure:** The nominal diameter of the TPV piston was 3.150 in and the average diameter of a concrete core was 2.729 in for 99 samples (COV = 2.5 %). Thus, the calculated areas were  $A_p = 7.793 \text{ in}^2$  and  $A_c = 5.849 \text{ in}^2$ . This leads to values for the force due to chamber pressure, acting on the piston, of:

$$F_{350 \text{ psi}} = (7.793 \text{ in}^2)(-0.35 \text{ ksi}) = -2.73 \text{ kip}$$

$$F_{700 \text{ psi}} = (7.793 \text{ in}^2)(-0.70 \text{ ksi}) = -5.46 \text{ kip}$$

These values are within 6 % and 2 % of the measured values (4.45 - 1.55 = 2.9 kip and 7.12 - 1.55 = 5.57 kip) at 350 psi and 700 psi, respectively, providing validation for the calculation used herein. Using the calculated values for the force due to the TPV pressure leads to corrections at 350 psi and 700 psi of:

$$F_{p,350\text{psi}} = (-0.35 \text{ ksi})(7.793 \text{ in}^2 - 5.849 \text{ in}^2) = -0.68 \text{ kip}$$

$$F_{p,700\text{psi}} = (-0.70 \text{ ksi})(7.793 \text{ in}^2 - 5.849 \text{ in}^2) = -1.36 \text{ kip}$$

**Total correction:** Based on the above estimates, the corrected force on the core specimens was given by (assuming F and P are negative quantities):

- For core specimens subjected to 350 psi confining pressure  
 $P = F - (-0.76 \text{ kip} + -0.79 \text{ kip} + -0.68 \text{ kip}) = F - (-2.23 \text{ kip})$
- For core specimens subjected to 700 psi confining pressure  
 $P = F - (-0.76 \text{ kip} + -0.79 \text{ kip} + -1.36 \text{ kip}) = F - (-2.91 \text{ kip})$

These corrections were used to correct the recorded peak force value to provide an estimate of the actual peak force experienced by the core specimens.

### 3.5.4 TPV Test Results and Data Analysis

#### 3.5.4.1 Test results

The raw data (before applying any correction based on above) from the triaxial testing is shown in Table 3-8. Note that the number of unconfined tests ( $f_l = 0$  psi) was larger than that shown in Table 3-7. This occurred when the extracted core from the blocks yielded three specimens, and as a result one confined test and two unconfined tests (instead of one as stipulated in the design of experiment, Section 3.5.2) were conducted.

Table 3-8. Raw data from triaxial testing of core specimens

Predictors			Response
Block	Region	Pressure, $f_i$ (psi)	Peak Load (kip)
ASR 3	1	348	27
ASR 3	1	0	19.91
ASR 3	1	345	38.4
ASR 3	1	0	19.36
ASR 3	1	0	20.69
ASR 3	1	698	47.73
ASR 3	1	0	21.32
ASR 3	1	0	18.13
ASR 3	3	698	45.82
ASR 3	3	0	20.43
ASR 3	3	0	17.15
ASR 3	3	348	33.32
ASR 3	3	0	17.29
ASR 3	3	0	20.1
ASR 3	3	348	37.24
ASR 3	3	0	18.6
ASR 3	3	0	21
ASR 1	1	348	43.82
ASR 1	1	0	25.8
ASR 1	1	705	55.8
ASR 1	1	0	20.73
ASR 1	1	0	25.21
ASR 1	1	348	44.38
ASR 1	1	0	27.52
ASR 1	1	0	21.44
ASR 1	3	348	39.75
ASR 1	3	0	20.54
ASR 1	3	0	25.14
ASR 1	3	0	26.72
ASR 1	3	348	32.67
ASR 1	3	706	56.61
ASR 1	3	0	23.65

The measured peak load for the confined tests was subsequently corrected based on the analysis in Section 3.5.3.2 and then the compressive strengths of the specimens were calculated. Because of the different strengths of the concrete mixtures for blocks ASR 1 and ASR 3, it was advantageous to normalize the confined concrete strengths by the unconfined concrete strength for each block separately. Table 3-9 shows the average unconfined compressive strength for cores extracted from blocks ASR 1 and ASR 3 after 28 days of concrete placement (see Section 3.4) and at the time of triaxial testing. The table shows significant difference between the strength of the cores from the two blocks at the time of TPV testing, signifying the higher strength degradation of the most reactive block ASR 3 (with larger expansion) compared with the low reactive block ASR 1. Note that the difference between the unconfined compressive strength for Regions 1 and 3 in a given block was within 5%. As a result, the confined strengths were normalized using the average unconfined strength of Regions 1 and 3 combined.

**Table 3-9. Average unconfined compressive strength of core specimens**

Block	Average 28-day strength of core specimens (psi)	Average strength of core specimens at time of triaxial testing (psi)
ASR 1	4998	4118
ASR 3	4667	3226

Based on the above discussion, the confined compressive strengths of core specimens were normalized to the average unconfined strength of the core specimens for each block at the time of triaxial testing, i.e., the confined strength of cores extracted from blocks ASR 1 and ASR 3 were normalized by dividing the corrected strength by 4118 psi and 3226 psi, respectively. The corrected and normalized data from the triaxial tests is presented in Table 3-10. The table shows for each block and region, the confinement pressure normalized to the average unconfined strength at the time of triaxial testing,  $f_l/f_{cu}$ , and the confined compressive strength normalized to the average unconfined strength at the time of triaxial testing,  $f_{cc}/f_{cu}$ . A summary of the corrected and normalized data from Table 3-10 is shown in Figure 3-48. The figure also shows, for the sake of comparison, the predictions from the commonly used confinement models by Mander *et al.* (1988) and Richart *et al.* (1928) for non-reactive concrete. The Mander *et al.* (1988) and Richart *et al.* (1928) formulae are shown in Equations (3.3) and (3.4), respectively.

$$\frac{f_{cc}}{f_c} = -1.254 + 2.254 \sqrt{1 + 7.94 \frac{f_l}{f_c}} - 2 \frac{f_l}{f_c} \quad (3.3)$$

$$\frac{f_{cc}}{f_c} = 1 + 4.1 \frac{f_l}{f_c} \quad (3.4)$$

**Table 3-10. Corrected and normalized data using average unconfined strength at time of triaxial testing**

Predictors			Response
Block	Region	$f_l/f_{cu}$	$f_{cc}/f_{cu}$
ASR 3	1	0.105	1.27
ASR 3	1	0	1.02
ASR 3	1	0.104	1.86
ASR 3	1	0	1.00
ASR 3	1	0	1.06
ASR 3	1	0.210	2.30
ASR 3	1	0	1.10
ASR 3	1	0	0.93
ASR 3	3	0.210	2.21
ASR 3	3	0	1.05
ASR 3	3	0	0.88
ASR 3	3	0.105	1.60
ASR 3	3	0	0.89
ASR 3	3	0	1.03
ASR 3	3	0.105	1.80
ASR 3	3	0	0.96
ASR 3	3	0	1.08
ASR 1	1	0.085	1.73
ASR 1	1	0	1.07
ASR 1	1	0.171	2.20
ASR 1	1	0	0.86
ASR 1	1	0	1.05
ASR 1	1	0.085	1.75
ASR 1	1	0	1.14
ASR 1	1	0	0.89
ASR 1	3	0.085	1.56
ASR 1	3	0	0.85
ASR 1	3	0	1.04
ASR 1	3	0	1.11
ASR 1	3	0.085	1.26
ASR 1	3	0.171	2.23
ASR 1	3	0	0.98

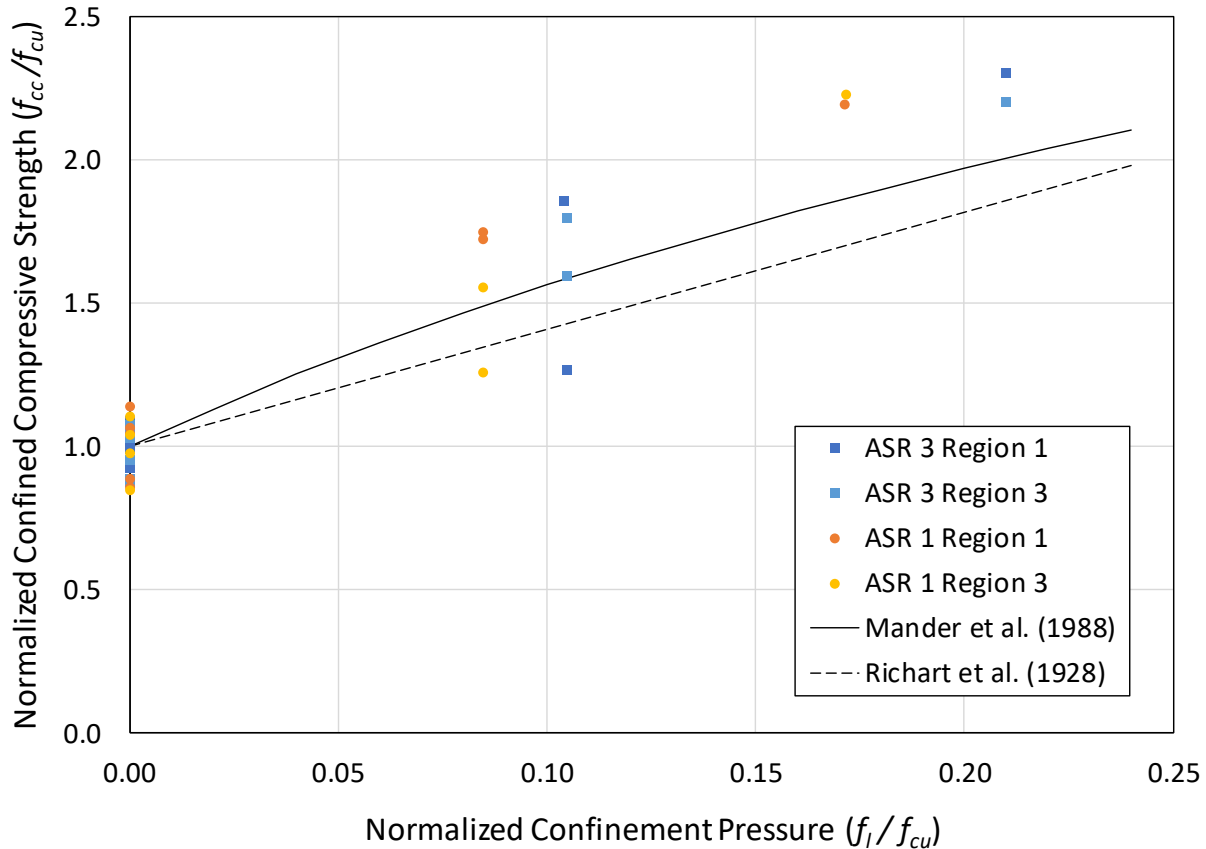


Figure 3-48. Corrected and normalized triaxial test data using average unconfined strength at time of testing

#### 3.5.4.2 Statistical Analysis of TPV Test Data

The statistical analysis aimed to: (1) develop an expression to describe the relationship between  $f_l/f_{cu}$  and  $f_{cc}/f_{cu}$  and examine if the relationship is linear (e.g., Richart *et al.*, 1928) or curved (e.g., Mander *et al.*, 1988) and (2) examine if the relationship between  $f_l/f_{cu}$  and  $f_{cc}/f_{cu}$  changes with the concrete mixture (ASR 1 and ASR 3), or confinement region (Regions 1 and 3); i.e., if an interaction between  $f_l/f_{cu}$ , block, and region does exist.

To address these objectives, least absolute shrinkage and selection operator (LASSO) regularized linear regression was utilized. The LASSO regularization method for generalized linear models was first introduced in Tibshirani (1996), and it acts as an automated way to select the most important regression terms. The selection occurs because LASSO regularization can force the coefficient for a regression term to be exactly zero. Those input variables for which the regression coefficients are exactly zero are deemed less important for predicting the response than those with non-zero coefficients because the zero valued coefficients remove the impact of the term on predicting the response. The *glmnet* package (Friedman *et al.*, 2010) for R (R Core Team 2020) was used for the computation. In addition, the parametric bootstrap described in Section 6.2 of Hastie *et al.* (2015) was used to assess uncertainty due to sampling variability.

The regression model that was fitted using the LASSO procedure is

$$\begin{aligned}
 f_{cc}/f_{cu} = & 1 + \beta_1 \left[ f_l/f_{cu} \right] + \beta_2 \left[ \left( f_l/f_{cu} \right)^2 \right] + \beta_3 \left[ f_l/f_{cu} \cdot B \right] + \beta_4 \left[ f_l/f_{cu} \cdot R \right] \\
 & + \beta_5 \left[ \left( f_l/f_{cu} \right)^2 \cdot B \right] + \beta_6 \left[ \left( f_l/f_{cu} \right)^2 \cdot R \right] + \beta_7 \left[ f_l/f_{cu} \cdot B \cdot R \right] \\
 & + \beta_8 \left[ \left( f_l/f_{cu} \right)^2 \cdot B \cdot R \right] + \epsilon
 \end{aligned}
 \tag{3.5}$$

The  $\beta_i$ 's in Equation (3.5) are the regression coefficients to be estimated, and the  $\epsilon$  term represents a random error.  $B$  identifies the block (ASR 1 or ASR 3) and  $R$  identifies the region (Region 1 or 3). In the analysis,  $B$  and  $R$  were assigned the values -1 and 1 to numerically represent the two levels associated with each parameter. Equation (3.5) allows for a separate quadratic relationship between  $f_l/f_{cu}$  and  $f_{cc}/f_{cu}$  for each of the four combinations of block and region. Figure 3-49 depicts the estimates and associated uncertainties of the  $\beta_i$ 's.

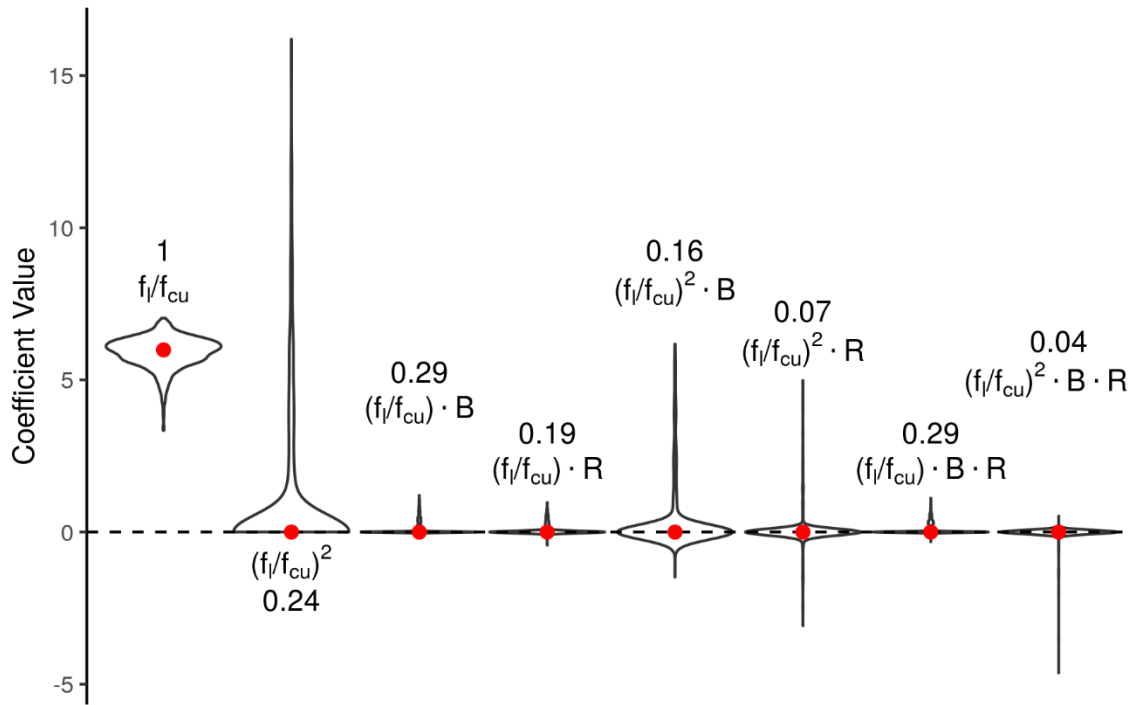


**Figure 3-49. Estimates and associated uncertainties for the  $\beta_i$ 's in Equation (3.5). The red points are the estimates, and the violin plots depict the bootstrap distributions, which quantify uncertainty. The numbers are the proportions of the bootstrap datasets for which the coefficients are estimated to be non-zero.**

The red points in Figure 3-49 are the estimated values for the  $\beta_i$ 's in Equation (3.5). The only non-zero estimate is for  $\beta_1$ ; the coefficient associated with the linear  $f_l/f_{cu}$  term. This indicates that the relationship between  $f_{cc}/f_{cu}$  and  $f_l/f_{cu}$  appears to be linear and can be described as:

$$f_{cc}/f_{cu} = 1 + k \left[ f_l/f_{cu} \right] \quad (3.6)$$

where the value of  $k$ , the rate of strength increase with increasing lateral pressure, was estimated to be 6, with the associated 95% confidence interval [4.7, 6.7]. The zero estimates for the rest of the  $\beta_i$ 's show that the relationship does not appear to change with block or region, i.e.,  $f_l/f_{cu}$  does not interact with block or region. This finding, however, does not consider sampling variability, i.e., would the same conclusion be reached if the experiment were run again, and a new set of measurements collected. The statistical bootstrap attempts to mimic what would happen if a new set of measurements were collected. Specifically, a bootstrap data set was generated, and the same LASSO procedure that was used on the original data set was applied to the bootstrap dataset. The violin plots in Figure 3-49 depict the results from 1000 bootstrap data sets and are referred to as the bootstrap distributions. The numbers are the proportion of times that the  $\beta_i$ 's was estimated to be non-zero. Clearly, the linear  $f_l/f_{cu}$  term was the most important since it was never estimated to be zero for any of the bootstrap data sets, and its bootstrap distribution was concentrated far away from zero. None of the other regression terms appeared to be very important for predicting  $f_{cc}/f_{cu}$  because the bootstrap distributions for their associated coefficients were all concentrated around zero. Further, the proportion of times that their associated coefficients were estimated to be non-zero was well below 50 %. Thus, the above findings are robust to sampling variability.

To complete the statistical analysis, the developed expression and associated uncertainty in Equations (3.5) and (3.6) were compared with two equations developed in previous work, namely Richart *et al.* (1928) and Mander *et al.* (1988). Figure 3-50 presents that comparison. The figure shows the developed expression (thick black line), 1000 bootstrap replicates of the estimate (grey lines), the measurements from Table 3-10 (black points), and the equations from Richart *et al.* (1928) and Mander *et al.* (1988) (colored curves). The uncertainty depicted by the bootstrap replicates represents only uncertainty due to sampling variability. That is, how the estimated expression might change if the experiment were run again with the same design, similar concrete blocks (same materials, processing, etc., but different physical blocks), and the same measurement system. The uncertainty does not represent what might happen to the estimated relationship if a major component of the experiment were to change, e.g., a consequential part of the measurement system. Figure 3-50 is divided into the four combinations of block and region because some of the bootstrap replicates estimated non-zero coefficients for the interaction terms (e.g.,  $f_l/f_{cu} \cdot B$ ). Note that the thick black line and the colored curves are identical between the four plots, but the grey curves may not be. Figure 3-50 implies that while the developed expression for the relationship between  $f_l/f_{cu}$  and  $f_{cc}/f_{cu}$  is linear just as in Richart *et al.* (1928), the equation developed in Richart *et al.* (1928) was not consistent with Equation (3.6) because the bootstrap replicates did not envelope the Richart *et al.* (1928) relationship. On the other hand, while the developed expression between  $f_l/f_{cu}$  and  $f_{cc}/f_{cu}$  is linear, and the equation in Mander *et al.* (1988) is not, the equation developed in Mander *et al.* (1988) is consistent with Equation (3.6) because the bootstrap replicates did envelope the Mander *et al.* (1988) curve.

In summary, the proposed regression equation represents the average response when incorporating sampling uncertainty and this regression is statistically consistent with Mander *et al.* (1998). For practical purposes, however, the equation by Richart *et al.* (1928) can serve as a

conservative lower bound for estimating the effects of confinement when taking into account the effects of sampling uncertainty.

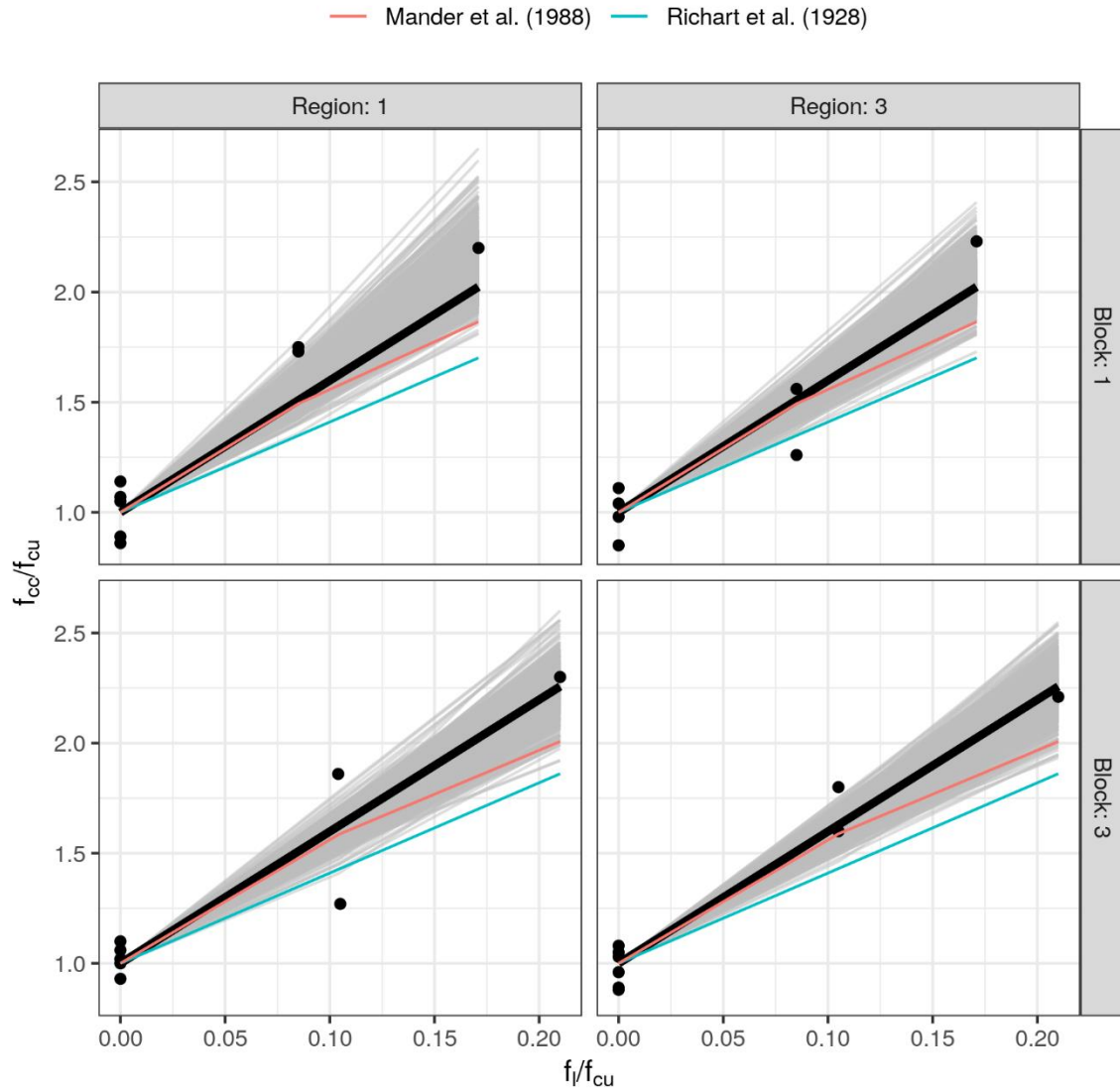


**Figure 3-50. Comparison of developed expression with equations from Richart *et al.* (1928) and Mander *et al.* (1988). The thick black line is the developed expression in Equation (3.6), and the grey lines are 1000 bootstrap replicates conveying uncertainty due to sampling variability. The black points are the observed measurements from Table 3-10.**

## Chapter 4

# FINDINGS AND CONCLUSIONS

---

---

### 4.1 SUMMARY

This Task 1 study utilized three large concrete block specimens made with reactive aggregates, along with one control, non-reactive, block specimen. Each block consisted of three separate regions containing three different amounts of longitudinal and transverse reinforcements to facilitate examination of the influences of different degrees of confinement on the ASR-induced expansion behavior of the blocks. All blocks were cast and kept in a large environmental chamber where they were subjected to predetermined curing regime with specified temperature and humidity to accelerate their ASR expansion.

The block specimens were heavily instrumented. The instruments allowed measurements of strains in concrete at the center of the blocks and in reinforcing bars at various locations, along with internal concrete temperature and relative humidity. External measuring devices, including a laser tracker, a high-precision caliper, and an optical microscope, were used in measuring ASR-induced expansion and crack developments on the surface of the reactive block specimens.

Core samples extracted from the reactive block specimens after different numbers of days, and companion concrete cylinders prepared during concrete placement, were used in mechanical property testing to quantify the effects of ASR on concrete's properties, including uniaxial compressive strength, modulus of elasticity, and splitting tensile strength. The measured mechanical properties of ASR-affected concrete were compared with ACI code equations for evaluation of their applicability to concrete affected by ASR.

Effect of confinement pressure on compressive strength of ASR-affected concrete was also quantified using the NIST-designed TPV test apparatus that allowed simultaneous application of radial confinement pressure of up to 700 psi and uniaxial compressive stress.

In the sections that follow, Section 4.2 presents the primary findings based on measurements, observations, and analysis of test results obtained in this experimental program, and Section 4.2 provide the conclusions of this Task 1 study.

### 4.2 FINDINGS

This section summarizes the findings and conclusions from this Task 1 experimental program:

#### 4.2.1 Strain Developments in Reinforcing Bars

- In the three reactive blocks, the tensile strains measured in the reinforcements were not symmetric with respect to the vertical axis even though the cross section of the blocks was symmetrical both in geometry and in amount of reinforcement. This lack of symmetry may be attributed to (1) a non-uniform ASR expansion within each specimen and (2) to a lesser extent the uneven extraction of core samples from the blocks (cores were not extracted in a symmetric fashion).

- For each block, the strains in Region 1 (mid-confinement) were slightly but consistently larger than those in Region 3 (high-confinement). This trend was expected to occur due to the higher confinement in Region 3 compared with Region 1.
- In general, for a given block and a given region, the strains on the bottom reinforcing bars were smaller than those on the higher bars. This may be due to the friction provided by the ground and/or the larger compaction and overburden pressure, which may have induced higher constraint and resulted in less expansion, on the lower portion of the block.
- Block ASR 3, which was designed to be the most reactive, had the largest expansion of the three reactive blocks at the end of Task 1 duration. Blocks ASR 1 and ASR 2 had lower and similar levels of expansion.
- Most reinforcing bars in block ASR 3 yielded due to the ASR expansion, having strains in excess of their yield strain of typically 0.20 % to 0.23 %. A few reinforcing bars in block ASR 1 also yielded. No reinforcing bars in block ASR 2 yielded.

#### 4.2.2 Concrete Core Strains

- For each reactive block, the expansions measured in the center of concrete using tri-directional concrete strain transducers in Region 2 were larger than those measured in Region 1 (no data was available from Region 3). This result was expected since Region 2 had virtually no confinement compared with Region 1.
- Consistent with the finding from the strain development using strain gages in the reinforcement above, the most reactive block ASR 3 (the most reactive block) had the largest measured concrete expansion at its center among the three reactive blocks. Concrete strains at cores of blocks ASR 1 and ASR 2 had lower and similar expansion values.
- Discrepancies observed between the measured strains in concrete at the center of the blocks and the measured strains on the reinforcing bars, which were located close to the exterior of the blocks (just inside the concrete cover), showed that strains at the exterior of the blocks were larger than those at the center. A similar observation was made using surface expansion measurements taken for Region 2. These measurements showed that the surfaces of the blocks without reinforcing bars had higher strains than what was measured by the concrete strain gages at the centers of the three reactive blocks.
  - This highlights one of the challenges associated with evaluation of large ASR-affected concrete structures, where the unconfined expansion is not a single-value, but in reality, an expansion field that can be largely affected by, among other variables, size, exposure to moisture, and potential for alkali leaching.
  - While previous studies provided the mechanical properties of ASR-affected concrete as a function of expansion based on measurements taken from standard prisms, this study provided the mechanical properties of an in-situ structure or element as a function of the measured expansion field (see Section 3.4).

### 4.2.3 Surface Expansion and Crack Mapping

- A reasonable correlation was observed between the average surface strains/displacements (along target lines in a given region) and the corresponding reinforcing bar strains for blocks ASR 1 and ASR 2, which had maximum measured reinforcing bar strains at or less than about 0.15 %. The correlation was much poorer for block ASR 3, which had maximum measured strains between 0.15 % and 0.35 % where the average surface strains were smaller than the measured strains on reinforcing bars. These contrasting results suggest that surface expansion measurements may only provide a reasonable estimate of strains at low expansion levels.
- Surface expansion measurements taken using a high-precision caliper were consistent with those taken using the laser tracker. The minor inconsistencies that do exist in the data were likely due to different measurement methodologies, human error, and to a lesser extent small differences in dates of measurements and slight differences in gage length.
- The cracking index (CI) method developed by the Federal Highway Administration (Fournier *et al.*, 2010) yielded results that were not consistent with the surface expansion measurements using the laser tracker and high-precision caliper devices. In general, the CI results were smaller than the surface strains obtained from the other two techniques, and there was a large scatter in the ratio of the CI to the average surface strains resulting in a coefficient of variation of about 50 %.
- The inability of the surface expansion measurements and the CI method to estimate the level of concrete expansion (or strains on reinforcing bars) was likely because the behavior and thus strains developed in the concrete cover are different from those within the confining reinforcing bars. The surface expansion measurements and the CI method remain as useful tools to monitor the progression of ASR, but they do not provide an accurate estimate of the level of expansion.

### 4.2.4 Mechanical Properties of ASR-Affected Concrete

- Plots of uniaxial compressive strength, modulus of elasticity, and splitting tensile strength (from cylinders and core specimens) versus time and versus unconfined expansion based on (1) Region 2 concrete strain gages and (2) Region 2 surface expansion measurements were developed. Results showed that:
  - *Unconfined uniaxial compressive strength*: Cores from blocks ASR 1 and ASR 2 showed no reduction in the unconfined uniaxial compressive strength compared with the 28-day strength. Cores from block ASR 3 exhibited a reduction in compressive strength of 13 %  $\pm$  15 % compared with the 28-day compressive strength. Samples from the control block continued to gain strength over time.
  - *Modulus of elasticity*: Cores from the three reactive blocks showed a reduction of the elastic modulus of 28 %  $\pm$  9 % to 41 %  $\pm$  6 % compared with the 28-day elastic modulus. On the other hand, samples from the control block exhibited an increase in the modulus of elasticity over time.
  - *Splitting tensile strength*: cores from blocks ASR 2 and ASR 3 showed no reduction in the tensile strength compared with the 28-day tensile strength. Cores from block ASR 1

showed a reduction of  $15 \% \pm 13 \%$  in tensile strength. For the control block, the splitting tensile strength remained nearly constant over time.

- Modulus of elasticity-compressive strength relationship versus current code:  
At the early age of the three reactive blocks, the modulus of elasticity of the cores remained, for the most part, within the  $\pm 20 \%$  range of the ACI 318-14 equation ( $E_c = 57000 \sqrt{f'_c}$  [psi]). At increased age (corresponding to increased levels of ASR expansion) of the blocks, the measured modulus of elasticity became significantly lower than that predicted by the ACI equation. This indicates that the modulus of elasticity degraded faster than the compressive strength of concrete with increased ASR expansion.
- Splitting tensile strength-compressive strength relationship versus current code:  
At the early age of the reactive blocks, the splitting tensile strength of the cores remained, for the most part, within the  $\pm 20 \%$  range of the ACI 318-14 equation ( $f_{ct} = 6.7 \sqrt{f_{cm}}$  [psi]). At increased age (corresponding to increased levels of ASR expansion), the measured splitting tensile strength became higher, on average, than the ACI equation. However, the large scatter in the data prevented definitive conclusions to be drawn regarding the validity of the ACI tensile strength equation for ASR-affected concrete.
- No discernable trend was found regarding the influence of region (i.e., level of confinement) on the uniaxial compressive strength of extracted cores.
- Cores were extracted from both the lower and upper portions of each region in each ASR-affected block. No discernable trend was found regarding the influence of core-height on uniaxial compressive strength of extracted cores.

#### 4.2.5 Effect of Confinement Pressure on Compressive Strength of ASR-Affected Concrete

Based on TPV triaxial compression test results and rigorous statistical analysis, an expression was developed to relate the uniaxial confined compressive strength of cores,  $f_{cc}$ , that were extracted from ASR-affected specimens; the applied lateral pressure,  $f_l$ ; and the uniaxial compressive strength of cores,  $f_{cu}$ , obtained under standard (unconfined) conditions at the time of the triaxial testing. The expression was found to have the familiar form:

$$f_{cc}/f_{cu} = 1 + k f_l/f_{cu},$$

where the value of  $k$ , the rate of strength increase with increasing lateral pressure, was estimated to be 6, with the associated 95 % confidence interval [4.7, 6.7].

The above expression was not found to depend on the concrete mixture, and therefore the level of ASR induced expansion at the time of testing, or the region where the cores were extracted, which had two different levels of confinement. The expression was consistent with the relationship proposed by Mander *et al.* (1988), commonly used for conventional concrete, within the uncertainty due to sampling variability estimated by a parametric bootstrap algorithm, while the equation proposed by Richart *et al.* (1928) may be used as a conservative lower bound.

### 4.3 CONCLUSIONS

For the ranges of experimental parameters examined in this study, i.e. concrete mixtures considered in this experiment with an ultimate ASR-induced target expansion  $\varepsilon_{ASR}$  of 0.5 % (based on measurements taken on standard prisms) and a maximum volumetric reinforcement ratio  $\rho_v$  of 1.14 %, the following conclusions can be drawn:

- For large structures, ASR-induced expansion is a complex field that varies both by location on the concrete surface and through depth of concrete member. The variation depends on several factors, including degree of confinement and, restraint by surrounding conditions. In the block specimens in this test program, the ASR expansion field varies with the largest expansion observed on or near the specimen surface and the smallest expansion at the center of the specimen.
- Both surface expansion measurements and the CI method are useful tools for monitoring the progressions of ASR-induced surface expansion, but may not be used to determine the actual expansion field in the structure.
- ASR expansion causes degradation of concrete's mechanical properties typically used in structural design (compressive strength and elastic modulus). For the concrete mixtures considered in this study, the degradation varies differently for each property:
  - *Compressive strength*: a reduction of 13 %  $\pm$  15 % of compressive strength obtained using standard uniaxial compression test method compared with 28-day compressive strength can be observed for the most reactive concrete (block ASR 3), while no discernable reduction was observed for concretes with lower reactivity (blocks ASR 1 and ASR 2).
  - *Modulus of elasticity*: modulus of elasticity was found to degrade faster with increased ASR expansion than compressive strength. Within the range of ASR reactivity studied in this test program, the reduction in modulus of elasticity ranged from 28 %  $\pm$  9 % to 41 %  $\pm$  6 % compared with the 28-day modulus.

Note that, in normal concrete (without ASR), both compressive strength and elastic modulus are expected to continue to increase as function of time.

- The current ACI code equation for the modulus of elasticity versus compressive strength relationship ( $E_c = 57000 \sqrt{f'_c}$  [psi]) is unconservative and not applicable for ASR-affected concrete. In general, the ACI empirical equation became unconservative for larger expansions. Note that this conclusion is based on isolated core/material uniaxial testing with no regard to structural surroundings or context, which might enhance the stiffness of the structure.
- Degree of reinforcement confinement (represented by volumetric reinforcement ratio,  $\rho_v$ , in this study) and location of concrete core samples (with higher locations in the blocks corresponding to less overburden pressure experienced by the core samples) were found not to have an influence on the uniaxial compressive strength of ASR-affected concrete. This suggests that the uncertainty in compressive strength obtained from field-procured core specimens due to sampling location on the structure may be small. Accordingly, for field core extraction for determining in-situ compressive strength of concrete of real structure, cores can

be taken at any locations on the structure as long as they are in the region affected by ASR with careful consideration of site conditions, structural loads that might restrain expansion, and moisture condition.

In-situ compressive strength of ASR-affected concrete, i.e., compressive strength measured under triaxial stress state (with radial confinement pressure) that simulates the confinement condition of the specimen, is higher than the compressive strength measured under the current, conventional ASTM uniaxial compression test condition. This increase in in-situ compressive strength varies linearly with increasing confinement pressure. The in-situ compressive strength of ASR-affected concrete  $f_{cc}$  can be estimated based on the confinement pressure  $f_l$  and compressive strength  $f_{cu}$  determined based on standardized uniaxial compression test at the time of triaxial testing following this empirical expression:

$f_{cc}/f_{cu} = 1 + k f_l/f_{cu}$ , where the value of  $k$ , the rate of strength increase with increasing lateral pressure, was estimated to be 6, with the associated 95 % confidence interval [4.7, 6.7]. This expression is valid for the range of confinement pressure of up to 700 psi and the range of ASR expansions studied in this test program. This expression is consistent with the relationship proposed by Mander *et al.* (1988), commonly used for conventional concrete, within the uncertainty due to sampling variability estimated by a parametric bootstrap algorithm. The relationship proposed by Richart *et al.* (1928) may also be used as a conservative lower bound for estimating the effects of confinement on the ASR-affected concrete. In an existing structure, determination of confinement pressure is based on the structural context, i.e., amount of external loading, reinforcing bar cage, intersecting/abutting elements, etc.

## REFERENCES

---

---

ACI 207.2R-07. Report on Thermal and Volume Change Effects on Cracking of Mass Concrete, American Concrete Institute, Farmington Hills, MI, 2007.

ACI 318-14. Building Code Requirements for Structural Concrete, American Concrete Institute, Farmington Hills, MI, 2014.

ASTM C1293-08b-15. Standard Test Method for Determination of Length Change of Concrete Due to Alkali-Silica Reaction, ASTM International, West Conshohocken, PA, 2015.

ASTM C138/C138M-17a. Standard Test Method for Density (Unit Weight), Yield, and Air Content (Gravimetric) of Concrete, ASTM International, West Conshohocken, PA, 2017.

ASTM C143/C143M-15a. Standard Test Method for Slump of Hydraulic-Cement Concrete, ASTM International, West Conshohocken, PA, 2015.

ASTM C150/C150M-16 Standard Specification for Portland Cement, ASTM International, West Conshohocken, PA, 2016.

ASTM C172/C172M-14a. Standard Practice for Sampling Freshly Mixed Concrete, ASTM International, West Conshohocken, PA, 2014.

ASTM C33/C33M-16. Standard Specification for Concrete Aggregates, ASTM International, West Conshohocken, PA, 2016.

ASTM C39/C39M-17a. Standard Test Method for Compressive Strength of Cylindrical Concrete Specimens, ASTM International, West Conshohocken, PA, 2017.

ASTM C231/C231M-17a. Standard Test Method for Air Content of Freshly Mixed Concrete by the Pressure Method, ASTM International, West Conshohocken, PA, 2017.

ASTM C469/C469M-14. Standard Test Method for Static Modulus of Elasticity and Poisson's Ratio of Concrete in Compression, ASTM International, West Conshohocken, PA, 2014.

ASTM C494/C494M-16. Standard Specification for Chemical Admixtures for Concrete, ASTM International, West Conshohocken, PA, 2016.

ASTM C496/C496M-17. Standard Test Method for Splitting Tensile Strength of Cylindrical Concrete Specimens, ASTM International, West Conshohocken, PA, 2017.

Bamforth, P. B., Price, W. F., Widdows, S. J., and Davies, D. R., (1992), "Evaluation of the Susceptibility to ASR of Concrete Mixes Containing Marine Dredged Aggregate," *9<sup>th</sup> International Conference on Alkali Aggregate Reaction in Concrete*, London, UK.

Bracci, J. M., Gardoni, P., Eck, M. K., and Trejo, D., (2012), "Performance of Lap Splices in Large-Scale Column Specimens Affected by ASR and/or DEF, Report 0-5722-1, Texas Transportation Institute, Texas A&M University, College Station, Texas.

- Feldman, S., Eason, R., Bajcsy, P., and Snyder K.A., (2020), "Material Research Support for the Structural Performance of Nuclear Power Plant Concrete Structures Affected by Alkali-Silica Reaction," NIST TN XXXX (under review), National Institute of Standards and Technology, Gaithersburg, Maryland.
- Fournier, B., Berube, M-A, Folliard, K. J., and Thomas, M. (2010), "Report on the Diagnosis, Prognosis, and Mitigation of Alkali-Silica Reaction (ASR) in Transportation Structures," FHWA-HIF-09-004, Washington D.C. 20590.
- Friedman, J., Hastie, T., and Tibshirani, R. (2010). "Regularization Paths for Generalized Linear Models via Coordinate Descent," *Journal of Statistical Software*, 33(1), 1-22. URL <http://www.jstatsoft.org/v33/i01/>.
- Hansen, W.C., (1944), "Studies Relating to the Mechanism by which the Alkali-aggregate Reaction Produces Expansion in Concrete", *Journal of the American Concrete Institute*, Vol. 15, p. 213-227.
- Hastie, T., Tibshirani, R., and Wainwright, M. (2015), "Statistical Learning with Sparsity: the Lasso and Generalizations", CRC press.
- Mander, J.B., Priestley, M.J.N., Park, R. (1988), "Theoretical Stress-Strain Model for Confined Concrete," *Journal of Structural Engineering*, ASCE, Volume 114(8), p.1804-1806.
- Phan, L.T., Sadek, F, Thonstad, T.E., Lew, H.S., Marcu, S., Philip, J., (2019), "Effects of Alkali-Silica Reaction on Mechanical Properties and Structural Capacities of Reinforced Concrete Structures" *Structural Mechanics in Reactor Technology (SMiRT) 25*, Charlotte, NC, United States, August 2019.
- R Core Team (2020). "R: A Language and Environment for Statistical Computing," R Foundation for Statistical Computing, Vienna, Austria. URL <https://www.R-project.org/>.
- Richart, F.E., Brandtzaeg, A., and Brown, R.L. (1928), "A Study of the Failure of Concrete under Combined Compressive Stresses," *Bulletin 185*, University of Illinois Engineering Experimental Station, Champaign, IL.
- Snyder, K., and Lew, H.S., (2013), "Alkali-Silica Reaction Degradation of Nuclear Power Plant Concrete Structures: A Scoping Study" NISTIR 7937, National Institute of Standards and Technology, Gaithersburg, Maryland.
- Stanton, T.E. (1940), "Expansion of Concrete Through Reaction Between Cement and Aggregate," *Proceedings, American Society of Civil Engineers*, Vol. 66, p. 1781-1811.
- Taylor, H.F.W. (1990), *Cement Chemistry*, Academic Press, New York.
- Tibshirani, R. (1996), "Regression Shrinkage and Selection via the Lasso." *Journal of the Royal Statistical Society: Series B (Methodological)*, 58.1: 267-288.

## **APPENDIX A**

### **STRAIN GAGES ON REINFORCING BARS**

---

---

This appendix presents the location and number designation for all strain gages attached to the reinforcing bars inside the blocks used in this study. The plots are provided for strain gages used in reactive block ASR 1, hence the number (1) at the beginning of each designation. For other blocks, the first number should be replaced by the block number, e.g., the number (3) for block ASR 3 and the letter (C) for the control block. Note that while the strain gage layout for the three reactive blocks was identical, the control block used smaller number of gages as indicated in Chapter 2.

### A.1 STRAIN GAGES ON STIRRUPS

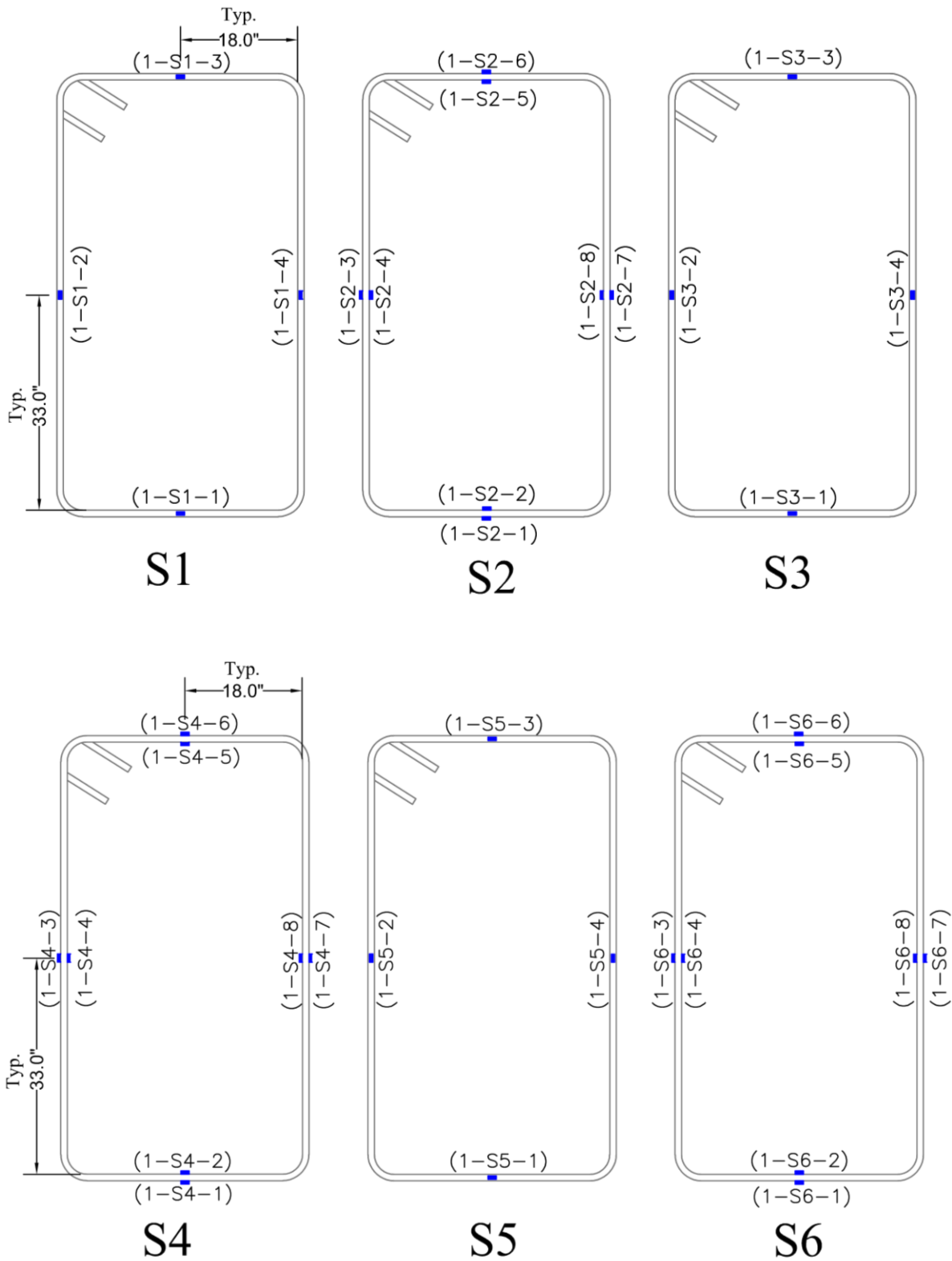


Figure A-1. Strain gages on stirrups in Region 1 of the blocks

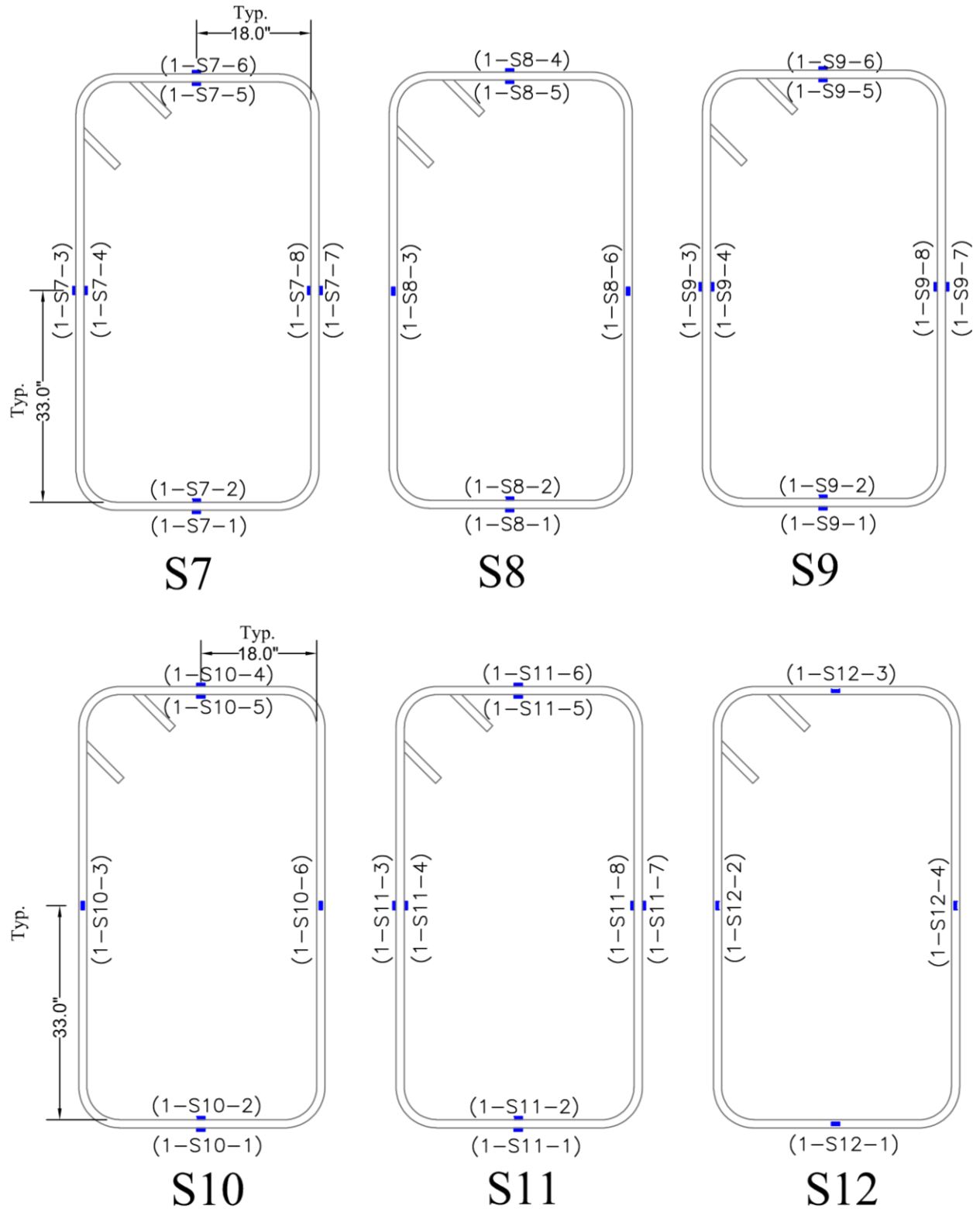


Figure A-2. Strain gages on stirrups in Region 3 of the blocks

## A.2 STRAIN GAGES ON LONGITUDINAL REINFORCING BARS

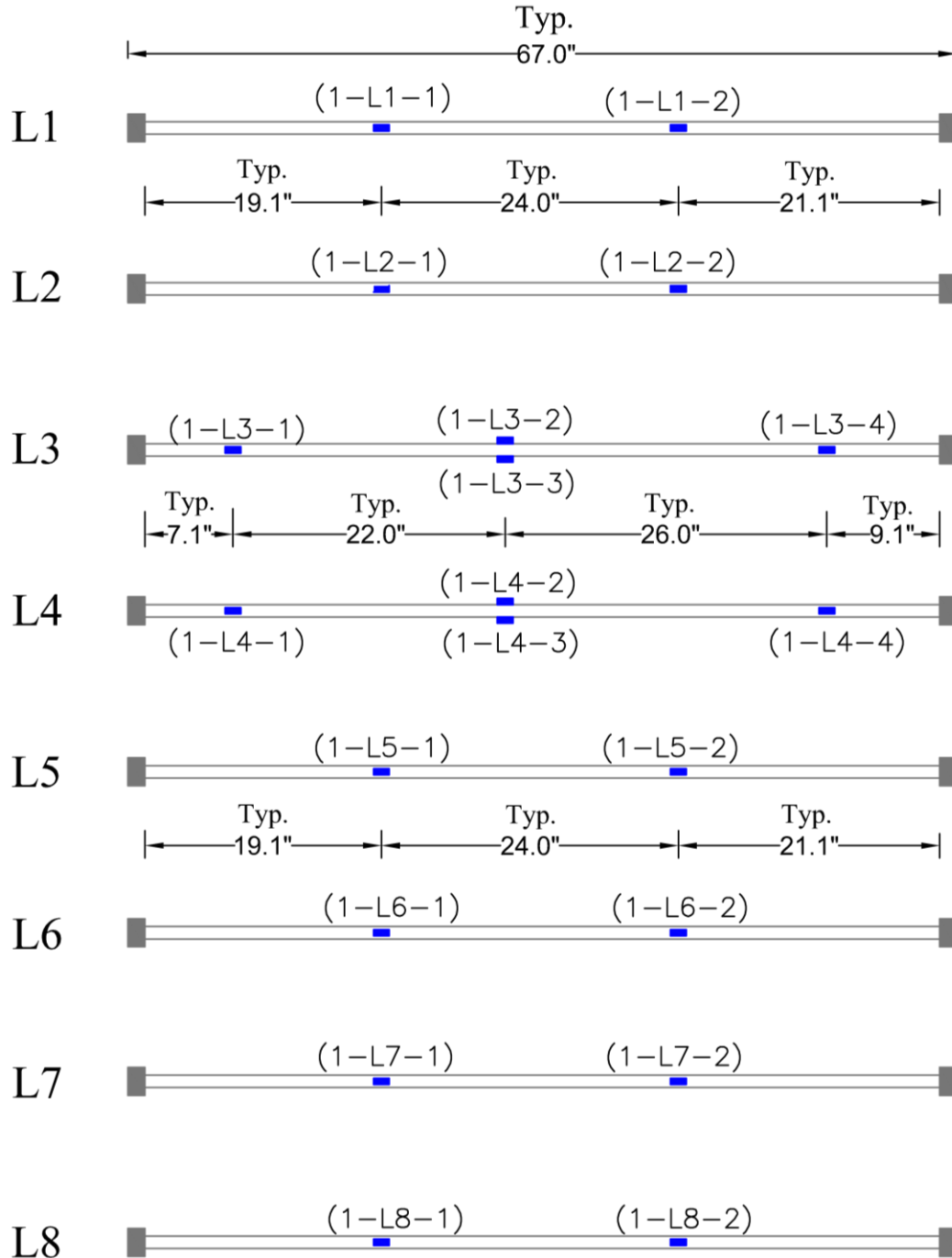


Figure A-3. Strain gages on longitudinal reinforcing bars in Region 1 of the blocks

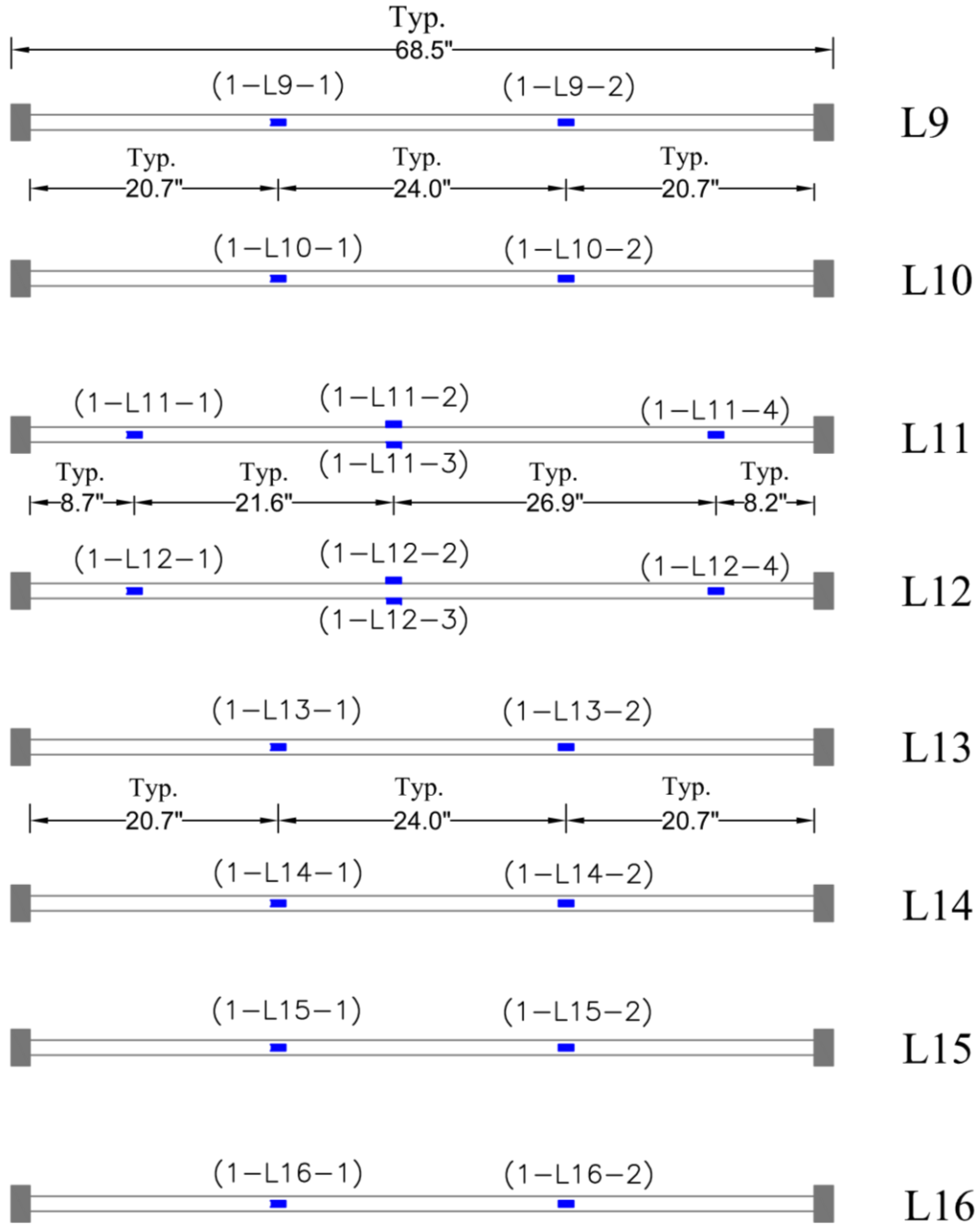
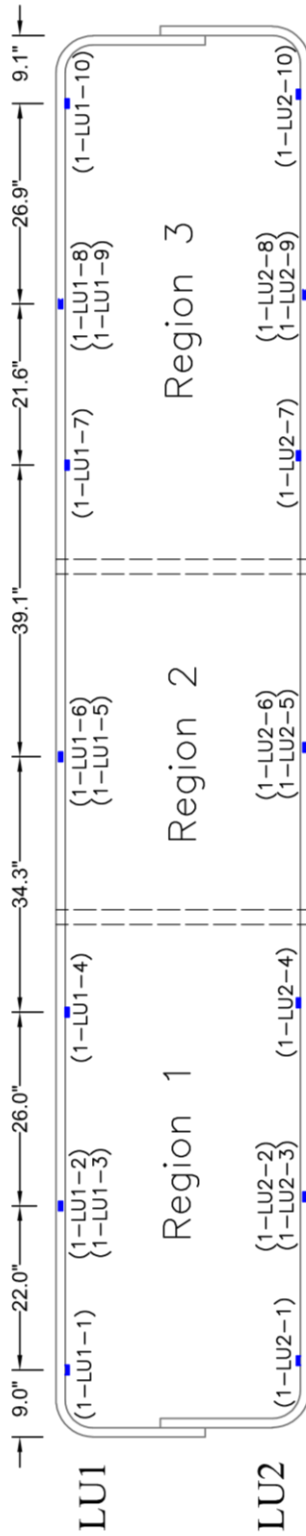


Figure A-4. Strain gages on longitudinal reinforcing bars in Region 3 of the blocks

**A.3 STRAIN GAGES ON CORNER REINFORCING BARS**



**Figure A-5. Strain gages on upper corner reinforcing bars**

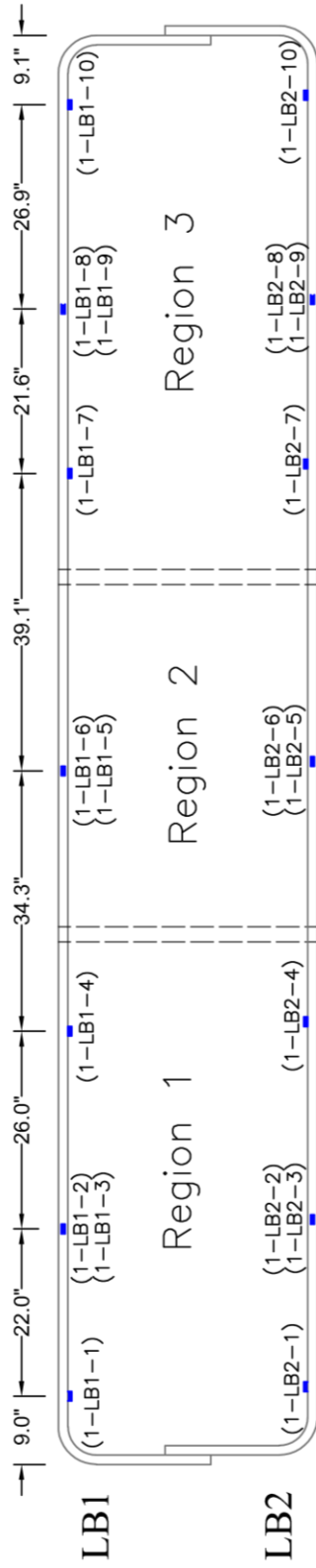
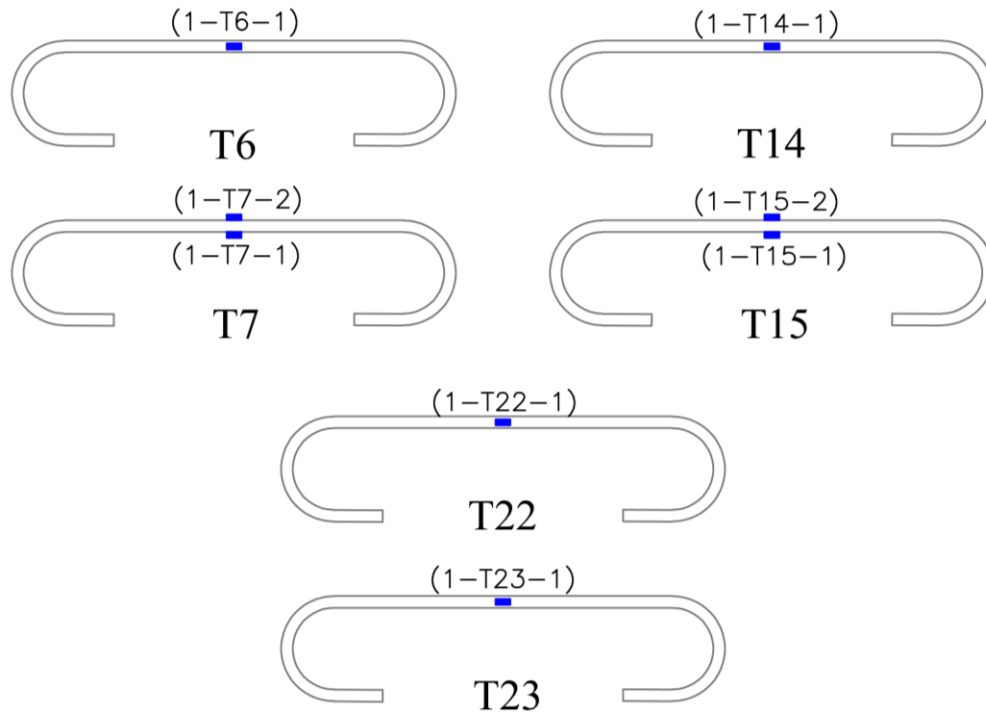


Figure A-6. Strain gages on lower corner reinforcing bars

**A.4 STRAIN GAGES ON CROSS TIES****Figure A-7. Strain gages on cross ties in Region 3 of the blocks**

## **APPENDIX B**

### **AVERAGE SURFACE STRAINS USING LASER MEASUREMENTS**

---

---

This appendix presents average surface strains using laser measurements, see Section 3.3.1. Separate plots are provided for blocks ASR 1, ASR 2, and ASR 3. North direction is defined in Figure 3-18.

ASR 1—East Face—Horizontal Strains

Strains %

Average, Laser Measurement  
Rebar Strain

Region 1	Region 2	Region 3
◦ 0.230 ◦ 0.169 ◦ 0.074 ◦ 0.210 ◦ 0.179 ◦ <b>0.118</b> <b>0.112</b>	◦ 0.036 ◦ 0.224 ◦ 0.230 ◦	◦ 0.171 ◦ 0.043 ◦ 0.149 ◦ 0.102 ◦ na ◦
◦ 0.140 ◦ 0.219 ◦ 0.071 ◦ 0.133 ◦ 0.175 ◦ <b>0.106</b>	◦ 0.330 ◦ 0.007 ◦ 0.107 ◦	◦ -0.494 ◦ 0.645 ◦ 0.125 ◦ 0.120 ◦ 0.098 ◦
◦ 0.187 ◦ 0.045 ◦ 0.141 ◦ 0.144 ◦ 0.165 ◦ <b>0.089</b>	◦ 0.180 ◦ 0.116 ◦ 0.107 ◦	◦ 0.061 ◦ 0.161 ◦ 0.125 ◦ 0.089 ◦ 0.120 ◦ <b>0.111</b>
◦ 0.128 ◦ 0.073 ◦ 0.155 ◦ 0.144 ◦ 0.093 ◦	◦ 0.178 ◦ 0.201 ◦ 0.102 ◦	◦ 0.031 ◦ 0.132 ◦ 0.122 ◦ 0.101 ◦ 0.119 ◦
◦ 0.222 ◦ 0.062 ◦ 0.053 ◦ 0.197 ◦ 0.116 ◦	◦ 0.163 ◦ 0.171 ◦ 0.153 ◦	◦ 0.117 ◦ 0.104 ◦ 0.021 ◦ 0.113 ◦ 0.180 ◦
◦ 0.180 ◦ 0.007 ◦ 0.144 ◦ <b>0.098</b> ◦ 0.120 ◦ 0.066 ◦	◦ 0.129 ◦ 0.192 ◦ 0.169 ◦	◦ <b>0.092</b> ◦ <b>0.143</b> ◦ ◦ 0.094 ◦ 0.124 ◦ 0.036 ◦ 0.165 ◦ 0.015 ◦
◦ 0.093 ◦ 0.115 ◦ 0.099 ◦ 0.129 ◦ 0.130 ◦	◦ 0.092 ◦ 0.122 ◦ 0.150 ◦	◦ 0.035 ◦ 0.042 ◦ 0.172 ◦ -0.087 ◦ 0.228 ◦ <b>0.088, 0.173</b> <b>0.114</b>

(a)

ASR 1—East Face—Vertical Strains

**Strains %**  
Average, Laser Measurement  
Rebar Strain

Region 1						Region 2				Region 3					
○	○	○	○	○	○	○	○	○	○	○	○	○	○	○	○
0.147	0.073	0.048	0.174	0.172	0.047	0.127	0.330	0.497	0.421	0.461	-0.008	0.103	0.163	-0.053	-0.262
○	○	○	○	○	○	○	○	○	○	○	○	○	○	○	○
0.177	0.210	0.236	0.225	0.150	0.318	0.183	0.142	0.116	0.181	0.180	0.192	0.190	0.167	0.232	0.180
○	○	○	○	○	○	○	○	○	○	○	○	○	○	○	○
0.205	0.217	0.159	0.190	0.196	0.192	0.314	0.439	0.212	0.135	0.065	0.029	0.119	0.074	0.032	0.222
○	○	○	○	○	○	○	○	○	○	○	○	○	○	○	○
0.194	0.110	0.135	0.161	0.061	-0.011	0.277	0.307	0.289	0.368	0.229	0.155	0.186	0.168	0.206	0.027
○	○	○	○	○	○	○	○	○	○	○	○	○	○	○	○
0.171	0.098	0.217	0.157	0.304	0.155	0.331	0.190	0.254	0.244	0.134	0.194	0.048	0.077	0.105	0.146
○	○	○	○	○	○	○	○	○	○	○	○	○	○	○	○
0.299	0.313	0.396	0.281	0.353	0.330	0.330	0.343	0.160	0.208	0.196	0.160	0.220	0.230	0.276	0.161
○	○	○	○	○	○	○	○	○	○	○	○	○	○	○	○

(b)

ASR 1—West Face—Horizontal Strains

**Strains %**

Average, Laser Measurement

Rebar Strain

Region 3	Region 2	Region 1
◦ 0.150 ◦ 0.222 ◦ 0.125 ◦ 0.117 ◦ 0.060 ◦	◦ 0.193 ◦ 0.290 ◦ 0.118 ◦	◦ 0.119 ◦ 0.152 ◦ 0.156 ◦ 0.124 ◦ 0.175 ◦ <b>0.152            0.123, 0.172            0.168</b>
◦ 0.067 ◦ 0.142 ◦ 0.097 ◦ 0.161 ◦ 0.105 ◦	◦ 0.197 ◦ 0.152 ◦ 0.062 ◦	◦ 0.050 ◦ 0.249 ◦ 0.074 ◦ 0.056 ◦ 0.214 ◦ <b>0.097</b>
◦ 0.158 ◦ 0.158 ◦ 0.058 ◦ 0.133 ◦ 0.021 ◦	◦ 0.325 ◦ -0.004 ◦ 0.081 ◦	◦ -0.020 ◦ 0.183 ◦ 0.211 ◦ 0.028 ◦ 0.148 ◦
◦ 0.096 ◦ 0.124 ◦ 0.113 ◦ 0.109 ◦ 0.055 ◦	◦ 0.164 ◦ 0.135 ◦ 0.063 ◦	◦ 0.076 ◦ 0.134 ◦ 0.087 ◦ 0.125 ◦ 0.165 ◦
◦ 0.169 ◦ 0.154 ◦ 0.044 ◦ 0.147 ◦ -0.001 ◦	◦ 0.240 ◦ -0.004 ◦ 0.198 ◦	◦ 0.088 ◦ 0.082 ◦ 0.093 ◦ 0.040 ◦ 0.122 ◦
◦ 0.108 ◦ 0.168 ◦ 0.040 ◦ 0.135 ◦ 0.037 ◦	◦ 0.504 ◦ -0.201 ◦ 0.088 ◦	◦ 0.110 ◦ 0.077 ◦ 0.124 ◦ 0.097 ◦ 0.046 ◦
◦ 0.281 ◦ 0.152 ◦ 0.092 ◦ 0.025 ◦ 0.121 ◦	◦ 0.201 ◦ 0.186 ◦ 0.031 ◦	◦ 0.109 ◦ 0.115 ◦ 0.105 ◦ -0.007 ◦ 0.110 ◦ <b>0.101, 0.116            0.084</b>

(c)

### ASR 1—West Face—Vertical Strains

**Strains %**

Average, Laser Measurement

Rebar Strain

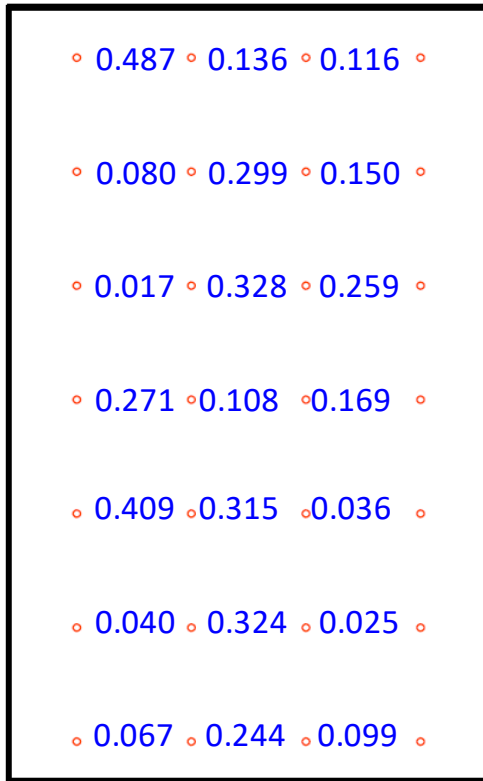
Region 3						Region 2				Region 1					
○	○	○	○	○	○	○	○	○	○	○	○	○	○	○	○
0.076	0.135	0.088	0.251	0.169	0.062	0.101	0.462	0.274	0.096	0.125	0.183	0.087	0.173	0.124	-0.042
○	○	○	○	○	○	○	○	○	○	○	○	○	○	○	○
0.252	0.180	0.181	0.167	0.198	0.172	0.297	0.212	0.224	0.343	0.197	0.176	0.239	0.214	0.336	0.443
○	○	○	○	○	○	○	○	○	○	○	○	○	○	○	○
0.079	0.100	0.196	0.215	0.160	0.127	0.267	0.198	0.221	0.184	0.223	0.281	0.104	0.212	0.169	0.115
○	○	○	○	○	○	○	○	○	○	○	○	○	○	○	<b>0.266</b>
0.286	0.166	0.103	0.091	0.130	0.196	0.259	0.252	0.174	0.387	0.135	0.069	0.169	0.061	0.152	0.111
○	○	○	○	○	○	○	○	○	○	○	○	○	○	○	○
0.062	0.100	0.147	0.081	0.171	0.174	0.275	0.249	0.392	0.238	0.237	0.185	0.257	0.154	0.110	0.190
○	○	○	○	○	○	○	○	○	○	○	○	○	○	○	○
0.354	0.170	0.038	0.377	0.206	0.071	0.170	0.375	0.258	0.246	0.064	0.106	0.185	0.149	0.210	0.106
○	○	○	○	○	○	○	○	○	○	○	○	○	○	○	○

(d)

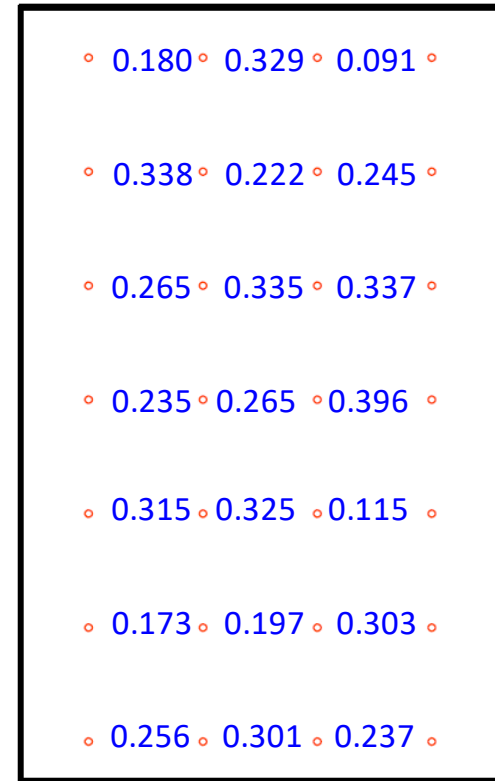
ASR 1—North and South Faces—Horizontal Strains

**Strains %**

Average, Laser Measurement  
Rebar Strain



Region 3  
North End



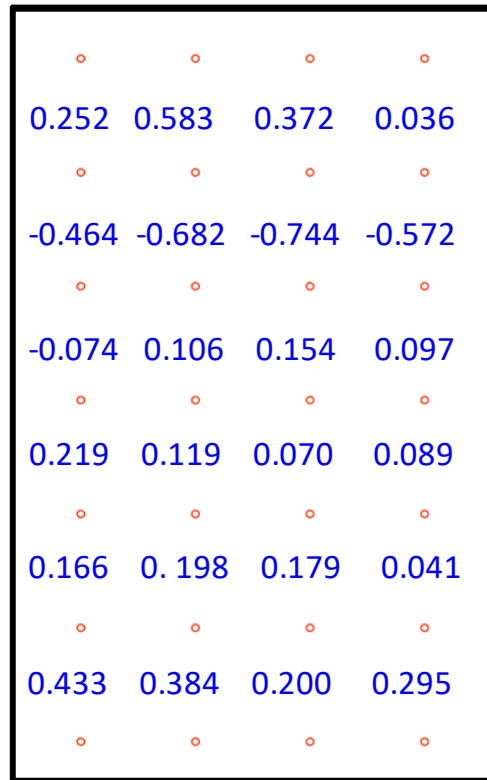
Region 1  
South End

(e)

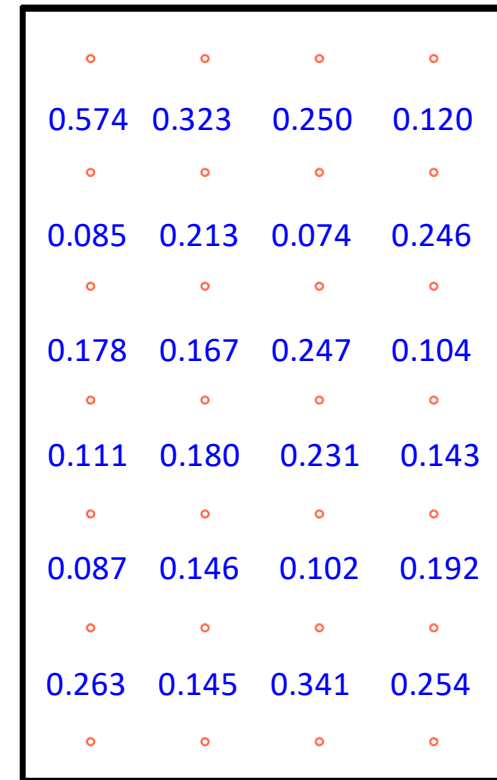
### ASR 1—North and South Faces—Vertical Strains

**Strains %**

Average, Laser Measurement  
Rebar Strain



Region 3  
North End



Region 1  
South End

(f)

Figure B-1. Average surface strains using laser measurements between neighboring targets for block ASR 1: (a) horizontal strains on east face, (b) vertical strains on east face, (c) horizontal strains on west face, (d) vertical strains on west face, (e) horizontal strains on north and south ends, and (f) vertical strains on north and south ends

ASR 2—North Face—Horizontal Strains

**Strains %**  
Average, Laser Measurement  
Rebar Strain

Region 1	Region 2	Region 3
◦ 0.050 ◦ 0.230 ◦ 0.091 ◦ 0.030 ◦ 0.176 ◦ <b>0.100</b>	◦ 0.337 ◦ 0.139 ◦ 0.092 ◦ <b>0.131</b>	◦ 0.074 ◦ 0.082 ◦ 0.124 ◦ 0.016 ◦ 0.467 ◦ <b>0.144, 0.141 0.127</b>
◦ 0.173 ◦ 0.045 ◦ 0.137 ◦ 0.104 ◦ 0.088 ◦	◦ 0.239 ◦ 0.049 ◦ 0.342 ◦	◦ 0.024 ◦ 0.041 ◦ 0.138 ◦ 0.139 ◦ 0.214 ◦
◦ 0.266 ◦ 0.050 ◦ 0.131 ◦ 0.103 ◦ 0.071 ◦ <b>0.083</b>	◦ 0.248 ◦ 0.087 ◦ 0.356 ◦	◦ 0.005 ◦ 0.044 ◦ 0.200 ◦ 0.094 ◦ 0.119 ◦
◦ 0.159 ◦ -0.067 ◦ 0.179 ◦ 0.092 ◦ 0.009 ◦	◦ 0.179 ◦ 0.116 ◦ 0.251 ◦	◦ 0.089 ◦ 0.056 ◦ 0.111 ◦ 0.059 ◦ 0.136 ◦
◦ 0.034 ◦ 0.094 ◦ 0.073 ◦ 0.187 ◦ -0.077 ◦	◦ 0.281 ◦ 0.091 ◦ 0.176 ◦	◦ 0.031 ◦ 0.066 ◦ 0.064 ◦ 0.005 ◦ 0.326 ◦
◦ 0.102 ◦ 0.044 ◦ 0.096 ◦ 0.055 ◦ 0.029 ◦	◦ 0.062 ◦ 0.104 ◦ 0.361 ◦	◦ 0.156 ◦ 0.028 ◦ 0.103 ◦ 0.011 ◦ 0.132 ◦
◦ 0.008 ◦ 0.125 ◦ 0.012 ◦ 0.123 ◦ -0.055 ◦ <b>0.079 0.056</b>	◦ 0.193 ◦ 0.014 ◦ 0.171 ◦	◦ 0.066 ◦ 0.058 ◦ 0.062 ◦ 0.072 ◦ 0.056 ◦ <b>0.071</b>

(a)

ASR 2—North Face—Vertical Strains

Strains %

Average, Laser Measurement

Rebar Strain

Region 1						Region 2				Region 3					
○	○	○	○	○	○	○	○	○	○	○	○	○	○	○	○
-0.094	-0.045	0.146	0.065	0.175	0.076	0.526	0.365	0.832	0.501	0.157	0.101	0.308	0.060	0.441	0.073
○	○	○	○	○	○	○	○	○	○	○	○	○	○	○	○
0.326	0.239	0.169	0.194	0.252	0.248	0.357	0.094	-0.250	0.040	-0.002	0.090	-0.060	0.271	0.199	0.113
○	○	○	○	○	○	○	○	○	○	○	○	○	○	○	○
0.303	0.156	0.051	0.214	0.136	0.133	0.370	0.225	0.137	0.319	0.217	0.271	0.222	0.171	0.041	0.053
○	○	○	○	○	○	○	○	○	○	○	○	○	○	○	<b>0.159</b>
0.033	0.213	0.219	0.094	0.148	0.126	0.164	0.233	0.239	0.051	0.357	0.071	0.136	0.185	0.246	0.323
○	○	○	○	○	○	○	○	○	○	○	○	○	○	○	○
-0.072	0.060	0.089	0.065	0.189	0.242	0.137	0.291	0.391	0.416	0.052	0.036	0.111	0.073	0.072	0.074
○	○	○	○	○	○	○	○	○	○	○	○	○	○	○	○
0.316	0.301	0.375	0.419	0.068	0.163	0.650	0.252	0.304	0.120	0.300	0.366	-0.114	-0.051	0.009	0.041
○	○	○	○	○	○	○	○	○	○	○	○	○	○	○	○

(b)

ASR 2—South Face—Horizontal Strains

**Strains %**  
Average, Laser Measurement  
Rebar Strain

Region 3	Region 2	Region 1
◦ 0.191 ◦ 0.254 ◦ 0.068 ◦ 0.103 ◦ 0.005 ◦	◦ Na ◦ 0.033 ◦ 0.219 ◦	◦ 0.115 ◦ 0.072 ◦ <b>0.116</b> ◦ 0.140 ◦ 0.177 ◦ <b>0.125</b>
◦ 0.164 ◦ 0.098 ◦ 0.120 ◦ -0.045 ◦ 0.133 ◦	◦ 0.079 ◦ 0.097 ◦ 0.078 ◦	◦ 0.095 ◦ 0.086 ◦ 0.103 ◦ <b>0.181</b> ◦ 0.147 ◦ <b>0.120</b>
◦ 0.016 ◦ -0.007 ◦ 0.121 ◦ 0.096 ◦ 0.109 ◦	◦ 0.285 ◦ 0.108 ◦ 0.122 ◦	◦ 0.076 ◦ 0.054 ◦ 0.107 ◦ 0.134 ◦ 0.155 ◦
◦ 0.240 ◦ 0.019 ◦ 0.111 ◦ 0.106 ◦ 0.228 ◦	◦ 0.291 ◦ -0.003 ◦ 0.074 ◦	◦ 0.054 ◦ 0.059 ◦ 0.163 ◦ -0.036 ◦ 0.303 ◦
◦ 0.127 ◦ 0.118 ◦ 0.062 ◦ 0.152 ◦ -0.083 ◦	◦ 0.082 ◦ 0.105 ◦ 0.284 ◦	<b>0.102</b> ◦ 0.082 ◦ 0.108 ◦ 0.127 ◦ -0.089 ◦ 0.210 ◦
◦ 0.196 ◦ -0.020 ◦ 0.038 ◦ 0.071 ◦ 0.046 ◦	◦ -0.013 ◦ 0.190 ◦ 0.200 ◦	◦ 0.062 ◦ 0.094 ◦ 0.067 ◦ 0.086 ◦ -0.028 ◦
◦ -0.018 ◦ 0.185 ◦ 0.060 ◦ 0.032 ◦ 0.109 ◦	◦ 0.179 ◦ 0.100 ◦ -0.050 ◦	◦ 0.101 ◦ -0.028 ◦ <b>0.101</b> ◦ 0.140 ◦ 0.124 ◦ <b>0.072</b>

(c)

### ASR 2—South Face—Vertical Strains

**Strains %**  
Average, Laser Measurement  
Rebar Strain

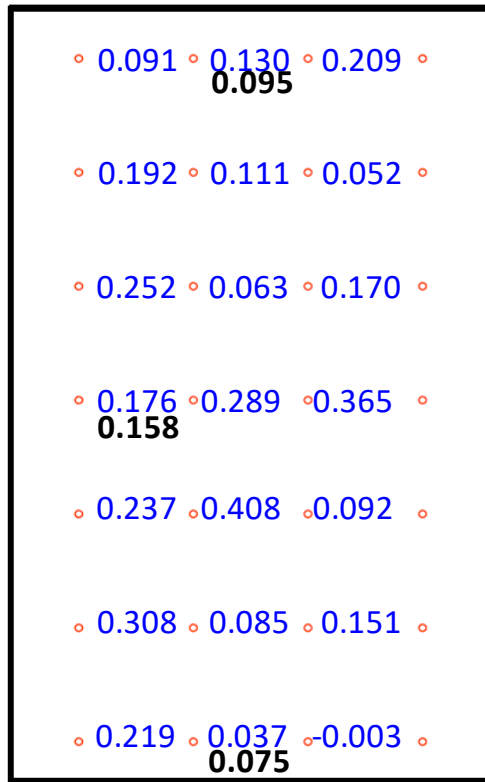
Region 3						Region 2				Region 1					
○	○	○	○	○	○	○	○	○	○	○	○	○	○	○	○
0.087	0.068	0.126	-0.136	0.042	0.140	0.021	0.017	0.123	0.169	0.159	0.096	0.111	0.033	0.193	0.234
○	○	○	○	○	○	○	○	○	○	○	○	○	○	○	○
0.093	0.182	0.057	0.378	0.099	0.105	0.388	0.120	0.291	0.249	0.093	0.191	0.127	0.233	0.220	0.409
○	○	○	○	○	○	○	○	○	○	○	○	○	○	○	○
0.090	0.016	-0.003	-0.066	0.249	0.213	-0.084	0.318	0.194	0.298	0.158	0.107	0.212	0.096	0.173	0.121
○	○	<b>0.144</b>	○	○	○	○	○	○	○	○	○	○	○	○	○
0.306	0.319	0.325	0.192	0.127	0.070	0.393	0.191	0.368	0.362	0.095	0.153	0.196	0.148	0.069	0.096
○	○	○	○	○	○	○	○	○	○	○	○	○	○	○	○
-0.004	0.010	0.048	0.127	0.040	0.083	0.178	0.291	0.209	0.062	0.199	-0.046	-0.033	-0.009	0.140	0.313
○	○	○	○	○	○	○	○	○	○	○	○	○	○	○	○
0.024	0.054	-0.046	0.287	0.248	0.344	0.380	0.271	-0.087	-0.063	0.196	0.459	0.384	0.707	0.431	0.255
○	○	○	○	○	○	○	○	○	○	○	○	○	○	○	○

(d)

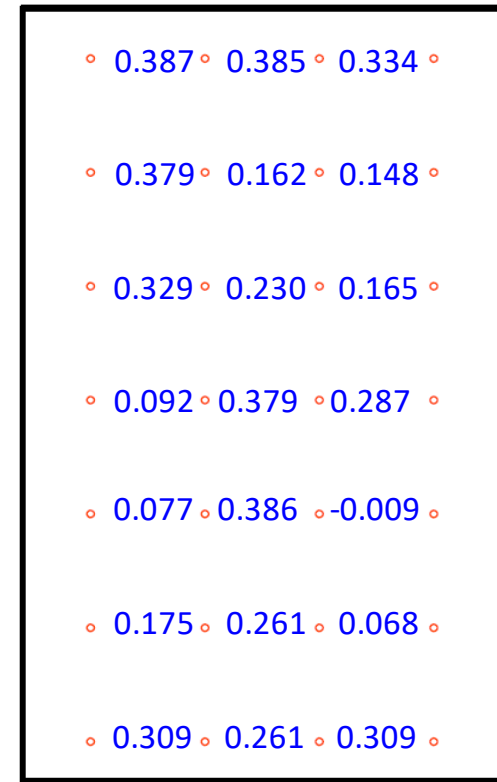
# ASR 2—East and West Faces—Horizontal Strains

## Strains %

Average, Laser Measurement  
Rebar Strain



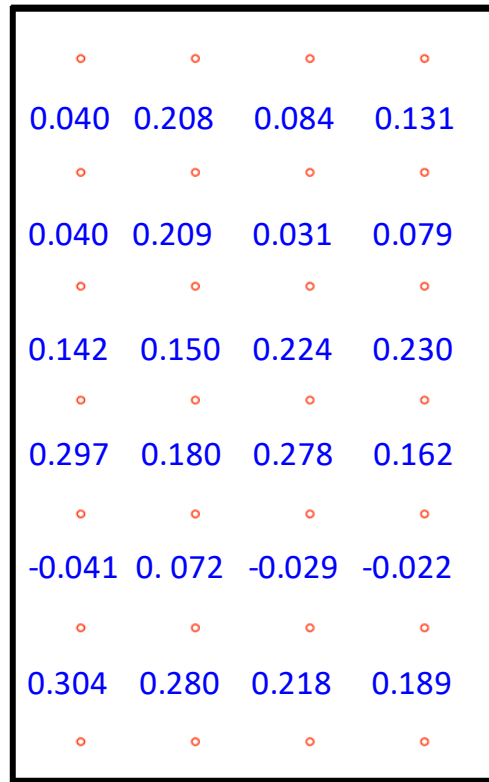
Region 3  
West End



Region 1  
East End

(e)

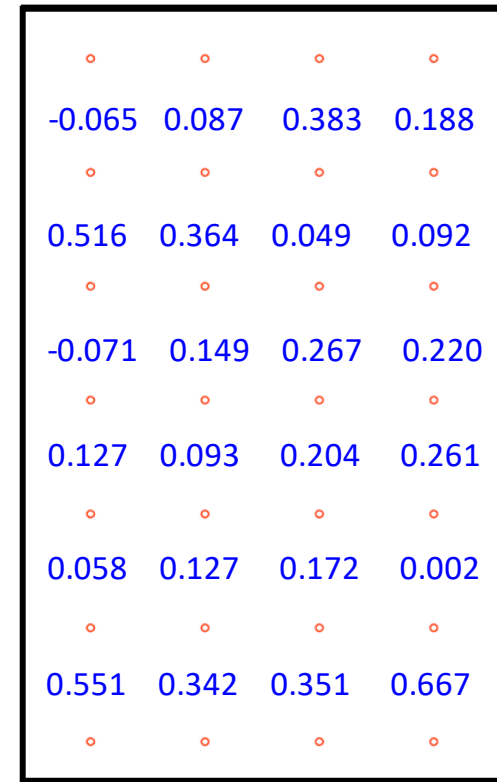
## ASR 2—East and West Faces—Vertical Strains



Region 3  
West End

### Strains %

Average, Laser Measurement  
Rebar Strain



Region 1  
East End

(f)

Figure B-2. Average surface strains using laser measurements between neighboring targets for block ASR 2: (a) horizontal strains on north face, (b) vertical strains on north face, (c) horizontal strains on south face, (d) vertical strains on south face, (e) horizontal strains on east and west ends, and (f) vertical strains on east and west ends

ASR 3—East Face—Horizontal Strains

**Strains %**

Average, Laser Measurement

Rebar Strain

Region 1	Region 2	Region 3
◦ 0.231 ◦ 0.095 ◦ <b>0.132</b> ◦ 0.108 ◦ <b>0.371</b> ◦ <b>0.350</b> ◦ <b>0.246</b>	◦ 0.155 ◦ 0.131 ◦ 0.122 ◦	◦ <b>0.013</b> ◦ <b>0.013</b> ◦ <b>0.189</b> ◦ <b>0.117</b> ◦ <b>0.085</b> ◦ <b>0.289</b> ◦ <b>0.335, 0.344</b> ◦ <b>0.319</b>
◦ 0.138 ◦ 0.094 ◦ 0.152 ◦ 0.122 ◦ 0.259 ◦	◦ 0.114 ◦ 0.108 ◦ 0.468 ◦	◦ 0.100 ◦ 0.052 ◦ 0.118 ◦ 0.067 ◦ 0.182 ◦
◦ 0.091 ◦ 0.165 ◦ 0.154 ◦ -0.064 ◦ 0.317 ◦	◦ 0.280 ◦ 0.091 ◦ 0.602 ◦	◦ <b>0.072</b> ◦ <b>0.108</b> ◦ <b>0.006</b> ◦ <b>0.185</b> ◦ <b>0.055</b> ◦ <b>0.234</b> ◦ <b>0.193, 0.304</b>
◦ 0.038 ◦ 0.115 ◦ 0.154 ◦ 0.015 ◦ 0.201 ◦	◦ 0.345 ◦ 0.376 ◦ 0.579 ◦	◦ -0.105 ◦ 0.121 ◦ 0.099 ◦ 0.061 ◦ 0.048 ◦
◦ 0.350 ◦ -0.068 ◦ 0.181 ◦ <b>0.202</b> ◦ 0.098 ◦ 0.095 ◦	◦ -0.154 ◦ 0.601 ◦ -0.031 ◦	◦ 0.128 ◦ 0.098 ◦ 0.039 ◦ 0.261 ◦ -0.014 ◦
◦ 0.053 ◦ <b>0.097</b> ◦ 0.124 ◦ <b>0.096</b> ◦ <b>0.013</b> ◦ <b>0.258</b> ◦ <b>0.210</b>	◦ 0.015 ◦ 0.276 ◦ 0.229 ◦	◦ 0.048 ◦ 0.184 ◦ 0.023 ◦ 0.105 ◦ 0.189 ◦
◦ 0.211 ◦ 0.011 ◦ 0.118 ◦ 0.114 ◦ -0.032 ◦	◦ 0.122 ◦ <b>0.021</b> ◦ 0.201 ◦ <b>0.313</b>	◦ 0.160 ◦ 0.143 ◦ <b>0.043</b> ◦ <b>0.097</b> ◦ <b>0.131</b> ◦ <b>0.243</b> ◦ <b>0.217</b>

(a)

ASR 3—East Face—Vertical Strains

**Strains %**  
Average, Laser Measurement  
Rebar Strain

Region 1						Region 2				Region 3					
○	○	○	○	○	○	○	○	○	○	○	○	○	○	○	○
0.061	0.234	0.160	0.178	0.185	0.269	-0.123	0.538	0.198	0.454	-0.179	-0.075	-0.082	0.054	0.080	0.022
○	○	○	○	○	○	○	○	○	○	○	○	○	○	○	○
0.247	0.357	0.184	0.213	0.264	0.045	0.188	0.189	0.250	0.342	0.267	0.177	0.143	0.211	0.118	0.193
○	○	○	○	○	○	○	○	○	○	○	○	○	○	○	○
0.092	-0.030	0.134	-0.028	-0.067	0.091	-0.025	-0.076	0.141	-0.224	-0.022	-0.085	-0.085	-0.059	0.061	0.124
○	○	○	<b>0.309</b>	○	○	○	○	○	○	○	<b>0.349, 0.206</b>	○	<b>0.376</b>	○	○
0.253	0.229	0.158	0.255	0.248	0.194	1.069	0.955	0.677	0.912	0.361	0.305	0.278	0.161	0.132	0.113
○	○	○	○	○	○	○	○	○	○	○	○	○	○	○	○
0.135	0.182	0.253	0.214	0.337	0.274	0.058	0.092	-0.031	-0.014	0.160	0.183	0.272	0.230	0.173	0.264
○	○	○	○	○	○	○	○	○	○	○	○	○	○	○	○
0.254	0.220	0.200	0.206	0.108	0.098	0.543	0.457	0.660	0.693	0.093	0.164	-0.028	0.221	0.360	0.226
○	○	○	○	○	○	○	○	○	○	○	○	○	○	○	○

(b)

ASR 3—West Face—Horizontal Strains

**Strains %**

Average, Laser Measurement

Rebar Strain

Region 3	Region 2	Region 1
◦ 0.426 ◦ 0.198 ◦ 0.130 ◦ 0.052 ◦ 0.050 ◦ <b>0.228</b>	◦ 0.409 ◦ 0.108 ◦ 0.476 ◦	◦ 0.358 ◦ 0.111 ◦ <b>0.111</b> ◦ 0.019 ◦ 0.292 ◦ <b>0.246</b> <b>0.300</b>
◦ 0.466 ◦ 0.042 ◦ 0.170 ◦ 0.063 ◦ 0.190 ◦ <b>0.321</b>	◦ 0.210 ◦ 0.210 ◦ 0.334 ◦	◦ 0.081 ◦ 0.015 ◦ 0.215 ◦ -0.001 ◦ 0.374 ◦ <b>0.273</b> <b>0.301</b>
◦ -0.054 ◦ 0.330 ◦ -0.021 ◦ 0.132 ◦ 0.133 ◦ <b>0.193</b>	◦ 0.136 ◦ 0.109 ◦ 0.445 ◦	◦ 0.123 ◦ 0.058 ◦ 0.090 ◦ 0.155 ◦ 0.166 ◦ <b>0.296</b> <b>0.324</b>
◦ 0.127 ◦ 0.109 ◦ -0.028 ◦ 0.186 ◦ 0.001 ◦ <b>0.255</b>	◦ -0.139 ◦ 0.387 ◦ 0.412 ◦	◦ 0.093 ◦ 0.133 ◦ 0.088 ◦ -0.003 ◦ 0.186 ◦
◦ 0.148 ◦ 0.211 ◦ 0.007 ◦ 0.010 ◦ 0.028 ◦	◦ 0.245 ◦ 0.126 ◦ 0.792 ◦	◦ 0.163 ◦ 0.113 ◦ 0.111 ◦ -0.043 ◦ 0.167 ◦
◦ 0.240 ◦ <b>0.210</b> ◦ 0.065 ◦ <b>0.199</b> ◦ 0.087 ◦	◦ 0.184 ◦ 0.039 ◦ 0.339 ◦	◦ 0.087 ◦ <b>0.245</b> ◦ 0.051 ◦ <b>0.289</b> ◦ 0.069 ◦
◦ 0.115 ◦ 0.027 ◦ 0.096 ◦ -0.014 ◦ 0.100 ◦ <b>0.213</b> <b>0.152</b> <b>0.202</b> <b>0.185</b>	◦ 0.130 ◦ 0.007 ◦ 0.190 ◦ <b>0.197</b>	◦ 0.064 ◦ 0.027 ◦ 0.045 ◦ 0.187 ◦ 0.018 ◦ <b>0.191</b>

(c)

ASR 3—West Face—Vertical Strains

**Strains %**

Average, Laser Measurement

Rebar Strain

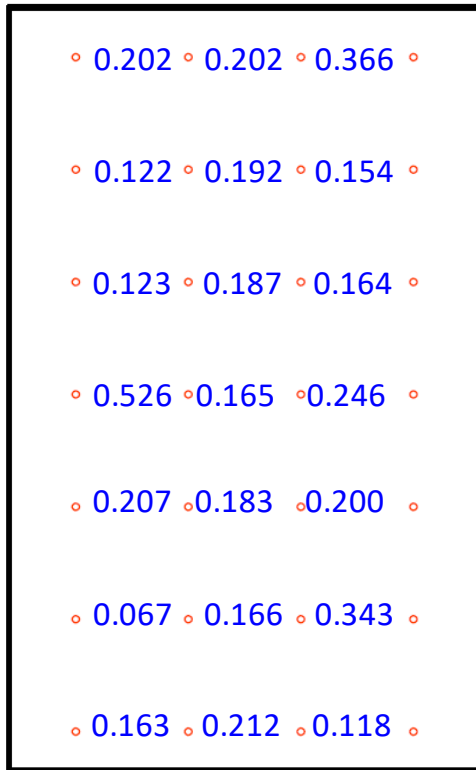
Region 3						Region 2				Region 1					
○	○	○	○	○	○	○	○	○	○	○	○	○	○	○	○
-0.001	0.246	0.058	0.101	-0.044	0.072	0.471	0.272	0.409	0.326	0.232	0.266	0.326	-0.089	-0.046	-0.131
○	○	○	○	○	○	○	○	○	○	○	○	○	○	○	○
0.265	0.133	0.253	0.200	0.340	0.376	0.183	0.096	-0.151	0.158	0.293	-0.069	0.045	0.333	0.379	0.415
○	○	○	○	○	○	○	○	○	○	○	○	○	○	○	○
0.099	0.159	0.003	-0.008	-0.008	0.106	0.158	0.346	0.802	0.429	0.192	0.351	0.017	0.210	0.109	0.134
○	○	○	<b>0.294</b>	<b>0.275</b>	<b>0.256, 0.257</b>	○	○	○	○	<b>0.289</b>	○	<b>0.321</b>	○	○	○
0.102	0.016	0.098	0.249	0.299	0.285	1.024	0.785	0.457	0.646	0.094	0.034	0.216	0.195	0.225	0.266
○	○	○	○	○	○	○	○	○	○	○	○	○	○	○	○
0.240	0.281	0.208	0.129	0.094	0.175	0.189	0.234	0.485	0.425	0.408	0.380	0.363	0.235	0.247	0.052
○	○	○	○	○	○	○	○	○	○	○	○	○	○	○	○
0.029	0.057	0.124	0.112	0.146	0.224	0.358	0.274	0.133	0.199	0.076	-0.022	-0.082	-0.046	0.084	0.324
○	○	○	○	○	○	○	○	○	○	○	○	○	○	○	○

(d)

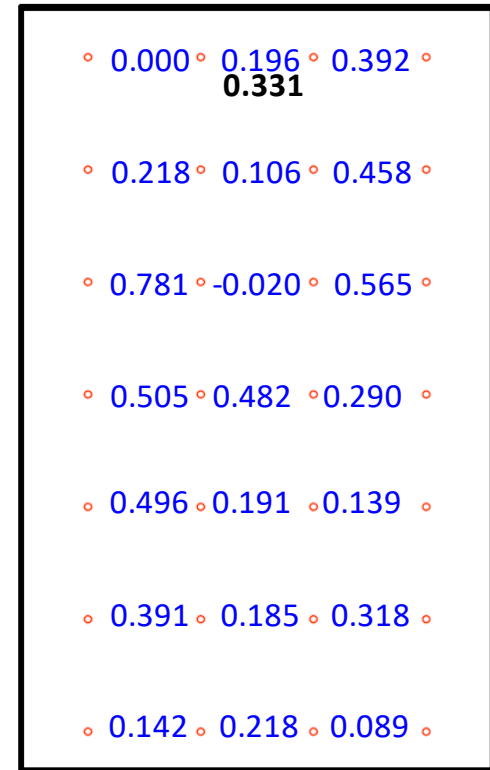
### ASR 3—North and South Faces—Horizontal Strains

**Strains %**

Average, Laser Measurement  
Rebar Strain



Region 3  
North End



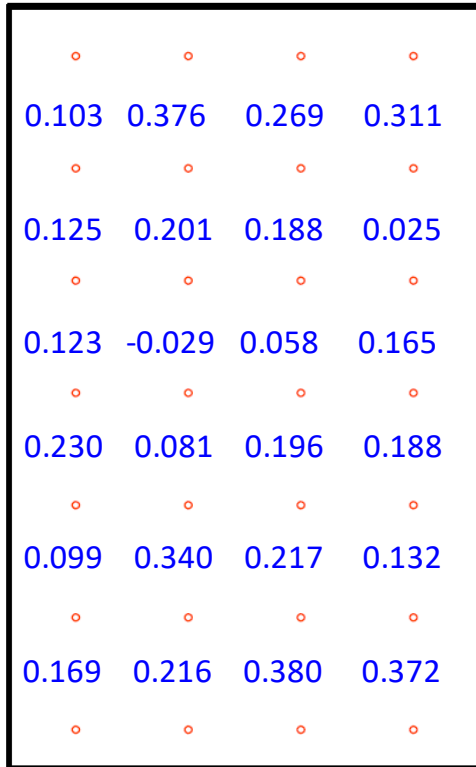
Region 1  
South End

(e)

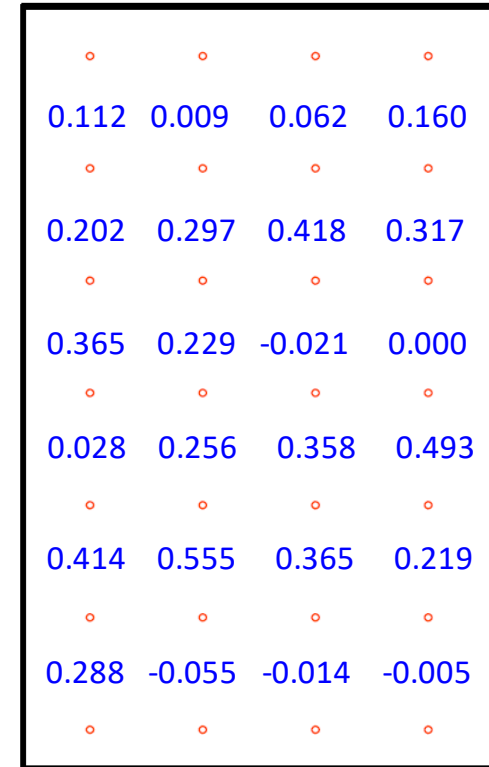
### ASR 3—North and South Faces—Vertical Strains

**Strains %**

Average, Laser Measurement  
Rebar Strain



Region 3  
North End

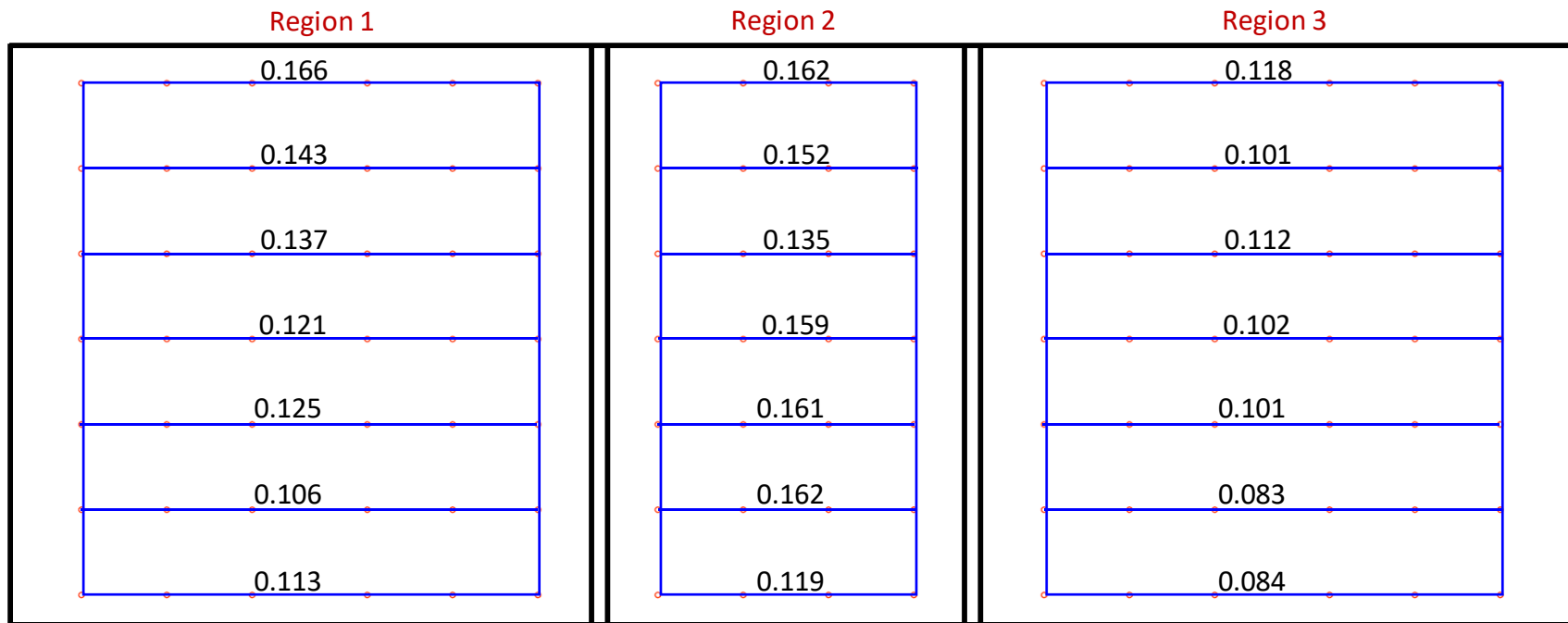


Region 1  
South End

(f)

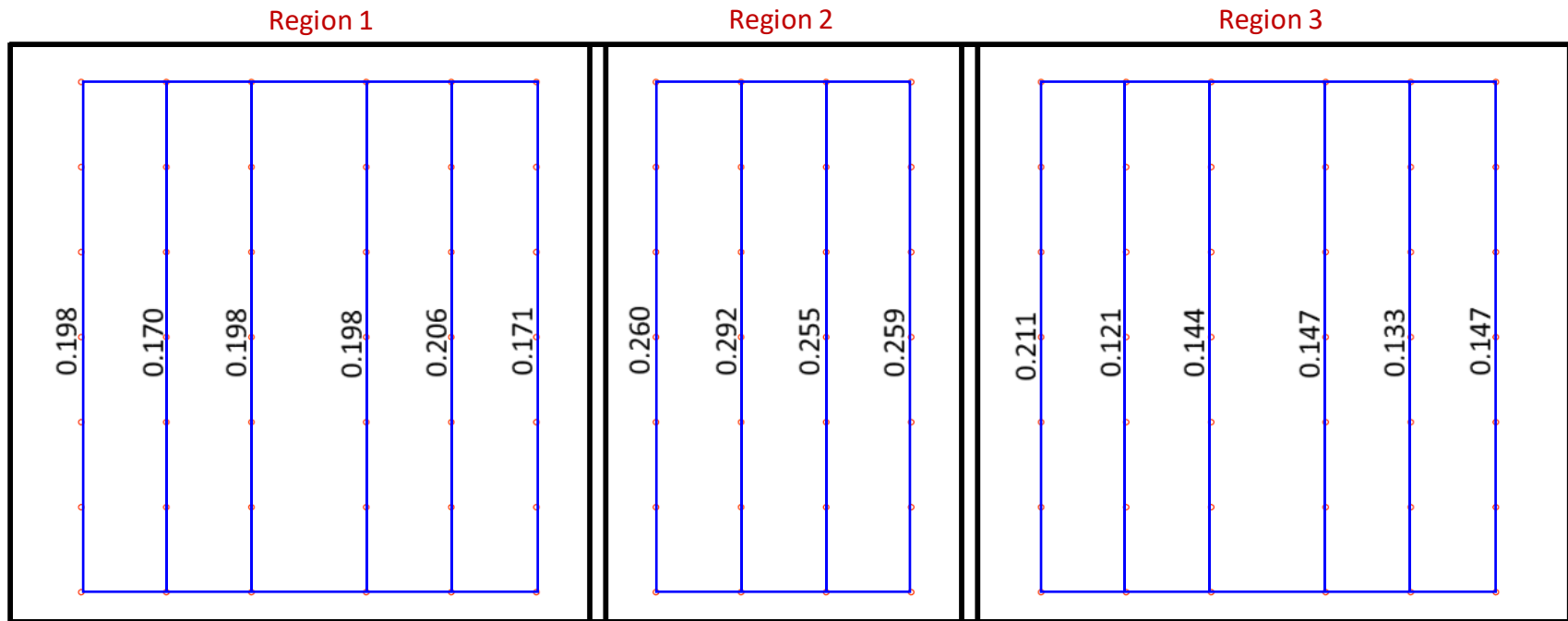
Figure B-3. Average surface strains using laser measurements between neighboring targets for block ASR 3: (a) horizontal strains on east face, (b) vertical strains on east face, (c) horizontal strains on west face, (d) vertical strains on west face, (e) horizontal strains on north and south ends, and (f) vertical strains on north and south ends

## ASR 1—East Face—Average Horizontal Strains



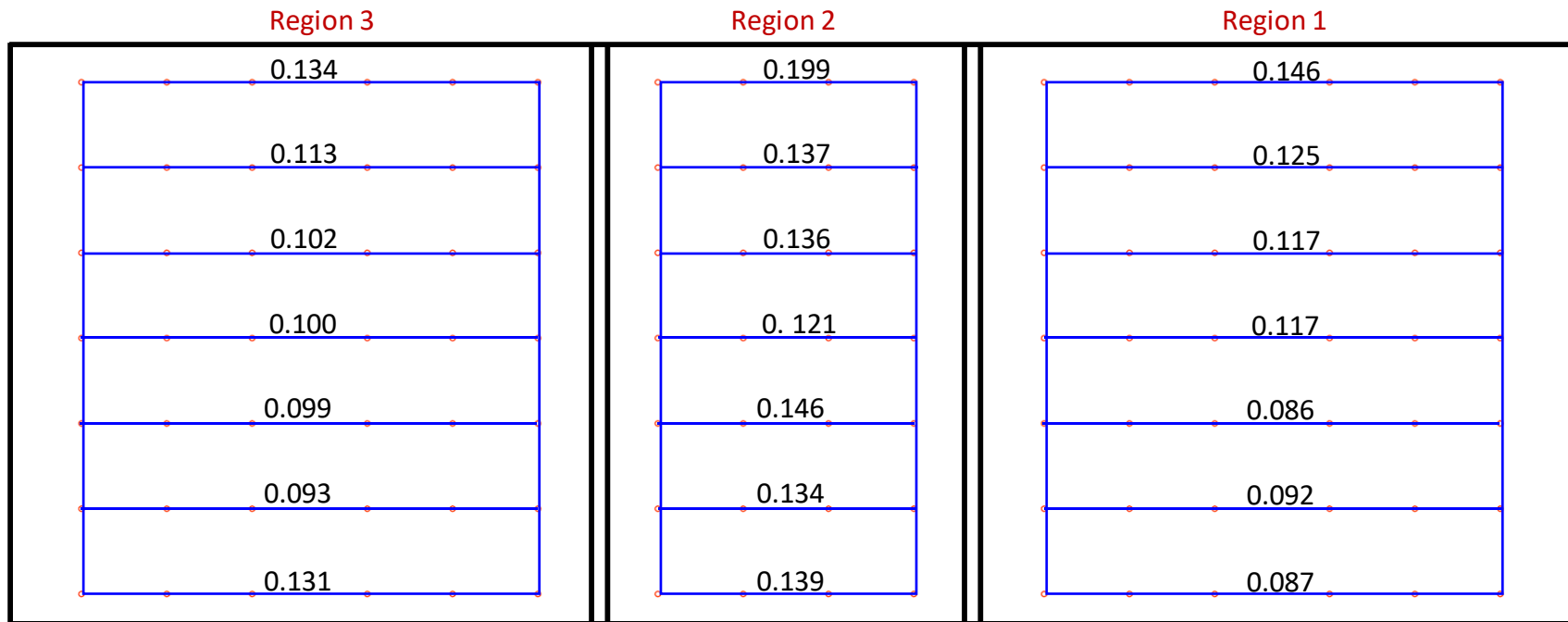
(a)

### ASR 1—East Face—Average Vertical Strains



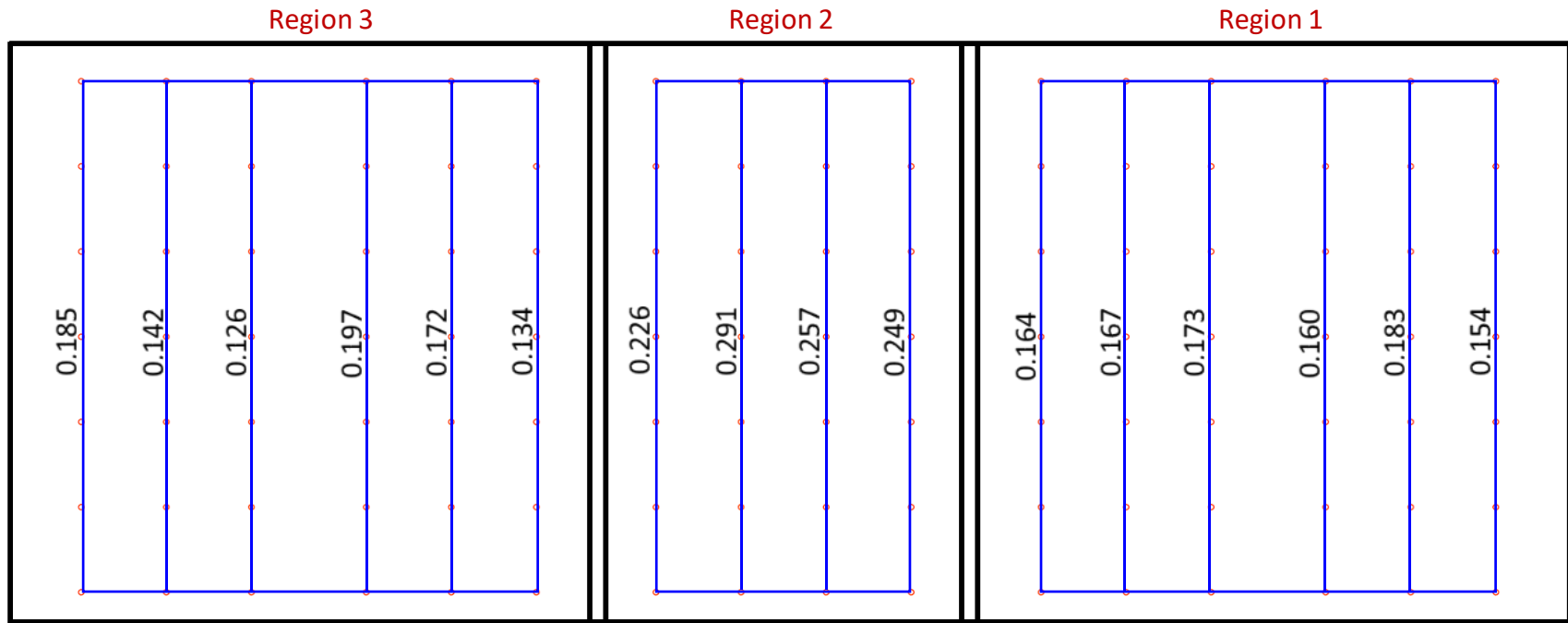
(b)

## ASR 1—West Face—Average Horizontal Strains



(c)

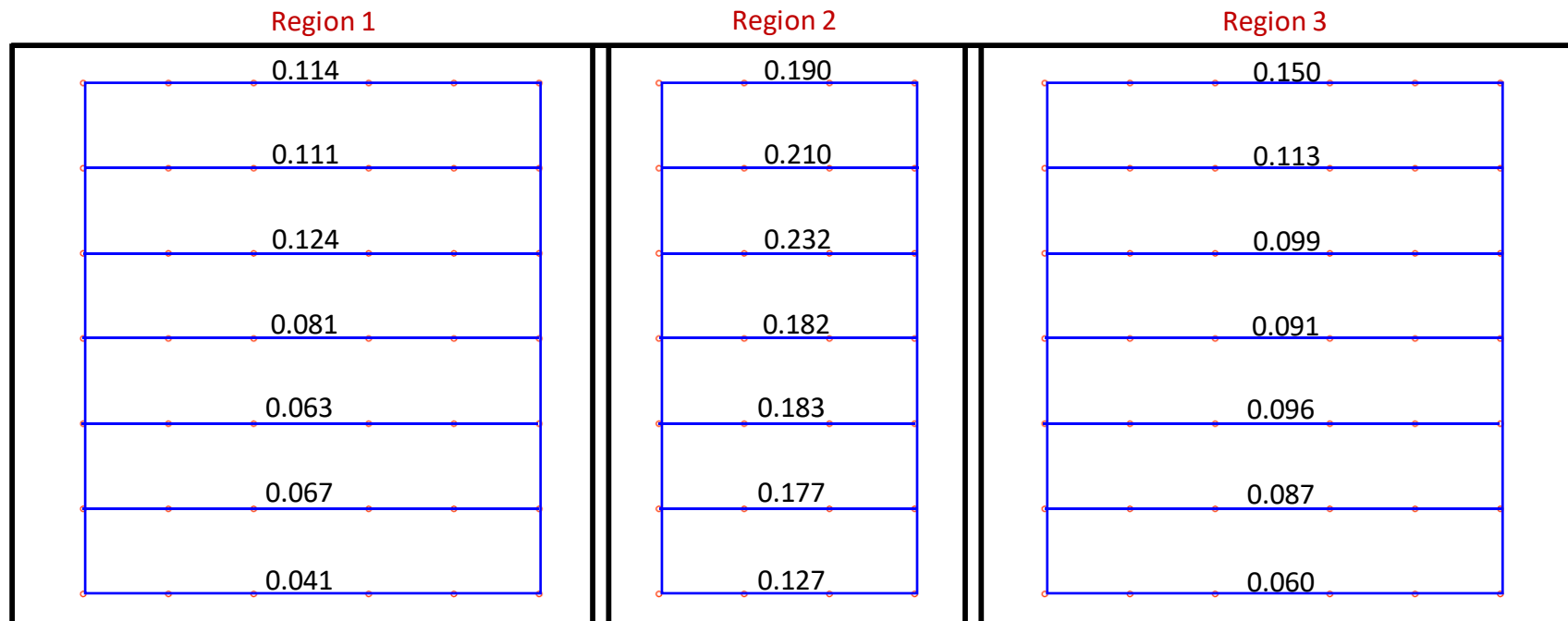
### ASR 1—West Face—Average Vertical Strains



(d)

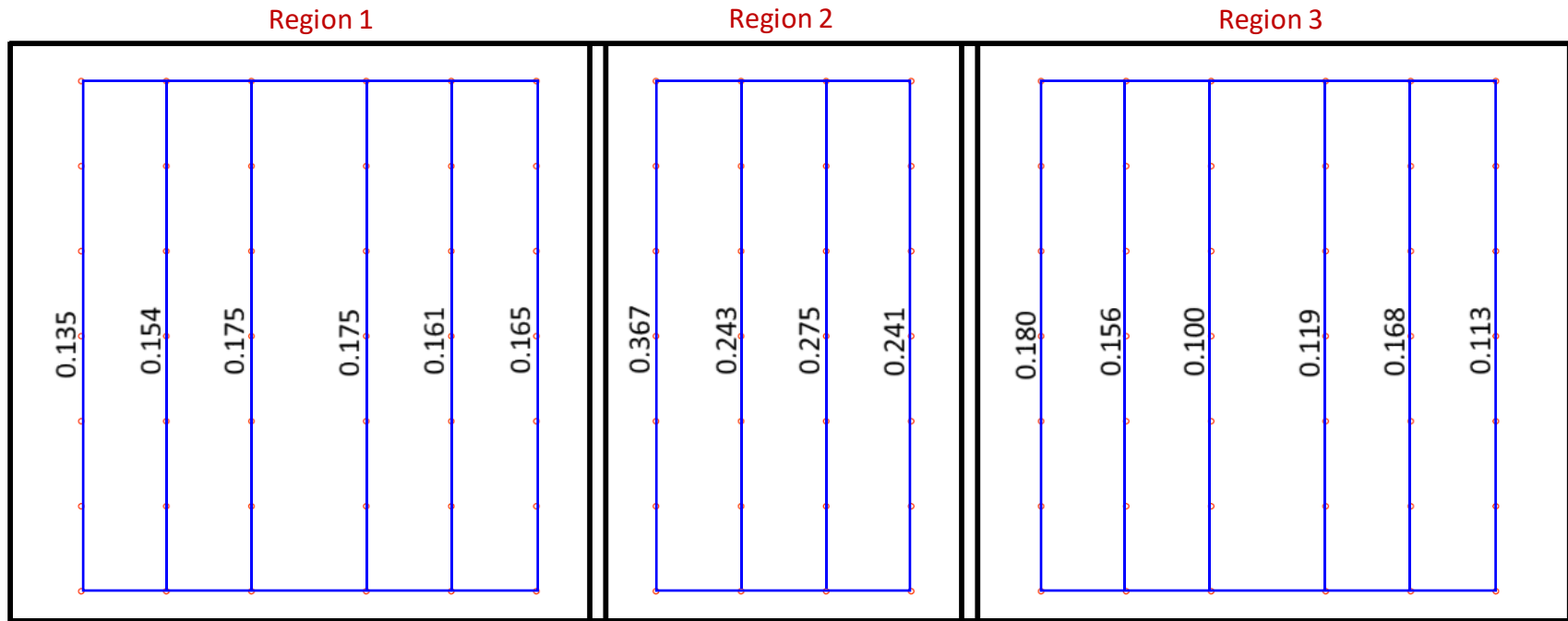
Figure B-4. Average surface strains using laser measurements along target lines for block ASR 1: (a) horizontal strains on east face, (b) vertical strains on east face, (c) horizontal strains on west face, and (d) vertical strains on west face

## ASR 2—North Face—Average Horizontal Strains



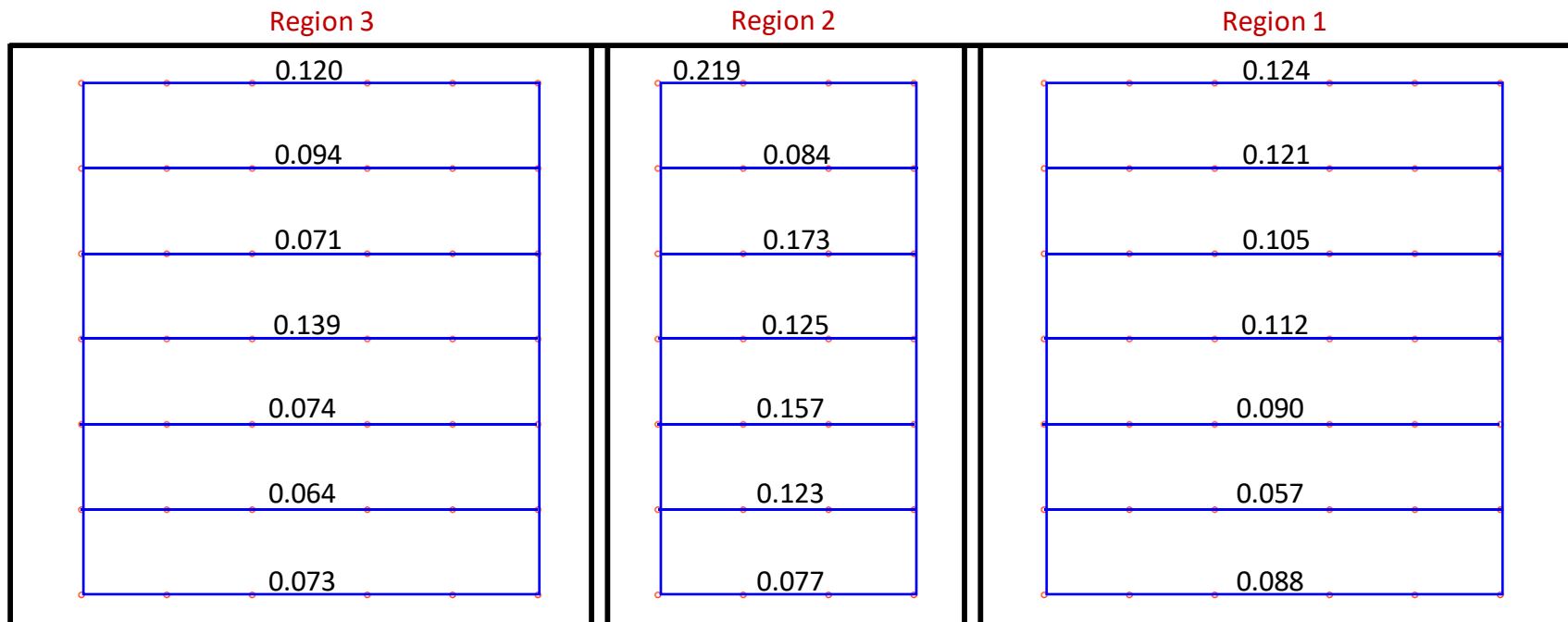
(a)

### ASR 2—North Face—Average Vertical Strains



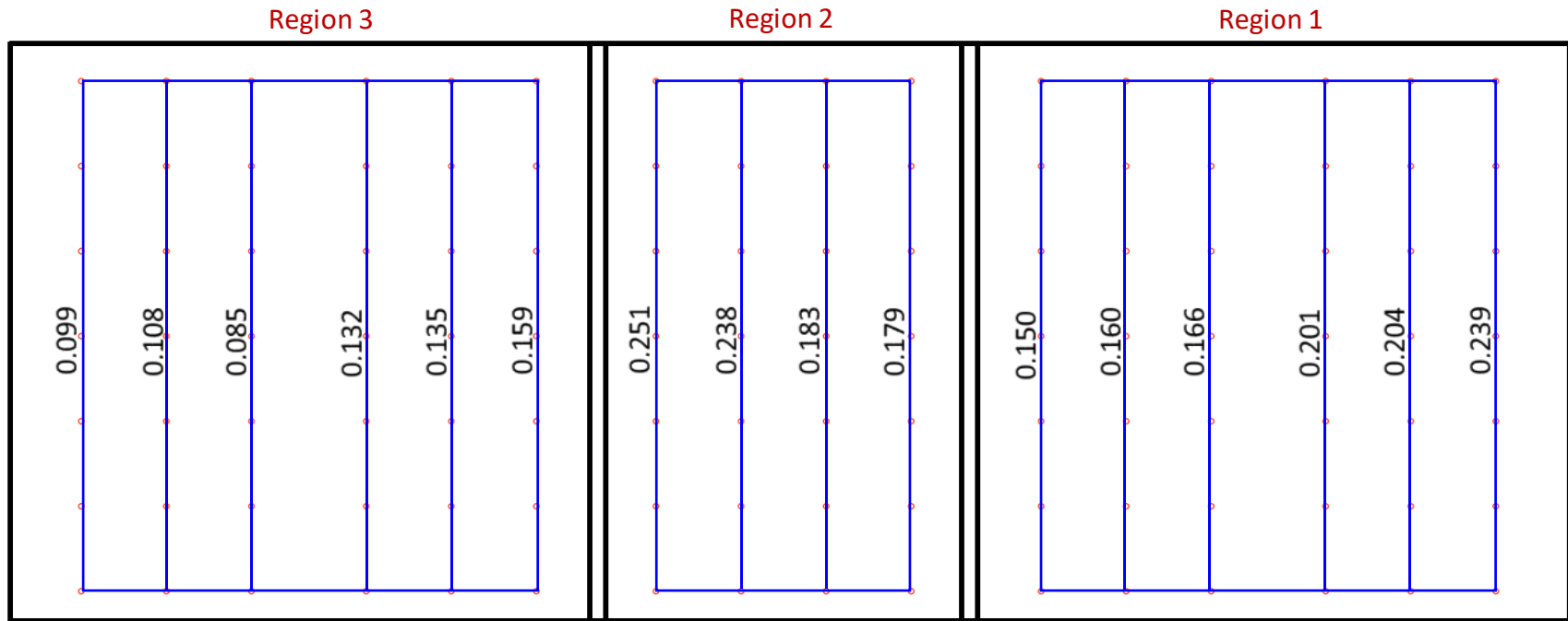
(b)

## ASR 2—South Face—Average Horizontal Strains



©

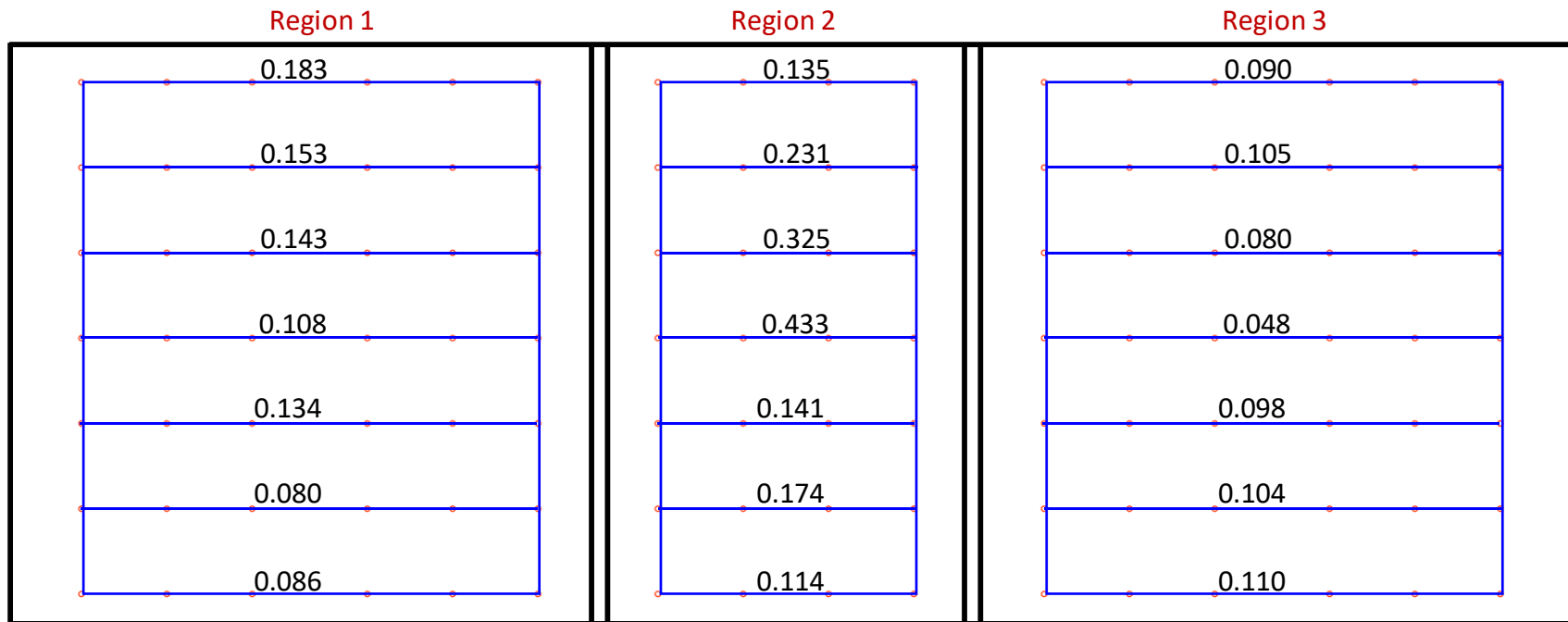
### ASR 2—South Face—Average Vertical Strains



(d)

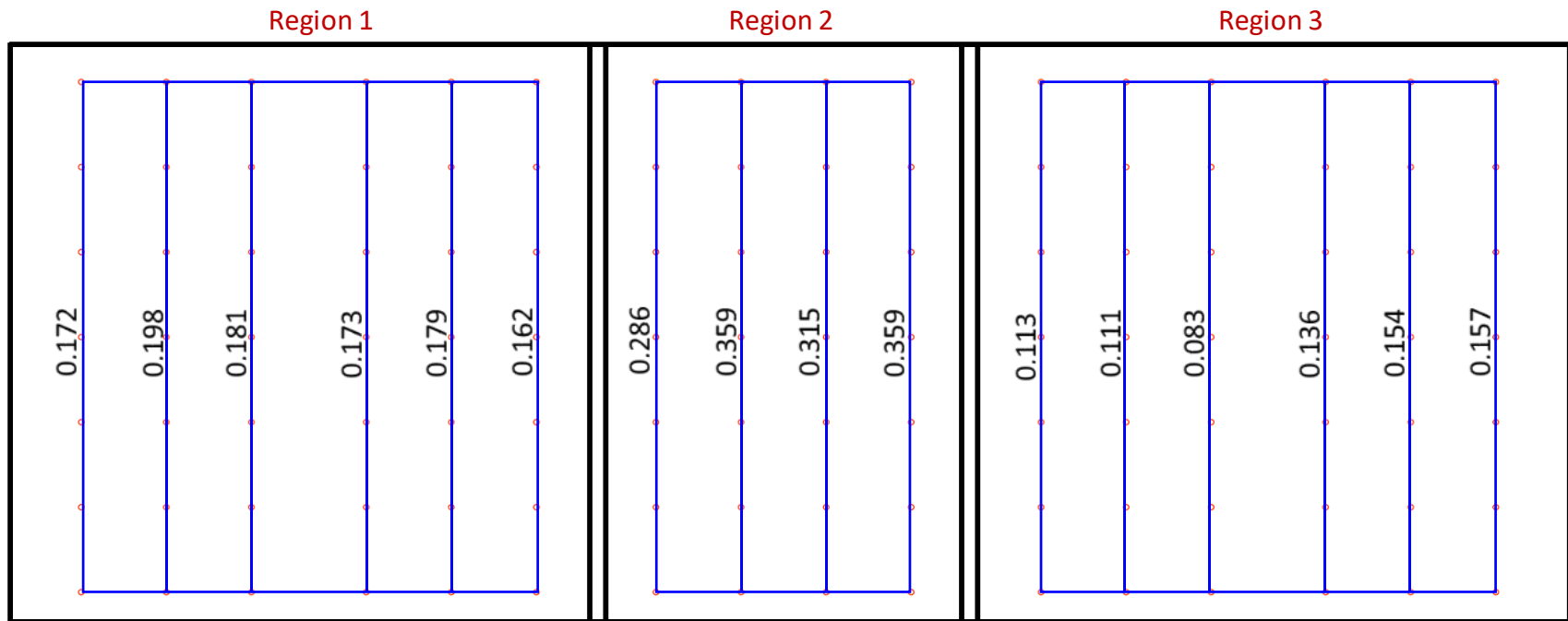
Figure B-5. Average surface strains using laser measurements along target lines for block ASR 2: (a) horizontal strains on north face, (b) vertical strains on north face, (c) horizontal strains on south face, and (d) vertical strains on south face

## ASR 3—East Face—Average Horizontal Strains



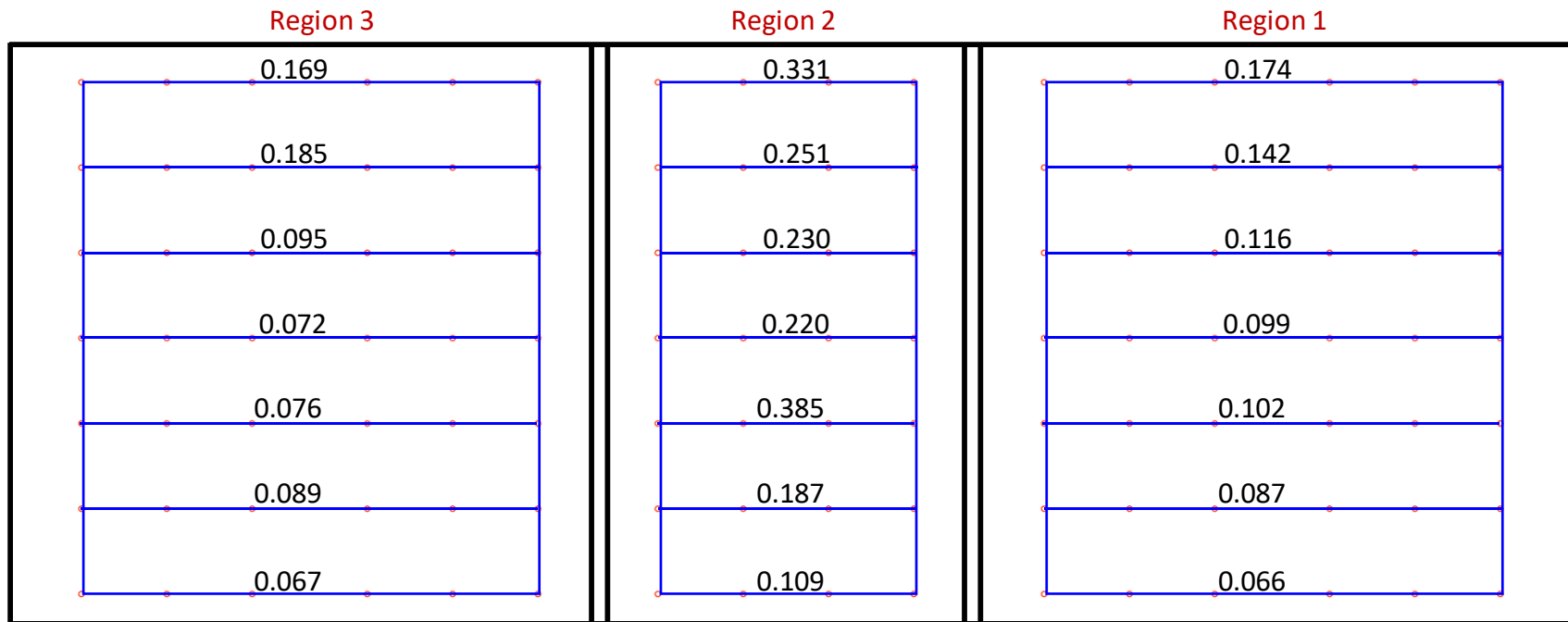
(a)

### ASR 3—East Face—Average Vertical Strains



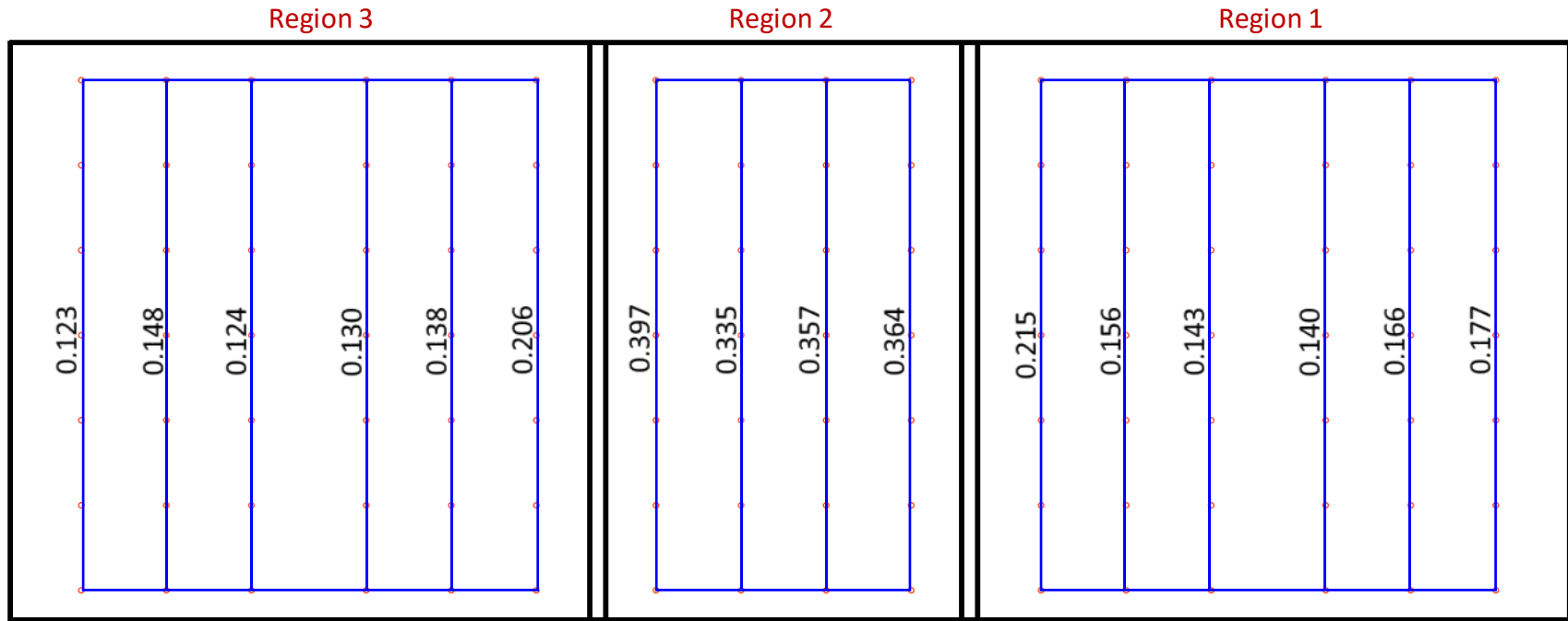
(b)

## ASR 3—West Face—Average Horizontal Strains



(c)

### ASR 3—West Face—Average Vertical Strains



(d)

Figure B-6. Average surface strains using laser measurements along target lines for block ASR 3: (a) horizontal strains on east face, (b) vertical strains on east face, (c) horizontal strains on west face, and (d) vertical strains on west face

This page intentionally left blank.

## **APPENDIX C**

### **AVERAGE SURFACE STRAINS USING LASER AND CALIPER MEASUREMENTS ALONG WITH CRACKING INDEX AND REINFORCING BAR STRAINS**

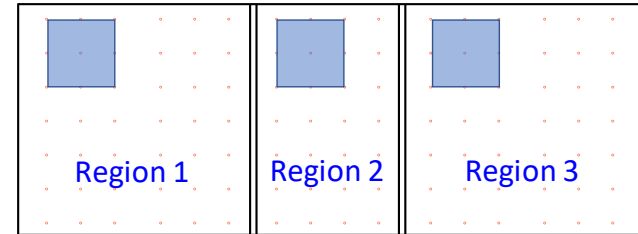
---

---

This appendix presents the average surface strains using laser and caliper measurements along with cracking index and reinforcing bar strains, see Section 3.3.2. Separate plots are provided for blocks ASR 1, ASR 2, and ASR 3. North direction is defined in Figure 3-18.

ASR 1—East Face

Average Strain, Laser Measurement  
 Average Strain, Caliper Measurement  
 Cracking Index  
 Rebar Strain

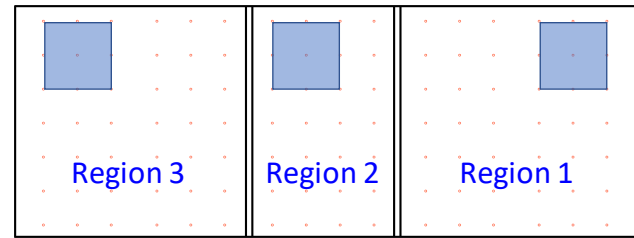


0.230	0.169	0.036	0.224	0.171	0.043
0.207	0.187	0.102	0.229	0.137	0.084
0.049	0.071	0.096	0.171	0.166	0.118
<b>0.118</b>	0.	0.	0.	0.	0.
0.147	0.073	0.127	0.330	0.461	-0.008
0.163	0.105	0.219	0.352	0.358	0.103
0.071	0.042	0.088	0.261	0.096	0.061
0.	0.	0.	0.	0.	0.
0.140	0.219	0.330	0.007	-0.494	0.645
0.151	0.186	0.252	0.120	0.103	0.049
0.194	0.167	0.095	0.038	0.103	0.101
0.	<b>0.106</b>	0.	0.	0.	0.
0.177	0.210	0.183	0.142	0.180	0.192
0.200	0.226	0.233	0.174	0.131	0.147
0.137	0.141	0.078	0.067	0.077	0.060
0.	0.	0.	0.	0.	0.
0.187	0.045	0.180	0.116	0.061	0.161
0.145	0.069	0.201	0.101	0.103	0.105
0.131	0.000	0.127	0.057	0.085	0.084
0.	0.	0.	0.	0.	0.

(a)

### ASR 1—West Face

Average Strain, Laser Measurement  
 Average Strain, Caliper Measurement  
 Cracking Index  
 Rebar Strain

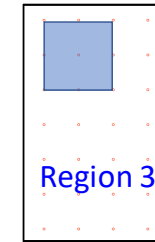


0.150 0.155 0.085 0. 0.076 0.139 0.078 0. 0.067 0.107	0.222 0.230 0.053 0. 0.135 0.143 0.266 0. 0.142 0.139	0.193 0.249 0.148 0. 0.101 0.222 0.131 0. 0.197 0.212	0.290 0.256 0.055 0. 0.462 0.400 0.207 0. 0.152 0.140	0.124 0.155 0.159 0. 0.173 0.200 0.138 0. 0.056 0.097	0.175 0.177 0.222 <b>0.168</b> 0.124 0.154 0.173 0. 0.214 0.190
0.252 0.231 0.095 0. 0.158 0.127 0.070 0.	0.180 0.183 0.148 0. 0.158 0.187 0.110 0.	0.297 0.303 0.285 0. 0.325 0.255 0.060 0.	0.212 0.222 0.198 0. -0.004 0.038 0.051 0.	0.214 0.194 0.085 0. 0.028 0.045 0.124 0.	0.336 0.263 0.145 0. 0.148 0.134 0.177 0.

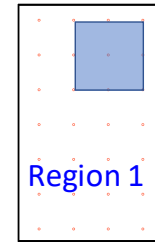
(b)

ASR 1—North and South Ends

Average Strain, Laser Measurement  
 Average Strain, Caliper Measurement  
 Cracking Index  
 Rebar Strain



North End



South End

	0.487 0.420		0.136 0.192	
	0.159		0.085	
	0.		0.	
0.252		0.583		0.372
0.264		0.498		0.372
0.070		0.182		0.095
0.		0.		0.
	0.080		0.299	
	0.118		0.234	
	0.085		0.074	
	0.		0.	
-0.464		-0.681		-0.744
0.125		0.111		0.164
0.049		0.053		0.099
0.		0.		0.
	0.017		0.328	
	0.044		0.273	
	0.018		0.237	
	0.		0.	

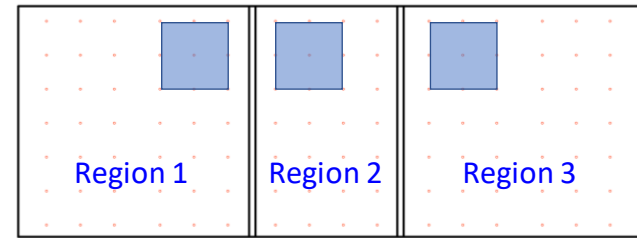
	0.329 0.282		0.091 0.158	
	0.124		0.085	
	0.		0.	
0.323		0.250		0.120
0.307		0.277		0.193
0.120		0.123		0.126
0.		0.		0.
	0.222		0.245	
	0.260		0.182	
	0.095		0.148	
	0.		0.	
0.213		0.074		0.246
0.209		0.166		na
0.192		0.106		na
0.		0.		0.
	0.335		0.337	
	0.342		na	
	0.211		na	
	0.		0.	

(c)

Figure C-1. Average surface strains using laser and caliper measurements along with cracking index and reinforcing bar strains for block ASR 1 on (a) east face, (b) west face, and (c) north and south ends (all values are percentages)

### ASR 2—North Face

Average Strain, Laser Measurement  
 Average Strain, Caliper Measurement  
 Cracking Index  
 Rebar Strain

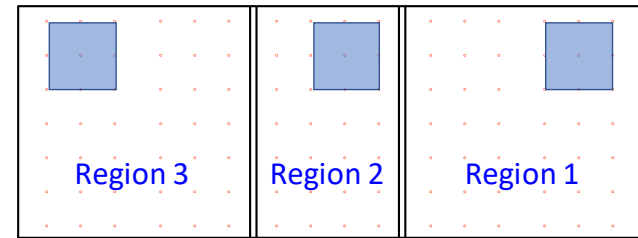


0.030	0.176	0.337	0.139	0.074	0.082
0.060	0.142	0.282	0.170	0.064	0.104
0.018	0.060	0.085	0.055	0.043	0.069
0.	<b>0.100</b>	0.	<b>0.131</b>	0.	0.
0.065	0.175	0.527	0.365	0.157	0.101
0.094	0.167	0.467	0.351	0.117	0.118
0.060	0.039	0.283	0.353	0.089	0.071
0.	0.	0.	0.	0.	0.
0.104	0.088	0.239	0.049	0.024	0.041
0.099	0.078	0.230	0.171	0.029	0.063
0.060	0.036	0.106	0.091	0.149	0.035
0.	0.	0.	0.	0.	0.
0.194	0.252	0.357	0.094	-0.002	0.090
0.117	0.129	0.281	0.140	0.028	0.080
0.060	0.078	0.229	0.060	0.000	0.077
0.	0.	0.	0.	0.	0.
0.103	0.071	0.248	0.087	0.005	0.044
0.072	0.075	0.257	0.106	0.031	0.075
0.084	0.078	0.177	0.073	0.035	0.084
0.	<b>0.083</b>	0.	0.	0.	0.

(a)

ASR 2—South Face

Average Strain, Laser Measurement  
 Average Strain, Caliper Measurement  
 Cracking Index  
 Rebar Strain

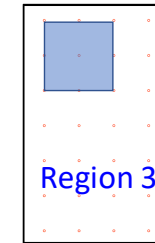


0.191	0.254	0.033	0.219	0.140	0.177
0.189	0.190	0.207	0.193	0.150	0.184
0.070	0.043	0.038	0.060	0.095	0.105
0.	0.	0.	0.	0	0.
0.087	0.068	0.123	0.169	0.033	0.193
0.144	0.107	0.148	0.215	0.076	0.173
0.053	0.036	0.106	0.106	0.025	0.089
0.	0.	0.	0.	0.	0.
0.164	0.098	0.097	0.078	0.181	0.147
0.152	0.054	0.160	0.089	0.151	0.132
0.078	0.053	0.081	0.060	0.068	0.088
0.	0.	0.	0.	<b>0.120</b>	0.
0.093	0.182	0.120	0.291	0.233	0.220
0.082	0.123	0.126	0.250	0.202	0.172
0.113	0.060	0.035	0.113	0.124	0.060
0.	0.	0.	0.	0.	0.
0.016	-0.007	0.108	0.122	0.134	0.155
0.037	0.008	0.083	0.150	0.107	0.144
0.042	0.018	0.046	0.060	0.060	0.078
0.	0.	0.	0.	0.	0.

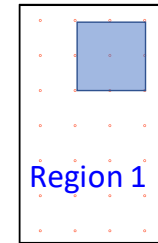
(b)

### ASR 2—East and West Ends

Average Strain, Laser Measurement  
 Average Strain, Caliper Measurement  
 Cracking Index  
 Rebar Strain



West End



East End

	0.091 0.107		0.130 0.133	
	0.035		0.179	
	0.		0.095	
0.040		0.208		0.084
0.077		0.198		0.071
0.025		0.123		0.060
0.		0.		0.
	0.192		0.111	
	0.108		0.117	
	0.043		0.078	
	0.		0.	
0.040		0.209		0.031
0.039		0.135		0.039
0.035		0.092		0.060
0.		0.		0.
	0.252		0.063	
	0.212		0.070	
	0.142		0.050	
	0.		0.	

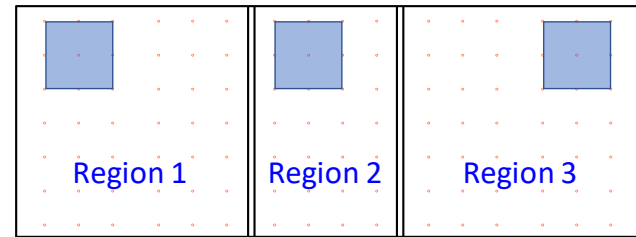
	0.385 0.296		0.334 0.346	
	0.096		0.067	
	0.		0.	
0.087		0.383		0.188
0.095		0.266		0.193
0.053		0.071		0.142
0.		0.		0.
	0.162		0.148	
	0.168		0.169	
	0.085		0.053	
	0.		0.	
0.364		0.049		0.092
0.268		0.122		0.132
0.106		0.035		0.085
0.		0.		0.
	0.230		0.165	
	0.218		0.168	
	0.106		0.053	
	0.		0.	

(c)

Figure C-2. Average surface strains using laser and caliper measurements along with cracking index and reinforcing bar strains for block ASR 2 on (a) north face, (b) south face, and (c) east and west ends (all values are percentages)

ASR 3—East Face

Average Strain, Laser Measurement  
 Average Strain, Caliper Measurement  
 Cracking Index  
 Rebar Strain

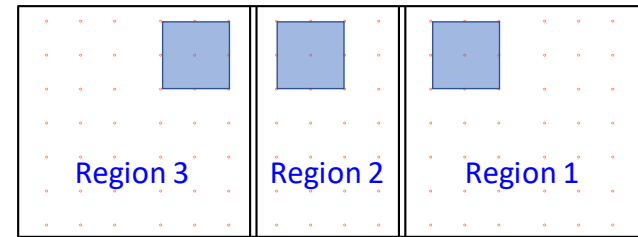


	0.231 0.193	0.095 0.111		0.155 0.208	0.131 0.153		0.117 0.146	0.085 0.100
	0.130 0.	0.074 0.		0.265 0.	0.113 0.		0.155 0.	0.071 0.319
0.061 0.117 0.120 0.		0.234 0.204 0.148 0.	0.160 0.147 0.096 0.	-0.123 0.026 0.071 0.	0.538 0.415 0.190 0.	0.198 0.210 0.179 0.	0.054 0.052 0.060 0.	0.080 0.077 0.060 0.
	0.138 0.122	0.094 0.097		0.114 0.178	0.108 0.113		0.067 0.087	0.182 0.148
	0.095 0.	0.053 0.		0.123 0.	0.095 0.		0.053 0.	0.088 0.
0.247 0.233 0.070 0.		0.357 0.243 0.103 0.	0.184 0.164 0.106 0.	0.188 0.205 0.106 0.	0.189 0.204 0.148 0.	0.250 0.243 0.113 0.	0.211 0.132 0.130 0.	0.118 0.093 0.060 0.
	0.091 0.075	0.165 0.151		0.280 0.266	0.091 0.119		0.185 0.140	0.055 0.072
	0.142 0.	0.300 0.		0.130 0.	0.140 0.		0.071 0.	0.049 0.

(a)

### ASR 3—West Face

Average Strain, Laser Measurement  
 Average Strain, Caliper Measurement  
 Cracking Index  
 Rebar Strain

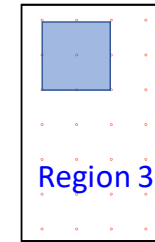


0.052	0.050	0.409	0.108	0.358	0.111
0.108	0.063	0.417	0.142	0.210	0.090
0.099	0.120	0.312	0.094	0.163	0.067
0.	<b>0.228</b>	0.	0.	0.	0.
0.101	-0.044	0.471	na	0.232	0.266
0.113	0.066	0.446	na	0.259	0.239
0.109	0.050	0.408	na	0.162	0.202
0.	0.	0.	0.	0.	0.
0.063	0.190	na	na	0.081	0.015
0.082	0.143	na	na	0.108	0.065
0.155	0.300	na	na	0.071	0.195
0.	0.	0.	0.	0.	<b>0.273</b>
0.200	0.340	0.183	na	0.293	-0.069
0.116	0.279	0.193	na	0.251	0.063
0.130	0.095	0.088	na	0.120	0.071
0.	0.	0.	0.	0.	0.
0.132	0.133	0.136	0.109	0.123	0.058
0.116	0.145	0.191	0.159	0.114	0.061
0.120	0.120	0.210	0.070	0.096	0.095
0.	0.	0.	0.	0.	0.

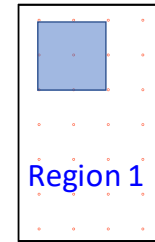
(b)

### ASR 3—North and South Ends

Average Strain, Laser Measurement  
 Average Strain, Caliper Measurement  
 Cracking Index  
 Rebar Strain



North End



South End

	0.202 0.236 0.096 0.	0.202 0.170 0.092 0.	
0.103 0.170 0.140 0.		0.376 0.311 0.189 0.	0.269 0.264 0.131 0.
	0.122 0.144	0.192 0.181	
0.125 0.076 0.035 0.	0.085 0.	0.130 0.	0.188 0.152 0.106 0.
	0.123 0.145	0.187 0.183	
	0.053 0.	0.078 0.	

	0.000 0.098 0.106 0.	0.196 0.216 0.248 0.331	
0.112 0.174 0.060 0.		0.009 0.139 0.088 0.	0.062 0.154 0.106 0.
	0.218 0.206	0.106 0.193	
0.202 0.242 0.229 0.	0.301 0.	0.120 0.	0.418 0.321 0.226 0.
	0.781 0.631	-0.020 0.080	
	0.320 0.	0.173 0.	

(c)

Figure C-3. Average surface strains using laser and caliper measurements along with cracking index and reinforcing bar strains for block ASR 3 on (a) east face, (b) west face, and (c) north and south ends (all values are percentages)

## APPENDIX D

### MEASUREMENT UNCERTAINTIES

This appendix presents measurement uncertainties for the instruments/devices used to measure structural responses in the Task 1 report.

**Table D-1. Measurement Uncertainty**

Measurement/Component	Type	Component Standard Uncertainty	Combined Standard Uncertainty	Total Expanded Uncertainty (k=2)
<i>Actuator position</i>				
Uncertainty in secondary standard	B	0.2 mm (0.006 in)	0.2 mm (0.007 in)	0.4 mm (0.015 in)
Uncertainty in calibration procedure (N=32)	A	0.2 mm (0.004 in)		
<i>Actuator load</i>				
Uncertainty in secondary standard	B	1.3 kN (0.3 kip)	1.3 kN (0.3 kip)	2.6 kN (0.6 kip)
Uncertainty in calibration procedure (N=32)	A	0.4 kN (0.1 kip)		
<i>Compressive Stress, 4 in x 8 in Concrete Cylinder (calculated using actuator load)</i>				
Uncertainty in secondary standard	B	165 kPa (23.9 psi)	174 kPa (25.2 psi)	347 kPa (50.4 psi)
Uncertainty in calibration procedure (N=32)	A	54.9 kPa (7.96 psi)		
<i>Compressive Stress, 6 in x 12 in Concrete Cylinder (calculated using actuator load)</i>				
Uncertainty in secondary standard	B	73.2 kPa (10.6 psi)	77.1 kPa (11.2 psi)	154 kPa (22.4 psi)
Uncertainty in calibration procedure (N=32)	A	24.4 kPa (3.54 psi)		
<i>Compressive Stress, 3 in x 6 in Concrete Core (calculated using actuator load)</i>				
Uncertainty in secondary standard	B	341 kPa (49.4 psi)	359 kPa (52.1 psi)	718 kPa (104 psi)
Uncertainty in calibration procedure (N=32)	A	114 kPa (16.5 psi)		

**Table D-1 (Continued): Measurement Uncertainty**

Measurement/Component	Type	Component Standard Uncertainty	Combined Standard Uncertainty	Total Expanded Uncertainty (k=2)
<i>Axial Extensometer, 4 in gage length</i>				
Uncertainty in secondary standard	A/B	1.52 $\mu\text{m}$ (0.00006 in)	16.9 $\mu\text{m}$ (0.00066 in)	33.7 $\mu\text{m}$ (0.00132 in)
Uncertainty in calibration procedure (N=20)	A	16.8 $\mu\text{m}$ (0.00066 in)		
<i>Axial Extensometer, 2 in gage length</i>				
Uncertainty in secondary standard	A/B	1.52 $\mu\text{m}$ (0.00006 in)	20.2 $\mu\text{m}$ (0.00079 in)	40.3 $\mu\text{m}$ (0.00158 in)
Uncertainty in calibration procedure (N=20)	A	20.1 $\mu\text{m}$ (0.00079 in)		
<i>Axial Compressive Strain, 4 in x 8 in Concrete Cylinder (calculated using 4 in gage length axial extensometer)</i>				
Uncertainty in secondary standard	A/B	15.0 $\mu\epsilon$	166 $\mu\epsilon$	331 $\mu\epsilon$
Uncertainty in calibration procedure (N=20)	A	165 $\mu\epsilon$		
<i>Axial Compressive Strain, 3 in x 6 in Concrete Core (calculated using 2 in gage length axial extensometer)</i>				
Uncertainty in secondary standard	A/B	30.0 $\mu\epsilon$	396 $\mu\epsilon$	792 $\mu\epsilon$
Uncertainty in calibration procedure (N=20)	A	395 $\mu\epsilon$		
<i>Displacement Transducer</i>				
Uncertainty in secondary standard (N=8)	A/B	2 $\mu\text{m}$ (0.00006 in)	0.3 mm (0.01 in)	0.6 mm (0.02 in)
Uncertainty in calibration procedure (N=20)	A	0.3 mm (0.01 in)		